



**DESIGN AND MANUFACTURING OF DIRECT
DRIVEN STANDALONE WIND ENERGY
CONVERSION SYSTEM**

BY:

MESFIN BELAYNEH

**BAHIR DAR UNIVERSITY
INSTITUTE OF TECHNOLOGY
SCHOOL OF CHEMICAL AND FOOD ENGINEERING
POSTGRADUATE PROGRAM IN SUSTAINABLE ENERGY
ENGINEERING**

November, 2011



**DESIGN AND MANUFACTURING OF DIRECT
DRIVEN STANDALONE WIND ENERGY
CONVERSION SYSTEM**

**A THESIS PRESENTED IN PARTIAL FULFILLMENT OF
THE REQUIREMENT FOR THE DEGREE OF MASTERS OF
SCIENCE IN SUSTAINABLE ENERGY ENGINEERING**

BY: Mesfin Belayneh

Advisor: Dr. Solomon T/M

Co. Advisor: Mr. Assefa Ayalew

**BAHIR DAR UNIVERSITY
INSTITUTE OF TECHNOLOGY
SCHOOL OF CHEMICAL AND FOOD ENGINEERING**

November, 2011



BAHIRDAR UNIVERSITY
INSTITUTE OF TECHNOLOGY
SCHOOL OF CHEMICAL AND FOOD ENGINEERING

**DESIGN AND MANUFACTURING OF DIRECT DRIVEN
STANDALONE WIND ENERGY CONVERSION SYSTEM**

BY:
MESFIN BELAYNEH

Approval by the board of examiners

----- Chair Graduate Committee	----- Date	----- Signature
----- Advisor	----- Date	----- Signature
----- Co. Advisor	----- Date	----- Signature
----- Examiner, internal	----- Date	----- Signature
----- Examiner, external	----- Date	----- Signature

Date _____

Declaration

I hereby declare that the work which is being presented in this thesis entitled ‘Design and Manufacturing of Direct Driven Standalone Wind Energy Conversion System’ is original work of my own, has not been presented for a degree of any other university and all the materials used for the thesis have been duly acknowledged. I certify that the above declaration is correct.

Mesfin Belayneh Ageze
(Candidate)

Signature: _____

ACKNOWLEDGMENT

To the very beginning, all praises and thanks to the almighty God ‘Egizabher’, everlasting Shepherd, most merciful!

‘Of all we shall thrust in God for he had bleed and condemned to clean us from our sin’

Looking back my study period, I found joyful experiences which are very helpful for my dreams I am intended to be. Unfortunately, there were many challenges to be tackled as well, and many people were there for me. It is my pleasure to express my appreciation to all of them for standing in my side.

My Advisor Dr. Solomon T/M and Co. Advisor Mr. Assefa Ayalew I am very thankful for their support and inspiration.

My special thanks goes to my colleagues and sweet friends for their valuable help especially during prototype development and of all I am very lucky to have you all.

My appreciation also goes to the School of Mechanical and Industrial Engineering and School of Electrical and Computing of Bahir Dar University for allow me to use the workshops to complete my prototype.

Particular thanks goes to my sponsor Horn of Africa Regional Environmental Center and Network, for the finical support.

Thank you all!

MESFIN BELAYNEH AGEZE

November 2011, Bahir Dar, Ethiopia

TABLE OF CONTENTS

Contents	Page No.
ACKNOWLEDGMENT	II
TABLE OF CONTENTS	III
LIST OF TABLES	VIII
LIST OF FIGURES	IX
NOMENCLATURE	XI
ABSTRACT	III
CHAPTER ONE: INTRODUCTION	1
1.1 BACKGROUND OF THE THESIS	1
1.2 OBJECTIVES	4
1.3 THESIS LAYOUT	4
CHAPTER TWO: THEORY OF WIND TURBINE	5
2.1 INTRODUCTION	5
2.2 CLASSIFICATION OF WIND TURBINE	6
2.2.1 Vertical Axis Wind Turbines	6
2.2.2 Horizontal Axis Wind Turbines	7
2.3 AERODYNAMICS OF HAWT	11
2.3.1 Actuator Disc Theory	11
2.3.2 Blade Element Theory	13
2.3.3 Blade Element Momentum Theory	14
2.3.4 Design Procedure of Wind Turbines	15
2.3.5 Performance Parameters of HAWT	16
2.3.6 Criteria in HAWT Design	16
2.4 WIND TURBINE SITTING	16
2.5 DIRECT DRIVEN PERMANENT MAGNET WIND GENERATOR	18
2.5.1 Generators with Field Winding	19
2.5.2 Axial Flux Permanent Magnet Wind Generator	19
2.5.3 Radial Flux Permanent Magnet Wind Generator	21
2.5.4 Transversal Flux Permanent Magnet Wind Generator	22
2.5.5 Generator Requirements	23
CHAPTER THREE: DATA COLLECTION AND CONCEPTUAL DESIGN	24

3.1 SITE SELECTION	24
3.2 DATA COLLECTION	25
3.3 WIND RESOURCE ASSESSMENT	25
3.3.1 Monthly Average Wind Speed	26
3.3.2 Diurnal Pattern of Strength	26
3.3.3 Wind Probability Density	27
3.3.4 Wind Speed Variation with Height	27
3.4 ELECTRICAL DEMAND DETERMINATION	28
3.4.1 Calculation of Primary Loads of the Site.....	29
3.4.2 Peak Load	32
3.4.3 Load Factor	32
3.5 SYSTEM CONFIGURATION	33
3.6 DESIGN TOPOLOGY	34
3.6.1 Rotor Axis Orientation: Horizontal or Vertical	34
3.6.2 Rotor Power Control.....	35
3.6.3 Rotor Position: Upwind Of Tower or Downwind of Tower.....	35
3.6.4 Rotor Speed: Constant or Variable	35
3.7 SELECTING HUB HEIGHT AND DESIGN SPECIFICATIONS	36
CHAPTER FOUR: DESIGN OF MECHANICAL COMPONENTS.....	38
4.1 INTRODUCTION	38
4.2 BLADE DESIGN	38
4.2.1 BLADE AERODYNAMICS ANALYSIS	40
A. Strip Theory for a Generalized Rotor with Wake Rotation	40
B. Tip Loss: Effect on Power Coefficient of Number of Blades.....	43
C. HAWT Flow States.....	45
D. Blade Shape for Optimum Rotor with Wake Rotation	46
E. Airfoil for Wind Turbines.....	47
F. Modification of Blade Geometry	48
G. Determination of Basic Rotor Parameters	49
H. Determination of the Performance the Rotor.....	55
4.2.2 BLADE STRUCTURAL ANALYSIS	57
A. Material Selection	60
B. Load Case A: Normal Operation	63
C. Load Case B: Yawing	68
D. Load Case C: Yaw Error	69
E. Load Case E: Maximum Rotational Speed.....	69
F. Load Case F: Short at Load Connection	69
G. Load Case G: Shutdown (Braking).....	70
H. Load Case H: Parked Wind Loading	71
I. Load Case I: Parked Wind Loading, Maximum Exposure	71
4.2.3 BLADE STABILITY ANALYSIS	72
A. Blade Vibration.....	72
B. Design for Buckling.....	74

4.3 JOINT DESIGN.....	75
A. Load Case A: Normal Operation	76
B. Load Case D and E Combined.....	78
4.4 HUB DESIGN	79
A. Material Selection	79
B. Load Case A: Normal Operation	80
C. Load Case B: Yawing	83
D. Load Case C: Yaw Error.....	83
E. Load Case E: Maximum Rotational Speed.....	84
F. Load Case F: Short at Load Connection	84
G. Load Case G: Shutdown (Braking).....	84
H. Load Case H: Parked Wind Loading	84
I. Load Case I: Parked Wind Loading, Maximum Exposure	84
4.4 MAIN SHAFT DESIGN AND ANALYSIS.....	85
4.4.1 MAIN SHAFT STRUCTURAL DESIGN	85
A. Material Selection	85
B. Load Case A: Normal Operation	87
C. Load Case B: Yawing	91
D. Load Case D: Maximum Thrust	91
E. Load Case E: Maximum Rotational Speed.....	91
F. Load Case F: Short at Load Connection	92
G. Load Case G: Shutdown (Braking).....	92
H. Load Case H: Parked Wind Loading	93
I. Load Case I: Parked Wind Loading, Maximum Exposure	93
4.4.2 MAIN SHAFT DEFLECTION	94
4.4.3 MAIN SHAFT VIBRATION	95
4.4.4 DESIGN FOR BUCKLING	96
CHAPTER FIVE: ELECTRICAL COMPONENT DESIGN	97
5.1 INTRODUCTION	97
5.2 CORELESS AXIAL FLUX PMG.....	98
5.2.1 Rotor Assembly	99
5.2.2 Stator Assembly.....	100
5.2.3 Permanent Magnet Materials	102
5.2.4 Coreless Stator Winding	104
5.3 MAGNETIC MODELING.....	106
5.3.1 Air Gap Modeling	106
5.3.2 Slot Modeling	108
5.3.3 Magnetic Circuit Analysis	110
5.4 PRELIMINARY ANALYTICAL ANALYSIS	113
5.4.1 Fixed parameters.....	113
5.4.2 Electrical Speed of the Generator	114
5.4.3 Number of Slots and Magnet Poles	114
5.4.4 Coil-Pole Fraction.....	114
5.4.5 Geometrical Parameter	115
5.4.6 Distribution Factor	116
5.4.7 Pitch Factor	116

5.4.8 Skew Factor	116
5.4.9 Magnet Fraction	117
5.4.10 Flux Concentration Factor	117
5.4.11 Permeance Coefficient	117
5.4.12 Magnet Leakage Factor.....	117
5.4.13 Effective Air Gap for Carter Coefficient	117
5.4.14 Carter Coefficient	117
5.4.15 Air Gap Area.....	118
5.4.16 Air Gap Flux Density.....	118
5.5 EQUIVALENT CIRCUIT.....	119
5.5.1 Induced Phase Voltage.....	120
5.5.2 Phase Resistance	121
5.5.3 Stator Inductance	121
5.5.4 Eddy Current Loss	122
5.5.5 Electromagnetic Torque.....	123
5.5.6 Cut in Speed of the Generator.....	124
CHAPTER SIX: MANUFACTURING	126
6.1 INTRODUCTION	126
6.2 BLADE MANUFACTURING.....	126
6.3 HUB MANUFACTURING.....	129
6.3.1 Casting Design Steps	131
6.3.2 Sand Casting Processes.....	131
6.4 MAIN SHAFT MANUFACTURING.....	132
6.5 ROTOR MANUFACTURING	134
6.6 STATOR MANUFACTURING.....	134
6.5 PROTOTYPE MANUFACTURING	136
CHAPTER SEVEN: OVERALL TECHNO-ECONOMICAL ANALYSIS	145
7.1 CAPITAL INVESTMENT COSTS	145
7.2 ANNUAL COSTS	147
7.2.1 Operation and Maintenance Cost (O&M).....	147
7.2.2 Replacement Cost	148
7.3 ANNUAL BENEFITS.....	148
7.4 ECONOMICAL EVALUATION OF THE SYSTEM.....	149
7.4.1 Real Interest Rate	149
7.4.2 Annual Saving.....	149
7.4.3 Cost Benefit Ratio (CBR)	149
7.4.4 Net Present Value (NPV).....	150
7.4.5 Internal Rate of Return (IRR)	151
7.4.6 Amortization	151

7.4.8 Cash Flow	153
CHAPTER EIGHT: CONCLUSION AND RECOMMENDATION	155
CONCLUSION	155
RECOMMENDATION.....	157
REFERENCE	158
ANNEX A	164
WIND RESOURCE ASSESSMENT RESULT.....	164
Wind Resource Assessment Result for Aykel: 1989	164
Wind Resource Assessment Result for Aykel: 2005	165
ANNEX B	166
AIRFOIL PROFILE FOR NACA 4412	166
ANNEX C	167
PART DRAWINGS	167
ANNEX D	174
ITERATION RESULT.....	174
ANNEX E.....	176
MANUFACTURING COST OF COMPONENTS.....	176
ANNEX F.....	177
INTERNAL RATE OF RETURN USING MICROSOFT EXCEL.....	177

LIST OF TABLES

Table No.	Description	Page No.
Table 1.1:	Overview of Renewable Energy Resources in Ethiopia	1
Table 2.1:	Number of Blades.....	15
Table 3.1:	Wind Speed Potential of Aykel City: Wind Resource Assessment Result	27
Table 3.2:	Comparison of Compact Fluorescent and Incandescent Bulbs	30
Table 3.3:	Typical Wattage Requirements for Electric Appliance.....	30
Table 3.4:	Household Energy Demand of Ch'andiba Keble	30
Table 3.5:	Institutions Daily Energy Demand	31
Table 3.6:	Ethiopian Population Growth Rate	31
Table 3.7:	Load Factor of Different Energy Technology	32
Table 3.8:	Design Specifications	37
Table 4.1:	Suggested Blade Number, B, for Different Tip Speed Ratio, λ	51
Table 4.2:	Results of Analysis Based on Spread Sheet Iteration.....	52
Table 4.3:	Comparison of the Designed and Linearized Chord Distribution of the Blade	55
Table 4.4:	End Condition Factor	75
Table 4.5:	Joint Loads Developed During Different Load Cases	76
Table 4.6:	SAE Bolts Strength Catalogue	77
Table 4.7:	Hub Material Specification	80
Table 4.8:	Result of the Strength Analysis for the Hub.....	85
Table 4.9:	Physical Properties of Shaft Material	87
Table 4.10:	Shaft Material Specification	89
Table 4.11:	Result of the Strength Analysis for the Main Shaft	94
Table 5.1:	Magnetic Properties of NdFeB.....	104
Table 5.2:	Physical Properties of NdFeB	104
Table 5.3:	Fixed Parameters of the Generator	113
Table 5.4:	Results of the Analysis for Preliminary Parameters of the Generator	115
Table 5.5:	Calculated Value of the Geometrical Parameters and Factors of the Generator ...	119
Table 5.6:	Characteristics of the Design Generator under Rated Conditions.....	125
Table 6.1:	Female Mold Width and Twisting Angle Distribution along the Span.....	128
Table 6.2:	Casting Processes, Mold and Metal Details	130
Table 6.3:	Flow Chart for Shaft Manufacturing	132
Table 6.4:	Dimension of the Blade of the Prototype	136
Table 6.5:	Dimension of the Generator of the Prototype	141
Table 7.1:	Raw Material Costs	145
Table 7.2:	Manufacturing Costs of Components.....	146
Table 7.3:	Miscellaneous Costs	146
Table 7.4:	Calculation of the Operation and Maintenance Cost of the System.....	147
Table 7.5:	Life Time Cash Flow of the System.....	153
Table 7.6:	Summary of Economic Analysis.....	154

LIST OF FIGURES

Figure No.	Description	Page No.
Figure 2.1:	The Energy Extracting Stream Tube of a Wind Turbine	5
Figure 2.2:	Darrieus Type Wind Turbine	7
Figure 2.3:	Savonius Type Wind Turbine	7
Figure 2.4:	Different Types of Horizontal Axis Wind Turbine.....	9
Figure 2.5:	Major Components of Horizontal Wind Turbine.....	10
Figure 2.6:	Control Volume for the Analysis of Momentum Theory	12
Figure 2.7:	Rotating Annular Stream Tube; Notation (a), Blade Element Model (b).....	14
Figure 2.8:	Axial Flux Generator	20
Figure 2.9:	Radial Flux Generator	21
Figure 2.10:	Transverse Flux Generator	22
Figure 3.1:	The Location of the Site Selected ‘Ch’andiba’ Village	24
Figure 3.2:	Flow Chart for the Wind Resource Assessment in HOMER.....	26
Figure 3.3:	Mean Wind Speed Variation with Height for Aykel City	28
Figure 3.4:	System Configuration of Wind Generator without Backup.....	34
Figure 3.5:	Power versus Rotor Diameter for Different Hub Height	36
Figure 4.1:	Blade Design Flow Chart.....	39
Figure 4.2:	Blade Element Theory, Geometry of the Airfoil	44
Figure 4.3:	Wind Turbine Flow States, the Axial Induction Factor and Thrust of Rotor	47
Figure 4.4:	Sample $CP- \Lambda$ Curve for High Tip Speed Ratio Wind Turbines.....	50
Figure 4.5:	Designed Chord Distribution of the Blade.....	53
Figure 4.6:	Linearized Chord and Designed Chord Distribution of the Blade.....	53
Figure 4.7:	Designed Twist Angle Distribution along the Blade Span	54
Figure 4.8:	Linearized Twist Angle and Designed Chord Distribution of the Blade.....	55
Figure 4.9:	Definition of the System of Axes for HAWT	59
Figure 4.10:	Tensile Failure Strength (Psi) for Laminated Douglass Fir/Epoxy	62
Figure 4.11:	Fatigue Failure Strength (psi) For Laminated Douglas Fir/Epoxy	62
Figure 4.12:	Approximation of Airfoil Cross Section to Triangular Area	63
Figure 4.13:	Design of Hub Flow Chart.....	79
Figure 4.14:	Design of Main Shaft Flow Chart	86
Figure 4.15:	Shaft Loading for Deflection Calculation.....	94
Figure 5.1:	Three Dimensional View of Axial Flux Permanent Magnet Generator	99
Figure 5.2:	Rotor Assembly for Twelve Pole Generator.....	100
Figure 5.3:	Stator Assembly for Axial Flux Generator	101
Figure 5.4:	Historical Development of the Rare Earth Magnets	103
Figure 5.5:	Coreless Winding of a Three Phase, Eight Pole AFPM Stator.....	105
Figure 5.6:	Connection Diagram of 3ϕ , Nine-Coil Winding of AFPM Brushless Stator	105
Figure 5.7:	Flux Flow through the Air Gap.....	106
Figure 5.8:	Air Gap Permeance Model.....	107

Figure 5.9: Circular Arc, Straight Line Permeance Model.....	108
Figure 5.10: Slotted Structure.....	109
Figure 5.11: Basic Translational Permanent Magnet Generator Structure.....	111
Figure 5.12: Equivalent Magnetic Circuit	111
Figure 5.13: Simplified Equivalent Magnetic Circuit	111
Figure 5.14: Equivalent Circuit of the AFPM Generator	120
Figure 5.15: Phasor Diagram of the AFPM Generator.....	124
Figure 6.1: Grain Orientation in Laminate and Illustration of Type of Laminate Joints	127
Figure 6.2: Twist of the Blade Airfoil	128
Figure 6.3: The Shape of the Laminated Wood/Epoxy Blade.....	129
Figure 6.4: Casting Components for Hub Casting	129
Figure 6.5: Creating the Taper of the Blades.....	137
Figure 6.6: Carving the Twisted Windward Face.....	138
Figure 6.7: Carving the Thickness.....	139
Figure 6.8: Carve the Curved Shape on the Back of the Blade	140
Figure 6.9: Photo of Blade Hub Assembly of the Prototype	140
Figure 6.10: Photo of One of the Rotor Assemblies of the Prototype.....	141
Figure 6.11: Photo of the Stator Assembly of the Prototype.....	143
Figure 6.12: Photo of the Assembling Frame of the Prototype	143
Figure 6.13: Photo of Assembled Prototype.....	144
Figure 7.1: Cash Flow of the System	154

NOMENCLATURE

Abbreviation: Meaning

AFPMG: Axial Flux Permanent Magnet Generator	FEA: Finite Element Analysis
BEM: Blade Element Momentum	HAWT: Horizontal Axis Wind Turbine
BEMT: Blade Element Momentum Theory	IEC: International Electrotechnical Commission
DDPMG: Direct Driven Permanent Magnet Generator	PM: Permanent Magnet
DFIG: Double Fed Induction Generator	NMSA: National Meteorology Service Agency
EMF: Electromotive Force	NdFeB: Neodymium Iron Boron
EPCO: Ethiopian Electric Power Corporation	SWT: Small Wind Turbine

Symbol: Meaning

a : axial induction factor	g_e : effective air gap length
a' : angular induction factor	I : area moment of inertia
A : cross sectional area	I_s : Peak slot current
A_g : air gap area	I_{ph} : Phase current
B : number of blades	J_{max} : Peak conductor current density
B_g : air gap flux density	k_c : carter coefficient
$ B_s _{max}$: Peak slot flux density	k_{cp} : Conductor packing factor
c : chord length of the airfoil	k_{ml} : magnet leakage factor
C_L : lift of coefficient	k_d : Distribution factor
C_D : drag of coefficient	k_p : Pitch factor
C_p : power coefficient	k_s : Skew factor
C_T : thrust coefficient	k_{st} : Stacking factor
C_ϕ : Flux concentration factor	l_m : magnte length
dF_x : thrust force	L_g : Air gap inductance
dr : differential radius	L_s : Slot leakage inductance
dQ : torque	L_e : End turns inductance
f : tip loss coefficient	L_{ph} : Phase inductance
f : electrical frequency	M : bending moment
g : air gap length	n_f : factor of safety
g : gravitational accleration	n_{rotor} : rotational speed of the rotor

n_s :	Number of turns per slot	P_{ml} :	line permeance
N_s :	Number of stator slots	P_c :	permeance coefficient
N_{spp} :	number of slots per pole per phase	P_r :	Ohmic power loss
N_m :	number of magnet poles facing the air gap	Re :	Reynolds number
N_{sm} :	Number of slots per pole	R_s :	slot resistance
N_{ph} :	number of phases	R_e :	End turn resistance
N_{sp} :	Number of slots per phase	R_i :	inner radius of the rotor
P_i :	pressure	R_{ph} :	phase resistance
P_{cr} :	critical bucking load	S_{ut} :	ultimate strength
P_g :	air gap permeance	S_e :	endurance limit
P_f :	fringing permeance	T_{el} :	electrical torque
P_s :	straight line permeance	V_∞ :	free stream velocity
P_m :	magnet permeability	V_{st} :	Stator steel volume
		Y_i :	lateral deflection

Greek Symbol: Meaning

α_{si} :	Slot aspect ratio at the inner radius	τ_{ci} :	Inside coil pitch
α_m :	Magnet fraction	τ_{co} :	Outside coil pitch
α_{cp} :	Coil – pole fraction	τ_{si} :	Inside slot pitch
β, φ :	relative wind angle	μ_o :	permeability of free space
θ_p :	Angular pole pitch	η :	mechanical/electrical efficiency
θ_s :	Angular slot pitch	ϑ :	kinematic viscosity
θ_{se} :	Slot pitch, electrical radian	λ :	tip speed ratio
ϵ_{max} :	peak emf	ω :	wake angular speed
ρ :	density	ω_m :	mechanical speed
σ' :	Local solidity factor	ω_{bi} :	Back iron width
σ_f' :	fracture strength coefficient	ω_{sb} :	Slot bottom width
\emptyset_g :	air gap flux	ω_e :	electrical speed
τ_p :	magnet pole pitch	ω_{tbi} :	Tooth width at the inner radius
τ_{pi} :	Inside pole pitch	ω_n :	natural frequency
τ_{po} :	Outside pole pitch	Ω :	rotor angular speed

ABSTRACT

The electricity generation from wind power is very reliant on the wind speed potential of the site and the technological advancement incorporated for manufacturing of wind turbine components, in addition raw material availability as well. The average wind speed distribution of Ethiopia is, is in the range of 3.5 to 5.5 m/s [3]. This is the cut-in speed for most of commercial wind generators available in the market. The goal of this thesis work is to design and manufacture a direct driven, horizontal axis, standalone, wind energy conversion system to utilize the wind speed range stated, as an off grid electrification system.

Design of wind blade to achieve satisfactory aerodynamic performance and structural stability starts with knowledge of the aerodynamic forces acting on the blades. In this thesis, HAWT blade design from aerodynamic view as well as from structural aspects is carried out. Blade element momentum theory (BEMT) known as also strip theory, which is the current mainstay of aerodynamic design and analysis of HAWT blades, is used for HAWT blade design, with consideration of tip loss, wake rotation, finite number of blades, and drag. For airfoil selection XFOIL program was used to constructing the airfoil database.

Structural design of the wind turbine blades is based on a publication of International Electrotechnical Commission for small wind turbine design; wind turbines-part 2: Design Requirement for Small Wind Turbines (IEC-614002). The publication suggests ten load cases that the wind turbine components will exposed from transportation to the extreme loading conditions. In addition to this stability analysis is carried out based on mechanical design procedure. The design of hub, joint, and main shaft are also designed for these load cases based on mechanical engineering design both for strength(fatigue and ultimate) and stability.

Design of axial flux permanent magnet generator (AFPMG) is done based on steady state analytical relations after a brief conceptual and magnetic modeling discussion are completed. The mechanical aspects of the generator are done after the electrical and major dimensions are determined. The designed mechanical and electrical components are modeled on Solidworks 2007 and analyzed on COSMOSwork 2007. Then after, the manufacturing processes are discussed. To validate the design completed a prototype with 1:4.6 scale was manufactured and testing was done. An overall techno-economic analysis was done to evaluate the feasibility of the design system.

CHAPTER ONE

INTRODUCTION

1.1 BACKGROUND OF THE THESIS

In recent years, the application of renewable energy sources is increasing in an effort to reduce the world wide dependence of fossil fuel. Among the major search areas wind, solar, biomass and wave are very common. The world wind energy conference held on 2003 Cape Town reasserted the imperative role of wind energy for future power generation.

According to world energy 2000 report, there is an enormous energy resource potential in Ethiopia, which if employed, could reduce the present energy shortage prevailing in the country and increase the process of rural electrification. The country has a potential of 30000MW from hydropower, 5kWh/m² from solar per day, wind speed of 3.5-5.5m/s, 700MW from geothermal, 1120×10⁶ tons from wood, from agricultural waste 15-20×10⁹ m³, and from natural gas 75×10⁶ tons, averagely per year [2]. The share of each energy source are tabulated below, From the total reserves of the country only wood 50%, agriculture wastes 30% and hydropower 0.9% are in use [2].

Table 1.1: Overview of Renewable Energy Resources in Ethiopia [3]

No.	Energy resources	Energy in TCal per year			
		Potential	Share %	Exploitable	Share %
1	Primary solar radiation	1,953,550	99.71	954	73.08
2	Wind	4,779	0.24	239	8.94
3	Forest biomass	800	0.005	240	8.97
4	Hydropower	552.1	0.03	138	5.16
5	Animal waste	111.2	0.01	33.73	1.26
6	Crop residue	81.36	0.0004	40.63	1.52
7	Human waste	28.18	0.00014	2818	1.05
Total		1,959,901.93	100.00	2,673.54	100.00

The wind distribution of Ethiopia is ranges between 3.5 to 5.5 m/s with best available wind resources (based on current measured data), Nazareth with 9.3 m/s, Ashengoda with 8.3 m/s, Herena-Mossobo with 6.9 m/s wind speed. Unfortunately, these wind speeds are considered quite low when compared to an international market which designs for turbine cut-in speeds higher than Ethiopian highest average wind speed. Furthermore, the significant variance of

the average wind speeds decreases their useful potential. This indicates the need for technology specific to the low wind speed conditions of Ethiopia which is similar to that of some countries such as South Africa with average wind speed range of 3 to 7 m/s [60].

Exploiting wind energy through various means is a very old concept. The first known use of wind dates back, 5000 years to Egypt when boats used sails to travel from shore to shore. The first true wind mill was built as early as 2000B.C. in ancient Babylon. By the 10th century, wind mills with wind catching surface as long as 16 feet and as high 30 feet were used to grind grain in the area known as Eastern Iran and Afghanistan. Vertical axis wind mills were also used in china which is often claimed as their birth place. The primary applications of wind mill were apparently grain grinding and water pumping. From as early as the thirteen century, horizontal axis wind mill were an integral part of the rural economy and their uses were declined with advent of cheap fossil fuelled engines [1, 4].

The first use of a wind mill to generate electricity was a system built in Cleveland Ohio in 1888 by Charles F. Brush. In 1891, Dane Poul La Cour developed the first wind machine to incorporate the aerodynamic principle (i.e. low solidity and four blade rotor with primitive airfoil shapes) to generate electricity. By 1920s, the two dominant rotor configurations (fan type and sail) were tried and found to be inadequate for generating appreciable amounts of electricity. The further development of wind generation electrical system in United State was inspired by the design of airplane propeller, latter a lot of electricity producing wind turbines. One remarkable Smith Putnam wind turbine of capacity of 1250kW was constructed in USA in 1941 [1, 4].

The sudden rise in the price of fuel in 1973 simulated a number of substantial government funded programs towards research and development of renewable energy sources. In USA, this lead to construction of a series of prototype turbines starting with the 38meter diameter and 100kW capacity in 1975 and continuing 97.5meter diameter and 2.5MW capacity in 1987. Similarly programs were in United Kingdom, Germany and Sweden. After 1990, both in Asia and Europe, the installation of wind turbines are improved. Wind energy was identified as having a key role to play in the supply of renewable energy with an increase in installed wind turbine capacity from 2.5GW in 1995 to 40GW by 2010 [1, 4].

Indigenously, the application of wind for power generation and other uses is not very familiar as compared the available reserve. Ethiopia Electric Power Corporation (EEPCO) engaged exploring an alternative electric power supply with collaboration of different nongovernmental organization such as GTZ TERNA Wind Energy Program on behalf of the German Federal Ministry for Economic Cooperation and Development (BMZ), the Deutsche

Gesellschaft für Technische Zusammenarbeit (GTZ) GmbH and Austrian Development Agency (ADA) since 2004 and wind energy projects throughout the nation [6, 7, 8]. Among the major searches of this project the final sites selected are, Nazareth with best wind speed 9.3m/s, Ashengoda with 8.3m/s(which is now a day called Africa's largest wind farm and it is estimated that it will cover 15% of the country demand), and Herena-Mossobo with 6.91m/s annual wind speed in 40 meter above the ground. The economic analysis of this project shows that their benefit/cost ratio is between 1.89-1.09 with 10% discount. Clean mechanism assessment is also taken [8].

In other uses for example water pumping, as International Development Research Center website description, in 1978 with Canadian collaboration a project titled pump windmill system (Project Number 770020 Start Date 1977/07/04 Program Area/Group PB-CORP | Sunset) which is the second phase of the economical vertical axis wind mill developed by the wind experts of the country before that year for water pumping. The total funding was around 27,010 dollar and the recipient institute was University of Waterloo. And the other project was under Ethiopian Water Resource Authority for the purpose of ground water pumping in 1982 with Canadian collaboration (Project Number 770029 Start Date 1978/09/26 Program Area/Group PB-CORP | Sunset). The project is focus wind power generation for driving water pump. For this project around 128,200 dollar was funded. Additional projects are in some technical schools and in universities of the country which are student projects for academics evaluation. But commercially only three assemblers and dealers are available until 2001E.C. [9].

Energy is the foremost and the influential factor for a given country economic development and the existence of the people as well, as William Blake said 'energy is eternal delight', Even though every active of mankind is depend on it, the usefulness and the benefit extent is highly based on the source the energy extracted from. In 1999, Ethiopian energy consumption was reached 17,539 thousand metric tons of oil equivalent [10] and further more in current Ethiopian fiscal 2010/11 the oil import bill is projected to increase by 9.3 billion birr which is 53% compared to the budget allocated for the same during the previous fiscal year [10]. In the rural area of the country which are far from the national electric grid, wood, agricultural and animal waste are used for cooking purpose, and for lighting purpose kerosene is the most familiar. To address this challenge this thesis aimed to work on wind energy generation under the stated wind speed range of the country. The major compatible wind conversion system is small scale wind turbine with direct driven generator. The major advantage of this type of system is it has small cut in wind speed and can generate electricity

under the rated wind speed so that it is possible to collect electricity at the wind speed distribution Ethiopia have had.

1.2 OBJECTIVES

Design and manufacture a direct driven standalone horizontal axis wind energy conversion system for off grid electrification.

Specific objectives:

- Potential site selection for the application based on the metrological data and other related constrained.
- Demand determination, by visiting the site identifying and classifying demands in to primary and deferrable load based on the application requirement and calculate the total demand.
- Design wind energy conversion system for off grid electrification application to satisfy the demand identified.
- Manufacture the prototype of the direct driven permanent magnet wind energy conversion system.
- Economical analysis of the system to evaluate the feasibility of the designed system.

1.3 THESIS LAYOUT

The organization of the thesis is as follow,

Chapter 1: In this chapter the background of the thesis and objectives that this thesis stands for are included, Chapter 2: The basic science behind wind energy technology and aerodynamics of the wind turbine are included. In addition different types of electric generator are discussed, Chapter 3: The wind resource data collected is analyzed using HOMER, the energy demand of the site is collected and the peak demand is determined. The other issue included is a conceptual design towards the system topology and selecting system configuration, Chapter 4: This chapter describes the mechanical components design, such as blade, hub, shaft and joint. The blades design both aerodynamic and structural design is included in it. The hub design, shaft design and the joint design are also completed in this chapter for nine design load cases, Chapter 5: The axial flux generator design is included with magnetic modeling and theoretical discussions, Chapter 6: The manufacturing processes for the main components are included in this chapter. The prototype development process and its test result also discussed, Chapter 7: includes the techno-economic analysis of the system to evaluate the feasibility of the system, Chapter 8: Conclusion and recommendation.

CHAPTER TWO

THEORY OF WIND TURBINE

2.1 INTRODUCTION

A wind turbine is a device for extracting kinetic energy from the wind blowing. By removing some of its kinetic energy the wind must slow down but only that mass of air which passes through the rotor disc is affected. Assuming that the affected mass of air remains separate from the air which does not pass through the rotor disc and does not slow down a boundary surface can be drawn containing the affected air mass and this boundary can be extended upstream as well as downstream forming a long stream tube of circular cross section. No air flows across the boundary and so the mass flow rate of the air flowing along the stream tube will be the same for all stream wise positions along the stream tube. Because the air within the stream tube slows down, but does not become compressed, the cross sectional area of the stream tube must expand to accommodate the slower moving air fig. 2.1[34].

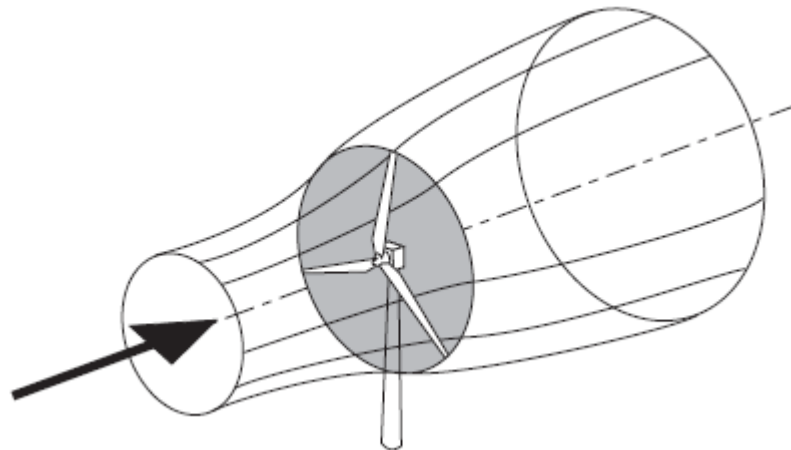


Figure 2.1: The Energy Extracting Stream Tube of a Wind Turbine [34]

Although kinetic energy is extracted from the airflow, a sudden step change in velocity is neither possible nor desirable because of the enormous accelerations and forces this would require. Pressure energy can be extracted in a step like manner, however, and all wind turbines, whatever their design is they operate in this way. The presence of the turbine causes the approaching air, upstream, gradually to slow down such that when the air arrives at the rotor disc its velocity is already lower than the free stream wind speed. The stream tube expands as a result of the slowing down and, because no work has yet been done on, or by, the air its static pressure rises to absorb the decrease in kinetic energy. As the air passes through the rotor disc, by design, there is a drop in static pressure such that, on leaving, the air is below the atmospheric pressure level. The air then proceeds downstream with reduced

speed and static pressure this region of the flow is called the wake. Eventually, far downstream, the static pressure in the wake must return to the atmospheric level for equilibrium to be achieved. The rise in static pressure is at the expense of the kinetic energy and so causes a further slowing down of the wind. Thus, between the far upstream and far wake conditions, no change in static pressure exists but there is a reduction in kinetic energy [34].

2.2 CLASSIFICATION OF WIND TURBINE

There are different criteria's for the classification of wind turbines. Wind turbines can be classified into two major classes based on the axis about which the turbine rotates. Turbines that rotate around a horizontal axis are more common. Vertical axis turbines are less frequently used. Wind turbines can also be classified by the location in which they are to be used. Onshore, offshore, or even aerial wind turbines have unique design characteristics. Wind turbines may also be used in conjunction with a solar collector to extract the energy due to air heated by the Sun and rising through a large vertical solar updraft tower.

2.2.1 Vertical Axis Wind Turbines

These types of wind turbines have rotor rotating about vertical axis. Key advantages of this arrangement are that the generator and/or gearbox can be placed at the bottom, near the ground, so the tower doesn't need to support it, and that the turbine doesn't need to be pointed into the wind. Drawbacks are usually pulsating torque that can be produced during each revolution and drag created when the blade rotates into the wind. It is also difficult to mount vertical axis turbines on towers, meaning they must operate in the often slower, more turbulent air flow near the ground, resulting in lower energy extraction efficiency.

Windmill with Rotational Sails: are new inventions and starts making electricity above a wind speed of 2m/s. Its sales contract and expand as the wind speed changes. These windmills have 3 sails of variable surface area. The speed is controlled through a magnetic revolution counter that expands or contracts the sails according to wind speed. A microprocessor type control unit controls the sails either manually or automatically. In case of a control unit failure, strong winds would tear the sails, but the frame would remain intact [12].

Darrieus Wind Turbine: Sometimes they are called "Eggbeater" turbines, they have good efficiency, but produce large torque ripple and cyclic stress on the tower, which contributes to poor reliability. Also, they generally require some external power source, or an additional Savonius rotor, to start turning, because the starting torque is very low. The torque ripple is

reduced by using 3 or more blades which results in a higher solidity for the rotor. Solidity is measured by blade area over the rotor area. Newer Darrieus type turbines are not held up by guy wires but have an external superstructure connected to the top bearing [12].

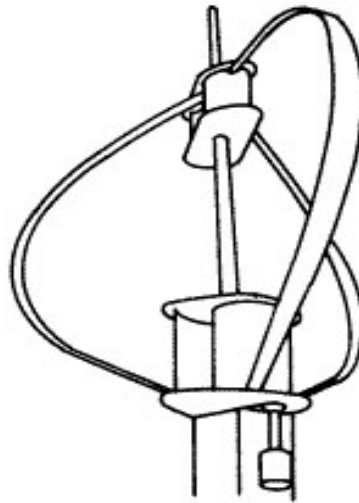


Figure 2.2: Darrieus Type Wind Turbine [13]

Savonius Wind Turbine: are drag type devices with two (or more) scoops that are used in anemometers, the flettner vents (commonly seen on bus and van roofs), and in some high reliability low efficiency power turbines. They are always self-starting, if there are at least three scoops. They sometimes have long helical scoops to give a smooth torque [12].

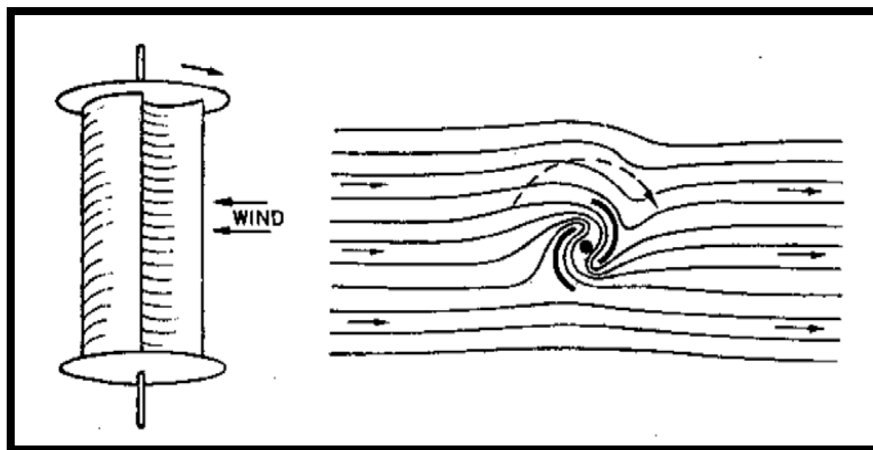


Figure 2.3: Savonius Type Wind Turbine [13]

2.2.2 Horizontal Axis Wind Turbines

Horizontal axis wind turbines (HAWT) have the main rotor shaft and electrical generator at the top of a tower, and must be pointed into the wind. Small turbines are pointed by a simple wind vane, while large turbines generally use a wind sensor coupled with a servo motor. Most have a gearbox, which turns the slow rotation of the blades into a quicker rotation that is more

suitable for generating electricity. Turbine blades are made stiff to prevent the blades from being pushed into the tower by high winds. Additionally, the blades are placed a considerable distance in front of the tower and are sometimes tilted up a small amount.

Modern Rural Windmills: these windmills, invented in 1876 by Griffiths Bros and Co (Australia), were used by Australian and later American farmers to pump water and to generate electricity. They typically had many blades, operated at tip speed ratios (defined below) not better than one, and had good starting torque. Some had small direct current generators used to charge storage batteries, to provide a few lights, or to operate a radio receiver. The American rural electrification connected many farms to centrally generated power and replaced individual windmills as a primary source of farm power in the 1950's. Such devices are still used in locations where it is too costly to bring in commercial power.

Common Modern Wind Turbines: usually three bladed, sometimes two bladed or even one bladed (and counterbalanced), and pointed into the wind by computer controlled motors. The rugged three bladed turbine types have been championed by Danish turbine manufacturers. These have high tip speeds of up to 6 times wind speed, high efficiency, and low torque ripple which contribute to good reliability. This is the type of turbine that is used commercially to produce electricity. The blades are usually colored light gray to blend in with the clouds and range in length from 20 to 40 meters (60 to 120 feet) or more.

Physical Principles of Rotor Rotation

It is important to note that modern wind turbines are based on the concept of speed of rotation rather than the amount of work done by the rotation of the rotor. This is evident in the difference seen between the wind turbine & windmill, whereas the former is designed for speed, the latter is designed for work. It must therefore be concluded that the relative physical load of modern wind turbines is light.

The physical principles affecting the speed of rotor rotation can be summarized as follows;

- The surface area, number of, & angle of the rotors to the wind direction.
- The angular momentum of the rotor piece which is dependent on the design and weight distribution of the rotor piece.
- Air resistance to rotation (i.e. drag when the rotors are rotating faster than the wind).
- Internal friction and electromagnetic force resistance to magnet rotation in the generator [15].

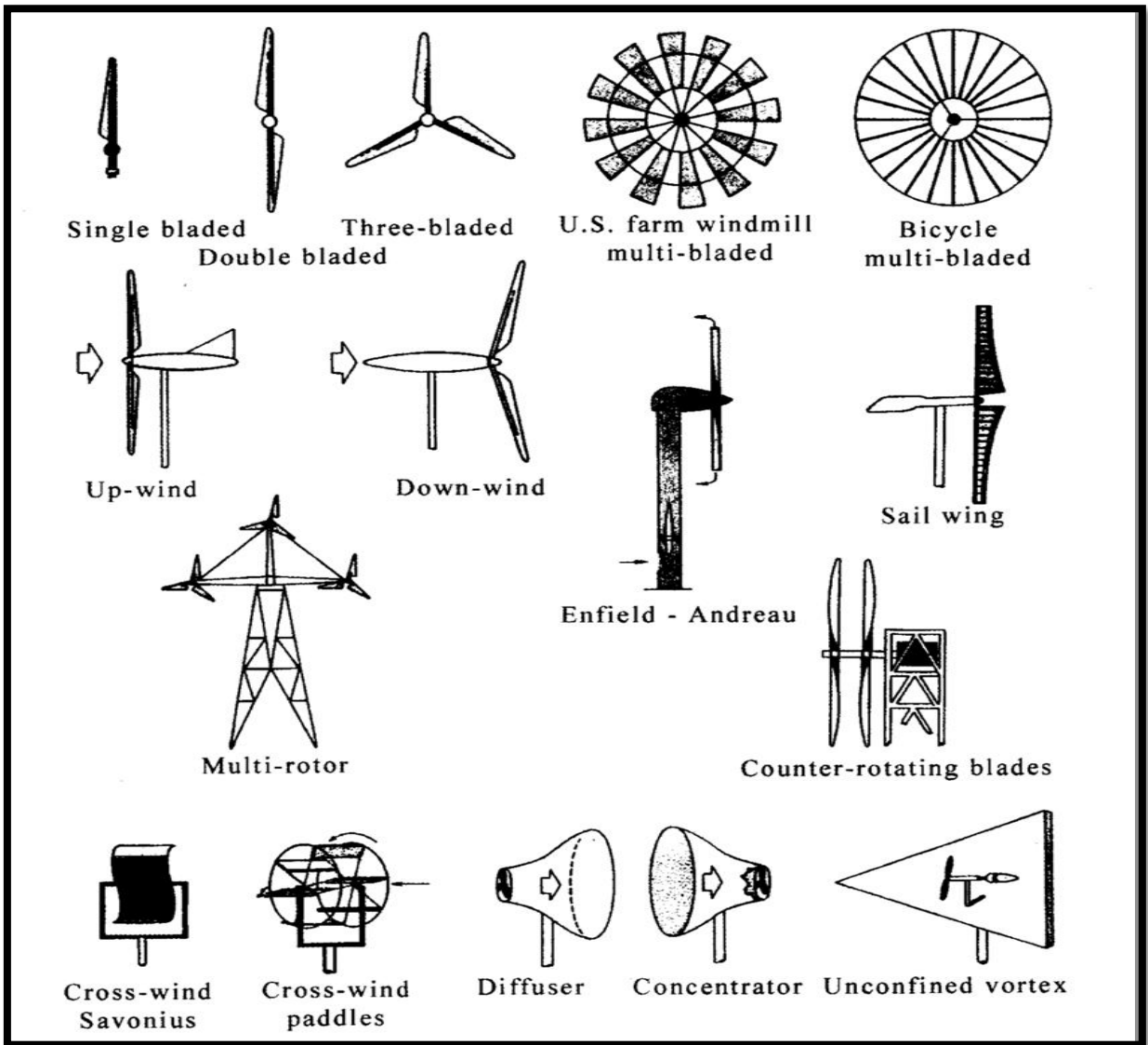


Figure 2.4: Different Types of Horizontal Axis Wind Turbine [5]

Components of HAWT

The major components of horizontal axial wind turbine system are stated in the following paragraphs;

The rotor subsystem: The rotor consists of the hub and blades of the wind turbine. These are often considered to be its most important components from both performance and overall cost standpoint. The rotor may be single, double, three, or multi bladed. A single-bladed wind rotor requires a counter weight to eliminate vibration but this design is not practical where icing on the one blade could throw the machine out of balance. The two bladed rotor was the most widely used because it is strong and simple and less expensive than the three-bladed rotor, but in the recent times three bladed rotor type becomes more widely used one in that the three bladed rotor distributes stresses more evenly when the machine turns, or yaws, during changes in wind direction.

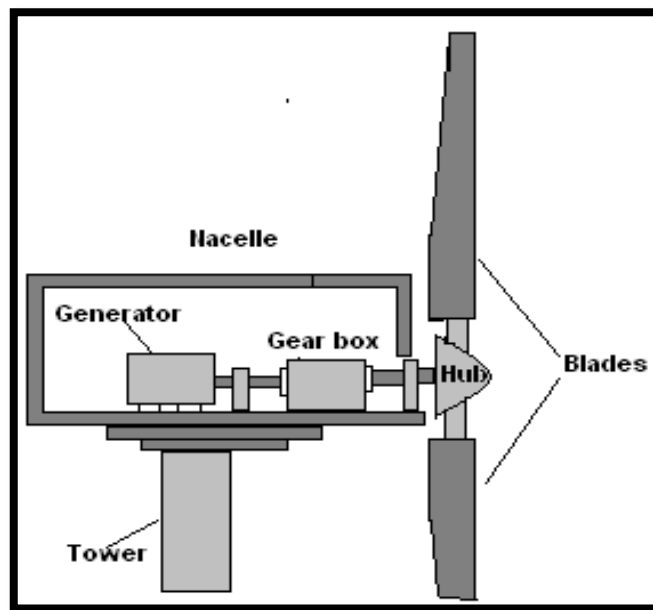


Figure 2.5: Major Components of Horizontal Wind Turbine [13]

Two general types of rotor hubs are rigid and teetered. In a typical rigid hub, each blade is bolted to the hub and the hub is rigidly attached to the turbine shaft. The blades are, in effect, cantilevered from the shaft and therefore transmit all of their dynamic loads directly to it. To reduce this loading on the shaft, a two bladed HAWT rotor usually has a teetered hub, which is connected to the turbine shaft through a pivot called a teeter hinge. Teeter motion is a passive means for balancing air loads on the two blades, by cyclically increasing the lift force on one while decreasing it on the other. Teetering also reduces the cyclic loads imposed by a two bladed rotor on the turbine shaft to levels well below those caused by two blades on a rigid hub. A three-bladed rotor has usually a rigid hub. In this case, cyclic loads on the turbine shaft are much smaller than those produced by a two-bladed rotor with a rigid hub, because three or more blades form a dynamically symmetrical rotor: one with the same mass moment of inertia about any axis in the plane of the rotor and passing through the hub. A wide variety of materials have been used successfully for HAWT rotor blades, including glass fiber composites, laminated wood composites, steel spars with non structural composite fairings and welded steel foils. Whatever the blade materials are, HAWT rotor hubs are almost always fabricated from steel forgings, castings or weldments.

The power train subsystem: The power train of a wind turbine consists of the series of mechanical and electrical components required to convert the mechanical power received from the rotor hub to electrical power. A typical HAWT power train consists of a turbine shaft assembly (also called a primary shaft), a speed increasing gearbox, a generator drive shaft (also called a secondary shaft), rotor brake and an electrical generator, plus auxiliary equipment for control, lubrication and cooling functions.

The nacelle structure subsystem: The HAWT nacelle structure is the primary load path from the turbine shaft to the tower. Nacelle structures are usually a combination of welded and bolted steel sections. Stiffness and static strength are the usual design drivers of nacelle structures.

The tower subsystem and the foundation: A HAWT tower raises the rotor and power train to the specified hub elevation, the distance from the ground to the center of the swept area. The stiffness of a tower is a major factor in wind turbine system dynamics because of the possibility of coupled vibrations between the rotor and tower.

The controls: The control system for a wind turbine is important with respect to both machine operation and power production. Wind turbine control involves the following three major aspects and the judicious balancing of their requirements [2]:

- Setting upper bounds on and limiting the torque and power experienced by the drive train,
- Maximizing the fatigue life of the rotor drive train and other structural components in the presence of changes in the wind direction, speed, as well as start-stop cycles of the wind turbine,
- Maximizing the energy production.

The balance of electrical subsystem: In addition to the generator, the wind turbine utilizes a number of other electrical components. Some examples are cables, switchgear, transformers and power electronic converters, yaw and pitch motors.

2.3 AERODYNAMICS OF HAWT

2.3.1 Actuator Disc Theory

A simple model, generally attributed to Betz (1926) can be used to determine the power from an ideal turbine rotor, the thrust of the wind on the ideal rotor and the effect of the rotor operation on the local wind field. The simplest aerodynamic model of a HAWT is known as ‘actuator disk model’ in which the rotor becomes a homogenous disk that removes energy from the wind. Actuator disk theory is based on a linear momentum theory developed over 100 years ago to predict the performance of ship propeller.

The theory of the ideal actuator disk is based on the following assumptions [14]:

- No frictional drag,

- An infinite number of blades,
- There is continuity of velocity through the disk,
- Homogenous, Incompressible, steady state fluid flow,
- The pressure increment or thrust per unit area is constant over the disk,
- The rotational component of the velocity in the slipstream is zero. Thus the actuator disk is an ideal mechanism which imparts momentum to the fluid in the axial direction only.

A complete physical representation of this actuator disk may be obtained by considering a close pair of tandem propellers or turbine blades rotating in opposite direction and so designed that the element of torque at any radial distance from the axis has the same value for each blade in order that there shall be no rotational motion in the slipstream;

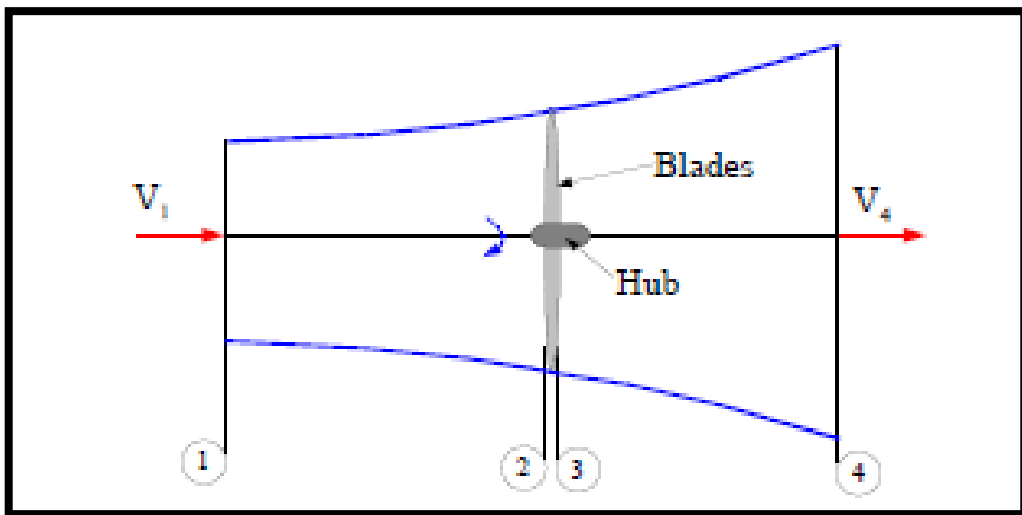


Figure 2.6: Control Volume for the Analysis of Momentum Theory [23]

also each turbine actual blade must be replaced with its small number of blades by another of the same diameter having a very large number of very narrow equal frictionless blades, the solidity at any radius being the same as for the actual turbine and finally to have the blade angles suitably chosen to give a uniform distribution of thrust over the whole disk. The analysis of the actuator disk theory assumes a control volume, in which the control volume boundaries are the surface of a stream tube and two cross sections of the stream tube as shown in Figure 2.6.

Consider the stream tube around a wind turbine shown in Figure 2.6. Four stations are shown in the diagram, 1 some way upstream of the turbine, 2 just before the blades, 3 just after the blades and 4 some way downstream of the blades. Between 2 and 3 energy is extracted from the wind and there is a change in pressure as a result. Assume $p_1 = p_4$ and that $V_2 = V_3$. We

can also assume that between 1 and 2 and between 3 and 4 the flow is frictionless so we can apply Bernoulli's equation. After some algebra:

$$P_2 - P_3 = \frac{1}{2\rho(V_1^2 - V_4^2)} \quad 2.1$$

Noting that force is pressure times area we find that:

$$dF_x = (P_2 - P_3)dA \quad 2.2$$

$$dF_x = 1/2\rho(V_1^2 - V_4^2)dA \quad 2.3$$

Define the axial induction factor 'a' as:

$$a = \frac{V_1 - V_2}{V_1} \quad 2.4$$

And also; $V_2 = V_1(1 - a)$ and $V_4 = V_1(1 - 2a)$

Substitution yields,

$$dF_x = 1/2\rho V_1^2 [4a(1 - a)] 2\pi r dr \quad 2.5$$

Then by considering rotating annular element and by defining angular induction factor as,

$$a' = \frac{\omega}{2\Omega} \quad 2.6$$

We find the torque as,

$$dT = 4a'(1 - a)\rho V_1 \pi r^3 dr \quad 2.7$$

Momentum theory has therefore yielded equations for the axial and tangential force on an annular element of fluid.

2.3.2 Blade Element Theory

Blade element theory relies on two key assumptions: [5]

- There are no aerodynamic interactions between different blade elements
- The forces on the blade elements are solely determined by the lift and drag coefficient

Consider a blade divided up into N elements as shown in Figure 2.7. Each of the blade elements will experience a slightly different flow as they have a different rotational speed (Ωr), a different chord length (c) and a different twist angle (γ). Blade element theory involves dividing up the blade into a sufficient number (usually between ten and twenty) of elements and calculating the flow at each one. Overall performance characteristics are determined by numerical integration along the blade span.

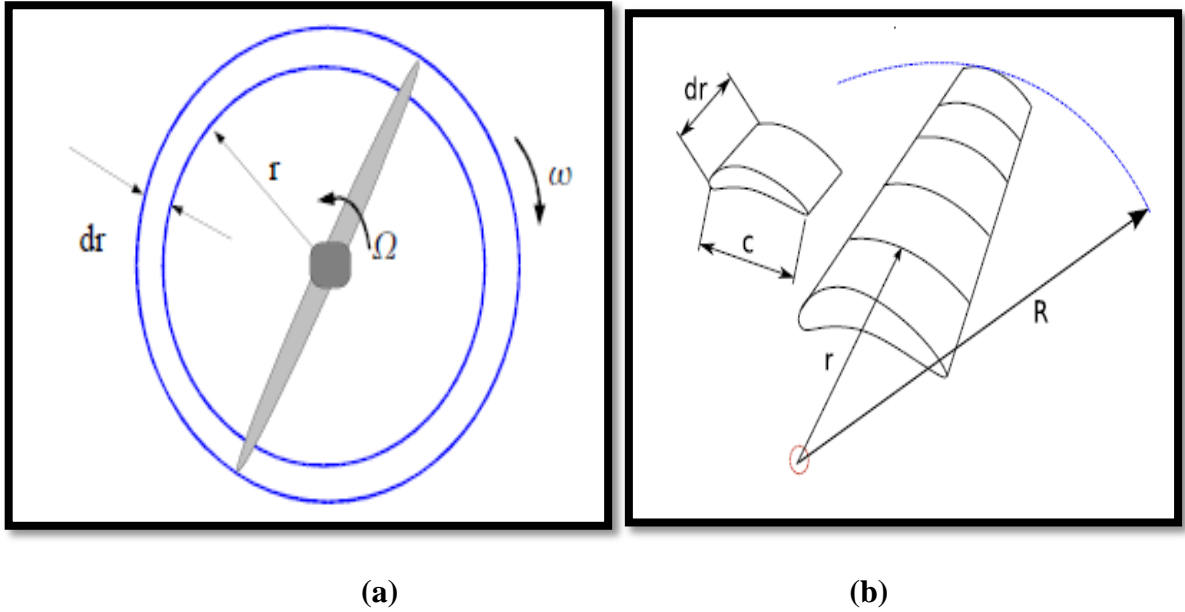


Figure 2.7: Rotating Annular Stream Tube; Notation (a), Blade Element Model (b) [23]

After series of algebraic manipulation the differential forces defined as follow;

$$dF_x = \sigma' \pi \rho \frac{V_1^2 (1-a)^2}{\cos^2(\beta)} (C_L \sin \beta + C_D \cos \beta) r dr \quad 2.8$$

$$dT = \sigma' \pi \rho \frac{V_1^2 (1-a)^2}{\cos^2(\beta)} (C_L \cos \beta - C_D \sin \beta) r^2 dr \quad 2.9$$

Where: σ' is the local solidity and defined as;

$$\sigma' = \frac{Bc}{2\pi r} \quad 2.10$$

2.3.3 Blade Element Momentum Theory

This theory is formulated by combining the last equations from the two preceding theories, to calculate rotor performance Equations 2.5 and 2.7 from a momentum balance are equated with Equations 2.8 and 2.9. Once this is done the following useful relationships arise:

$$\frac{a}{1-a} = \frac{\sigma' (C_L \sin \beta + C_D \cos \beta)}{4Q \cos^2(\beta)} \quad 2.11$$

$$\frac{a'}{1-a} = \frac{\sigma' (C_L \cos \beta - C_D \sin \beta)}{4Q \lambda_r \cos^2(\beta)} \quad 2.12$$

Where: Q = tip loss correction.

These equations will be used for design of blades, by introducing addition loss factor such as tip loss factor. The detail analysis for optimum wind blade design is discussed in chapter four of this documentation.

2.3.4 Design Procedure of Wind Turbines

1. Determine the diameter of the turbine required from the site condition and

$$P = 1/2 \times \rho \times C_p \times \eta \times U_\infty^3 \times \pi \times R^2 \quad 2.13$$

Where: P is the power output, C_p is the expected coefficient of performance (0.4 for a modern three bladed wind turbine), η is the expected electrical and mechanical efficiencies (0.9 would be a suitable value), R is the tip radius.

2. Choose a tip speed ratio for the machine. For water pumping pick $1 < \lambda < 3$ (Which gives a high torque) and for electrical power generation pick $4 < \lambda < 10$,
3. Choose a number of blades B , using Table 2.1, which is based on practical experience
4. Select an aerofoil, for $\lambda < 3$ curved plates can be used.

Table 2.1: Number of Blades

λ	B
1	8-24
2	6-12
3	3-6
4	3-4
More than 4	1-3

5. Obtain and examine lift and drag coefficient curves for the aerofoil in question. Note that different aerofoil's may be used at different spans of the blade; a thick aerofoil may be selected for the hub to give greater strength.
6. Choose the design aerodynamic conditions for each aerofoil. Typically select 80% of the maximum lift value.
7. Divide the blade into N elements. Typically 10 to 20 elements would be used.
8. As a first guess for the blade twist and chord, use the blade shape derived with wake rotation, zero drag and zero tip losses. Note that these equations provide an *initial guess only*. The equations are given as follows:

$$\beta = 90^\circ - \frac{2}{3} \tan^{-1} \left(\frac{1}{\lambda_r} \right) \quad 2.14$$

$$a = \left(1 + \frac{4 \cos^2(\beta)}{\sigma' C_L \sin \beta} \right)^{-1} \quad 2.15$$

$$a' = \frac{1 - 3a}{4a - 1} \quad 2.16$$

9. Calculate rotor performance and then modify the design as necessary, this is an iterative process [23]

In addition to these theories there are many methods for design and modeling, and corrections to take account other aerodynamics of the turbines blade such as wake rotation and losses.

2.3.5 Performance Parameters of HAWT

The power performance parameters of a HAWT can be expressed in dimensionless form, i.e. the power coefficients, C_p and is given by equation 2.17.

$$C_p = \frac{P}{1/2 \times \rho \times U_\infty^3 \times \pi \times R^2} \quad 2.17$$

2.3.6 Criteria in HAWT Design

During the design and construction of horizontal axis wind turbines there major criteria's to be considered for better outcome some of them according to ref [14] are listed below;

- Number of turbine blades
- Turbine torque regulation
- Hub design; rigid, teetering or hinged
- Turbine speed; fixed or variable rotor speed
- Rotor orientation; downwind or upwind rotor
- Blade material, construction method and profile (airfoil section)
- Orientation by self-aligning action (free yaw) or direct control (active yaw)
- Type of tower; steel or reinforced concrete shell or steel truss with tension cables
- Power control via aerodynamic control (stall control) or variable pitch blades (pitch control)
- Types of mechanical transmission and generator; synchronous or induction generator; gearbox or direct drive transmission

2.4 WIND TURBINE SITTING

Wind turbine can be installed as a single plant or a combination of many towers to form an array towers or of wind farm. The installation of individual wind turbines and wind farms requires a significant amount of planning, coordination and design work. Before wind turbines can be installed and connected to an electrical system, the exact locations for the future turbines need to be determined. A primary consideration is maximizing energy capture,

but numerous constraints may limit where turbines can be situated, the process of locating the area for wind farm is generally called wind turbine sitting and has the following major steps;

1. Identification of geographic areas needing further study
 - Areas with high average wind speeds within the region of interest are identified using a wind resource atlas and any other available wind data.
 - The characteristics of turbine types or designs under consideration are used to establish the minimum useful wind speed for each type.
2. Selection of candidate sites
 - Potential windy sites within the region are identified where the installation of one or more wind turbines appears to be practical from engineering and public acceptance standpoints.
 - If the nature of the terrain in the candidate region is such that there is significant variation within it, then a detailed analysis is required to identify the best areas.
 - At this stage, topographical considerations, ecological observations, and computer modeling may be used to evaluate the wind resource.
 - Geologic, social, and cultural issues are also considered
3. Preliminary evaluation of candidate sites
 - In this phase, each potential candidate site is ranked according to its economic potential, and the most viable sites are examined for any environmental impact, public acceptance, safety, and operational problems that would adversely affect their suitability as a wind turbine site.
 - Once the best candidate sites are selected, a preliminary measurement program may be required.
4. Final Site Evaluation
 - For the best remaining candidate sites, a more comprehensive measurement may be required. At this point, the measurements should include wind shear and turbulence in addition to wind speed and prevailing wind directions.
5. Micrositting
 - Once a site is chosen, or possibly as part of the final site evaluation, the exact location of the turbines and their energy production needs to be determined [5]

After the exact location for the wind farm is identified the installation process will follow, the installation of a wind power project is a complex process involving a number of steps and legal and technical issues. The process starts with securing legal rights and permit approvals. Once permits are obtained, the site needs to be prepared and the turbine transported to the site

and erected. Only after the turbine is connected to the grid and commissioned does regular operation commence. At this point the owner is responsible for oversight of the turbine, safe operation and maintenance.

The Installation and Operation Issues can be summarized in the following major activities; [5]

1. Predevelopment work and permitting,
2. Site preparation,
3. Turbine transportation,
4. Turbine assembly and erection,
5. Grid connection,
6. Commissioning,
7. Turbine operation.

2.5 DIRECT DRIVEN PERMANENT MAGNET WIND GENERATOR

Basically, there are three commonly used generator system for wind turbine application, these are stated below,

Constant speed wind turbines: it was built till late 1990 s with power levels below 1.5 MW using a multistage gearbox and a standard squirrel cage induction generator, directly connected to the grid.

Variable speed wind turbines: Since the late 1990s, most wind turbine manufacturers have changed to variable speed wind turbines for power levels from roughly 1.5MW, mainly to enable a more flexible match with requirements considering audible noise, power quality, and energy yield. They have used a multistage gearbox, a relatively low cost standard DFIG (Doubly Fed Induction Generator) and a power electronic converter feeding the rotor winding with a power rating of approximately 30% of the rated power of the turbine.

Direct driven system: Since 1991, there have been wind turbine manufacturers proposing gearless generator systems with the so called direct drive generators, mainly to reduce failures in gearboxes and to lower maintenance problems. A power electronic converter for the full rated power is then necessary for the grid connection. The low speed high torque generators and the fully rated converters for these wind turbines are rather expensive.

Direct driven permanent magnet wind generator seems much more attractive because the active material weight of the generator for the same air gap diameter is nearly halved, while the energy yield is a few percent higher. It has the highest energy yield. However, compared to the generator systems with gearbox, it is more expensive. Further improvements of this

generator system may be expected because the cost of the permanent magnets and the power electronics is decreasing and because further optimization and integration of the generator system is possible. In principle, the DDPMG could be the best solution because it does not have brushes or a gearbox that wears, it has the advantages of a fully rated converter and it is very compact and integral design so that low cost for transport [14].

There are different alternatives of the design of directly driven wind generator. It can be an asynchronous machine, a permanent magnet synchronous machine or a synchronous machine excited by a traditional field winding. Furthermore, the machine can be a radial, an axial or a transverse flux machine. The stator core can be slotted or slotless, and there can, for example, be a toroidal stator winding in an axial flux machine. Many different generators have been proposed in the literature as directly driven wind turbine generators [18].

2.5.1 Generators with Field Winding

Radial flux synchronous machine excited by a traditional field winding is one alternative for making a directly driven wind generator. The diameter of the machine in a large wind power plant will be large and the length small. The pole pitch must be large enough in order to arrange space for the excitation windings and pole shoes. The frequency must usually be lower than 50Hz, typically 10–20Hz, and a frequency converter is needed. The generator can be directly connected to a simple and cheap diode rectifier. However, the machine demands regular maintenance [22].

The first commercial directly driven generator in the power range of some hundreds of kilowatts is a synchronous machine excited by a traditional field winding. The first prototype was built in 1992. The outer diameter of the 500kW generator is about 5 meters and the length 0.6meter. The wind power plant is designed to be used with a frequency converter and the rotational speed varies between 18–38rpm. Nowadays, this type of 200kW – 1.5MW gearless turbine is on the market [22].

2.5.2 Axial Flux Permanent Magnet Wind Generator

Today, most of the low speed wind turbine generators available are permanent magnet (PM) machines. The characteristics of permanent magnet materials are improving and the material prices are decreasing. PM generators are usually axial or radial flux machines. The axial flux machines usually have slotless air gap windings. A design without slots simplifies the winding design. The magnets used can be of a flat shape, which is easy to manufacture. The length of the axial flux machine is short compared to the radial flux machine. Many axial flux

machines can easily be connected directly to the same shaft. The machine may have high axial force between the stator and rotor discs. Practical problems may arise in maintaining a small air gap in a large diameter machine and the structural stability of the large diameter discs [22].

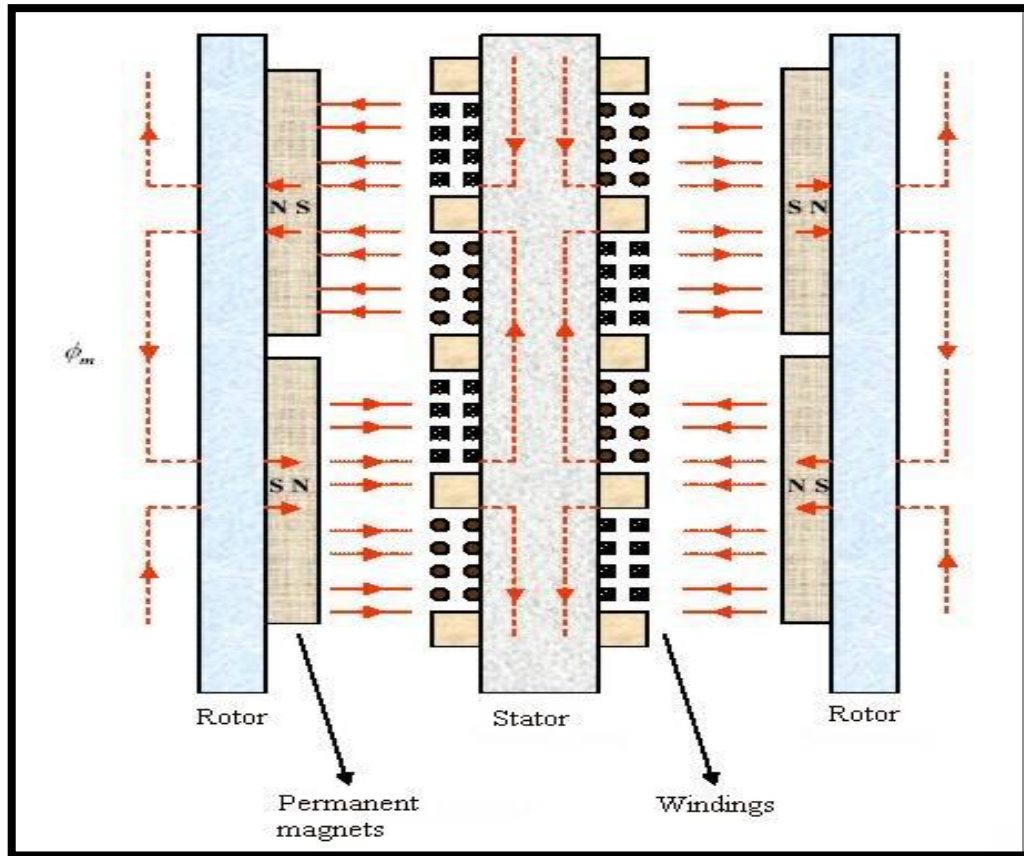


Figure 2.8: Axial Flux Generator [24]

In an axial flux machine with toroidal air gap winding, NdFeB permanent magnets are mounted on two rotor discs on both sides of the stator. Special attention must be paid to the choice of structural materials. If the casing is too close to the rotating magnets, the leakage flux will induce eddy currents causing extra losses and heating [22].

The advantages of the axial flux machine are: [22]

- Small length of the machine,
- Low cogging torque and noise,
- The fact that many machines can be mechanically connected with each other.

The disadvantages are:

- The need for a large outer diameter of the machine,

- Structural instability of the large diameter discs, and large amount of magnet material in the slotless design,
- The output of the experimental machines is in most cases rather low, only some kilowatts, but a 100kW machine is also under construction.

2.5.3 Radial Flux Permanent Magnet Wind Generator

Radial flux permanent magnet generators may be divided into two main types, surface magnet and buried magnet machines. The simple way to construct a rotor having a great number of poles is to mount the magnets onto the surface of a rotor core. However, it is necessary to use high energy magnets such as NdFeB magnets to provide an acceptable flux density in the air gap. The high energy magnets are very expensive and the magnet material should be used effectively. Furthermore, the surface mounted magnets should be mechanically protected by a band surrounding the rotor. Cheaper ferrite magnet material can be used in a buried magnet machine. The cost of the magnet material is relatively low but the assembly is complicated and costly. More magnet material is needed in a machine with ferrite magnets than in a machine with rare earth magnets and, therefore, the weight of the rotor becomes rather high. Different generator designs for gearless wind turbines have been used, i.e. electrically excited synchronous machines, surface magnet and buried magnet radial flux PM machines, axial-flux PM machines, transverse flux PM machines, switched reluctance machines and a linear induction machine. Some directly driven generators are used in low power commercial gearless wind turbines. The first commercial directly driven generator in the power range of some hundred kilowatts is a synchronous machine excited by a traditional field winding. Many low speed experimental machines have been built and tested [22].

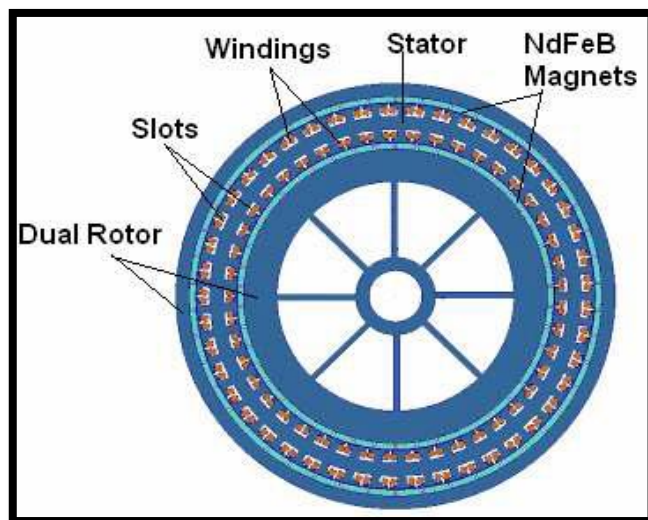


Figure 2.9: Radial Flux Generator [20]

The conventional asynchronous machine and the switched reluctance machine are large and heavy and they will not be very suitable designs for a large directly driven generator compared to the other designs. The transverse flux machine is small, efficient and light compared to the other designs, but the mechanical design is very complicated. The electrically excited synchronous machine is larger, heavier and less efficient than the PM synchronous machine. The radial flux PM synchronous machine has smaller outer diameter and it is cheaper than the axial flux machine. Cheap ferrite magnet material can be used in the buried magnet machine, but the rotor is heavier and the mechanical design more complicated than those in the surface magnet machine with high energy magnets. The radial flux PM machine with surface mounted magnets seems to be a good choice for the design of a large scale directly driven wind turbine generator [22].

2.5.4 Transversal Flux Permanent Magnet Wind Generator

The transversal flux machine has the simplest one-phase winding imaginable: the solenoid. Also, the TFM has fabled torque density; however, TFM's are not really expected to excel in standalone generation. At the very least, high phase inductance will make the electronics more costly. Transversal flux machine with axial air gap field and an axially magnetized permanent magnet, construction has extremely few parts six per phase four of which are distinct. If these parts could be manufactured by warm compacting SMC powder, the manufacturability of the whole generator would be superior to other options [22].

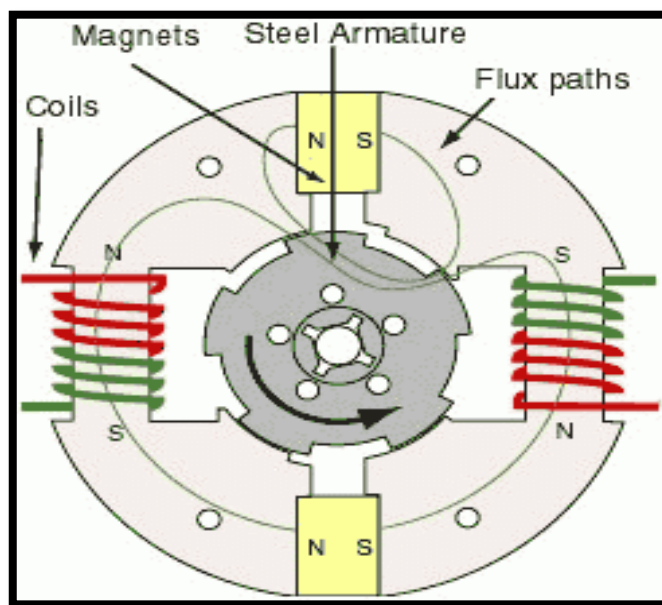


Figure 2.10: Transverse Flux Generator [21]

2.5.5 Generator Requirements

For the generator to work well in combination with a stall regulated wind turbine in a tiny wind power plant, the following qualities are desirable.

- *Permanent magnets:* All small scale wind power plants use permanent magnet generators. Electric magnetization is impossible because no brushes can be tolerated and because there is no grid.
- *Turbine startup:* Turbine startup is moderately difficult due to the very small torque produced at standstill. Therefore, a good generator has as small no load torque as possible.
- *Good efficiency at partial loads:* Since the generation takes place between 2 and 12 m/s, operation at nominal point of the generator is quite rare. Therefore, good efficiency at partial loads is desirable.
- *Passive cooling:* Since the tiny wind power plant is expected to operate in isolation from the electric grid, no forced cooling can be provided. Good conductive cooling from armature winding to the machine casing is desirable.
- *Small phase inductance:* If the generator has a small synchronous inductance, it is possible to use a diode rectifier. This way, the converter can be more stupid and cheaper.
- *High torque density:* The outer diameter of the tiny wind power plant generator is limited by aesthetic and aerodynamic considerations.
- *High short-circuit torque:* Since the primary storm protection method is short circuiting the generator, a large short circuit torque is preferable to keep the turbine stalled to as high a wind speed as possible.
- *Small outer diameter:* Since the turbine, for which the generators are too designed, has a diameter of 1.3 m, the outer diameter of the generator should not be greater than 200 mm.
- *Protective casing:* Small wind power plants are often subjected to marine air. The casing must protect active parts from both salt and humidity, and the armature should be resin cast.

In this chapter the science behind wind turbine systems were discussed, in the subsequent chapters the main findings of this thesis will be discussed.

CHAPTER THREE

DATA COLLECTION AND CONCEPTUAL DESIGN

3.1 SITE SELECTION

The major criteria's for the selection of the site to apply this thesis work are the following,

- Potential for wind energy generation,
- Rural area far from the national electric grid,
- Availability of wind speed data for the site,
- Compact population with demand of electricity.

The major potential areas in Amhara regional state are Debrebrhan, Gondar, Debremarkos, Aykel, Gorgora, Dangla, Kombolcha, Woreta, and Bahirdar. Among these areas the thesis select Aykel as a working site because of its wind speed potential, rural area far from national grid (even though the city Aykel has electricity source from the national grid there are many villages around Aykel city which are not suitable for the grid to address them. Based on the above points, the thesis selects '*ch'andiba*' village (which is under Amhara Regional State, North Gondar,) as target area. The site is located at [12°25'0"N 37°3'0"E], average elevation of 2,085 meter above sea level, and 52 km from Gondar city the capital of north Gondar district. The site is very close to the Lake Tana offshore, so that it has a promising wind energy potential.



Figure 3.1: The Location of the Site Selected '*Ch'andiba*' Village

3.2 DATA COLLECTION

The nearest wind speed measuring station is located at Aykel city so that the analysis is based on this station data, the available wind speed data for the site is for 10 years (1989-1993 and 2001-2005) but only the for 8 years is full measured and it is reliable only if the thesis only based on these years wind speed data. The source of the wind speed data for the site is taken from National Meteorology Service Agency. Wind resource assessment for the site for the selected years (i.e. 1989, 1991, 1992, 1993, 2001, 2004 and 2005) is done using software called HOMER. HOMER stands for Hybrid Optimization Model for Electric Renewable, and is a stand-alone hybrid system optimization program released by the US National Renewable Energy Lab (NREL) in 2000. The wind speed assessment result of the software is available at annex A, it include monthly average, diurnal pattern strength, probability density function and wind speed profile.

3.3 WIND RESOURCE ASSESSMENT

The study of wind resource of a site is useful because, the amount of power in the wind is very dependent on the speed of the wind, i.e. the power in the wind is proportional to the cube of the wind speed, and small differences in the wind speed make a large difference in the power that can be collected. A 10% difference in speed makes about a 33% change in power. This gives rise to the primary reason for wind resource assessment. In order to more accurately predict the potential benefits of a wind power installation, wind speeds and other characteristics of a site's wind regime must be accurately understood. There are also important technical reasons for studying a site's wind characteristics. Wind speeds, wind shear, turbulence and gust intensity all need to be specified when procuring a wind turbine, designing its foundation, etc.

The wind speed data collected from the national metrology agency is not full filled and has some gaps, so that have good outcome these gaps should filled properly. The unmeasured data are filled using linear interpolation. In addition some measured data is above the expected value this because of some technical and typing error, so that eliminating these values was done. After these all processes the data was filled to HOMER to evaluate the wind resource potential of the site. The wind speed assessment result of the software is available at annex A, it include monthly average, diurnal pattern strength, probability density function and wind speed profile with height. The wind resource assessment procedure shown is in the flow chart shown below at figure 3.2.

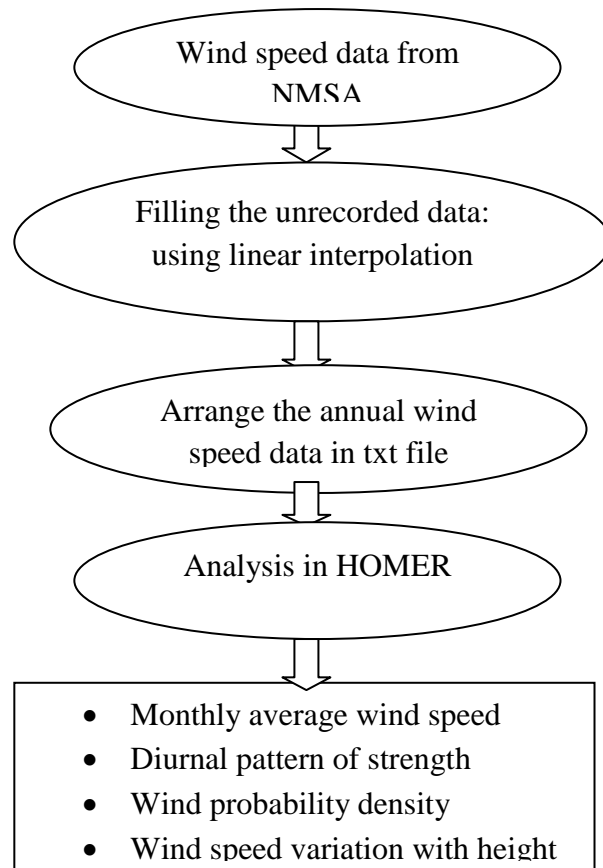


Figure 3.2: Flow Chart for the Wind Resource Assessment in HOMER

3.3.1 Monthly Average Wind Speed

Significant variations in seasonal or monthly averaged wind speeds are common. Most of high wind speed occur in sunny season of the month for example in Ethiopia finding significant amount of wind speed in summer (June, July and August) is not possible in turn wind speed is very high in dry season of the month. That is in February, March and April wind speed is considerable [28].

3.3.2 Diurnal Pattern of Strength

The diurnal pattern strength is a measure of how strongly the wind speed tends to depend on the time of day. Because the wind is typically affected by solar radiation, most locations show some diurnal (or daily) pattern in wind speed. In order to measure the strength of the diurnal pattern, we can calculate the average diurnal profile. Each of the 24 values of the average diurnal profile represents the annual average wind speed for that hour. HOMER then fits a cosine function to this average diurnal profile [28].

3.3.3 Wind Probability Density

The likelihood that the wind speed has a particular value can be described in terms of a probability density function (pdf). Experience has shown that the wind speed is more likely to be close to the mean value than far from it, and that it is nearly as likely to be below the mean as above it. The probability density function that best describes this type of behavior for turbulence is the Gaussian or normal distribution. The probability density function of the wind speed provides a means of the likelihood of particular values of wind speed. It provides no information, however, about what the speed is likely to be [28].

3.3.4 Wind Speed Variation with Height

Since most of the case wind speed measured above the earth surface about 10 m from the earth surface, and also it obvious that as altitude increase the wind speed also increase logarithmically. Therefore, including this in wind resource assessment is very vital [28].

Table 3.1: Wind Speed Potential of Aykel City: Wind Resource Assessment Result

Month	Year							
	Monthly average wind speed (m/s) at 10 meter hub height							
	1989	1990	1991	1992	1993	2002	2004	2005
January	2.412	2.450	3.159	2.615	2.663	2.255	2.431	2.702
February	2.647	2.559	3.178	3.006	2.962	2.327	2.928	2.832
March	2.589	3.129	2.629	3.303	2.962	2.117	2.824	2.821
April	2.500	3.162	2.722	2.978	3.091	2.746	2.599	2.856
May	2.173	3.533	2.604	2.812	2.847	2.592	2.841	3.065
June	2.380	3.554	2.549	3.109	2.868	2.559	2.403	2.688
July	2.246	2.762	2.617	2.493	2.622	2.127	2.342	2.137
August	2.125	2.927	2.644	2.436	2.689	2.512	1.999	2.198
September	1.728	2.507	2.273	2.373	2.548	1.836	1.956	2.118
October	1.795	2.224	2.099	2.142	2.353	1.913	2.089	1.700
November	1.790	2.331	2.234	2.137	2.107	1.884	2.067	2.035
December	2.064	2.482	2.342	2.561	2.419	1.972	2.589	2.027
Mean speed	2.49	3.06	2.52	2.89	2.91	2.18	2.64	2.67
Average of the mean wind speed of these 8 years in m/s							2.67	

So that the mean wind speed that the design will based is 2.67 meter at hub height of 10 meter. The wind speed variation with height can be related by using two major method such as power law and logarithmic method. Form these two method power law is chosen for this work and it is stated below as [5],

$$V_z = V_{zref} \left(\frac{z}{zr} \right)^a \quad 3.1$$

Where: V_{zref} = wind speed at the reference height

$Zref$ = reference height (10 meter is the reference elevation for this data)

Z = height of the hub

V_z = the wind speed at the required hub height

a = a factor to take account the surface roughness of the site, it vary for different terrain.

The value of a can be determined using empirical relation to take account the site geographical features. One can expect that any irregularities on the earth's surface will modify the wind flow, thus compromising the applicability of these prediction tools. So that take account the effect of terrain is a concrete point to focus during the wind resource of a site. In some literatures the value of a is tabulated with the different condition of the terrain. For this thesis work 'a' taken as 0.5 based on [5].

Substituting the power exponent in equation 3.1 the wind speed variation with height will look like as shown in the following figure.

$$V_z = 2.67 \left(\frac{Z}{10} \right)^{0.5}$$

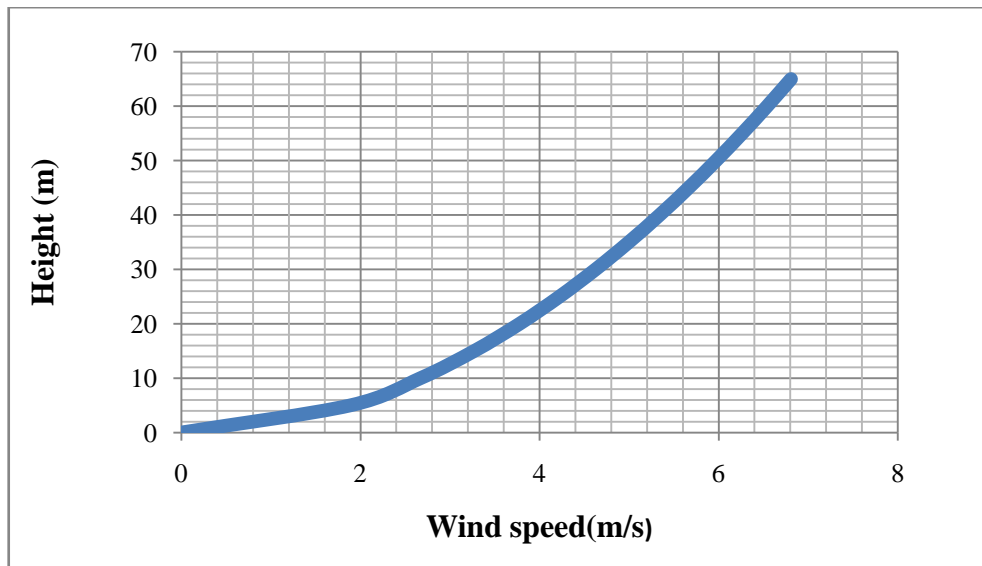


Figure 3.3: Mean Wind Speed Variation with Height for Aykel City

3.4 ELECTRICAL DEMAND DETERMINATION

In broad sense, electrical demand of a given site is categorized as primary load and deferrable load, based on the demand time limitation and application. Primary load is electrical demand that the power system must meet at the required time. Electrical demands associated with lights, radio, TV are primary load as per the community requirement. When a consumer

switches on a light, the power system must supply electricity to that light immediately the load cannot be deferred until later. Deferrable load is electrical demand that can be met anytime within a defined time interval. Water pump is an example of deferrable load because the storage inherent to each of those loads allows some flexibility as to when the system can serve them. The ability to defer serving a load is often advantageous for systems comprising intermittent renewable power sources, because it reduces the need for precise control of the timing of power production. If the renewable power supply ever exceeds the primary load, the surplus can serve the deferrable load rather than going to waste. By the current practice, the community used hand pump for drinking water supply and diesel pump for irrigation purpose, so that the thesis adopt as there is no deferrable load unless using the other electrically operating electrical pumps, it will be discussed on load management section of this documentation.

Based on the data collected from the village administration in the site '*ch'andiba*', there are 85 families with average of five family members at each. In addition, there is one church, and one elementary school.

3.4.1 Calculation of Primary Loads of the Site

Information obtained from village administration and from the survey conducted in the village showed that currently the communities are primarily using kerosene for lighting, and dry cells, wood for cooking. All households and institution establishments require lighting for 5 hours per day. Currently this is being met primarily with kerosene, candle and dry cells. Based on information obtained, the quantitative non cooking energy usage and expenditure pattern assessment survey, the energy needs of rural households and commercial establishments is characterized as follows. This has been done as per the '*ch'andiba*'s community requirement. Primary load is electrical demands associated with lights, radio, and TV as per the community requirement. Concerning about lighting, there are three different types of lamps options such as incandescent, fluorescent/compact fluorescent and light emitting diode (LED). It has been selected compact fluorescent lamp which is superior efficiency and longevity compared to an incandescent lamp. It consumes quarter of the energy compared to an incandescent lamp and these bulbs generally work in either alternating or direct current system though the ballast must much the system's nominal voltage and current type. The comparison between compact fluorescent and incandescent is given in table below at table 3.2.

Table 3.2: Comparison of Compact Fluorescent and Incandescent Bulbs [70]

Incandescent (watt)	Fluorescent (watt)	Same light output range (lumen)
40	7	400-500
50-60	10	500-600
75	11-15	600-1150
90	18	1150-1250
100	20-27	1250-1750

The type and power rating of the electric appliances that are going to be used by the community is given on the following table 3.3, so that it enable to estimate all the power required by the household and institution in the site.

Table 3.3: Typical Wattage Requirements for Electric Appliance [71]

Appliance	Wattage (W)	Remark
Compact florescent *	16	Equivalent with 60 watt incandescent lamp
Radio receiver/Caste player	15	-
14'' television	50	-
21'' television	65	-

The energy demand requirement of the households in the given village is different depend on their current economic status. Therefore, the community is classified in to four family classes according to their energy demand size as it shown in table 3.4.

Table 3.4: Household Energy Demand of Ch'andiba Keble [72]

Family class	Appliance	No. of family	Operation hour	Wattage (W) per family	Daily power use of household [Wh/day]
First	2bulb+1radio/tape recorder	40	5	47	9,400
Second	3bulb+1radio/tape recorder + 14'' television	20	5	113	11,300
Third	4bulb+1radio/tape recorder + 14'' television	15	5	129	9,675
Fourth	4bulb+1radio/tape recorder + 21'' television	10	5	144	7,200
Total energy demand per day					37,575

Table 3.5: Institutions Daily Energy Demand

Institution	No.	Consumption(Watt)	Operation hour	Daily energy consumption(Wh/day)
Church	1	160	5	800
School	1	320	5	1600
Total				2400

$$E_{total} = E_{houshold} + E_{scho\&church} = 37,575 + 2400 = 39.975kWh/day$$

The demand of the given site will increase as the population so that it is an instinct to consider the population increment before design energy supply. To consider of number of community families increment each year, first let's calculate the future population increment in the village as follows. The formula to calculate future population given current population and a growth rate is [25]

$$F_p = P_p \times [1 + PGR]^{yrs} \quad 3.4$$

Where: P_p = The present estimated population number is 425 people,

PGR = The average population growth rate of the community, for the country Ethiopia the population growth rate has the following trend according to World Bank report (table 3.6).

Table 3.6: Ethiopian Population Growth Rate [26]

Year	2000	2001	2002	2003	2004	2005	2006	2007	2008	2009	average
PGR	2.7	2.6	2.6	2.6	2.6	2.6	2.6	2.6	2.6	2.6	2.61

yrs = The number of year required to effect is 20 years (it is based on most of modern wind turbines are designed for around 20 years' operation or 120,000hours [26]).

$$F_p = 425 \times [1 + 0.0261]^{20} = 710$$

Then the future population number will increase to 710 after twenty years. Hence, on a daily and hourly basis 40% of power level has been added to the calculated load. Therefore, the required demand of the village will be;

$$E_{final} = (1 + 0.4) \times E_{total} = 1.4 \times 39.975 = 55.965kWh/day$$

The design of wind turbine is based on the peak load of the site, but to find the peak load of a given site it is necessary to determine the variation on electricity generation of the plant, this is directly related to the load factor the energy technology.

3.4.2 Peak Load

The demand of a given site varies with the time of the day, but the maximum requirement of the wind turbine system will exist when all the appliances are turn ON at the same time and this load is called the peak load of the system. The peak load can be found by dividing the total daily demand of the site with the operating hour of the appliances, i.e.

$$Peak\ load(kW) = \frac{electricity\ Demand(kwh)}{hour\ of\ operation} = \frac{55.965kWh/day}{5hour} = 11.193kW$$

3.4.3 Load Factor

Wind energy is often passing on judgment for being unreliable or intermittent supply. Wind turbines generate electricity for 70-85% of the time, but not always at full output. Most wind turbines start generating power at wind speeds of around 3 or 4 m/s (when the output is a few kilowatts), generate maximum (rated) power at around 15 m/s and shut down to prevent storm damage at 25 m/s or above. The proportion of time that wind turbine is generating between these wind speeds depends on the average wind speed at the site. Load factor deals with the day to day productivity of electricity generating plant. Different energy technologies have different load factors, no individual power plants is always available to supply electricity. All power stations are unavailable at certain times, whether for routine maintenance or for unexpected reasons. The load factor of an energy technology is the ratio (expressed as a percentage) of the net amount of electricity generated by a power plant to the net amount which it could have generated if it were operating at its net output capacity. Wind farms can be treated statistically in exactly the same way as conventional power plant. For any type of power plant it is possible to calculate the probability of it not being able to supply the expected load. As wind is variable, the probability that it will not be available at any particular time is higher [27].

Table 3.7: Load Factor of Different Energy Technology [27]

Energy Technology	Load factor
Sewage Gas	90%
Farmyard Waste	90%
Energy Crops	85%
Landfill Gas	70-90%
Combined Cycle Gas Turbine (CCGT)	70-85%
Waste Combustion	60-90%
Nuclear Power	65-85%
Hydropower	30-50%
Wind Energy	25-40%

The load factor of wind varies according to the site and the type of turbine, but it is generally around 30%. It is higher during the winter than the summer [27].

$$\begin{aligned} \text{Peak load}(kw)_{corrected} &= \frac{\text{peak load}}{\text{Load Factor}} && 3.5 \\ &= \frac{11.193}{0.4} = 27.08kW \end{aligned}$$

Therefore, the design load of the system is 27.08kW.

3.5 SYSTEM CONFIGURATION

The site selected for this work is located far from the national electric grid so that the electric source that is going to be designed should be a standalone system. In order to achieve this need there are different alternatives configurations, such as;

- Wind hybrid system with other renewable or nonrenewable source,
- Wind with battery storage system,
- Wind without any storage or backup source by increasing the load factor and by designing the system for the peak load of the site demand.

Wind hybrid with others sources such as PV, diesel and the like needs a series of analysis to determine the possible and optimum combination of each sources for a given demand, in addition to reduce the scope of the work, the thesis chose to work on the last alternative design from the list. But it should note that the selection of system configuration must be done after series of comparative studies are done, this can be taken as the limitation of this work. Wind energy system without any backup source used to reduce the use of any backup system so that the wind generator by itself can supply the demand required at any time. The design load for this type of configuration is the peak load (when all loads are turn ON at the same time the wind generator should supply that much electricity). The major drawback of this system is once it is designed for the peak load it will supply that much load where there is a demand or not, but this can be overcome by using deferrable load at the off peak load time. For this type of configuration the total peak load will be the power requirement when all the appliances are turn ON at the same time that is 11.93kW and by treating with load factor the final peak load will be, 27 kW.

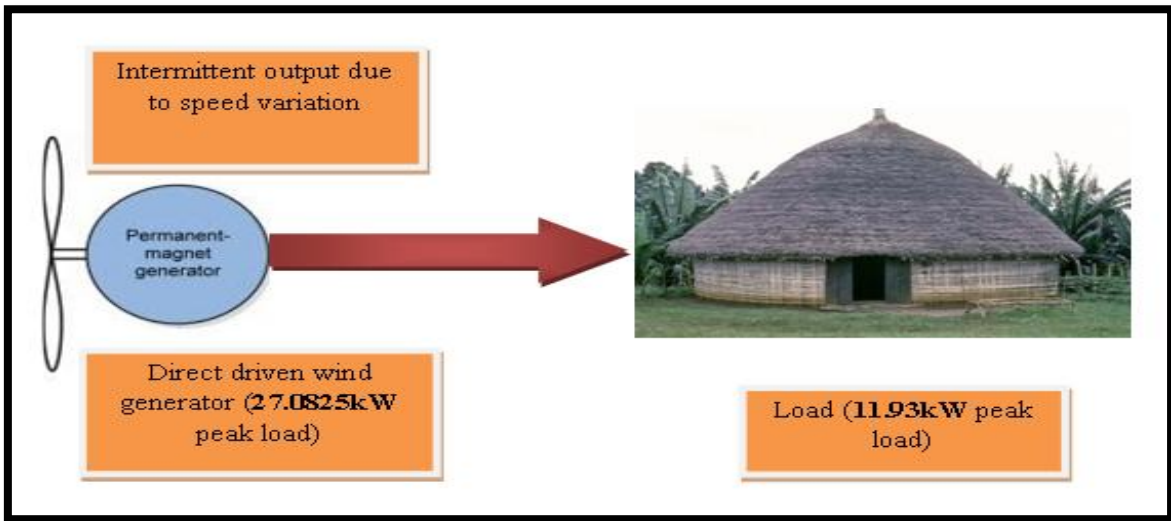


Figure 3.4: System Configuration of Wind Generator without Backup

The wind generator system is direct driven system so that the wind turbine is directly coupled to the generator, no gear box or other speed increasing mechanism included. The electric generator is an axial flux permanent magnet generator which is compatible for low speed applications. For the selected system configuration the design topology and design specification are stated in the next two articles so that the design will be carried out those specifications.

3.6 DESIGN TOPOLOGY

The design of a wind energy conversion system need to determine the basic design topology based on the design constraints. The major design topologies for this thesis are stated below;

3.6.1 Rotor Axis Orientation: Horizontal or Vertical

The most fundamental decision in the design of a wind turbine is probably the orientation of the rotor axis. In most modern wind turbines the rotor axis is horizontal (parallel to the ground), or nearly so. The turbine is then referred to as a ‘horizontal axis wind turbine’ (HAWT). Two of the main advantages of horizontal axis rotors are the following: The rotor solidity of an HAWT (and hence total blade mass relative to swept area) is lower when the rotor axis is horizontal (at a given design tip speed ratio). This tends to keep costs lower on a per kW basis. The average height of the rotor swept area can be higher above the ground. This tends to increase productivity on a per kW basis [5].

3.6.2 Rotor Power Control

There are a number of options for controlling power aerodynamically. The selection of which of these is used will influence the overall design in a variety of ways. Stall control takes advantage of reduced aerodynamic lift at high angles of attack to reduce torque at high wind speeds. For stall to function, the rotor speed must be separately controlled, most commonly by an induction generator connected directly to the electrical grid. Blades of stall controlled machines are fastened rigidly to the rest of the hub, resulting in a simple connection. The nature of stall control, however, is such that maximum power is reached at a relatively high wind speed. The drive train must be designed to accommodate the torques encountered under those conditions, even though such winds may be relatively infrequent. Stall controlled machines invariably incorporate separate braking systems to ensure that the turbine can be shutdown under all eventualities [5]. As stated earlier stall regulated need less effort to apply and the blades are fixed to the hub so that it improve the stability of the system even if it has some drawbacks related to reduce the output above the rated speed. Based on the above discussion active stall controlled wind turbine blade is selected.

3.6.3 Rotor Position: Upwind Of Tower or Downwind of Tower

The rotor in a horizontal axis turbine may be either upwind or downwind of the tower. A downwind rotor in principle allows the turbine to have free yaw, which is simpler to implement than active yaw. Another advantage of the downwind configuration is that it is easier to take advantage of centrifugal forces to reduce the blade root flap bending moments. This is because the blades are normally coned downwind, so centrifugal moments tend to counteract moments due to thrust. On the other hand, the tower produces a wake in the downwind direction, and the blades must pass through that wake every revolution. This wake is a source of periodic loads, which may result in fatigue damage to the blades and may impose a ripple on the electrical power produced. Blade passage through the wake is also a source of noise. The effects of the wake (known as ‘tower shadow’) may, to some extent, be reduced by utilizing a tower design which provides minimal obstruction to the flow [5].

3.6.4 Rotor Speed: Constant or Variable

Most rotors on grid connected wind turbines have operated at a nearly constant rotational speed, determined by the electrical generator and the gearbox. In many turbines today, however, the rotor speed is allowed to vary. Variable speed rotors can be operated at the optimum tip speed ratio to maximize power conversion in low wind and at lower tip speed

ratios in high winds to reduce loads in the drive train. On the other hand, variable-speed rotors may require more complicated and expensive power conversion equipment in the drive train or electrical components of the wind turbine [5]. For this thesis work the load the wind generator are connected directly or it is standalone, so that the rotor speed is variable for this application.

3.7 SELECTING HUB HEIGHT AND DESIGN SPECIFICATIONS

The hub height of a given wind turbine tower is directly related to the power production and the cost as well. Increasing the hub height will reduce the rotor diameter but increase the tower height and the cost as well, and the vice versa is true. Before selecting the hub height let us plot the power production characteristics for different hub height.

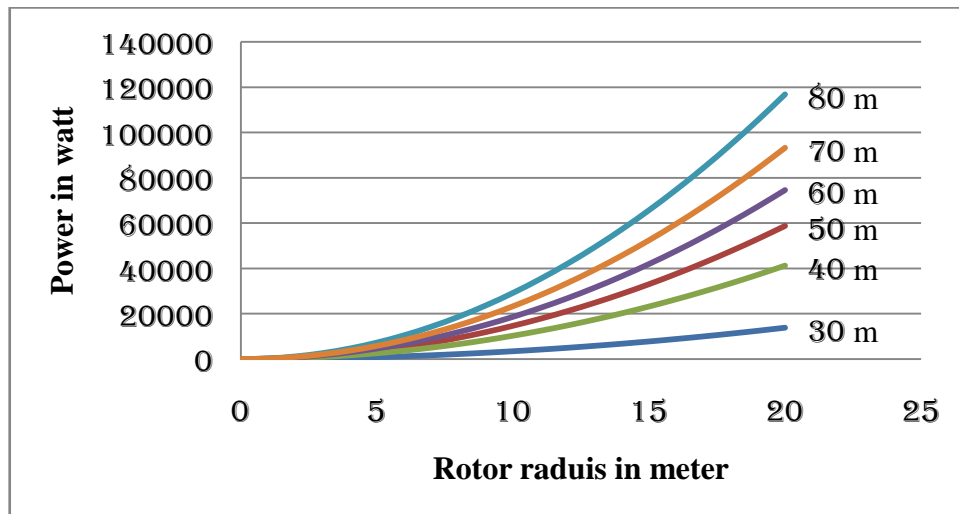


Figure 3.5: Power versus Rotor Diameter for Different Hub Height

From previous calculation we find out that the total peak load of the site is $27.0825kW$ and based on figure 4.2 only it will be achieved for 30 meter hub height at 29, for 40 meter hub height at 17 or above, for 50 meter hub height at 14, for 60 meter hub height at 13, for 70 meter hub height at 11 and for 80 meter hub height at 9 meter or above rotor radius. The most limitations of wind energy application are its cost of manufacturing, cost of transportation and installation. Among these cost of transportation and installation high based on the tower height and size of the rotor. To enhance the application and production of wind turbine application under technology limitation it is necessary to reduce the size and increasing the number of wind turbines to be installed for a given demand. By taking these reasoning in mind this thesis adopt the following specifications (stated at table 3.8).

Table 3.8: Design Specifications

Specifications	Value
Hub height	50 meter
Total number of wind turbines required	6
Peak load for each wind turbines	4.5kW
Mean wind speed at the hub height	6m/s
Total plant output	27kW

In this chapter data collection and analysis was completed, in addition the basic design topologies and the design specification are determined. Based on the results from this chapter the design of components will be followed in the preceding chapters.

CHAPTER FOUR

DESIGN OF MECHANICAL COMPONENTS

4.1 INTRODUCTION

In the preceding chapter the conceptual design and data analysis was done, the wind resource assessment and electrical demand determination was completed which is followed by selection of system configuration and design specifications. In this chapter the detail analysis and design of the mechanical components mainly the **blade, joint, hub, and main shaft** of the wind conversion system will be performed with theoretical discussion of the basic science behind horizontal axis wind turbines components such as aerodynamics, structural design, material selection. The other components of the system such as the bearings, the tower, nacelle cover, the foundation system, and the yawing controller are taken from standard catalogue. In the first section of the chapter, the theoretical and analytical concept of blades design, more specifically BEM theory by taking in to account, tip loss, drag, wake rotation and finite number of blades will be discussed which will be followed by aerodynamics design based on the BEM theory for the specified site conditions and demand requirement and structural design using IEC 6400-2: *design of small wind turbines* publication as a guide line.

In the subsequent sections the design analysis of the bolted joint between the blades and the hub, the fixed hub and the main shaft will be conducted for different load case they are expected to be exposed. The final stage of the design process is to model and check the analytical design completed manually using Solidwoks 2007 and COSMOSworks 2007 packages.

4.2 BLADE DESIGN

The design of the horizontal axis wind turbines is begin with aerodynamic analysis to determine the basic dimensions of the blade such as the radius of the blade, the chord distribution, the twist angle distribution; in addition the aerofoil selection is also complete at the aerodynamic analysis of the blade after the aerodynamic analysis is completed the structural design of the blade will follow. Before the force and stress analysis start material selection must be carried out considering the system requirements such as light weight, strong and low cost. The blades are exposed to different loadings during its transportation to operation, these loading types are called load case and the blades must be checked for this load case and determine whether the factor of safety for each load case is above the safe limit. The blade design will be completed by blade stability analysis which includes vibration,

deflection and buckling. Based on this design flow in the section 4.2 the aerodynamic design of the blade will be discussed. The blade design procedure is based on the flow chart shown at figure 4.1.

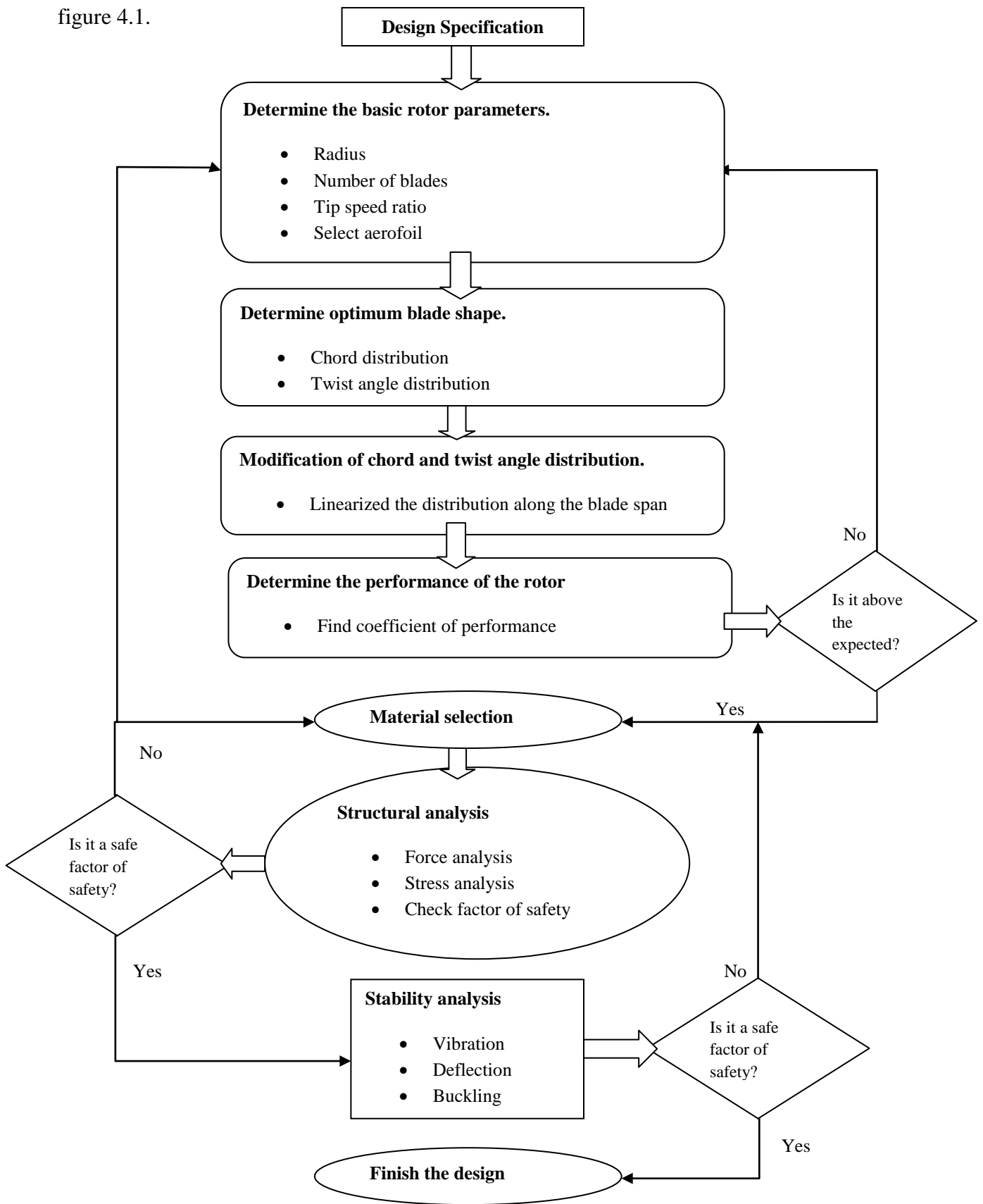


Figure 4.1: Blade Design Flow Chart

4.2.1 BLADE AERODYNAMICS ANALYSIS

There are many design theories for wind turbine blades analysis such as blade element theory, momentum theory, blade element momentum and the like. The analytical design of for this thesis work is based on the generalized rotor design procedure for optimum blade shape of a rotor with wake rotation, as presented at [5]. The effect of tip loss factor is introduced to take account the loss due to the phenomena that is the pressure on the suction side of the blade is lower than on the pressure side, air tends to flow around the tip from the lower to upper surface, reducing the lift and hence power production at the tip. There are many approaches developed to estimate the tip loss factor this thesis uses the one developed by Prandtl and is stated at [5]. During really wind turbine rotor operation the flow behind the rotor rotates in the opposite direction to the rotor, in reaction to the torque exerted by the flow on the rotor. This generation of kinetic energy without wake results in less energy extraction by the rotor than would expected without wake rotation, so that it is straightforward to see slow running wind turbines (with low rotational speed and a high torque) experience more wake rotation losses than high speed wind machines with low torque. The design analysis for this work has made the following assumptions;

- There is wake rotation behind the rotor,
- Tip loss effect should have to be introduced,
- Finite number of blades,
- The drag force coefficient is non-zero.

A. Strip Theory for a Generalized Rotor with Wake Rotation

As stated in the previous paragraphs the blade design analysis is based on BEM theory with wake rotation, tip losses and the like, this approach is selected to achieve a result that is a wind turbines performance that is not far from the actual value that is expected to be. The analysis is starts with the four equations derived from momentum and blade element theories, in addition it is assumed that the chord and twist distributions of the blade are known. The angle of attack is not known, but additional relationships can be used to solve for the angle of attack and performance of the blade.

Momentum theory

From axial momentum: as stated in equation 2.8

$$dT = \rho V_1^2 [4a(1 - a)] \pi dr \quad 4.1$$

From angular momentum: from equation 2.10

$$dQ = 4a'(1-a)\rho V_1 \pi r^3 dr \quad 4.2$$

Blade element theory

From blade element theory:

$$dF_N = B \times \frac{1}{2} \times \rho \times V_{rel}^2 \times (C_L \sin\beta + C_D \cos\beta) c dr \quad 4.3$$

$$dQ = B \times \frac{1}{2} \times \rho \times V_{rel}^2 \times (C_L \sin\beta - C_D \cos\beta) \times c \times r dr \quad 4.4$$

Where the thrust, dT is the same force as the normal force, dF_N therefore after series of algebraic manipulation the differential forces defined as follow;

$$dF_N = \sigma' \pi \rho \frac{V_1^2 (1-a)^2}{\cos^2(\beta)} (C_L \sin\beta + C_D \cos\beta) r dr \quad 4.5$$

$$dQ = \sigma' \pi \rho \frac{V_1^2 (1-a)^2}{\cos^2(\beta)} (C_L \cos\beta - C_D \sin\beta) r^2 dr \quad 4.6$$

Where: σ' is the local solidity and defined as;

$$\sigma' = \frac{Bc}{2\pi r} \quad 4.7$$

Blade element momentum theory

In the calculation of induction factor, a and a' , an accepted practice is to set the drag coefficient to zero, this simplification introduce negligible error. So when the torque equation from momentum and blade element theory are combined will give us,

$$\frac{a}{1-a} = \frac{\sigma' (C_L \sin\beta + C_D \cos\beta)}{4Q \cos^2(\beta)} \quad 4.8$$

$$\frac{a'}{1-a} = \frac{\sigma' (C_L \cos\beta - C_D \sin\beta)}{4Q \lambda_r \cos^2(\beta)} \quad 4.9$$

From blade element theory based on the geometrical consideration we have,

$$\tan\varphi = \frac{V(1-a)}{\Omega r (1+a')} = \frac{V(1-a)}{\lambda_r (1+a')} \quad 4.10$$

And equations 2.14 and 2.15 the following results are developed,

$$C_l = 4 \times \sin\varphi \frac{(\cos\varphi - \lambda_r \sin\varphi)}{\sigma' (\sin\varphi + \lambda_r \cos\varphi)} \quad 4.11$$

$$\frac{a'}{(1+a')} = \frac{\sigma' \times C_l}{4 \cos\varphi} \quad 4.12$$

$$a/a' = \lambda_r / \tan\varphi \quad 4.13$$

$$a = 1 / \left[1 + 4 \times \sin^2\varphi / (\sigma' \times C_l \times \cos\varphi) \right] \quad 4.14$$

$$a' = 1 / \left[\left(4 \times \cos\varphi / (\sigma' \times C_l) \right) - 1 \right] \quad 4.15$$

There are two basic methods to find the solutions for the above equations to determine the flow conditions and forces at each blade sections.

Method 1: solving for C_l and a since $\theta = \alpha + \theta_p$, for a given blade geometry and operating conditions, there are two unknowns in equation 4.11, i.e. C_l and φ at each section. To find these values, one can use the empirical C_l Vs a curves for the chosen airfoil, then find C_l and a from the empirical data to satisfy equation 4.11. This can be done either numerically or graphically [5].

Method 2: iterative solution for 'a' and 'a'', this method starts with guesses for a and a', from which flow condition and new induction factors are calculated.

1. Guess values of a and a',
2. Calculate the angle of the relative wind from equation 4.10,
3. Calculate the angle of attack from $\theta = \alpha + \theta_p$ and then C_l and C_d
4. Update a and a' from equation 4.14 and 4.15.

This process will continue until the induction factors calculated is within the accepted tolerance of the previous one, specifically less than 1% difference.

Calculation of power coefficient

Once 'a' has been obtained from each section, the overall rotor power coefficient may be calculated from the following equation as stated in [5], originally (Wilson and Lissaman, 1974):

$$C_P = \left(8/\lambda^2 \right) \int_{\lambda_h}^{\lambda} \lambda_r^3 \times a' (1 - a) \left[1 - \left(C_d/C_l \right) \times \cot\varphi \right] d\lambda_r \quad 4.16$$

Where: λ_h is the local speed ratio at the hub, or equivalently (de Vries, 1979):

$$C_P = \left(8/\lambda^2 \right) \int_{\lambda_h}^{\lambda} \sin^2\varphi (\cos\varphi - \lambda_r \sin\varphi) (\sin\varphi + \lambda_r \cos\varphi) \left[1 - \left(C_d/C_l \right) \times \cot\varphi \right] \lambda^2 d\lambda_r \quad 4.17$$

B. Tip Loss: Effect on Power Coefficient of Number of Blades

During operation of wind turbines blades, the pressure on the side of a blade is slower than that on the pressure side, air tends to flow around the tip from the lower to upper surface, reducing lift and hence power production near the tip. There are a number of methods have been suggested for including the effect of the tip loss. Among those methods the one which is developed by L. Prandtl is the most recommended model for the following reasons;

- Prandtl model prediction are in qualitative agreement with the behavior of HAWT rotors,
- Calculations of rotor power and thrust made with Prandtl model are in good agreement with test data,
- BEM theory calculations made with Prandtl model show good agreement with calculations made with vortex theory,
- The Prandtl model is easier to program and use.

According to this method, a correction factor, F, must be introduced in to the previously discussed equations. This correction factor is a function of the number of blades, the angle of relative wind, and the position on the blades,

$$F = (2/\pi) \cos^{-1} \left[\exp \left(- \left\{ \frac{(B/2)[1 - (r/R)]}{(r/R) \sin \varphi} \right\} \right) \right] \quad 4.18$$

Where the angle resulting from the inverse cosine function assumed to be in radians and F is always between 0 and 1.

Since the tip loss affects the forces derived from momentum theory (the forces derived from blade element theory remain unchanged) they should have to be corrected wit tip loss factor as shown below;

$$dT = F \rho V_1^2 [4a(1 - a)] \pi dr \quad 4.19$$

$$dQ = 4F a' (1 - a) \rho V_1 \pi r^3 dr \quad 4.20$$

By equating these equations with those equations from blade element theory we found the following relations;

$$\frac{a'}{(1 - a)} = \frac{\sigma' \times C_l}{4F \lambda_r \sin \varphi} \quad 4.21$$

$$\frac{a}{(1 - a)} = \frac{\sigma' \times C_l \times \cos \varphi}{4F \sin^2 \varphi} \quad 4.22$$

$$C_l = 4 \times F \times \sin\varphi \frac{(\cos\varphi - \lambda_r \sin\varphi)}{\sigma'(\sin\varphi + \lambda_r \cos\varphi)} \quad 4.23$$

$$\frac{a'}{(1+a')} = \frac{\sigma' \times C_l}{4F \cos\varphi} \quad 4.24$$

$$a = 1 / \left[1 + \frac{4 \times F \sin^2\varphi}{(\sigma' \times C_l \times \cos\varphi)} \right] \quad 4.25$$

$$a' = 1 / \left[\left(\frac{4 \times F \cos\varphi}{(\sigma' \times C_l)} \right) - 1 \right] \quad 4.26$$

$$V_{rel} = \frac{V(1-a)}{\sin\varphi} = \frac{V}{\left(\frac{\sigma' \times C_l}{4F} \right) \cot\varphi + \sin\varphi} \quad 4.27$$

Therefore the power coefficient can be calculated as equation 4.28 or equation 4.29.

$$C_P = \left(\frac{8}{\lambda^2} \right) \int_{\lambda_h}^{\lambda} F \lambda_r^3 \times a' (1-a) \left[1 - \left(\frac{C_d}{C_l} \right) \times \cot\varphi \right] d\lambda_r \quad 4.28$$

$$C_P = \left(\frac{8}{\lambda^2} \right) \int_{\lambda_h}^{\lambda} F \sin^2\varphi (\cos\varphi - \lambda_r \sin\varphi) (\sin\varphi + \lambda_r \cos\varphi) \left[1 - \left(\frac{C_d}{C_l} \right) \cot\varphi \right] \lambda^2 d\lambda_r \quad 4.29$$

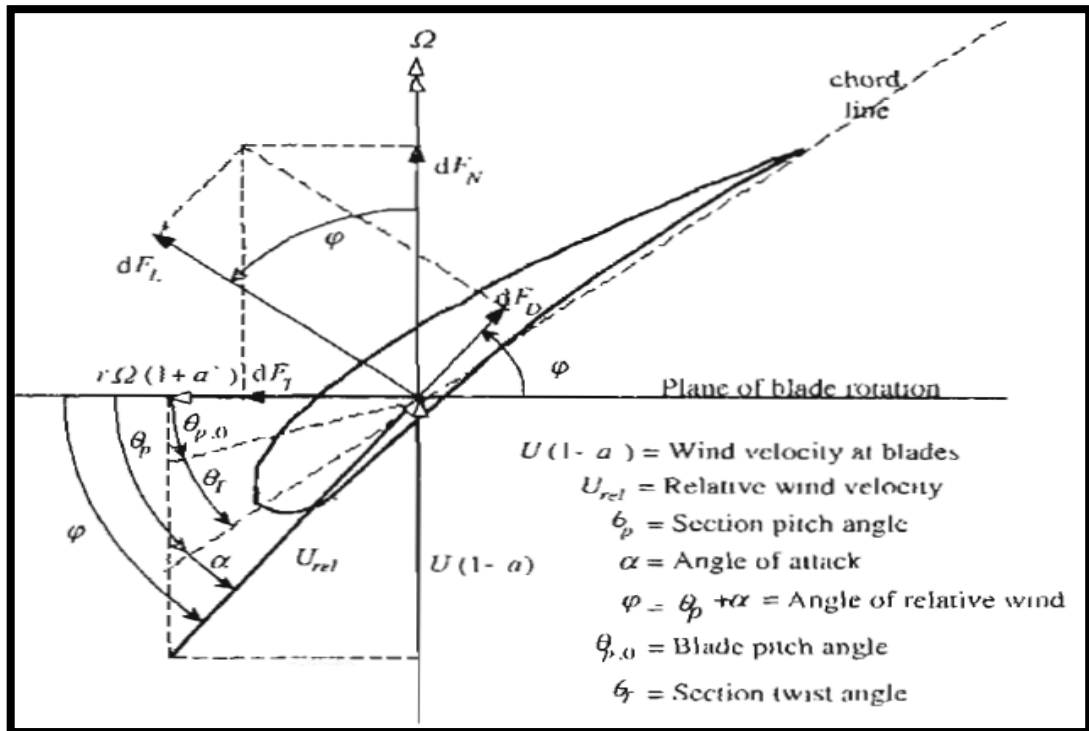


Figure 4.2: Blade Element Theory, Geometry of the Airfoil [5]

C. HAWT Flow States

The real wind turbines performance closely approximates the results of BEM theory at low axial induction factor and the general momentum theory is no longer valid at the axial induction factor greater than 0.5, because above this value the far wake wind velocity would be negative. In practice the induction factor can be greater than 0.5 but the flow pattern through wind turbine will become more complex than that can be predicted by using the momentum theory. A number of operating states for a rotor have been identified. The operating states relevant to wind turbines are design the windmill state and the turbulent wake state. The windmill state is a normal wind turbines operating state. The turbulent wake state occurs under operation in high winds. The windmill state is characterized by the flow conditions described by momentum theory for axial induction factors less than about 0.5. Above $a = 0.5$, in the turbulent wake state, measured data indicate that thrust coefficients increase up to about 2.0 at an axial induction factor of 1.0. This state is characterized by a large expansion of the slipstream, turbulence and recirculation behind the rotor. While momentum theory no longer describes the turbine behavior, empirical relationships between C_T and the axial induction factor are often used to predict wind turbine behavior.

In turbulent wake states, an empirical relation developed by Glauert, is used to relate the axial induction factor to the thrust coefficient including the tip loss factor as shown below.

$$a = \left(\frac{1}{F}\right) \left[0.143 + \sqrt{0.0203 - 0.6427(0.889 - C_T)}\right] \quad 4.30$$

It is valid for $a > 0.4$ or equivalently for $C_T > 0.96$.

The Glauert empirical relationship was determined for the overall thrust coefficient for a rotor. It is customary to assume that it applies equally to equivalent local thrust coefficients for each blade section. (Wilson et al., 1976) defined local thrust coefficient for each annular rotor section as shown below;

$$C_{T_r} = \frac{dF_N}{\frac{1}{2}\rho U^2 2\pi r dr} \quad 4.31$$

And using normal force relation from blade element theory, the local thrust coefficient will be,

$$C_{T_r} = \sigma'(1-a)^2 \left((C_L \cos\varphi + C_D \sin\varphi) / \sin^2\varphi \right) \quad 4.32$$

The solution procedure can then be modified to include heavily loaded turbines blade design and power prediction of HAWTs which are operating at high tip speed ratios.

D. Blade Shape for Optimum Rotor with Wake Rotation

Designing a blade shape from a known airfoil type for an optimum rotor means determining the blade shape parameters; chord length distribution and twist distribution along the blade length for a certain tip speed ratio at which the power coefficient of the rotor maximum. To find a general relationship can be found between an optimum relative wind angle and local tip speed ratio which will be applicable for any airfoil type by taking the partial derivate of the integral relation for definition of C_p taking $C_d = 0$ and $F = 1$;

$$\frac{\partial[\sin^2\varphi(\cos\varphi - \lambda_r \sin\varphi)(\sin\varphi + \lambda_r \cos\varphi)]}{\partial\varphi} = 0$$

Then we found,

$$\lambda_r = \frac{\sin\varphi(2\cos\varphi - 1)}{[(1 - \cos\varphi)(2\cos\varphi + 1)]} \quad 4.33$$

Some more algebra reveals that:

$$\varphi = (2/3)\tan^{-1}(1/\lambda_r) \quad 4.34$$

$$c = \frac{8\pi r}{BC_L}(1 - \cos\varphi) \quad 4.35$$

Induction factor can be defined as;

$$a' = \frac{1 - 3a}{4a - 1} \quad 4.36$$

$$a = \frac{1}{[1 + 4 \times \sin^2\varphi / (\sigma' \times C_l \times \cos\varphi)]} \quad 4.37$$

The blade solidity can be found from the ratio the area of the blades to swept area,

$$\sigma = \frac{1}{\pi R^2} \int_{r_h}^R c dr \quad 4.38$$

And when the blade is modeled as a set of N blade sections of equal span, the solidity can be calculated from:

$$\sigma \cong \frac{B}{N\pi} \left(\sum_{i=1}^N c_i / R \right) \quad 4.39$$

Note that; B: number of blades, c: airfoil chord length, r: blade section radius, R: rotor radius, tip speed ratio, and φ : angle of relative wind.

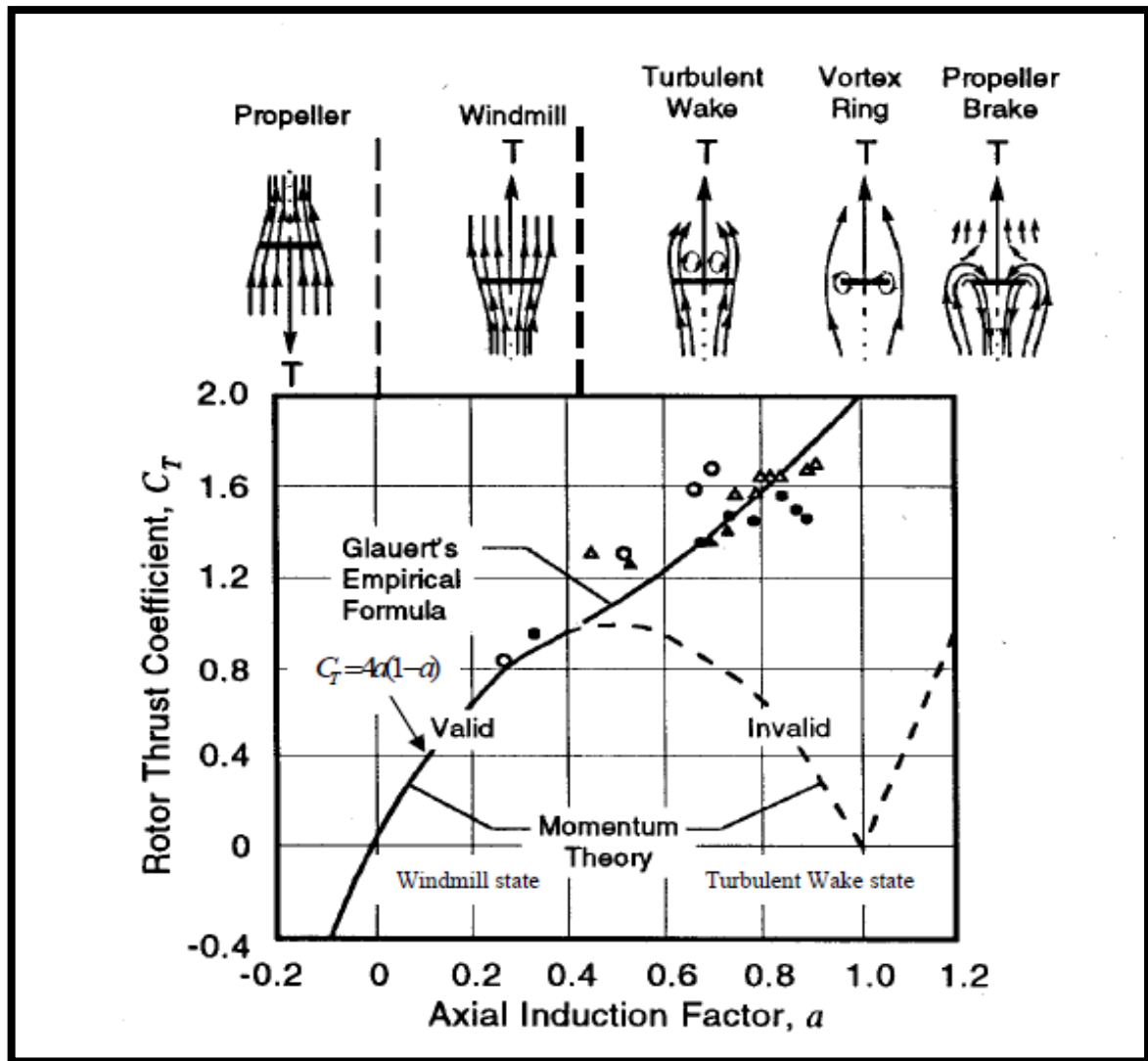


Figure 4.3: Wind Turbine Flow States, the Axial Induction Factor and Thrust of Rotor [29]

E. Airfoil for Wind Turbines

HAWT blades use flat plates and less sophisticated profiles for low tip speed ratios and for high tip speed ratios an airfoil will be used to develop mechanical power. The width and the length of the blade are functions of the desired aerodynamic performance, the maximum desired rotor power, the assumed airfoil parameters and strength calculations. Hence designing HAWT blades depends on the knowledge of the properties of airfoils.

The most significant factor that influences the behavior of airfoils is that of the viscosity of the fluid and airfoil combination which is characterized by the Reynolds number (Re) and defined

as below; it should be noted that there are significant differences in the airfoil behavior at different Reynolds numbers, so that it is necessary make sure the correct Reynolds number data is used for the design.

$$Re = \frac{V_{rel} \times c}{\nu} \quad 4.40$$

The drag and lift characteristics of airfoil show also significant aspect ratio dependence at angles of attack larger than 30 deg. But fully attached region in which HAWT is operating under windmill state are not greatly affected by aspect ratio, so that two dimensional (i.e. infinite aspect ratio) data can be used in blade design at low angles of attack. However, when two dimensional data are used, tip loss factor must be added.

According to [5], in the 1970s and early 1980s, wind turbine designers felt that minor differences in airfoil performance characteristics were far less important than optimizing blade twist and taper. For this reason, little attention was paid to the task of airfoil selection. Thus, airfoils that were in use by the helicopter industry were chosen because the helicopter was viewed as a similar application. Aviation airfoil such as the NACA 44xx and NACA 230xx were popular airfoil choices because they had high maximum lift coefficients, low pitching moment and low minimum drag coefficient.

F. Modification of Blade Geometry

In general, a rotor is not of the optimum shape because of fabrication difficulties, furthermore, when an ‘optimum’ blade is run at different tip speed ratio than the one for which it is designed, it is no longer ‘optimum’. Thus, blade shapes must be designed for easy of fabrication and for overall performance over the range of the wind and rotor speeds that they will encounter. That is, one can assume a blade shape and predict its performance, try another shape and repeat the prediction until a suitable blade has been chosen. Thus, blade shape is generally modified for the purpose of decreasing the thrust force and torque acting on the blade during its operation by trying to keep the design power coefficient close to the one which is obtained for the designed blade and for easy of manufacturing.

Modification of chord length distribution

The chord variation across the span of the blade of a designed blade shape is not linear and near the root the blade chord increasing steeply. This type of variation is not an easy to manufacture so that it is not an optimum shape. To achieve good result this variation should have to be modified to make the variation linear. But while transforming the designed blade shape to a linear taper shape the area of the chord to length of each blade element for both

shapes should remain the same. At least the one of linear taper shapes whose blade elements' chord lengths are the closest to the designed blade elements' chord lengths should be selected. Also it should be kept in mind that most power is generated by the outer part of the blade (between $r / R = 0.5$ and $r / R = 0.9$) [24]. For this reason a blade is linearized through these points of the ideal blade shape seems to be a good choice. Generally, an iterative approach is used. That is, a blade shape can be assumed and predicted its performance and another blade shape is assumed and the prediction of performance is repeated until a suitable blade shape has been chosen.

Modification of twist distribution

When the twist distribution of a designed blade shape is analyzed, we can see a designed blade has to be twisted strongly, especially near the root again as it occurs in the chord-length variation of the same blade. For that reason twist distribution can also be modified considering the ease of fabrication. So that the twist variation should have to be linearized across the blade length as we done to the chord variation.

G. Determination of Basic Rotor Parameters

At this step the basic parameters will be determined. The design inputs are, the power requirement that is as calculated in chapter three is 4.5kW for each wind turbine, the wind speed at the hub height is 6m/s, the air density is adapted to be 1.2kg/m³, the total electrical and mechanical efficiency is expected to be 90%. So that based on one dimensional momentum theory we have the following relation to find the rotor radius,

$$P = \frac{1}{2} \times C_p \times \eta \times \rho \times \pi \times R^2 \times V^3 \quad 4.41$$

Where: P is power required, i.e. 4.5kW, C_p is expected coefficient of performance, 0.4 for modern three bladed wind turbines, R is tip radius, U is mean wind speed at the hub height, 6m/s, η is expected mechanical and electrical efficiency (0.9 would be a suitable value), ρ is density of air at the site, taken as 1.22kg/m³. Therefore, the rotor radius calculated to be,

$$R = \sqrt{\frac{2P}{C_p \times \eta \times \rho \times \pi \times V^3}} = \sqrt{\frac{2 \times 4.5}{0.4 \times 0.9 \times 1.22 \times \pi \times 6^3}} = 5.5 \text{ meter.}$$

Tip Speed Ratio

The choice of tip speed ratio is depend on the application area that the wind turbine going to be incorporated. It is suggested by many literatures that, for water pumping windmill higher torque are required, therefore tip speed ratio between 1 and 3 is suitable, and for electric power generation it is recommended to use a tip speed ratio between 4 and 10. The higher

speed machines use less material in the blades but require more sophisticated airfoil. The system planned to be used for this thesis work is a direct drive configuration with the generator so that the tip speed ratio should be large as possible because the power output of the generator is directly related to the rotational speed of the rotor shaft. In addition the tip speed ratio has a great effect of the coefficient of performance of the turbines, a typical C_p - λ at figure 4.3 show us the relation between each other.

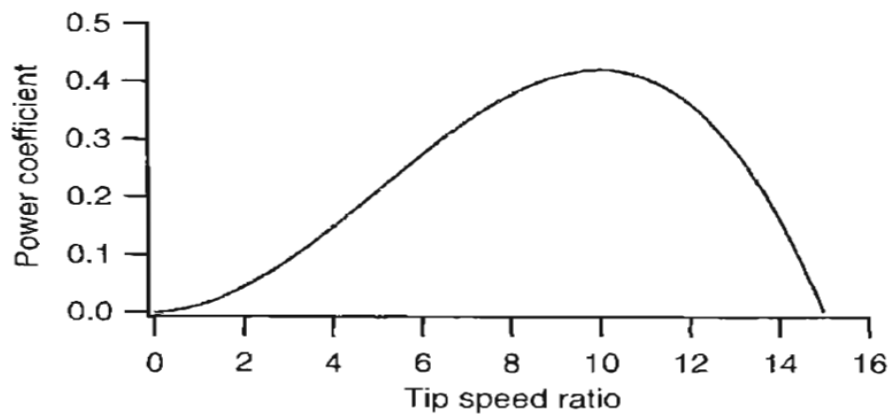


Figure 4.4: Sample C_p - λ Curve for High Tip Speed Ratio Wind Turbines [5]

As stated in the previous sections of this chapter the design of wind turbines is an iterative process to achieve maximum rotor performance. So that for this thesis work from 6 to 10 tip speed ratio will be take in to consideration, the best will be selected at the end of design process that will be give us maximum performance.

Numbers of Blades

The number of blades has also a great impact on the performance of a rotor. In addition number of blades on the rotor must be considering the structural stability of the total system. Single bladed wind HAWT will have higher cyclic stress because when it is at the lower position it will have lower thrust force and at the upper position a higher one due to the difference in wind speed at those positions. Furthermore, due to the lack of balance it will lead to instability of the other components such as hub, shaft, drive train and the tower, but single bladed wind turbine has lower cost. Multibladed wind turbines have good stability and solidity, high performance, but need high material and starting torque then this will reduce the feasibility of the system. With present manufacturing techniques it is generally advantageous to have as few blades as possible; this is primarily because of the fixed costs in fabricating the blades. In addition, when there are more blades (for a given solidity) they will be less stiff and may have higher stresses at the roots, at the present time all commercial wind turbines have either two or three blades. Reference [5] suggest table 4.1 for selecting number of blades.

Table 4.1: Suggested Blade Number, B, for Different Tip Speed Ratio, λ [5]

λ	B
1	8-24
2	6-12
3	3-6
4	3-4
>4	1-3

Based on the table the blade number for this specific design condition is between 1-3, and considering structural stability and to increase solidity, the number of blades is taken to be three.

Selecting an Airfoil

The design procedure this thesis aimed to follow is based on a known airfoil profile and to achieve good performance by generating an optimum blade shape. There are many different types of standard airfoil such as, NACA, RIS ϕ , FFA, SG, S, DAE, Lissaman and the like. The major selection criteria for the airfoil is, lower drag coefficient and fairly large lift coefficient. In modern large scale wind turbines it is a usual practice to use different airfoil at the different section of the blade to improve the performance as well as strength at the root. But using different airfoil will result high cost of manufacturing and complicated technology, for this application the wind turbines to be design is a small scale wind turbine and it is fair decision to use single airfoil with different thickness and chord, this will improve the manufacturability of the system. In other side as per reference [5], it is a better way to focus on the shape of the blade rather than the airfoil to achieve good performance. Among the different airfoil profiles, NACA 230xx, NACA 44xx, NACA 63 2xx, SERI 804-808, DAE 21 and 11, and Lissaman 7769 are compared. The profile data for the selected airfoil is attached at annex B.

By now the major ingredient for the design are selected, the remaining task is to find the optimum blade shape using an iterative methods stated before. The design is based on the optimum blade shape prediction procedure suggested by [5].

First the blade need to be divided in to N numbers of sections along the span, the more the number of the section and more the accurate result will obtained, the length of the blade is only 5.5meter so that dividing the blade in to 10 elements will be a suitable choice. All values to be calculated for each section are based on the radius at the center of each section. The local speed ratio for each section can be calculated as;

$$\lambda_i = \lambda \times \left(\frac{r_i}{R} \right) \quad 4.42$$

And the optimum relative wind angle is given by,

$$\varphi = (2/3)\tan^{-1}\left(1/\lambda_r\right) \quad 4.43$$

The chord at each section is given by;

$$c = \frac{8\pi r}{BC_L}(1 - \cos\varphi) \quad 4.44$$

The twist angle for each section is;

$$\theta_{T_i} = \theta_{p_i} - \theta_{p_o} \quad 4.45$$

But the pitch angle for each section can be found from the following relation.

$$\varphi_i = \theta_{p_i} + \alpha_{design_i} \quad 4.46$$

The design angle of attack is should have to be a value which is corresponding to the minimum drag to lift coefficient ratio. Most literatures recommend the design angle of attack to be the corresponding value of the 80% of the maximum lift coefficient. The design process includes much repetitive iteration for different airfoils and for different tip speed ratio. To determine the best alternative airfoil a preliminary analysis using Microsoft Excel 2007 is made based on the result NACA 4412 is adopted for this design. For different tip speed ratio, starting from 6 to 10 the iteration process was made, the result is available at annex c by comparing the final coefficient of performance 10 tip speed ratios is the satisfactory. In addition the design configuration of this system is direct driven so that the 10 tip speed ratio is a good ratio; because of the power output of the generator is directly affected by the rotation speed of the rotor. The results at this tip speed ratio are tabulated below at table 4.2.

Table 4.2: Results of Analysis Based on Spread Sheet Iteration

Section n	Radius (m)	Local speed ratio	phi	Section pitch	Section twist	r/R	Chord(M)
1	0.25	0.5	42.311415	34.31141	38.50242	0.05	0.3891372
2	0.825	1.5	22.471437	14.47143	18.66244	0.15	0.3742844
3	1.375	2.5	14.541644	6.541644	10.73265	0.25	0.2631808
4	1.925	3.5	10.635655	2.635655	6.826662	0.35	0.1975912
5	2.475	4.5	8.3567750	0.356775	4.547781	0.45	0.1570138
6	3.025	5.5	6.8733821	-1.126617	3.064389	0.55	0.1298974
7	3.575	6.5	5.8337322	-2.166267	2.024739	0.65	0.1106238
8	4.125	7.5	5.0656636	-2.934336	1.256670	0.75	0.0962650
9	4.675	8.5	4.4754934	-3.52450	0.666500	0.85	0.0851721
10	5.225	9.5	4.0080358	-3.99196	0.199042	0.95	0.0763532
tip	5.5	10	3.8089930	-4.19100	0	1	0.0725901

From the result we can see that the twist and the chord distributions along the blade length are not linear and it is recommended to have linear relation so that the fabrication process will be easy with optimum performance as well. To find a linear relation a curve fitting technique of the least square method is used.

Modification of the Chord Distribution

The designed chord distribution is looks like as shown below;

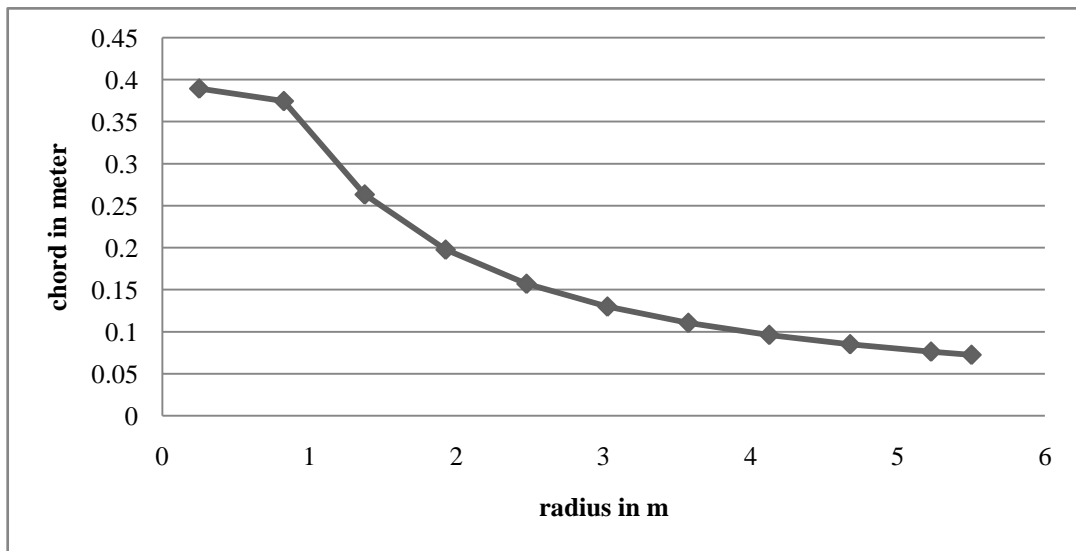


Figure 4.5: Designed Chord Distribution of the Blade

From figure 4.4, for the first sections, i.e. section1 and 2, the variation is very small but at the middle of the span the variation of the chord is steeply and it will goes similar to the first two sections at the end of the span.

So the following approximation is taken,

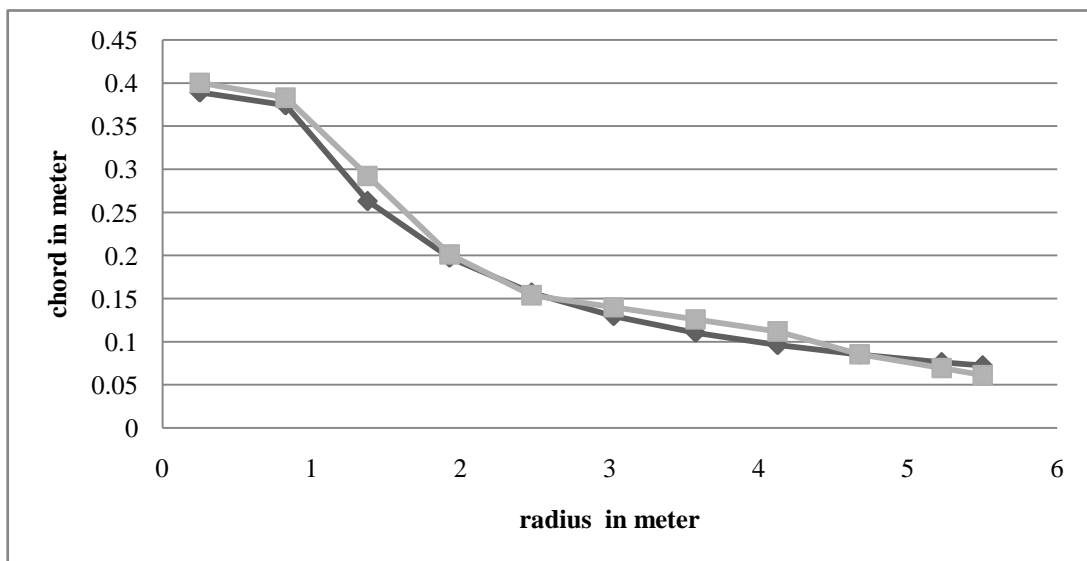


Figure 4.6: Linearized Chord and Designed Chord Distribution of the Blade

Series 1: the designed chord distribution, **Series 2:** the chord distribution linearized, for the first section the chord is taken to be .40m, for the next sections (i.e. 2, 3 and 4 $c = -0.165 \times r + 0.519$), for middle sections (i.e. 5 $c = -0.014 \times r + 0.217$), and for the tip sections (i.e. sections 9 and 10, $c = -0.029 \times r + 0.221$) are used to linearized the chord distributions.

The chord distribution along the span of the blade was linearized to have easy of manufacturing as shown at figure 4.5. Series1 represent the design chord distribution and series2 represent the linearized chord distribution.

Modification of the twist angle

The designed twist distribution across the blade is show below, from the figure, after 2 meter the variation is very slow rather at the root section it is very steeply, as far as it is said the most of the energy is extracted by the tips section of the blade it is necessary to make good approximation at this areas. To do so to linear approximation equations are used for the two sections as shown. The variation is approximated by two linear equations for the first three sections, $\theta_{T_i} = -24.683 \times r + 44.69425 \text{ degree}$, and for the remaining sections, $\theta_{T_i} = -1.91 \times r + 10.508 \text{ degree}$.

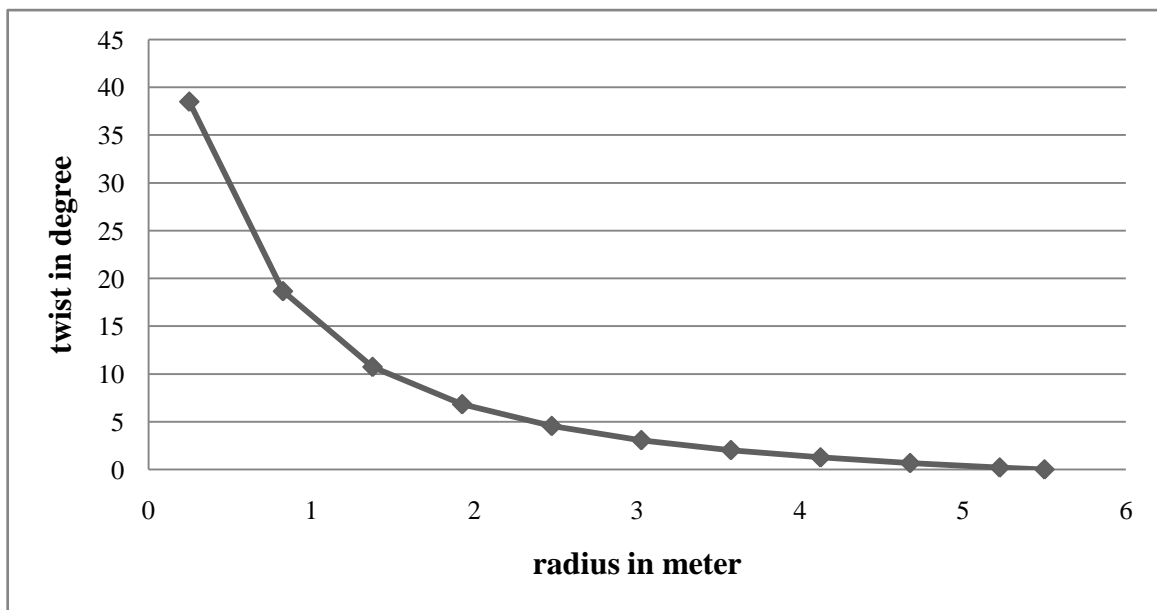


Figure 4.7: Designed Twist Angle Distribution along the Blade Span

From the figure 4.6, the twist angle distribution at section one and two change very fast but at the rest of the section is almost linearized. The twist angle distribution is linearized as shown in figure 4.7.

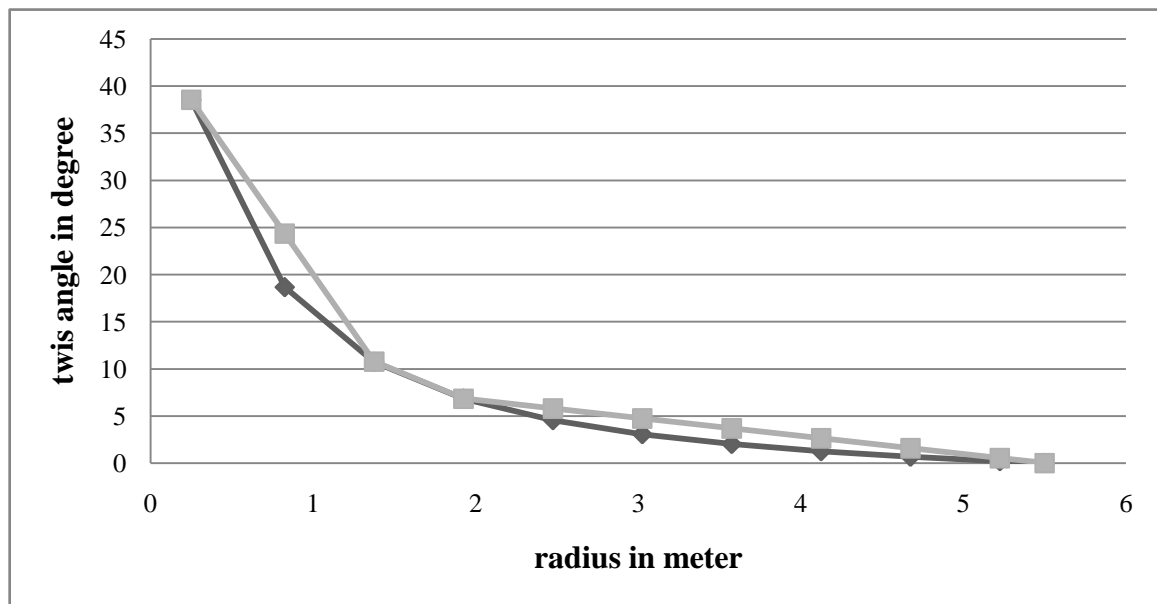


Figure 4.8: Linearized Twist Angle and Designed Chord Distribution of the Blade

Series 1: the designed twist angle, **Series 2:** the linearized variation of the twist angle, the modified results of the chord and the twist angle are tabulated below,

Table 4.3: Comparison of the Designed and Linearized Chord Distribution of the Blade

Section	Designed value		Modified value		Blade solidity	difference	
	Chord in meter	Twist in degree	Chord in meter	Twist in degree		chord	twist
1	0.389	38.502	0.4	38.523	0.764	0.010	0.021
2	0.374	18.662	0.382	24.330	0.225	0.008	5.668
3	0.263	10.732	0.292	10.755	0.096	0.028	0.022
4	0.198	6.826	0.201	6.831	0.051	0.003	0.004
5	0.157	4.547	0.154	5.780	0.030	0.003	1.232
6	0.129	3.064	0.14	4.730	0.020	0.010	1.66
7	0.110	2.024	0.126	3.679	0.016	0.015	1.655
8	0.096	1.256	0.112	2.629	0.013	0.015	1.372
9	0.085	0.666	0.085	1.578	0.008	0.001	0.912
10	0.076	0.199	0.069	0.528	0.006	0.006	0.329
tip	0.072	0	0.062	0	0.005	0.011	0

H. Determination of the Performance the Rotor

The determination of the performance of the rotor is an iterative procedure to achieve an optimum blade shape. There two approaches to solve the equation for the blade performance as stated in the previous sections that are method one and two. For this thesis work will be

taken as the first chose but between the iteration processes if the axial induction factor is above the 0.5 method two will be used.

This method is solving the actual C_L and the angle of attack for the center of each section, using the equations 4.23, 4.18, and 4.47.

$$\sigma' = B \times c_i / 2\pi r_i \quad 4.47$$

The procedure is , based on the optimum relative wind angle find the blade solidity the tip loss factor then find the lift coefficient and then find the actual angle of attack from the airfoil profile curve for the C_L and α , and then find the modified relative wind angle by using the following relation.

$$\varphi_{i_{j+1}} = \theta_{p1} + \alpha_{i_j} \quad 4.48$$

Where, 'i' the section number and 'j' the number of iteration,

Finally find the axial and angular induction factor till the difference between the successive iteration values. Use the following relation to find axial and angular induction factors.

$$a = 1 / [1 + 4 \times F \sin^2 \varphi / (\sigma' \times C_l \times \cos \varphi)] \quad 4.49$$

$$a' = 1 / \left[\left(4 \times F \cos \varphi / (\sigma' \times C_l) \right) - 1 \right] \quad 4.50$$

When the iteration is completed calculate the coefficient of performance of the blade using the following relation,

$$C_P = \left(8 / N \lambda^2 \right) \sum_{i=1}^N \left[F \sin^2 \varphi (\cos \varphi - \lambda_{r_i} \sin \varphi) (\sin \varphi + \lambda_{r_i} \cos \varphi) \left[1 - \left(C_d / C_l \right) \cot \varphi \right] \lambda_{r_i}^2 \right]$$

N is the number of sections.

Then, if the calculated performance is below the expected one repeat the design by changing the parameters at the early stage of the design such as the chord distribution even the tip speed ratio and others. For this design thesis from 6 to 10 tip speed ratio using different airfoil was analyzed and the 10 tip speed ratio is already selected. Seven iteration was made the results are attached at annex d. And the final result for each section will be,

Table 4.4: Final Result of the Aerodynamic Design Analysis of the Blade

Section	Section Cp	Total Cp	Airfoil
1	0.042	0.424	NACA 4412
2	0.164		NACA 4412
3	0.292		NACA 4412
4	0.383		NACA 4412
5	0.522		NACA 4412
6	0.563		NACA 4412
7	0.558		NACA 4412
8	0.561		NACA 4412
9	0.564		NACA 4412
10	0.587		NACA 4412

Based on the previous design analysis the total power coefficient for the blade design after optimization of the shape is 0.424, which is more than the expected value i.e. 0.4, so that the design optimization is satisfactory. The optimization process is based on a spread sheet iteration using Microsoft Excel 2007. In the preceding section the aerodynamic design of the wind turbine blades was done, in the next section the structural and stability analysis of the blade will continue using the results from the aerodynamic analysis.

4.2.2 BLADE STRUCTURAL ANALYSIS

Imposed loads and dynamics interactions produce forces and motions in wind turbines which need to be understood during the design process. The effects of all the various types of loads, (static, steady, cyclic, transient, impulsive and stochastic) need to be determined.

There are many approaches available for analyzing the forces and motions of wind turbines two of them are, simple ideal rigid rotor model which focuses on steady turbine loads, and linearized hinged spring blade rotor model which used to illustrate the nature of the turbine response to steady and cyclic loads. In addition to the above simple models there are many detailed dynamic models which are more accurately predict turbines response to stochastic or transient loads, but tends to be quit complex [5].

The accuracy of the analysis is highly based on the model selected; hence the selection should consider the design conditions as well the effort available. As it is stated in the previous aerodynamics analysis it was assumed that the drag, the wake, the tip loss and the finite number of blades, so that it is more suitable to use more accurate model to simulate the response of each forces on the blade structure. The linearized hinge spring blade rotor model as stated at [5] used to analysis the loads on the rotor. The rotor topology which was designed under this thesis was a stall controlled, constant pitch, upwind, and the hub type is a fixed

type hub, so the use of this linearized hinge spring blade rotor model is proper angle of attack towards the solutions.

In addition to the type of approach to be used, design integrity and interchangeability should have to be considered. This is for the purpose of design standardization. According to the International Electrotechnical Commission (IEC), the designer should be aware of these standards, since a turbine's ability to meet these conditions must be demonstrated if it is intended for use in any country which enforces those standards. Hence, the design and load determination for this thesis work is based on IEC 6400-2 publication [32].

The International Electromechanical Commission (IEC) begins work on the first publication standards in 1988. IEC 6400-1 and IEC 6400-2 identifies four different class of wind turbines to suit differing site wind conditions with increasing class designation number corresponding to reduce wind speed. The wind speed parameters for each class are given at table 4.5.

Based on the table the wind class that this design will aimed to satisfy is class IV with annual average wind speed of 6m/s at the hub.

Table 4.5: Wind Class and Their Parameters [32]

Parameters	Class I	Class II	Class III	Class IV
Reference wind speed	50	42.5	37.5	30
Annual average wind speed	10	8.5	7.5	6
50 year return gust speed	70	59.5	52.5	42
1 year return gust speed	52.5	44.6	39.4	31.5

The publication by International Electrotechnical Commission (i.e. IEC 6400-2, design requirements for small wind turbines) states two major models for analysis of small scale wind turbines these are simplified load model, aeroelastic modeling and mechanical load testing. The best and compatible for this system topology we are working on is the simplified load model. The turbine configurations that are able to use this model shall meet all of the following requirements;

- Horizontal axis rotor,
- Two or more bladed propeller type rotor,
- Cantilever blades,
- Rigid hub (not teetering or hinged).

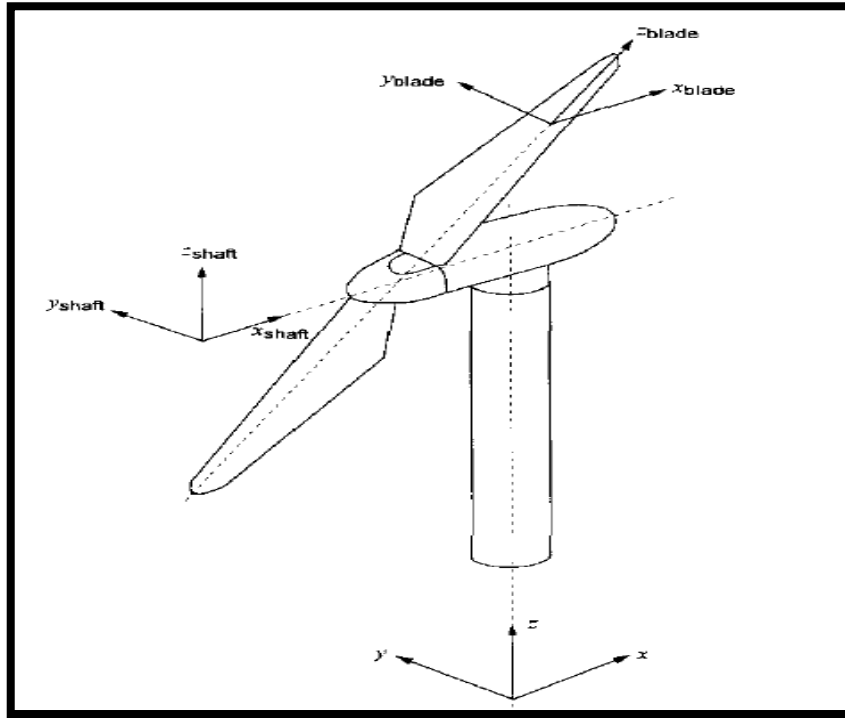


Figure 4.9: Definition of the System of Axes for HAWT [32]

The turbine configuration may use an upwind or downwind; it may operate at either variable or constant speed; it may have an active or passive pitch mechanism, as well as fixed pitch; and it may furl about furl about vertical, horizontal, or intermediate axes, as well as not furling. The coordinate system for the design of the components is based on the figure 4.8.

Table 4.6: Load Case for Small Wind Turbine Analysis [32]

Design situation	Load cases	Wind inflow	Analysis
Power production	A Normal operation		F
	B Yawing	$V_{hub} = V_{design}$	U
	C Yaw error	$V_{hub} = V_{design}$	U
	D Maximum thrust	$V_{hub} = 2.5V_{aver}$	U
Power production plus occurrence of fault	E Maximum rotational speed		U
Shutdown	F Short at load connection	$V_{hub} = V_{design}$	U
	G Shutdown (braking)	$V_{hub} = V_{design}$	U
Parked, idle or stand still	H Parked wind loading	$V_{hub} = V_{e50}$	U
Parked and fault	I Parked wind loading,	$V_{hub} = V_{ref}$	U
Transport, assembly, and maintenance	J To be stated by manufacturer		U

Note that ‘F’ is stands for analysis of fatigue loading, and ‘U’ stand for analysis of ultimate loads such as exceeding the maximum material strength, tip deflection, stability analysis. Other load case may be introduced, if it is required by the design condition specified. In the following sections the design loads at different load cases and stresses developed are determined.

A. Material Selection

It is evident that glass and carbon fiber composites (GFRP and CFRP) have a substantially higher compressive strength to weight ratio compared with the other materials. However, this apparent advantage is not as decisive as it appears, for two reasons. First of all, the fibers of some of the plies making up the laminated blade shell have to be aligned off axis (typically at 45degree) to resist shear loads, giving reduced strengths in the axial direction. Secondly, the relatively low Young’s modulus of these composites means that resistance to buckling of the thin skins governs the design rather than simple compression yielding. The likelihood that buckling will govern is inversely related to the plane stability parameter, $E = (UCS)^2$ so that materials with high values, such as wood composites will be least sensitive to buckling. As a result wood composite blades are generally lighter than equivalent glass fiber composite blades.

It should be noted that the low strength of wood laminate compared with other materials renders it unsuitable for blades with slender chords operating at high tip speed, where the flapwise bending moments during operation are inevitably high in relation to blade thickness.

Fatigue performance is conveniently measured by mean fatigue strength at 10^7 cycles, as a percentage of ultimate compressive strength. Clearly, carbon fiber and khaya/epoxy perform best with a value of about 30 percent. The low value for welded steel (10 percent), combined with steel’s low strength to weight ratio, renders it uncompetitive for large diameter machines where gravity fatigue loading becomes important, although it was chosen for some of the early prototype megawatt scale machines when the fatigue properties of composite materials were less well understood. The stiffness to weight ratio determines blade natural frequency. Apart from CFRP, the strength of the mentioned materials are all in a relatively small range (18–27 GPa), so that material choice will generally only have a marginal effect on dynamic behavior.

From the above brief survey, it is apparent that the material with the best all round structural properties is carbon fiber composite. However, it has not found common use because it is an

order of magnitude more costly than other materials. Instead, the most popular material is glass/polyester, followed by glass/epoxy and wood/epoxy.

In addition to material strength properties the manufacturability and availability with local market are crucial factors for selecting the blade material. Based on market and industries capability survey (only for the domestic ones) wood/epoxy is the most suitable and recommended.

The basic principle of laminating wood has been used effectively for many years. The major difference between a standard wood laminate (such as plywood) and the new wood resin composite developed by GBI is that as much as 20 to 25 percent of this new material is resin. The main reason for this change in approach is to provide the wood fiber with maximum protection against moisture. A second reason is to provide sufficient resin to fill the inevitable voids and gaps that can occur with low pressure bonding and thus reduce the number of defects that might act as nuclei for failures. The basic success of the wood/resin composite depends on the ability of the resin system to both affect an adequate bond and resist the passage of moisture. Dry rot has been eliminated by keeping the moisture content below that required for dry rot activity and also by sealing the wood from any oxygen source. This removes two of the necessary ingredients for the rot spore to function. Early in the GBI wood composite development, the Douglas fir species was chosen as the best available to fulfill all long term needs. The reason for this decision was primarily economic, but it was also recognized that the Douglas fir species possesses excellent specific physical properties, better than those of many other readily available wood species. Of particular interest was Douglas fir's ideal density for use in many types of high performance structures. Its density is high enough to give needed strength, yet low enough to provide efficient buckling stability.

Douglas fir, widely traded as a commodity in a veneer form, supports a large plywood industry. An active reforestation effort with this species has meant that a significant portion of the market is in second growth trees that range from 20 to 30 in. in diameter. These trees, cut into 8ft lengths called peeler logs, are efficiently turned into veneers with a minimum of waste. At historic growth rates the present reforestation efforts should ensure an ample supply of this species through the next century.

The NASA Lewis Research Center began a series of projects in 1977 to develop low cost rotor blades for megawatt scale wind turbines. And the organization conduct a static and fatigue strength test for laminated wood material made from Douglass fir and epoxy. The results are corrected for different variables which have an impact on the strength of the

material such as wood grade, moisture size, and type of joint used. The blade material static and fatigue strength data for this thesis work is based on this publication [31].

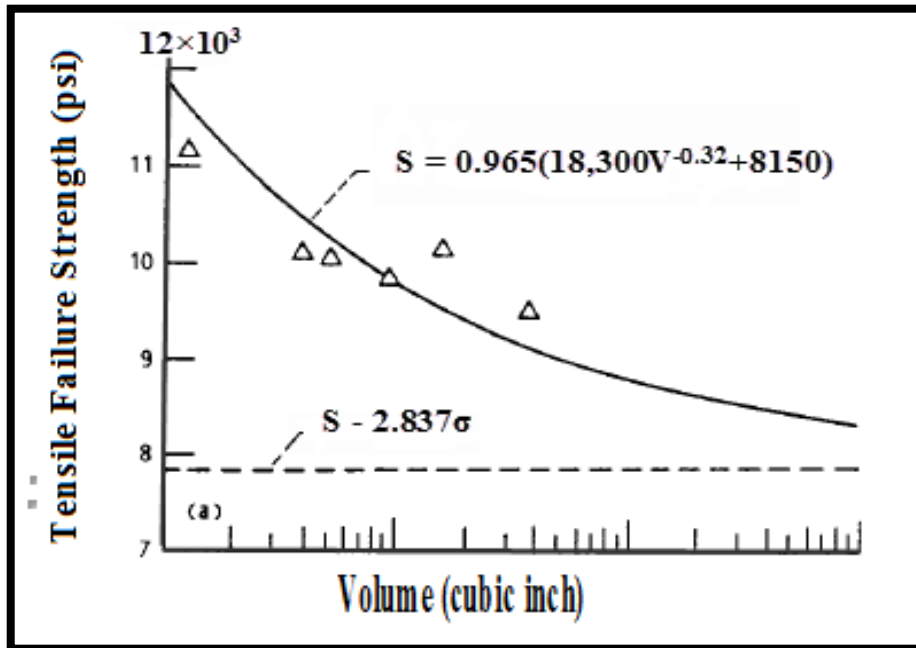


Figure 4.10: Tensile Failure Strength (Psi) for Laminated Douglas Fir/Epoxy, [31]

Based on the graph (figure 4.9) the tensile strength is related to the volume of the material and given by the following relation, $S_{ut} = 0.965(18,300V^{-0.32} + 8,150)psi$. The fatigue strength of the Douglas fir/epoxy laminated is related with life cycle of the component and showed below at figure 4.10.

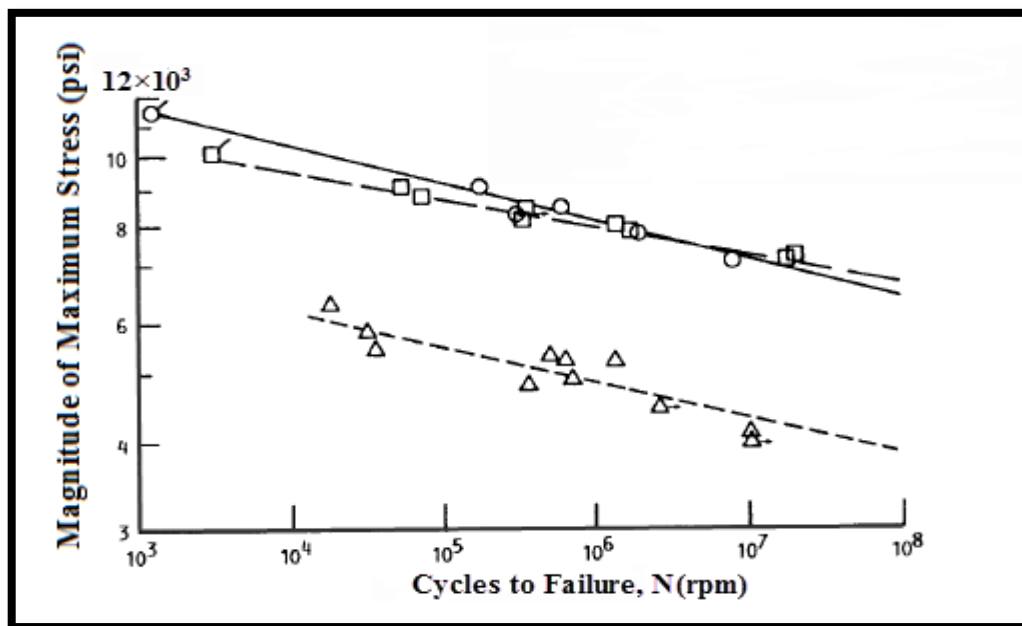


Figure 4.11: Fatigue Failure Strength (psi) For Laminated Douglas Fir/Epoxy, ‘O’ Tension-Tension Fatigue: $S = 16,842N^{-0.0527}Psi$, ‘□’ Compression-Compression Fatigue: $S = -13,550N^{-0.03997}Psi$, ‘Δ’ Tension-Compression Fatigue: $S = 9585N^{-0.05017}Psi$ [31]

B. Load Case A: Normal Operation

The design load for ‘Normal operation’ load case is a fatigue load. The load case assumes constant range of fatigue loading for the blade and shaft, these ranges are given below. The ranges are to be considered in the fatigue assessment as peak to peak values. The mean values of the load ranges can be ignored.

Force analysis: the major load during this load case is the centrifugal force and the edge and flapwise bending moments. They are calculated as follow,

Centrifugal force:

$$\Delta F_{ZB} = 2m_B R_{cog} \omega_n^2 design \quad 4.51$$

Where: m_B is mass of the blade, $\omega_n design$ is design rotational speed, 10.6rad/sec, R_{cog} is radial distance between the center of gravity of a blade and the rotor center, 2.5m. The mass of the blade can be estimated by assuming uniform cross section from the tip to the root and by approximating the cross section as triangular area.

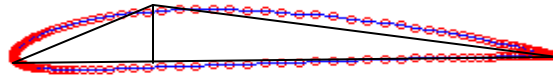


Figure 4.12: Approximation of Airfoil Cross Section to Triangular Area

$$Volume = \frac{1}{2} \times base \times height \times length = \frac{1}{2} \times 0.4 \times 0.12 \times 0.4 \times 6 = 0.0576m^3$$

And the density of the material selected i.e. Douglas fir(mountain type) is 0.446g/cc, then the mass of the blade calculated as; $m_B = 57600cc \times \frac{0.446g}{cc} = 25.6896kg$, Therefore, the centrifugal force will be, $\Delta F_{ZB} = 2 \times 25.6896kg \times 2.5 \times 10^2 = 1,284.48N$.

Blade edgewise bending moment (bending moment about x axis): it is given by,

$$\Delta M_{XB} = \frac{Q_{design}}{B} + 2m_B g R_{cog} \quad 4.52$$

Where: Q_{design} is design torque, B is Number of blades, i.e. 3, g and is Gravitational acceleration, 9.81 m/s. The design torque is given by for each radial blade sections;

$$dQ = 4a'(1 - a)\rho V_1 \pi r^3 dr \quad 4.53$$

And when it is integrated through the span of the blade we got, $Q_{design} = 36,240.74 Nm$. Finally, the bending moment range about x axis calculated as, $\Delta M_{XB} = 13,340.29Nm$.

Blade flapwise bending moment (bending moment about y axis):

$$\Delta M_{YB} = \lambda_{design} \frac{Q_{design}}{B} \quad 4.54$$

Where: λ_{design} : design tip speed ratio, i.e.10, $\Delta M_{YB} = 10 \times \frac{36240.74 Nm}{3} = 120,802.47 Nm$

The fatigue loading on the blade would be considered to occur at the airfoil root junction or at the root hub junction, whichever is determined to have the lowest ultimate strength. The calculate stresses are the combination of the centrifugal loading and the bending moment.

Stress Analysis

Axial load along the span of the blade: based on the force analysis completed the centrifugal load on the blade is calculated in range between the peak values, so that the stress can be calculated as;

$$\Delta \sigma_{ZB} = \frac{\Delta F_{ZB}}{A_B} \quad 4.55$$

Where: A_B = the area of the blade at the root, the cross section of the blade is rectangular and the exact size will be determined from the following fatigue assessment. The relation between the length and the width is taken to be as the chord and the maximum thickness. $A_B = L \times 0.12L = 0.12L^2$

Therefore,

$$\Delta \sigma_{ZB} = \frac{1,284.48N}{0.12L^2 m^2} = 10.704kPa/L^2$$

Bending stress about x axis: due to the bending moment about x axis there is a bending stress varying compression and tension based on the turbine operation, and it is given by;

$$\Delta \sigma_{MXB} = \frac{\Delta M_{xB} \times c}{I_{xb}} \quad 4.56$$

Where: c: the distance between the neutral axis and the outer part of the blade, $L/2$, I_{xb} is Area moment of inertial at the root taking x axis through the center of the rectangular, for rectangular section is given by,

$$I_{xb} = \frac{b \times h^3}{12} = \frac{0.12L \times (L)^3}{12} = 0.01L^4 m^4$$

Therefore,

$$\Delta \sigma_{MXB} = \frac{13,340.29Nm \times L/2}{0.01L^4 m^4} = 0.667MPa/L^3$$

Bending stress about y axis: due to the bending moment about y axis there is a bending stress varying compression and tension based on the turbine operation, and it is given by;

$$\Delta\sigma_{MyB} = \frac{\Delta M_{yB} \times c}{I_{yb}}$$

Where: c : For this axis it is $0.12L/2$.

Similarly the moment of inertial about y axis is given by;

$$I_{yb} = \frac{L \times (0.12L)^3}{12} = 144 \times 10^{-6}(L)^4 m^4$$

Therefore the stress will be;

$$\Delta\sigma_{MyB} = \frac{120,802.47Nm \times 0.12L/2}{144 \times 10^{-6}(L)^4 m^4} = 50.33MPa/L^3$$

The total bending stress at the root of the blade will be the sum of the two bending moments calculated above, therefore,

$$\Delta\sigma_{MB} = 0.667MPa/L^3 + 50.33MPa/L^3 = 51MPa/L^3$$

And the total stress variation can be calculated as equivalent stress as shown below, the combined stress may be include the shear stress due to the torque. But when it is compared to the bending moment stress and axial stress, it has negligible impact on the equivalent stress of the blade so that it is ignored by this work as suggested by [32]. Therefore the equivalent stress will be,

$$\Delta\sigma_{equ} = \Delta\sigma_{MB} + \Delta\sigma_{ZB} \tag{4.57}$$

Substitution will give us,

$$\Delta\sigma_{equ} = \frac{51MPa}{L^3} + \frac{0.01MPa}{L^2} \cong \frac{51MPa}{L^3}$$

Note that $\Delta\sigma_{equ}$ is the peak stress so that it will be used as amplitude for the alternating stress, in addition the fatigue loading is a completely reversed stress. The blade material selected was a composite Douglass fir/epoxy laminated and its properties are as stated in the material selection section of this documentation.

The total life time cycle of the wind turbine components is calculated as,

$$N_L = 60kn_{rotor} H_{op} Y \tag{4.58}$$

Where: k is the number of cyclic events per revolution, i.e. 1, n_{rotor} is the rotational speed of the rotor, $95.5RPM$, H_{op} is operating hours in a year, $8760hours$, Y is number of years of operation, 20 years.

Therefore,

$$N_L = 60 \times 1 \times 95.5 \times 8760 \times 20 = 10^9 \text{ cycle}$$

$$S_{ut} = 0.965(18,300V^{-0.32} + 8,150)psi = 9,160psi = 63.2MPa$$

$$S_e = 9585 \times N_L^{-0.05017} psi = 9585 \times (10^9)^{-0.05017} = 3,388.9psi = 23.3MPa$$

The endurance limit of the given material will reduce because of different defects during processing and other related tasks. To take account these effects and other external conditions the following factors are used.

- 1. Surface factor (K_a)** : it is to consider the final surface finish of the blade.

$$K_a = aS_{ut}^b LN(1, c)$$

The constants for different surface finish are tabulated below at table 4.7;

Table 4.7: Surface Finish Factors for Different Manufacturing Techniques, [33]

Surface finish	Constants		
	a (MPa)	b	c
Ground	1.58	-0.086	0.120
Machine / cold rolled	4.45	-0.265	0.058
Hot rolled	56.1	-0.719	0.110
As forged	271	-0.995	0.145

The surface finish that is aimed to used for blade manufacturing is grounding and substitution for the constants for this surface finish will give us the surface factor to be, $K_a = 0.72$

- 2. Size factor (K_b)** : this factor is to take account to the reduction to endurance because of the component, it is estimated by the following equation.

$$\begin{cases} K_b = \left(d/7.62\right)^{-0.107} & \text{for } 2.79 \text{ to } 51\text{mm diameter} \\ K_b = 0.859 - 0.000837d & \text{for } 51 \text{ to } 254\text{mm diameter} \end{cases}$$

The maximum dimension of the blade is at the root and it is the chord length i.e. 40mm, and the size factor will be, $K_b = 0.82552$.

- 3. Miscellaneous effects factor (K_c)**: it is to take account other external and uncounted factor, and is adopted to be $K_c = 0.88$.

Therefore, the final endurance limit of the material will be;

$$S_e = S_e' K_a K_b K_c = 23.3 \text{MPa} \times 0.72 \times 0.82552 \times 0.88 = 12.2 \text{MPa}$$

Then, the factor of safety for this load case taken as 1.25 as recommended at [33].

$$n_f = \frac{12.2 \text{MPa}}{\frac{51 \text{MPa}}{L^3}} = 1.25$$

Therefore, solving for L will result,

$$L = \sqrt[3]{\frac{12.2}{51 \times 1.25}} = 0.58 \text{m and the thickness } t = 0.069 \text{m}$$

To take account the effects of manufacturing defects $L = 0.7 \text{m}$ and $t = 0.084 \text{m}$ are taken.

And using equation 4.57 the alternating stress calculated to be $\sigma_a = 148.7 \text{MPa}$

Now let us find the fatigue life of the blade, the number of fatigue life of the turbine can be calculated from the following relation.

$$N = \left(\frac{\sigma_a}{a}\right)^{\frac{1}{b}} \quad 4.59$$

Where:

$$\begin{aligned} b &= -\frac{\log\left(\frac{\sigma_f'}{S_e}\right)}{\log(2N_e)} \\ &= \frac{-\log(579.159/12.2)}{\log(2 \times 10^8)} = -0.2 \end{aligned} \quad 4.60$$

σ_f' = Fatigue strength coefficient and is the true strength corresponding to fracture, 579.159 MPa, N_e = elastic limit cycle, from [33], $N_e = 10^8$. Then the final constant required to find the fatigue life is a, and calculated as,

$$a = \frac{f^2 S_{ut}^2}{S_e} \quad 4.61$$

Where:

$$f = \sigma_f \times (2 \times 10^3)^b / S_{ut} \quad 4.62$$

Then substitution will give us $f = 2.0$ and $a = 685.7\text{MPa}$, Therefore, the fatigue life of the blade will be,

$$N = \left(\frac{148.7}{685.7}\right)^{\frac{1}{-0.2}} = 2085.047\text{cycles}$$

C. Load Case B: Yawing

For this loading case, the ultimate loads (gyroscopic forces and moments) shall be calculated assuming the maximum yaw speed $\omega_{yaw\ max}$ occurring with n_{design} . The topology of this system is a passive yaw system, so that the analysis is based on the approach for passive yaw system as suggested by IEC. For passive yaw system, the maximum yaw rate is given by the following equation;

$$\omega_{yaw\ max} = 3 - 0.01(\pi R^2 - 2) \quad 4.63$$

For all turbines with a swept rotor area of less than $2m^2$, the maximum yaw rate shall be determined by measurement in calm wind. If the maximum yaw rate is expected to occur under special conditions such as emergency yawing at higher rate, the active yaw rate shall be measured under those conditions.

During yawing process the blade exposed to a flapwise bending moment. It is a function of the total mass of the blades, yawing rate and also the rotational speed of the rotor. The flapwise bending moment at the root of each blade is given by,

$$M_{YB} = m_B \omega_{yaw}^2 L_{rt} R_{cog} + 2\omega_{yaw} I_B \omega_n + \frac{R}{g} \Delta F_{x\ shaft} \quad 4.64$$

Where: L_{rt} is the distance between the rotor center and the yaw axis, 0.5m, ω_n is rotor rotational speed, $10.6\text{rad}/\text{se}$, I_B is mass moment of inertia of the blade about the blade root flap axis, the cross section of the blade root is a rectangular shape so that it is I_B is given by,

$$I_B = \frac{1}{2} m_B (H^2 + T^2) \quad 4.65$$

$\Delta F_{x\ shaft}$ is the axial thrust force and given by,

$$\Delta F_{x\ shaft} = \frac{3}{2} \frac{\lambda_{design} Q_{design}}{6} \quad 4.66$$

The flapwise bending moment develop a bending stress at the root section of the blades, it is necessary to analysis for the developed stress and check whether it is in the safe region. In this load case the components are only need ultimate strength analysis.

D. Load Case C: Yaw Error

All turbines operate with a certain yaw error. In this load case, a yaw error of 30° is assumed. Yawing error similar to the yawing load case develop a flapwise bending moment and then a bending stress at the root of each blade. The flapwise bending moment (bending moment about y axis) for at each blade because of this load case is given by,

$$M_{YB} = 1/8 \rho A_{projectB} C_{Lmax} R^3 \omega_n^2 design \left(1 + \frac{4}{3\lambda_{design}} + \left(\frac{1}{\lambda_{design}} \right)^2 \right) \quad 4.67$$

Where: ρ is air density, $1.22kg/m^3$, $A_{projectB}$ is The component area projected on to a plane perpendicular to the wind flow, i.e. $5.5 \times 0.4 = 2.2m^2$, C_{Lmax} : The maximum lift coefficient, i.e. 2.

During load case D i.e. maximum thrust loading the maximum exposure will occur on the shaft rather than the blades and the IEC 6400-2 only focus the thrust load on the shaft, so that the load by this load case on the blade is ignored.

E. Load Case E: Maximum Rotational Speed

The centrifugal load in the blade root F_{ZB} due to centrifugal load and rotor unbalance shall be calculated from equations below. The maximum possible rotor speed $\omega_n max$ shall be derived by measurements. The maximum rotor speed can be found from wind speed data by identifying the maximum wind speed. From the wind speed data of year 2005 for the site selected the maximum wind speed is $10.62m/s$. Therefore, the maximum rotor speed will be,

$$\omega_n max = (10.62 \times 10/6) = 17.7rad/s$$

The centrifugal force on each blade due to the maximum rotational speed of the rotor is given by,

$$F_{ZB} = m_B R_{cog} \omega_n^2 max \quad 4.68$$

During power production, the occurrence of the maximum rotation is an expected event. The centrifugal load because of this phenomenal will develop a tensile stress on the blades of turbine.

F. Load Case F: Short at Load Connection

After a wind turbine is installed it will be connected to a load to be powered. But during its operation there might be a short current winch will generate a reaction torque and it may damage the structure of the wind rotor. In case of a direct electrical short at the output of the

SWT or internal short in the generator, a high moment is created about the rotor shaft due to the short circuit torque of the alternator. In the absence of any values proven to be more accurate, two times the design torque is to be taken as the short circuit torque acting on the generator shaft. Therefore,

$$M_{X\ shaft} = GQ_{design} \quad 4.69$$

Then, this short circuit torque develops an edgewise bending moment, and can be calculated by,

$$M_{X\ B} = \frac{M_{X\ shaft}}{B} \quad 4.70$$

G. Load Case G: Shutdown (Braking)

In the case of wind turbines with a mechanical or electrical braking system in the drive train the braking moment can be greater than the maximum driving moment. In these cases, the braking moment derived from testing or calculated shall be used in design calculation of the SWT.

The maximum shaft torque is assumed to be equal to the braking plus the applied while the generator still delivers design torque.

$$M_{Xshaft} = M_{brake} + Q_{design} \quad 4.71$$

M_{brake} , shall be multiplied by the gearbox ratio if the brake is on the high speed shaft, but for this specific thesis work the topology selected was direct driven so that no need to multiply to take account the effect of the gearbox. The brake should deliver a torque to stop the rotor at any operational speed so the brake torque must be equivalent to the maximum rotor torque. The design condition for the brake will be based on the reference wind speed for the wind class specified for this thesis work, $V_{ref} = 30m/s$.

$$M_{brake} = \int_{r_h}^R 4a'(1-a)\rho V_{ref} \pi r^3 dr \quad 4.72$$

The blade load during shutdown is assumed to be determined by the torque and blade mass. Thus being,

$$M_{X\ B} = \frac{M_{X\ shaft}}{B} + m_B g R_{cog} \quad 4.73$$

If the turbine has a gearbox and a high speed shaft brake, the shaft torque calculated in equation above should be increased to account for drive train dynamics. In the absence of any proven more accurate values, the shaft torque shall be multiplied by a factor of two.

H. Load Case H: Parked Wind Loading

In this load case, the wind turbine is parked in the normal way. The loads on the exposed parts of the SWT shall be calculated assuming wind speed of V_{e50} .

For turbines which will be parked, the out of plane blade root bending moment is dominated by drag and thus defined as;

$$M_{YB} = C_d \frac{1}{4} \rho V_{e50}^2 A_{project} BR \quad 4.74$$

Where: C_d is drag coefficient and shall be taken as 1.5, V_{e50} is the expected extreme wind speed (averaged over 3 seconds) with a recurrence time interval of 50 years. It is can be calculated as,

$$V_{e50} = 1.4 \times V_{ref} = 1.4 \times 6 = 8.4m/s$$

For turbines that have their root spinning at V_{e50} , it is expected that, at some loading on the root $C_{L_{max}}$ will occur on one of the blades due to variations in wind direction. Thus the blade root bending moment is;

$$M_{YB} = C_{L_{max}} \frac{1}{6} \rho V_{e50}^2 A_{project} BR \quad 4.75$$

I. Load Case I: Parked Wind Loading, Maximum Exposure

In the case of a failure in the yaw mechanism, the SWT can be exposed to the wind from all directions. Thus, for design purposes, the forces on the SWT blades, nacelle, tower, and tail (if applicable) shall be calculated for all possible exposures including winds from the front side or rear of the rotor.

During maximum exposure the load on each component is given by;

$$F = C_f \frac{1}{2} \rho V_{ref}^2 A_{project} \quad 4.76$$

Where: C_f : Force coefficient

$A_{project}$: is component area (in its most unfavorable position) that is appropriate for the force coefficient. For blunt (or bluff) loading (for example nacelle covers and tower section), they are shall be the projected area on a plane perpendicular to the wind direction. For airfoil shapes, the area shall be the platform area.

During the maximum exposure for wind blowing from front of the rotor flapwise bending moment will developed, and during exposure from side edgewise bending moment will developed at the root of the blades.

The blades strength for the load cases stated is analyzed and the results such as the loads and stress developed and the factor of safety for each loading are determined (table 4.8).

Table 4.8: Result of the Strength Analysis for the Blades

Load case	Load type	Value	Stress type	Value	Factor of safety
Load Case B: Yawing	Flapwise Bending Moment	55,745.4Nm	Bending Stress	67.66MPa	1.2
Load Case C: Yaw Error	Flapwise Bending Moment	16,571.0Nm	Bending Stress	20.11MPa	3.14
Load Case E: Maximum Rotational Speed	Centrifugal Force	20,120.74N	Tensile Stress	0.34MPa	185.88
Load Case F: Short at Load Connection	Edgewise Bending Moment	24,160.5Nm	Bending Stress	3.52MPa	17.95
Load Case G: Shutdown (Braking)	Edgewise Bending Moment	73,111.5Nm	Bending Stress	10.7MPa	5.9
Load Case H: Parked Wind Loading	Flapwise Bending Moment	284.074Nm	Bending Stress	0.52MPa	121.5
Load Case I: Parked Wind Loading, Maximum Exposure	Flapwise Bending Moment	14,493.6Nm	Bending Stress	17.6MPa	3.6
	Edgewise Bending Moment	10,540.8Nm	Bending Stress	1.54MPa	41.04

The blade structural result showed that the blades with the specified size and material type can withstand the loads that are expected to expose during its life time operation. To complete the design and have reliable result the stability analysis must conducted. In the next section the stability analysis will discussed.

4.2.3 BLADE STABILITY ANALYSIS

The blade stability analysis includes investigating the natural frequency of the blade, the deflection and the buckling load is in the safe limit.

A. Blade Vibration

During the operation of wind turbine the blades will be subjected to bending moments from both flapwise and edgewise, and these bending moments lead to failures of blade. The major phenomenon's that may lead to the failure of the blades are, a physical contact between the

tower and the blades tip during maximum thrust loading and then deflection and resonance because of the blade running at the natural frequency of the blade. The vibration aspects of wind turbine blade are similar to that of a cantilever beam.

The vibration of the blade can be modeled either uniform cantilever beams or cantilever beam with finite number of mass attached together. For this work the blade vibration is modeled as uniform cantilever beam (is was recommended to use such a simplified model for a rotor with simple arrangement) [5, 33] and the following assumptions are assumed,

- Uniform material properties throughout the span
- Constant cross section
- Ideal beam and it can be modeled using analytical equation called the Euler equation for beams.

This equation is particularly useful because it allows first order approximations of natural frequencies to be made very easily for many beams. The Euler equation for deflection of uniform beam is stated as follow,

$$Y_i = A \left\{ \cosh\left(\frac{(\beta L)_i}{L} x\right) - \cos(\beta x)_i - \frac{\sinh(\beta L)_i - \sin(\beta L)_i}{\cosh(\beta L)_i + \cos(\beta L)_i} \left[\sinh\left(\frac{(\beta L)_i}{L} x\right) - \sin\left(\frac{(\beta L)_i}{L} x\right) \right] \right\} \quad 4.77$$

The value of $(\beta L)_i$ can be determined from the following relation,

$$\cosh(\beta L)_i \times \cos(\beta L)_i + 1 = 0 \quad 4.78$$

The above equation has infinite solution but the most crucial values are smaller values because of the blade is rotating under smaller speeds so that there is no fear for the maximum rotational speed which will lead to resonance and the first three of them are 3.52, 22.4 and 61.7. The value of ‘A’ in the equation stated above can be determined by limiting the maximum deflection of the tip of the blade. The natural frequency of the system is directly related to the parameter $(\beta L)_i$, modulus of elasticity density per unit length and area moment of inertia and can be defined as follow;

$$\omega_n = \frac{(\beta L)_i^2}{L^2} \sqrt{\frac{EI}{\bar{\rho}}} \quad 4.79$$

Where: E is modulus of elasticity, 9.6GPa, L: radius of the blade, 5.5m, $(\beta L)_i$: A set of constants, 3.52, 22.4, 61.7and etc.

$$\bar{\rho} = \rho_B c t$$

Where: ρ_B is mass density of the blade material, $446kg/m^3$, c is the chord of the airfoil, t is the thickness of the airfoil, I is Area moment of inertial; $I = ct^3/12$.

Substitution will give us,

$$\omega_n = \frac{(\beta L)_i^2}{L^2} \sqrt{\frac{E ct^3/12}{\rho_B ct}} = \frac{(\beta L)_i^2}{L^2} t \sqrt{\frac{E}{12\rho_B}} \quad 4.80$$

The result for the first three vibration mode shapes are as tabulated at table 4.9;

Table 4.9: Vibration Analysis Results

Vibration mode	$(\beta L)_i$	ω_n (rad/se)	A
1	3.52	26.33	-0.5
2	22.4	1066.3	0.769
3	61.7	8011.8	0.833

Note that for the determination of the constant the maximum deflection at the tip is limited to be 0.4m, which is very safe since the distance between the rotor axis and the tower is 0.5m. Substitution for the constants will give us the following deflection mode for the blade,

For mode 1:

$$Y_i = -0.5\{cosh(0.59x) - \cos(3.52x) - [sinh(0.59x) - \sin(0.59x)]\}$$

For mode 2:

$$Y_i = 0.769\{cosh(3.7x) - \cos(22.4x) - [sinh(3.7x) - \sin(3.7x)]\}$$

For mode 3:

$$Y_i = 0.769\{cosh(10.3x) - \cos(61.7x) - [sinh(10.3x) - \sin(10.3x)]\}$$

And the maximum, deflection for all mode is 0.4m so that there will be no strike between the tower and the blades.

B. Design for Buckling

The critical buckling load for column subjected to compression load is given by,

$$P_{cr} = C \frac{\pi^2 EI}{L^2} \quad 4.81$$

Where: C is a constant to take account the end condition of the beam, for different end condition its values are tabulated below; L is the radius of the blade, 5.5m, E is modulus of elasticity of the blade material, 9.6GPa, I is the area moment of inertia, $I = 3.7 \times 10^{-6}m^3$.

Table 4.4: End Condition Factor

End condition	Theoretical value of C	Conservative value of C	Recommended value of C
Fixed-free	1/4	1/4	1/4
Rounded-rounded	1	1	1
Fixed-rounded	2	1	1.2
Fixed-fixed	4	1	1.2

Based on the above equation the critical load that will lead the buckling of the blade is;

$$P_{cr} = 0.25 \times \frac{\pi^2 \times 9.6 \times 10^9 \times 3.7 \times 10^{-6}m^3}{5.5^2} = 2897.26N$$

But the buckling load that is acting on the blade is its weight, i.e. $m_B \times g = 256.896N$. Then the factor of safety will be;

$$n = \frac{P_{cr}}{w} = \frac{2897.26N}{256.896N} = 11.28$$

Now it is the final step of the blade design based on the above calculations the blade design is very safe for the targeted application. The detail part drawing is included at annex c.

4.3 JOINT DESIGN

In the preceding section the blade design and analysis was done, in this section the joint between the hub and the blades will be design. In broad sense there are two types of joints such as permanent and temporary, it is based on the time length of the application they stands. The major types of permanent joints are welded joint and riveted joint and for temporary type bolted and screwed are the most common. By taking account the advantage of bolted joint over the others it is selected for this application and the design procedure will continue in the following paragraphs.

The joint between the hub and the blades is subjected to the load case as that of the blade and the hub so that they should design in such a way that to withstand all the loads developed. The loads developed are tabulated at table 4.5.

Table 4.5: Joint Loads Developed During Different Load Cases

Load cases	Shear load	Tensile load
A Normal operation	$\Delta F_{ZB} = 1,2884.5N$ $\Delta M_{XB} = 13,340.29Nm$	ΔM_{YB} $= 120,802.29N$
B Yawing	1.	$M_{YB} = 55,745Nm$
C Yaw error	-	M_{YB} $= 16,571.06Nm$
D Maximum thrust	-	Thrust _{max} = 7,761.3N
E Maximum rotational speed	$F_{ZB} = 20,120.74N$	-
F Short at load connection	$M_{XB} = 24,160.5Nm$	-
G Shutdown (braking)	$M_{XB} = 73,111.5Nm$	-
H Parked wind loading	-	$M_{YB} = 284.074Nm$
I Parked wind loading, maximum exposure	-	Thrust _{max} = 32.287Nm

Then from the table we can see that the extreme loads are existed at the load case A, load case D and load case E. so that the design will carryout for fatigue loading and for the two extreme loadings.

A. Load Case A: Normal Operation

In this load case the joint is subjected completely reversed fatigue loading so that the mean stress is zero.

The amplitude of the shear force at each bolt is given by,

$$\Delta S = \Delta F_{ZB} + \frac{\Delta M_{XB}}{1/3 \times R} = 1,2884.5N + \frac{13,340.29Nm}{1/3 \times 6} = 8,561.0N$$

And the total tensile load,

$$\Delta T = \Delta M_{YB} = 120,802.29N / 1/3 \times R = 120,802.29N / 1/3 \times 6 = 65,892.256N$$

This tensile load share by each bolt , since this external load pass through the center of the joint the load will share by each load equally, therefore the tensile load by each load will be;

$$\Delta T_{bolt} = \Delta T / No. bolt = 65,892.256N / 9 = 7,321.8N$$

Then the equivalent tensile load for a bolt subjected to both shear and tensile load can be found using the following relation;

$$\Delta F_{T.equ} = \frac{1}{2} (\Delta T_{bolt} + \sqrt{\Delta T_{bolt}^2 + 4(\Delta S)^2}) = 12,974.6N$$

Stress Analysis

The equivalent tensile load develops a tensile stress on the bolts and it can be expressed as follow;

$$\sigma_a = \frac{\Delta F_{T.equ}}{A_{bolt}} = \frac{12,974.6N}{\frac{1}{4} \pi d_c^2} = \frac{16520}{d_c^2} N$$

Where: d_c = core diameter of the bolts

Table 4.6: SAE Bolts Strength Catalogue

SAE grade	Size in	Minimum proof strength, kpsi	Minimum tensile Strength, kpsi	Minimum yield strength, kpsi	Endurance strength, kpsi	Material
5	¼ -1	85	120	92	18.6	Medium carbon Q&T

According to Goodman fatigue criteria;

$$\frac{S_a}{S_e} + \frac{S_m}{S_{ut}} = 1 \tag{4.82}$$

But the mean stress is zero; therefore the above relation will give us;

$$S_a = S_e = 18.6 \text{ kpsi} = 128.2 \text{ MPa}$$

Then,

$$\frac{S_a}{\sigma_a} = fs \tag{4.83}$$

Where: fs = factor of safety = 3,

Then substitution will result,

$$\frac{128.2N/mm^2}{\frac{16520N}{d_c^2}} = 3, \quad d_c = \sqrt{\frac{16520N}{128.2N/mm^2}} = 19.7mm$$

Therefore, the core diameter of the bolts will be; $d_c = 19.7mm$. From catalogue the nearest standard value will be; M24 is selected.

B. Load Case D and E Combined

When the joint is subjected both the maximum rotational speed as well as maximum thrust loads it will have both extreme shear and tensile load on each bolt.

Force Analysis

The shearing force on each bolt is given by;

$$S_{bolt} = F_{ZB} = 20,120.74N$$

And the tensile load on each bolt is given by;

$$T_{bolt} = Thrust\ max / No.\ bolts = 7,761.3N / 9 = 862.4N$$

Then, the equivalent tensile load that can compile the combined effect of both tensile and shear loads is given by;

$$F_{T.equ} = \frac{1}{2} (T_{bolt} + \sqrt{T_{bolt}^2 + 4(S_{bolt})^2}) = 20,556.6N$$

Stress Analysis

The tensile stress developed at each bolt is given by;

$$\sigma_{T\ bolts} = \frac{F_{T.equ}}{A_{bolt}} = \frac{20,556.6N}{\frac{1}{4}\pi \times 20^2} = 65.4MPa$$

Then the factor of safety will be;

$$fs = \frac{S_{ut}}{\sigma_{T\ bolts}} = \frac{827.4MPa}{65.4MPa} = 12.7$$

Therefore, we can conclude that the joint is very safe for the planned application.

4.4 HUB DESIGN

The design of hub is based on the type of hub topology is selected, shape, and loading. The topology selected for this work was a fixed hub which is the connection between the blades and the hub is fixed. The general shape of the hub is shown below at annex d. The hub expected to expose for the same type of load cases as that of the blades so that the hub must be design for all load case. The general design low is shown at figure 4.13.

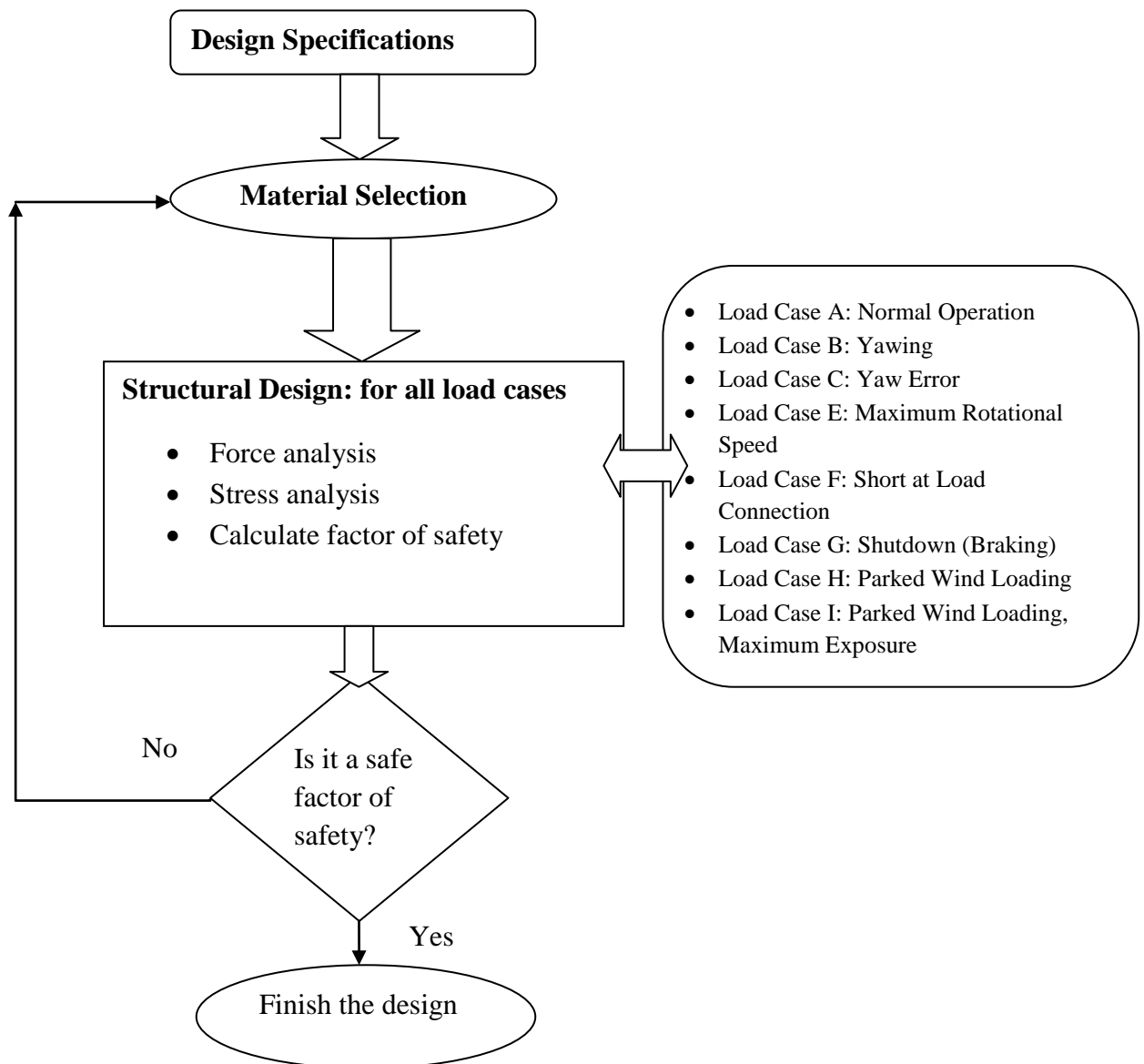


Figure 4.13: Design of Hub Flow Chart

A. *Material Selection*

The relatively complex three dimensional geometry of rotor hub favors the use of casting in their manufacturing process, with spheroid graphite iron being the material generally chosen. The physical properties of the selected material are tabulated at table 4.7.

Table 4.7: Hub Material Specification

Property	Value
Material	spheroid graphite cast iron
Grade(SNG)	24/17
Ultimate tensile strength/ S_{ut} (MPa)	370
Endurance limit (MPa)	$0.5S_{ut}=185$
Modulus of elasticity (GPa)	173

The hub is one of the major and crucial components of wind turbines. It is subjected to similar load case as that of the wind blades. The critical area that maximum stress developed is the cross sectional area that the bolts are crossing. Therefore the design analysis is based on this cross sectional area for each load case.

B. Load Case A: Normal Operation

The design load for ‘Normal operation’ is a fatigue load. The load case assumes constant range of fatigue loading for the blade and shaft, these ranges are given below. The ranges are to be considered in the fatigue assessment as peak to peak values. The mean values of the load ranges can be ignored.

Force Analysis

From the force analysis for the blades we have the following results,

Centrifugal force: $\Delta F_{ZB} = 1,284.48N$

Blade edgewise bending moment (bending moment about x axis): $\Delta M_{XB} = 13,340.29Nm$

Blade flapwise bending moment (bending moment about y axis): $\Delta M_{YB} = 120,802.47Nm$

Stress Analysis

Axial load along the span of the blade: based on the force analysis completed the centrifugal load on the blade is calculated in range between the peak values, so that the stress can be calculated as;

$$\Delta\sigma_{ZB} = \frac{\Delta F_{ZB}}{A_{HUB}}$$

Where: A_{HUB} = area of the hub at the joint, $A_{HUB} = 700mm \times t - 3 \times 24t = 628t \text{ mm}$, t: is the thickness of the hub, Then the stress will be;

$$\Delta\sigma_{ZHUB} = \frac{1,284.48N}{628t \text{ mm}} = 0.002045MPa/t$$

Bending stress about x axis: due to the bending moment about x axis there is a bending stress varying compression and tension based on the turbine operation, and it is given by;

$$\Delta\sigma_{MXB} = \frac{\Delta M_{xB} \times c}{I_{xhub}}$$

Where: c : the distance between the neutral axis and the outer part of the blade, $\frac{0.7}{2} = 0.35m$

I_{xHUB} : Area moment of inertial at the root taking x axis through the center of the rectangular, for rectangular section is given by,

$$I_{xHUB} = \frac{t \times 0.7^3}{12} - 3 \times \frac{t \times 0.024^3}{12} = 0.0286t \text{ m}^4$$

Therefore,

$$\Delta\sigma_{MXHUB} = \frac{13,340.29Nm \times 0.35m}{0.0286t \text{ m}^4} = 0.163Mpa/t$$

Bending stress about y axis: due to the bending moment about y axis there is a bending stress varying compression and tension based on the turbine operation, and it is given by;

$$\Delta\sigma_{MyHUB} = \frac{\Delta M_{yB} \times c}{I_{yb}}$$

c : For this axis it is, $t/2$

Similarly the moment of inertial about y axis is given by;

$$I_{yHUB} = \frac{0.7 \times (t)^3}{12} - 3 \times \frac{0.024 \times (t)^3}{12} = 0.052(t)^3m^4$$

Therefore the stress will be;

$$\Delta\sigma_{MyHUB} = \frac{120,802.47Nm \times t/2}{0.052(t)^3m^4} = 2.32MPa/t^2$$

The total bending stress at this section will be the sum of the two bending moments calculated above, therefore,

$$\Delta\sigma_{MB} = 0.163MPa/t + 2.32MPa/t^2$$

And the total stress variation can be calculated as equivalent stress as shown below, the combined stress may be include the shear stress due to the torque. But when it is compared to the bending moment stress and axial stress, it has negligible impact on the equivalent stress of the blade so that it is ignored by this work as suggested by [32]. Therefore the equivalent stress will be,

$$\Delta\sigma_{equ} = \Delta\sigma_{MB} + \Delta\sigma_{ZB} = \frac{0.163MPa}{t} + \frac{2.32MPa}{t^2} + \frac{0.002045MPa}{t} = \sigma_a$$

Note that $\Delta\sigma_{equ}$ is the peak stress so that it will be used as amplitude for the alternating stress, in addition the fatigue loading is a completely reversed stress. The total life time cycle of the wind turbine components is calculated as, $N_L = 10^9$ cycle.

Similarly the endurance limit reduction factors for the hub material are introduced as follow, using the equation stated earlier at the blade design section.

1. **Surface factor (K_a)** : it is to consider the final surface finish of the blade.

$$K_a = aS_{ut}^b LN(1, c) = 0.85$$

2. **Size factor (K_b)** : this factor is to take account to the reduction to endurance because of the component, it is estimated by the following equation.

$$\begin{cases} K_b = (d/7.62)^{-0.107} & \text{for 2.79 to 51mm diameter} \\ K_b = 0.859 - 0.000837d & \text{for 51 to 254mm diameter} \end{cases}$$

The dimension of the shaft is still not determine, but by rough estimation second equation is used taking average diameter of 100mm, $K_b = 0.7753$.

3. **Miscellaneous effects factor (K_c)**: it is to take account other external and uncounted factor, and is adopted to be $K_c = 0.88$.

Therefore, the final endurance limit of the material will be;

$$S_e = S_e' K_a K_b K_c = 185MPa \times 0.72 \times 0.7753 \times 0.88 = 90.9MPa$$

Then the factor of safety for this load case taken as 1.25 as recommended at [33].

$$n_f = \frac{90.9MPa}{\Delta\sigma_e} = 1.25 = \frac{90.9MPa}{\frac{0.165MPa}{t} + \frac{2.32MPa}{t^2}}$$

$$72.72 \times (t + 0.177) \times (t - 0.18) = 0$$

Some algebraic manipulation will give us the value of thickness of the hub; $t = 0.18m$

And the alternating stress,

$$\sigma_a = \frac{0.165}{t} + \frac{2.32MPa}{t^2} = 72.52MPa$$

$$I_{yHUB} = 0.052(t)^3 m^4 = 3.03 \times 10^{-4} m^4$$

$$I_{xHUB} = 0.0286t m^4 = 5.15 \times 10^{-3} m^4$$

$$A_{hub} = 0.7 \times 0.18 - 3 \times 0.024 \times 0.18 = 0.113m^2$$

Now let us find the fatigue life of the blade, the number of fatigue life of the turbine can be calculated from the following relation.

$$N = \left(\frac{\sigma_a}{a}\right)^{\frac{1}{b}}$$

Where: $b = -\log\left(\frac{\sigma_f'}{S_e}\right) / \log(2N_e)$, and substitution give us, $b = -0.141$, σ_f' = Fatigue strength coefficient and is the true strength corresponding to fracture, $S_{ur} + 345MPa = 705MPa = N_e$: elastic limit cycle, from [33], $N_e = 10^6$. Therefore,

$$f = \sigma_f \times (2 \times 10^3)^b / S_{ut} = 705MPa \times (2 \times 10^3)^{-0.141} / 360MPa = 0.67$$

Then the final constant required to find the fatigue life is a, and calculated as,

$$a = \frac{f^2 S_{ut}^2}{S_e} = \frac{0.67^2 \times 360MPa^2}{90.9MPa} = 640MPa$$

Therefore, the fatigue life of the blade will be, $N = 3.4 \times 10^6$ cycles

C. Load Case B: Yawing

For this loading case, the ultimate loads (gyroscopic forces and moments) shall be calculated assuming the maximum yaw speed $\omega_{yaw\ max}$ occurring with n_{design} . The topology of this system is a passive yaw system, so that the analysis is based on the approach for passive yaw system as suggested by IEC.

The loads developed at the blades will transmit to the hub through the joint; therefore the hub should withstand these loads. The hub is subjected to flapwise bending moment during this load case and then develops bending stress.

D. Load Case C: Yaw Error

All turbines operate with a certain yaw error. In this load case, a yaw error of 30° is assumed. Similarly at this load case the hub is subjected to the flapwise bending moment transferred from the blade. The flapwise bending moment on the hub has similar magnitude as that of the blades exposed to.

E. Load Case E: Maximum Rotational Speed

During power production, the occurrence of the maximum rotation is expected event. The centrifugal load because of this phenomenal will develop a tensile stress on the blades of turbine. Again this load and stress will transmit to the hub with similar magnitude as that of the blades.

F. Load Case F: Short at Load Connection

Due to the short circuit torque developed at the shaft the hub will be subjected to edgewise bending moment. The magnitude of the bending moment is equal to the bending moment developed at the root of the blades.

G. Load Case G: Shutdown (Braking)

The wind turbine system may be stopped for emergency purpose from its operating speed using brake. Due to this existence of phenomenal the wind turbine components will be subjected to edgewise bending moment and then stress.

H. Load Case H: Parked Wind Loading

In this load case, the wind turbine is parked in the normal way. The loads on the exposed parts of the SWT shall be calculated assuming wind speed of V_{e50} .

I. Load Case I: Parked Wind Loading, Maximum Exposure

In the case of a failure in the yaw mechanism, the SWT can be exposed to the wind from all directions. Thus, for design purposes, the forces on the SWT blades, nacelle, tower, and tail (if applicable) shall be calculated for all possible exposures including winds from the front side or rear of the rotor.

The bending moment on the hub due to maximum exposure is the summing up effect of the bending moments developed at the blade, nacelle and the hub itself. When the exposure it from the front flapwise bending moment or edgewise bending moment when exposure from side will develop.

The design analysis result of the hub is tabulated at table 4.8.

Table 4.8: Result of the Strength Analysis for the Hub

Load Case	Load Type	Value	Stress Type	Value	Factor of safety
Load Case B: Yawing	Flapwise Bending Moment	55,745.4Nm	Bending Stress	16.6MPa	21.9
Load Case C: Yaw Error	Flapwise Bending Moment	16,571.016Nm	Bending Stress	4.92MPa	73.2
Load Case E: Maximum Rotational Speed	Centrifugal Force	20,120.74N	Tensile Stress	0.178MPa	2022.5
Load Case F: Short at Load Connection	Edgewise Bending Moment	24,160.5Nm	Bending Stress	1.64MPa	220
Load Case G: Shutdown (Braking)	Edgewise Bending Moment	73,111.5Nm	Bending Stress	4.97MPa	72.43
Load Case H: Parked Wind Loading	Flapwise Bending Moment During Parked State	426.112Nm	Bending Stress	0.127MPa	2834.6
Load Case I: Parked Wind Loading, Maximum Exposure	Flapwise Bending Moment	14,647.3Nm	Bending Stress	4.35MPa	82.75
	Edgewise Bending Moment	10,590.76Nm	Bending Stress	0.72MPa	500

The design result for the hub shows that the hub with material selected and the dimensions specified is very safe for the targeted application.

4.4 MAIN SHAFT DESIGN AND ANALYSIS

As far as the main shaft is exposed to different load case like the blades do the shaft must be design to withstand the loads developed at each load cases. The design of the shaft based on the loading for each load case is completed in the following sections. The design flow is based on figure 4.11.

4.4.1 MAIN SHAFT STRUCTURAL DESIGN

The structural design of the main shaft start by material selection and then by stress analysis for each load cases it is expected to expose.

A. *Material Selection*

The shaft is also subjected to similar load case as that of the blades and other components so that the shaft material should withstand the loads developed. The major selection criteria's used for the selection of shaft material are the following,

- Component loading

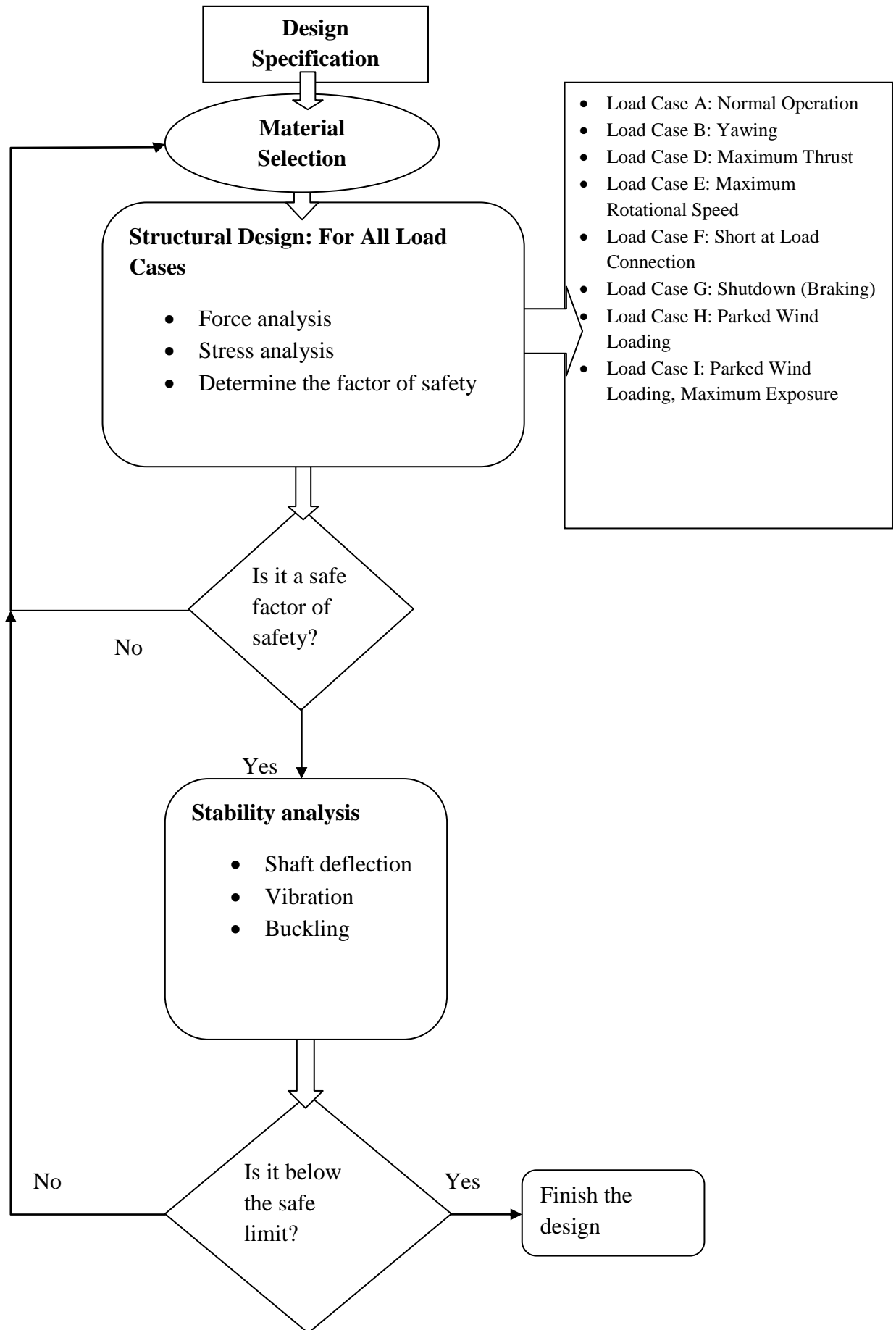


Figure 4.14: Design of Main Shaft Flow Chart

- Life time and external conditions
- Cost and availability within the local market
- Manufacturability with the local limited technological advancement

By taking these points in to consideration hot rolled steel with the parameters at table 4.9 from standard catalogue is selected.

Table 4.9: Physical Properties of Shaft Material

ISO Standard 1083	Tensile Strength MPa	Yield Strength MPa	Elongation %	Hardness (BHN)
350/22	350	215	22	107-130

B. Load Case A: Normal Operation

Force Analysis

Axial thrust load on the shaft: the load range of shaft at the normal operation of the wind turbine is given by the following equation,

$$\Delta F_{x-shaft} = \frac{3 \lambda_{design} Q_{design}}{2 R} \quad 4.84$$

Substitution for the values will give us,

$$\Delta F_{x-shaft} = \frac{3}{2} \times \frac{10 \times 36,240.74}{6} = 90,601.85N$$

Moments:

Torsional moment on the shaft:

$$\Delta M_{xshaft} = Q_{design} + 2m_r g e_r \quad 4.85$$

Where: e_r : Distance between the center of gravity of the rotor and axis of rotation. It can be calculated by the equation stated below unless experimental value is available.

$$e_r = 0.005R = 0.005 \times 6 = 0.03m$$

m_r : mass of the whole rotor including the hub, the blade, the shaft, since the major dimensions of the shaft and the hub is not identified there is no exact value for it. Hence rough estimation is required; the total mass of the rotor is assumed to be 3 times the mass of the

blade, 77.0688kg, at the end of the design process if the estimated value is much different from the real value the design will be modified.

$$\Delta M_{Xshaft} = 36,240.74 + 2 \times 77.0688 \times 9.81 \times 0.03 = 36,286.1Nm$$

Bending moment on the shaft:

$$\Delta M_{shaft} = 2m_r g L_{rb} + \frac{R}{6} \Delta F_{x-shaft} \quad 4.86$$

Where: L_{rb} : Distance between rotor center and first bearing, 0.25m

Substitution for the values will give us,

$$\Delta M_{shaft} = 2 \times 77.0688 \times 9.81 \times 0.25 + \frac{6}{6} \times 90,601.85N = 90,979.87Nm$$

Stress analysis

Axial compression stress: due to the thrust load the shaft will subjected to axial compression stress and can be calculated as follow,

$$\Delta \sigma_{x-shfat} = \frac{\Delta F_{x-shaft}}{A_{shaft}}$$

Where: A_{shaft} = the cross sectional area of the shaft, the exact size will be determined from the following fatigue assessment.

$$A_{shaft} = \pi r_{shaft}^2$$

Therefore,

$$\Delta \sigma_{x-shfat} = \frac{90,601.85N}{\pi r_{shaft}^2} = 28,854.1N / r_{shaft}^2$$

Torsional stress: due to this torsional moment on the shaft can be calculated form the following equation,

$$\Delta \tau_{shaft} = \frac{\Delta M_{Xshaft} \times c}{I_{shaft}}$$

Where: c: the distance between the neutral axis and the outer part of the blade, r_{shaft}

I_{shaft} : Area moment of inertial the shaft and given by

$$I_{shaft} = \frac{\pi r_{shaft}^4}{4}$$

$$\Delta\tau_{shaft} = \frac{36,286.1Nm \times r_{shaft}}{\frac{\pi r_{shaft}^4}{4}} = \frac{46,200.9}{r_{shaft}^3} Nm$$

Bending stress: due to this bending moment will be,

$$\Delta\sigma_{M-shaft} = \frac{\Delta M_{shaft} \times c}{I_{shaft}}$$

Where: : For this axis it is, r_{shaft} and $I_{shaft} = \frac{\pi r_{shaft}^4}{4}$

$$\Delta\sigma_{M-shaft} = \frac{90,979.87Nm \times r_{shaft}}{I_{shaft} = \frac{\pi r_{shaft}^4}{4}} = \frac{115,839.2}{r_{shaft}^3} Nm$$

The equivalent stress will combine the effect of each stress is given by the following relation,

$$\Delta\sigma_e = \sqrt{(\Delta\sigma_{M-shaft} + \Delta\sigma_{x-shaft})^2 + 3 \times (\Delta\tau_{shaft})^2} = \sigma_a \quad 4.87$$

Substitution will give us,

$$\Delta\sigma_e = \sqrt{\left(\frac{115,839.2}{r_{shaft}^3} + 28,854.1N/r_{shaft}^2\right)^2 + 3 \times \left(\frac{46,200.9}{r_{shaft}^3}\right)^2} = \sigma_a$$

This the amplitude of the alternating stress with a mean stress of zero, i.e. completely reversed loading. The material selected for the shaft is hot rolled steel with the following parameters,

Table 4.10: Shaft Material Specification

Specification	Value
SAE/AISI No.	1015/ hot rolled steel
S_{ut}	340 MPa
S_y	190 MPa
S_e	$0.56S_{ut}=190.4$ MPa
E	205GPa
N_e	10^6
σ_f	$S_{ut} + 345MPa = 685MPa$

Similarly the endurance limit reduction factors for shaft material are introduced as follow, using the equation stated earlier at the blade design section.

1. Surface factor (K_a) : it is to consider the final surface finish of the blade.

$$K_a = aS_{ut}^b LN(1, c) = 0.85$$

2. Size factor (K_b) : this factor is to take account to the reduction to endurance because of the component, it is estimated by the following equation.

$$\begin{cases} K_b = \left(d/7.62\right)^{-0.107} & \text{for 2.79 to 51mm diameter} \\ K_b = 0.859 - 0.000837d & \text{for 51 to 254mm diameter} \end{cases}$$

The dimension of the shaft is still not determine, but by rough estimation second equation is used taking average diameter of 100mm, $K_b = 0.7753$.

3. Miscellaneous effects factor (K_c): it is to take account other external and uncounted factor, and is adopted to be $K_c = 0.88$.

Therefore, the final endurance limit of the material will be;

$$S_e = S'_e K_a K_b K_c = 190.4\text{MPa} \times 0.72 \times 0.7753 \times 0.88 = 93.53\text{MPa}$$

Then the factor of safety for this load case taken as 1.25 as recommended at [33].

$$n_f = \frac{93.53\text{MPa}}{\Delta\sigma_e} = 1.25$$

Therefore, the radius of the shaft will be, $r_{shaft} = 0.12\text{m}$

And the alternating stress,

$$\sigma_a = \sqrt{\left(\frac{115,839.2\text{Nm}}{0.12\text{m}^3} + 28,854.1\text{N}/0.12\text{m}^2\right)^2 + 3 \times \left(\frac{46,200.9\text{Nm}}{0.12\text{m}^3}\right)^2} = 83.1\text{MPa}$$

Now let us find the fatigue life of the blade, the number of fatigue life of the turbine can be calculated from the following relation.

$$N = \left(\frac{\sigma_a}{a}\right)^{\frac{1}{b}}$$

Where:

$$b = -\log\left(\frac{\sigma_f'}{S_e}\right) / \log(2N_e) = -\log(685\text{MPa}/93.53\text{MPa}) / \log(2 \times 10^6) = -0.14$$

σ_f' = Fatigue strength coefficient and is the true corresponding to fracture, 685MPa, N_e = elastic limit cycle, from [33], $N_e = 10^6$

Therefore,

$$f = \sigma_f \times (2 \times 10^3)^b / S_{ut} = 685\text{MPa} \times (2 \times 10^3)^{-0.14} / 340\text{MPa} = 0.7$$

Then the final constant required to find the fatigue life is a, and calculated as,

$$a = \frac{f^2 S_{ut}^2}{S_e} = \frac{0.7^2 \times (340\text{MPa})^2}{93.53\text{MPa}} = 605.6\text{MPa}$$

Therefore, the fatigue life of the blade will be,

$$N = \left(\frac{\sigma_a}{a}\right)^{\frac{1}{b}} = \left(\frac{83.1\text{MPa}}{605.6\text{MPa}}\right)^{-0.14} = 1.45 \times 10^6 \text{cycles}$$

C. Load Case B: Yawing

For this load case, the ultimate loads (gyroscopic and moment) shall be calculated assuming the maximum yaw speed $\omega_{yaw \max}$ occurring with ω_n . The shaft ending moment due to this load case is depend on the number of the blade and for three bladed turbine the shaft bending moment is given by,

$$M_{shaft} = B\omega_{yaw \max} I_B \omega_n + m_r g L_{rb} + \frac{R}{6} \Delta F_{x-shaft} \quad 4.88$$

During load case C i.e. during yaw error the blade the major component which will suffer by the bending moment developed and so that the load on the shaft due to this load case is ignored as suggested at [33].

D. Load Case D: Maximum Thrust

The SWT can be exposed to high thrust loads on the rotor. The thrust load acts parallel to the rotor shaft and has maximum value given by;

$$F_{x \text{ shaft}} = 3.125 C_T \rho V_{aver}^2 \pi R^2 \quad 4.89$$

Where: C_T is the thrust coefficient, it is equal to 0.5, $V_{average}$ is the average wind speed for the wind class specified, i.e. 6m/s.

This thrust force on the shaft develop a compressional stress, so that the shaft should checked for this stress and buckling.

E. Load Case E: Maximum Rotational Speed

When the wind turbine exposed to maximum rotational speed there will high centrifugal force which further will result bending stress on the shaft. The bending moment on the rotor shaft is given by;

$$M_{shaft} = m_r g L_{rb} + m_r e_r \omega_{n \max}^2 L_{rb} \quad 4.90$$

Where: m_r is mass of the whole rotor including the hub, the blade, the shaft, since the major dimensions of the shaft and the hub is not identified there is no exact value for it. Hence rough estimation is required; the total mass of the rotor is assumed to be 3 times the mass of the blade, 77.0688kg, at the end of the design process if the estimated value is much different from the real value the design will be modified, e_r : Distance between the center of gravity of the rotor and axis of rotation. It can be calculated by, $e_r = 0.005R$, unless experimental value is available, L_{rb} is distance between rotor center and first bearing, 0.25m.

F. Load Case F: Short at Load Connection

In case of a direct electrical short at the output of the SWT or internal short in the generator, a high moment is created about the rotor shaft due to the short circuit torque of the alternator. In the absence of any values proven to be more accurate, two times the design torque is to be taken as the short circuit torque acting on the generator shaft. Therefore,

$$M_{X\ shaft} = GQ_{design} \quad 4.91$$

G. Load Case G: Shutdown (Braking)

In the case of wind turbines with a mechanical or electrical braking system in the drive train the braking moment can be greater than the maximum driving moment. In these cases, the braking moment derived from testing or calculated shall be used in design calculation of the SWT.

The maximum shaft torque is assumed to be equal to the braking plus the applied while the generator still delivers design torque.

$$M_{X\ shaft} = M_{brake} + Q_{design} \quad 4.92$$

M_{brake} , shall be multiplied by the gearbox ratio if the brake is on the high speed shaft, but for this specific thesis work the topology selected was direct driven so that no need to multiply to take account the effect of the gearbox. The brake should deliver a torque to stop the rotor at any operational speed so the brake torque must be equivalent to the maximum rotor torque. The design condition for the brake will be based on the reference wind speed for the wind class specified for this thesis work, $V_{ref} = 30m/s$.

$$M_{brake} = \int_{r_h}^R 4a'(1-a)\rho V_{ref} \pi r^3 dr \quad 4.93$$

H. Load Case H: Parked Wind Loading

In this load case, the wind turbine is parked in the normal way. The loads on the exposed parts of the SWT shall be calculated assuming wind speed of V_{e50} .

The thrust load:

1. For parked rotor the thrust load will be given by,

$$F_{X\ shaft} = BC_d \frac{1}{2} \rho V_{e50}^2 A_{project\ shaft} \quad 4.94$$

2. For a spinning rotor the thrust force is;

$$F_{X\ shaft} = 0.17 B A_{project} B \lambda_{e50}^2 V_{e50}^2 \quad 4.95$$

Where: λ_{e50} : tip speed ratio at V_{e50} , and can be estimated as,

I. Load Case I: Parked Wind Loading, Maximum Exposure

In the case of a failure in the yaw mechanism, the SWT can be exposed to the wind from all directions. Thus, for design purposes, the forces on the SWT blades, nacelle, tower, and tail (if applicable) shall be calculated for all possible exposures including winds from the front side or rear of the rotor.

The load on each component is given by;

$$F = C_f \frac{1}{2} \rho V_{ref}^2 A_{project\ component} \quad 4.96$$

Where: C_f is Force coefficient, $A_{project}$ is component area (in its most unfavorable position) that is appropriate for the force coefficient.

For blunt (or bluff) loading (for example nacelle covers and tower section), they are shall be the projected area on a plane perpendicular to the wind direction. For airfoil shapes, the area shall be the platform area.

Exposure from front side:

During exposure from front the shaft will subjected to compressional stress and bending stress due to the bending moment transferred from the other components of the rotor (the blade, hub, and nacelle).

Exposure from side:

During exposure from the side of the rotor the shaft will subjected to shear stress only due to the twisting moment from the other components of the rotor.

Table 4.11: Result of the Strength Analysis for the Main Shaft

Load Case	Load Type	Value	Stress Type	Value	Factor of safety
Load Case B: Yawing	Bending Moment	91,188.3Nm	Bending Stress	67.13MPa	5.06
Load Case D: Maximum Thrust	Compression Force	7,761.305N	Compressional Stress	172.5kPa	1971
Load Case E: Maximum Rotational Speed	Bending Moment	370.098Nm	Bending Stress	272kPa	1250
Load Case F: Short at Load Connection	Twisting Moment	72,481.48Nm	Shear Stress	53.36MPa	6.4
Load Case G: Shutdown (Braking)	Twisting Moment	217,444.4Nm	Bending Stress	160MPa	2.125
Load Case H: Parked Wind Loading	Thrust Force For Parked Rotor	426.112Nm	Compressional Stress	9.5kPa	35.8×10^3
	Thrust force for spinning rotor	12,648.69N	Compressional Stress	281.08kPa	1209
Load Case I: Parked Wind Loading, Maximum Exposure	Bending Moment	14,507.6Nm	Bending Stress	10.3kPa	33,009.7
	Twisting Moment	10,561.4Nm	Shear Stress	7.8MPa	43.6

4.4.2 MAIN SHAFT DEFLECTION

The shaft is exposed to radial loads which will deflect it from the normal operating position. The occurrence such a case will disturb the performance and reduce the life time of the components. The deflecting load for the shaft is the weight of the whole rotor assembly and the free body diagram is shown below at figure 4.12;

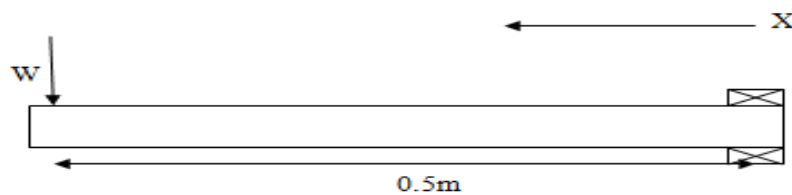


Figure 4.15: Shaft Loading for Deflection Calculation

The total mass of the rotor is 77.0689kg and the weight will be 770.689N. For a cantilevered beam with the above loading condition the deflection equation is given by equation 4.97.

$$Y = \frac{Wx^2}{6EI}(3L - x) \quad 4.97$$

Where: E is modulus of elasticity; 205Gpa, I is area moment of inertial, $\frac{\pi r_{shaft}^4}{4} = 1.63 \times 10^{-4}m^4$, L is shaft length, 0.5m, W is weight of the rotor assembly, 770.689N. Therefore,

$$Y = \frac{770.689x^2}{6 \times 205 \times 10^9 \times 1.64 \times 10^{-4}m^4}(3 \times 0.5 - x) = (0.6x^2 - 0.382x^3) \times 10^{-5}$$

And the maximum deflection at the end of the shaft is given by;

$$\delta_{max} = \frac{WL^3}{3EI} \quad 4.98$$

$$\delta_{max} = \frac{770.689 \times 0.5^3}{3 \times 205 \times 10^9 \times 1.64 \times 10^{-4}} = 9.55 \times 10^{-7}m$$

4.4.3 MAIN SHAFT VIBRATION

During its operation the shaft is subjected to a variation because of dynamic load and mass unbalance. When a shaft is turning, eccentricity causes a centrifugal force deflection, which is resisted by the shaft's flexural rigidity E I. As long as deflections are small, no harm is done. Another potential problem, however, is called critical speeds: at certain speeds the shaft is unstable, with deflections increasing without upper bound. It is fortunate that although the dynamic deflection shape is unknown, using a static deflection curve gives an excellent estimate of the lowest critical speed. Such a curve meets the boundary condition of the differential equation (zero moment and deflection at both bearings) and the shaft energy is not particularly sensitive to the exact shape of the deflection curve. Designers seek first critical speeds at least twice the operating speed. The shaft, because of its own mass, has a critical speed. The ensemble of attachments to a shaft likewise has a critical speed that is much lower than the shaft's intrinsic critical speed. Estimating these critical speeds (and harmonics) is a task of the designer. When geometry is simple, as in a shaft of uniform diameter, simply supported, the task is easy. It can be expressed as [33],

$$\omega_n = \left(\frac{\pi}{l}\right)^2 \sqrt{\frac{EI}{m}} \quad 4.99$$

Where: m is mass per unit length of the shaft, 356kg/m, E is modulus of elasticity of shaft material, 205GPa, I is area moment of inertia, $1.63 \times 10^{-4}m^4$, l is Length of the shaft, 0.5m

$$\omega_n = \left(\frac{\pi}{0.5}\right)^2 \sqrt{\frac{205 \times 10^9 \times 1.63 \times 10^{-4}m^4}{356}} = 12094.9rad/s$$

Which is very large from the actual rotational speed, 10rad/s or 95.5rpm, so that the shaft for vibration.

4.4.4 DESIGN FOR BUCKLING

During maximum exposure to thrust load the shaft will subjected to a bucking load. The total maximum thrust load can be found summing up the maximum thrust load from the blade and the hub.

$$F_{shaft-buckling} = F_B + F_{HUB} \quad 4.100$$

$$F_{shaft-buckling} = 7,246.8N + 1.5 \times 0.5 \times 1.22 \times 30^2 \times 0.8^2\pi = 11,289.2N$$

The critical load that the shaft can withstand is calculated by the following relation,

$$P_{cr} = C \frac{\pi^2 EI}{L^2} \quad 4.101$$

Where: C is constant to take account the end condition of the beam, for different end condition its values are tabulated below; L is The radius of the blade, 0.5m, E is Modulus of elasticity of the blade material, 205GPa, I is Area moment of inertia, $1.64 \times 10^{-4}m^4$, Therefore the critical load and the factor of safety for bucking are,

$$P_{cr} = 0.25 \times \frac{\pi^2 \times 205 \times 10^9 \times 1.64 \times 10^{-4}}{0.5^2} = 1.33 \times 10^9 N$$

$$n_f = \frac{P_{cr}}{F_{shaft-buckling}} = \frac{1.33 \times 10^9 N}{11,289.2N} = 1.17 \times 10^5$$

Both the structural and stability analysis of the main shaft proved as it can supply the required application with material selected and dimensions determined for the specified application.

In this chapter, the major mechanical components were designed for the application required. The blades are design for both aerodynamics and structural aspects and the result showed that they are very safe to the loads they are expected to expose. In addition the joint between the hub and the blades, the hub, and the main shaft are design to accomplish the required application. The other components of the wind turbine system which are not design such as, the bearings, the tower, the nacelle, the foundation, the yaw and the like are take to be selected from standard catalogue, and it is one of the limitation of the thesis. In the next section the major components of axial flux permanent magnet generator will be design after detail conceptual discussion done.

CHAPTER FIVE

ELECTRICAL COMPONENT DESIGN

5.1 INTRODUCTION

There are generally three types of PM machines: Radial, Axial and Transversal flux machines. The names arise from the direction of the magnetic flux in the air gap. The major concern of this thesis is axial flux permanent magnet generators so that a bird eye view discussion will follow in the subsequent sections.

Axial Flux Permanent Magnet (AFPM) machines with coreless stators are regarded as high efficiency machines for distributed power generation [43-45]. In these machines, the ironless stator avoids the direct magnetic attraction between rotors and stators [44]. Because of the absence of core losses, a generator with this type of design can potentially operate at a higher efficiency than conventional machines [44]. Besides, the compactness and disk shaped profile make these types of machines particularly suitable for mechanical integration with wind turbines [46].

Electric generators using an axial flux configuration were developed almost 150 years ago. However, their applications have been limited to fractional power due to some difficulties [47], [48]. One major problem is the centrifugal force acting on magnets that tends to move them from their place. Therefore, the rotation speed of AFPM generators is limited, and that leads to using such generators in low speed applications such as direct coupling with wind turbines [4]. In the past, some researchers have done work on AFPM generators with rated speeds equal to 200 rpm [46] and close to 1950 rpm [49]. In previous AFPM machines, to increase the power output, the pole-numbers were increased, for example, to 28 poles in [46] and 40 in [49]. Another way to reach the desired high outputs is to increase the rotation speed of the AFPM generator with lower pole numbers. A higher speed leads to higher induced voltage on stator windings. The AFPM generators with no cores always have low inductances and thus current increase does not change the machine performance [50]. One advantage of fewer numbers of magnets is the decrease in the generator cost.

In this chapter, after the presentation of the necessary formulas to obtain parameters and the performance of AFPM machines, an axial flux 3 phase coreless PM generator is designed. This generator has two outer disk rotors and one coreless stator in between. Neodymium-Iron-Boron (Nd-Fe-B) rare earth magnets produce the necessary excitation in the generator. These magnets are glued onto the two inner surfaces of rotor disks. After the preliminary design, and

for precision study, a three-dimensional (3-D) model of the machine is analyzed using finite element method (FEM) software (specifically COSMOSworks). From the results of FEM analysis, one can calculate the parameters of the machine. The experimental test will be conducted after the prototyping process is done and the result is presented in chapter six of this documentation.

5.2 CORELESS AXIAL FLUX PMG

AFPM machines with coreless stators have the stator winding wound on a non magnetic and non conductive supporting structure or mould. The stator core losses, i.e. hysteresis and eddy current losses do not exist. The losses in PMs and rotor solid steel disc are negligible. This type of design offers higher efficiency at zero cogging torque. In order to maintain a reasonable level of flux density in the air gap, a much larger volume of PMs in comparison with laminated stator core AFPM machine is required. The stator winding is placed in the air gap magnetic field generated by the PMs mounted on two opposing rotor discs. When operating at relatively high frequency, significant eddy current losses in the stator winding conductors may occur [37].

For axial flux machines, the minimum number of disks is two (single sided), but normally three disks (double sided) are used in order to get balanced axial forces and to increase the total air gap surface. The single sided axial flux permanent magnet machine topology has the drawback of a large uncompensated attractive force between the rotor and the stator, which implies the use of a bearing system capable of tolerating it [38]. For double sided axial flux machine structures, these mechanical concerns are cancelled out during machine operation because the double air gap system causes that the total axial force affecting the inner disk is negligible.

Regarding the stator(s) position(s) with respect to the rotor(s) position(s), slot or slotless stator(s) and the winding arrangements, several axial flux machine types can be used, giving freedom to select the most suitable machine structure into the considered application. The double-sided axial flux permanent generator with internal rotor is chosen, mainly due to simplified manufacturing process, placing the rotor between two stators, which are easily fixed to the frame. Compared to the opposite structure, in which the stator is located between the rotors [39], more space is available for winding, but, on the other hand, the copper losses are generally higher. Three dimensional view of axial flux double rotor permanent magnet generator with single coreless stator is shown at fig. 5.1. As it can be seen, rectangular flat shaped high energy Nd-Fe-B magnets are glued onto the inner surfaces of the two rotor disks.

The shaft diameter shown is not to the scale. It is only to state that the inner diameter of AFPM machine is relatively large.

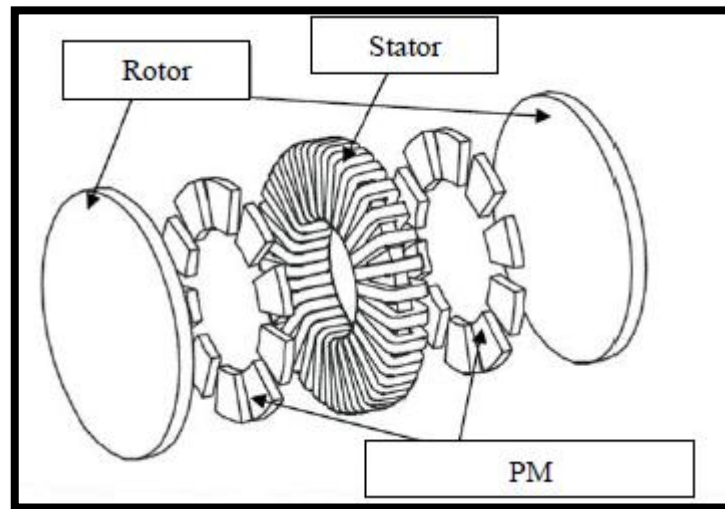


Figure 5.1: Three Dimensional View of Axial Flux Permanent Magnet Generator [40]

5.2.1 Rotor Assembly

The permanent magnets in the internal rotor of a double sided structure may be located on the surface or inside the rotor disk. Thereby, the main flux may flow axially through the rotor disk or flow circumferentially along the rotor disk. With the permanent magnets located at the surface of the rotor disk, it is not necessary a ferromagnetic rotor core and the axial length are substantially reduced, which consequently improves the power density of the machine. The chosen rotor structure consists in a holed nonmagnetic disk to support the permanent magnets. Compared to the surface mounted permanent magnets in a non-holed rotor disk, this solution involves the machining and the manipulation of half magnet pieces. The flux path associated with this machine topology is shown in fig. 5.2. The flux travels axially in the rotor structure and completes its path by returning circumferentially around the stators cores.

The rotor assembly is content the permanent magnets glued on to steel disks. The magnets are arranged in such a ways that opposite magnet polarization between two successive poles and between the two rotors concurrent poles. The general arrangement for twelve pole rotor is shown below at figure 5.2;

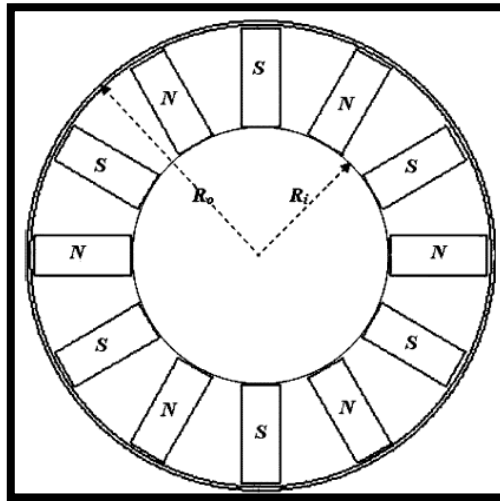


Figure 5.2: Rotor Assembly for Twelve Pole Generator [40]

Magnet placement

There are mainly two possible ways of mounting the permanent magnets in AFPM machines. The permanent magnets can either be mounted on the surface of the rotor disk or they can be embedded into the rotor disk. Surface mounting of permanent magnets is the preferred placement type due to the ease of the manufacturing of the smooth rotor disks, thereby, lowering the cost of the machine. Another advantage is that the surface-mounted permanent magnets naturally act as fans which have a ventilation effect on the stator windings at higher rotating speeds. The added cooling feature of the spinning permanent magnets allow for higher stator current densities before excessive stator winding temperatures damage or irreversibly demagnetize the permanent magnets [61]. As the direct drive AFPM generator has a low rotating speed, the resulting centrifugal force on the magnets created by the spinning rotor is relatively low. Lower centrifugal forces allows for the permanent magnets to be glued onto the surface of the rotor disks, instead of requiring further mechanical means such as through magnet fastening screws.

5.2.2 Stator Assembly

Although generator designs can have any number of phases, most small scale wind turbine manufacturers require a three phase machine. Slotted stators increase remarkably the amplitude of the air gap flux density due to the shorter air gap and consequently this reduces the required amount of permanent magnets, which yields savings in the generator price. Slotting may evoke undesired torque pulsations, but if the two windings are connected in series, then one stator may be rotated over a certain angle (usually one half of the slot pitch) with respect to the other which results in reduced slot ripple and space harmonic components [41]. It should be noted also that in slotted stators, the leakage and mutual inductances are

increased compared to the slotless stators, which is advantageous when using the generator connected to a solid state converter, as it helps reduce the current ripple due to converter switching.

The concentrated windings have phase coils wound around separate teeth, meaning that the radial build of the machine is shorter than machines with distributed windings which have typically long end windings, because the coil of a phase must cross the other phase coils. Thereby, the overall space, required by the machine with concentrated windings is decreased; this procedure also solves the problem how to arrange the end windings in the limited space between the shaft and the inner radius of the stators, which can be a problem for conventional three phase machines. Distributed windings use more insulation material than concentrated ones. This is translated to a more reliable insulation system and higher fill factors of concentrated windings. Compared with a conventional distributed winding with one slot per pole and phase, the concentrated winding has a low fundamental winding factor. The average electromagnetic torque is proportional to the winding factor. Disregarding the end windings effects, an electrical machine with low winding factor needs to compensate its lower torque with higher current density, which leads to higher Joule losses compared to a machine with a winding factor equal to 1, for the same torque, assuming equal slot fill factor and comparable magnetic design [42].

It's currently assumed that concentrated windings are an effective way to reduce Joule losses in low speed permanent magnet machines, due to shorter end windings. However they generate both odd and even harmonics, and some, also produce sub harmonics in the MMF. All extra harmonics create additional flux in the machine which results in high eddy current losses in a solid rotor and in the permanent magnets, which may cancel the benefits of the shorter end windings.

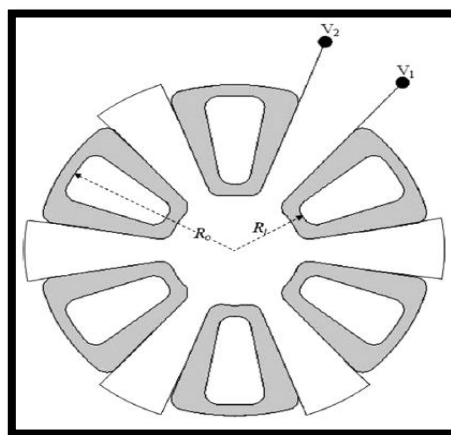


Figure 5.3: Stator Assembly for Axial Flux Generator [40]

Based on this discussion, coreless stators with three phase distributed windings have been chosen for this study. The two stator windings are connected in series and the star connection is used to avoid circulating currents.

5.2.3 Permanent Magnet Materials

The unusual properties of lodestone, known also as magnetite Fe_3O_4 , were known to the ancient Chinese and Greeks. The first known apparatus exploiting magnetism was a magnetic compass, invented by the Chinese around 3000 B.C. An important milestone in the research field of magnetism was set in 1600 when William Gilbert published his book “De Magnete”, which was the first systematic study related to the phenomenon of magnetism. The artificial permanent magnets discussed in “De Magnete” were made of sword steel and were used to lifting iron parts. According to present standards, the carbon steel used those days is an extremely poor permanent magnet material, offering a low coersivity, $H_c < 4 \text{ kA/m}$, and a low energy product, $BH_{max} < 2 \text{ kJ/m}^3$. This remained the quality level of artificial permanent magnets until about 1880 when the systematic study on alloy properties got started. The addition of tungsten and chromium was shown to rise H_c to some degree. An important discovery was the use of cobalt as an additional material and in 1917 K. Honda achieved the ultimate properties of steel magnets by adding to the alloy 35% of cobalt. The maximum energy product of this steel magnet was 8 kJ/m^3 and its coersivity was 20 kA/m [51, 52].

In 1931 T. Mishima patented the first hard magnetic alloy, based on aluminum, nickel and iron. This was the start of the development of the permanent magnet family known as AlNiCo. Due to the remarkably improved magnet properties the AlNiCo magnets were now made useful for many electrical engineering applications. Supported by a better understanding of material physics, further development of the artificial permanent magnet materials has been rapid since the 1940s. In the 1950s, another permanent magnet family, known as ferrites, became commercially available. Because of their better material properties and much lower material costs the ferrites became extremely popular for DC electric motor applications used in automobiles, hand tools, etc [52].

The development of rare earth permanent magnet materials started in the 1960's with the Samarium-Cobalt alloys. The material properties of $SmCo_5$ and Sm_2Co_{17} make these permanent magnet materials very suitable to be used in electric motors and generators, but they are expensive due to the rare raw material Cobalt. The newest, important addition to permanent magnet materials was made in 1983, when the high performance Neodymium-Iron-Boron permanent magnet material was introduced. Compared to SmCo permanent

magnets, Nd-Fe-B magnets offer compatible material properties but are essentially cheaper. A historical development of the rare earth permanent magnets is illustrated in fig. 5.4.

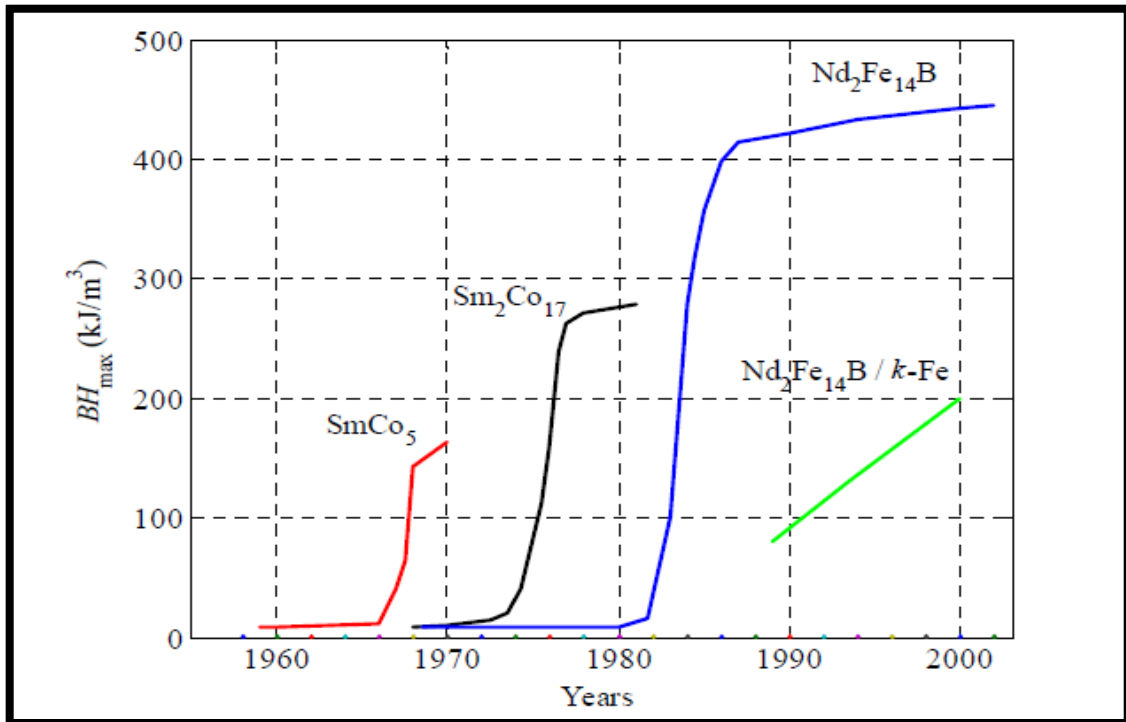


Figure 5.4: Historical Development of the Rare Earth Magnets [53]

Two types of the rare earth magnet exist, namely the SmCo magnet and NdFeB magnet, and presently approximately 98% of the total production quantity stems from the Nd family; with the NdFeB magnet acting as the rare earth magnet.

The NdFeB magnets consist of the sintered type and the bond type, and are made from a mixture of resin and plastics (etc.) with magnetic powder. The sintered magnet makes up the bulk of the magnet production, and the manufacturing process of the NdFeB magnet follows powder metallurgy. The difference in normal powder metallurgy has to do with compression the molding under the magnetic field. By arranging the crystal orientation of the fine powder to one direction using an external magnetic field, the mechanical pressure is applied to the mold, and the resulting product provides the magnetic anisotropy. The compactness of the pressured powder is then sintered at high temperature, and through the liquid phase sintering, the compacted matter shrinks, and the density increases to the near true density. The volume shrinks in the half; however obtaining true dimensional accuracy is difficult. After sintering, a diamond wheel does grinding, and the dimension and surface treatment is applied to achieve the final product. By considering availability and the cost, in addition to the technical aspects NdFeB permanent magnet is selected with the following properties and grade.

Table 5.1: Magnetic Properties of NdFeB [54]

Grade	B_r (Gauss)	H_c (Oersteds)	H_{ci} (Oersteds)	BH_{max} (MGOe)	Temp. Coefficient of B_r (%/°C)	Max. Op. Temp. (°C)	Density (lbs/in ³)
42H	13,300	12,700	17,000	43	-0.10	120	0.271

Table 5.2: Physical Properties of NdFeB [54]

Description	Value
Modulus of elasticity	22 x 10 ⁶ psi
Ultimate tensile strength	12 x 10 ³ psi
Density	7.4 g/cc
Perpendicular to orientation	-4.8 x 10 ⁻⁶ /°C
Parallel to orientation	3.4 x 10 ⁻⁶ /°C
Electrical resistivity	160μ ohm cm
Curie temperature	310°C
Reversible temperature coefficient of residual induction (-100°C to + 100°C)	-0.09 to -0.13% /°C
Recoil permeability	1.05
Max. service temperature*	150°C

* Maximum Service Temperature depends on permeance coefficient of magnetic circuit. Temperatures shown here are guidelines only.

5.2.4 Coreless Stator Winding

Coreless stator windings are used in twin rotor double sided AFPM machines. For the ease of construction, the stator winding normally consists of a number of single layer trapezoidal shaped coils. The assembly of the stator is made possible by bending the ends of the coils by a certain angle, so that the active conductors lie evenly in the same plane and the end windings nest closely together. The windings are held together in position by using a composite material of epoxy resin and hardener. Fig. 5.5 shows the coreless stator winding of a three phase, eight pole AFPM machine. Obviously, the relations used in the slotted stator windings can be directly used for coreless trapezoidal stator winding with the exception that the term “slot” is replaced by the “coil side”[56].

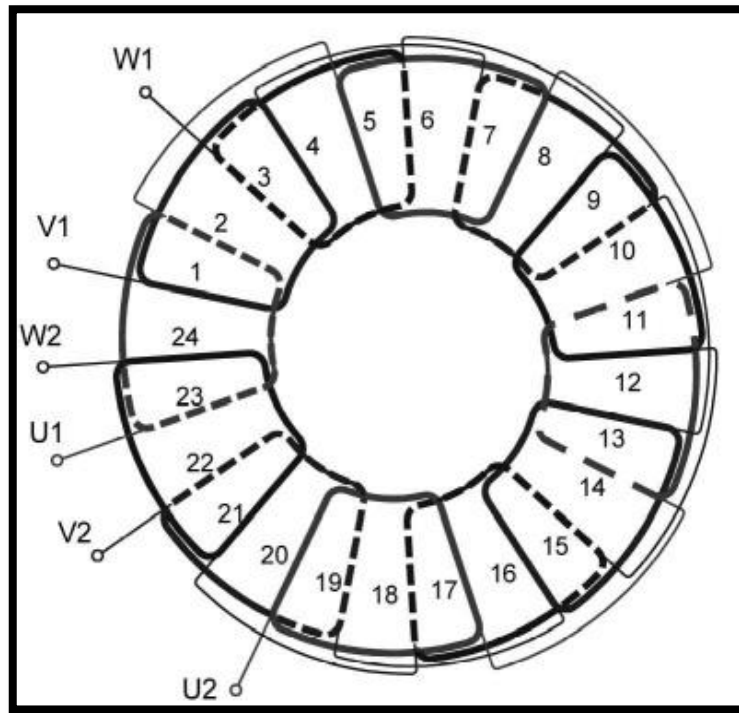


Figure 5.5: Coreless Winding of a Three Phase, Eight Pole AFPM Stator

Another coil profile that has been used in coreless stator AFPM machines is the *rhomboidal* coil. It has shorter end connections than the trapezoidal coils. The inclined arrangement of the coil's active sides makes it possible to place water cooling ducts inside the stator. The main drawback of rhomboidal coils is the reduction of the torque.

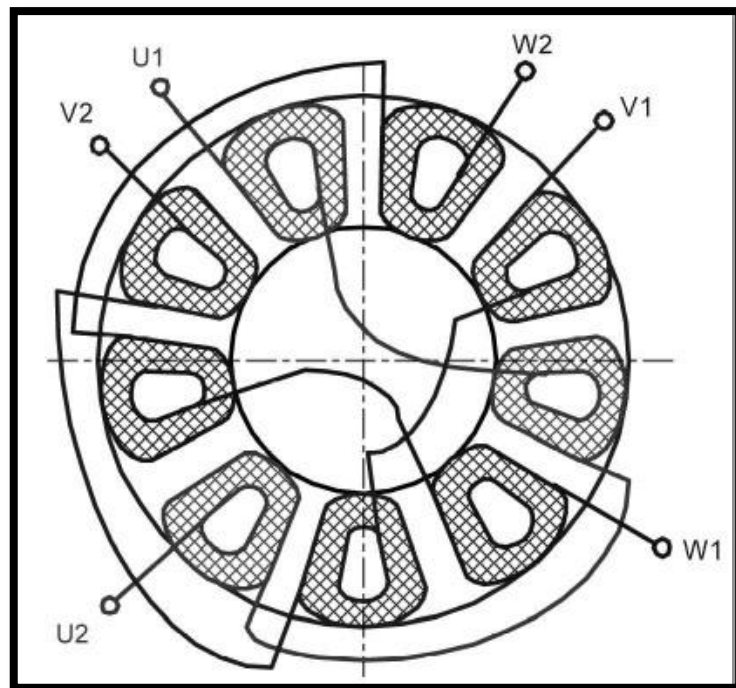


Figure 5.6: Connection Diagram of 3 ϕ , Nine-Coil Winding of AFPM Brushless Stator

5.3 MAGNETIC MODELING

5.3.1 Air Gap Modeling

In all AFPM machines, flux passes between the stator through an air gap. For this reason it is important to model the permeance or reluctance of the air gap. Consider the structure shown in figure 5.7, where an air gap is created between two blocks of highly permeable material. Flux flowing from one block to the other passes through the air gap and creates a *mmf* drop between the two blocks. The permeance of this air gap P_g is difficult to model because flux does not flow straight across the air gap near the edges of the blocks. This occurs because the air in the gap has the same permeability as the air fringing the gap; therefore, some flux will flow in the fringe area as shown in figure 5.7. The permeance of the gap depends on the exact magnetic field distribution in the gap. While this can be accurately approximated using finite element methods, it is possible to approximate the air gap permeance with sufficient accuracy for most applications using magnetic circuit concepts.

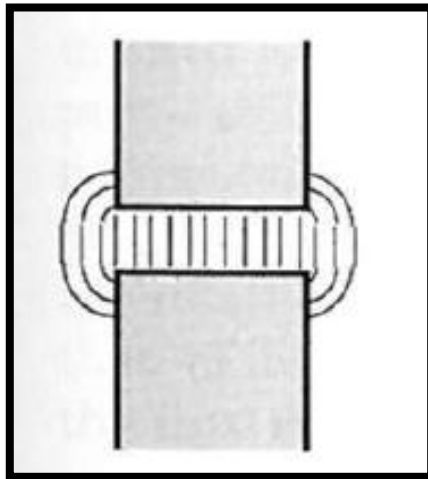


Figure 5.7: Flux Flow through the Air Gap

Depending on the degree of precision required, there are a number of techniques for modeling flux flow in an air gap as depicted in figure 5.8. The simplest model (figure 5.8a) ignores the fringing flux entirely, and then the permeance of the air gap will be,

$$P_g = \frac{\mu_o A}{g} \quad 5.1$$

Where: μ_o : permeability of free space = $4\pi \times 10^{-7}$ H/m

g : air gap length and A : cross sectional area

A refinement of the simplified model (figure 5.8b) which is accurate when g/A is small lets the permeance of the air gap,

$$P_g = \frac{\mu_o A'}{g} \quad 5.2$$

Where: the air gap length g is added to the perimeter of A to obtain A' .

Yet another refinement models the fringing flux as a separate permeance in parallel with the permeance of the direct flux path across the air gap. One method for doing this is shown in figure 5.8c. In this figure, the fringing flux is assumed to follow a circular arc from the side of one block, travel in a straight line across the gap area, and then follow a circular arc to the other block.

The calculation of the air gap permeance using this circular arc, straight line approximation utilizes the fact that permeances add in parallel just as electrical conductance do. The air gap permeance P_g in figure 5.9 is equal to the sum of P_s and $4P_f$ (one P_f each side of the block). While the straight line permeance P_s is computed, the fringing permeance P_f requires more work. As depicted in Fig. 5.9, P_f is an infinite sum of differential width permeances, each of length $g + \pi x$, i.e.,

$$P_f = \sum \frac{\mu_o dA}{l} = \sum \frac{\mu_o L dx}{g + \pi x} \quad 5.3$$

Where: dA : is the crosssectional area of each differential permeance and L is the depth of the block into the page. Because this equation involves the sum of differential elements, its solution is given by the integral.

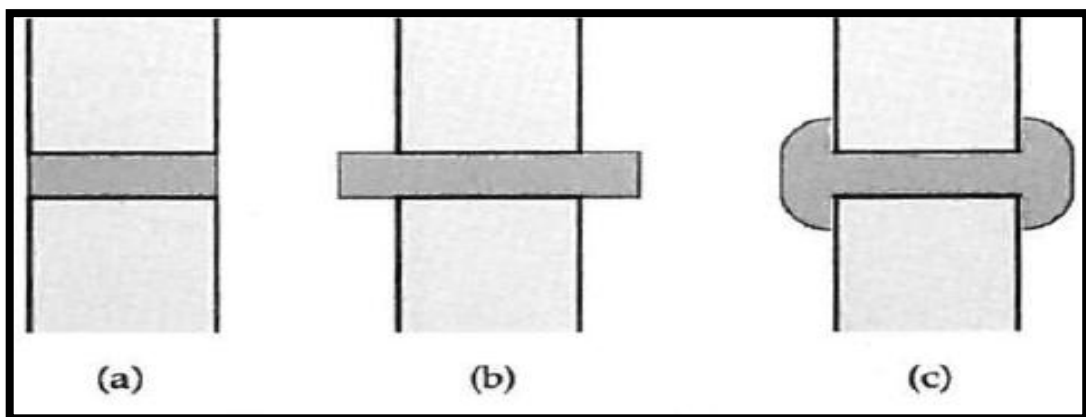


Figure 5.8: Air Gap Permeance Model

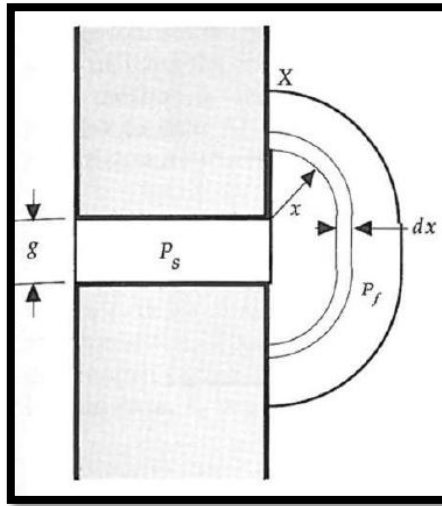


Figure 5.9: Circular Arc, Straight Line Permeance Model

5.3.2 Slot Modeling

The same as the air gap in electrical machines there are slots facing an air gap which hold current carrying windings. Since the windings are nonmagnetic, flux crossing an air gap containing slots will try to avoid the low relative permeability of the slot area. This adds another factor that must be considered in determining the permeance of an air gap. There are several ways to approximate the air gap permeance.

The simplest and crudest method is to ignore the slot by assuming that it contains material of permeability equal to that of the rest of the block. In this case, the permeance is simply,

$$P_g = \frac{\mu_o A}{g} \quad 5.4$$

Where: A is the total cross sectional area facing the gap. Obviously, this is a poor approximation because the relative permeability of the slot is orders of magnitude lower than that of block material.

Another crude approximation is to ignore the flux crossing the gap over the slot, giving a permeance,

$$P_g = \frac{\mu_o (A - A_s)}{g} \quad 5.5$$

Where: A_s is the cross sectional area of the slot facing the air gap. Neither of these methods is very accurate, but they do represent upper and lower bounds on the air gap permeance, respectively.

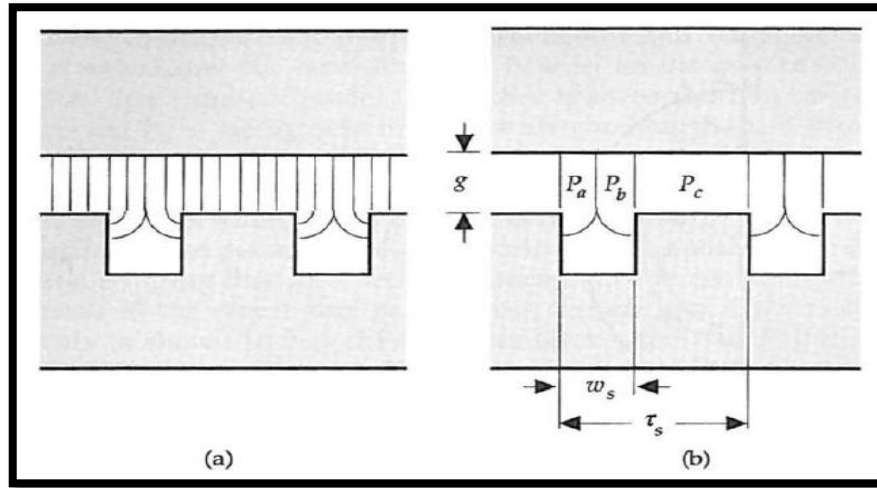


Figure 5.10: Slotted Structure

There are two more accurate ways of determining air gap permeance in the presence of slotting. The first is based on the observation that the flux crossing the gap over the slot travels a further distance before reaching the highly permeable material across the gap. As a result, the permeance can be written as,

$$P_g = \frac{\mu_o A}{g_e} \quad 5.6$$

Where; $g_e = gk_c$ is an effective air gap length, $k_c > 1$ is a correction factor that increases the entire air gap length to account for the extra flux path distance over the slot, and it is called carter coefficient which is approximated by the following two equations, the one given by Nasar (1987).

$$k_c = \left[1 - \frac{1}{\frac{\tau_{si}}{\omega_s} \left(5 \frac{g_c}{\omega_s} + 1 \right)} \right]^{-1} \quad 5.7$$

And the other which was given by, Ward and Lawrenson (1977),

$$k_c = \left[1 + \frac{2\omega_s}{\pi\tau_{si}} \left\{ \tan^{-1} \left(\frac{\omega_s}{g} \right) \right\} - \frac{g}{\omega_s} \ln \left(1 + \left(\frac{\omega_s}{g} \right)^2 \right) \right]^{-1} \quad 5.8$$

The other more accurate method for determining the air gap permeance utilizes the circular arc, straight line modeling discussed earlier. This method is demonstrated in figure 5.10b, the permeance of the air gap can be written as;

$$P_g = P_a + P_b + P_c = \mu_o L \left[\frac{\tau_s - \omega_s}{g} + \frac{4}{\pi} \ln \left(1 + \frac{\pi\omega_s}{4g} \right) \right] \quad 5.9$$

But for this case the carter coefficient is give by,

$$k_c = \left[1 + \frac{\omega_s}{\tau_{si}} + \frac{4g}{\pi\tau_{si}} \ln \left(1 + \frac{\pi\omega_s}{4g} \right) \right]^{-1} \quad 5.10$$

One important consequences of slotting is that the presence of slots squeezes the air gap flux into a cross sectional area $\left(1 - \frac{\omega_s}{\tau_{si}} \right)$ times smaller than the cross sectional area of the entire air gap. Thus the average flux density at the base of the teeth is greater by a factor of $\left(1 - \frac{\omega_s}{\tau_{si}} \right)^{-1}$.

The importance of this phenomenon cannot be understated. Since this flux density level is sufficient to saturate (i.e., dramatically reduce the effective permeability of) most magnetic materials, there is an upper limit to the achievable air gap flux density in a motor. Later this will be shown to be a limiting factor in motor performance.

5.3.3 Magnetic Circuit Analysis

Magnetic circuits of rotors consist of PMs and mild steel backing rings or discs. Since the air gap is somewhat larger that in similar RFPM counterparts, high energy density PMs should be used. Normally, surface magnets are glued to smooth backing rings or rings with cavities of the same shape as magnets without any additional mechanical protection against normal attractive forces. Epoxy, acrylic or silicon based adhesives are used for gluing between magnets and backing rings or between magnets. There were attempts to develop interior PM rotor for AFPM machines. According to [57], rotor poles can only be fabricated by using soft magnetic powders [57]. The main advantage of this configuration is the improved flux weakening performance. However, the complexity and high cost of the rotor structure discourage further commercializing development.

Depending on the need for accuracy and calculation speed different methods can be used. In general there have been used three levels of calculations for finding the flux during the design and analysis. First the very simple method using magnet and air gap length to find the magnetic flux density in the air gap, together with the electric and magnetic loading to identify the main dimensions, then a lumped circuit model to get the final main dimensions, and finally FEA analysis with linear and nonlinear 2D and 3D time stepping and rotation. These three steps above describe the process of the design from the crude design of the first meetings, to the final analysis of the machine.

The magnetic circuit analysis is based on the equivalent magnetic circuit for the single rotor as shown at figure 5.11;

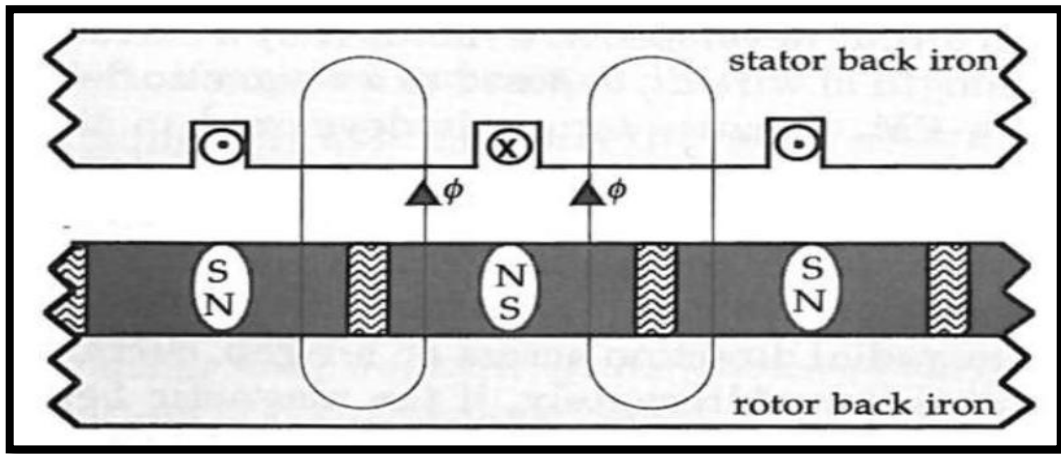


Figure 5.11: Basic Translational Permanent Magnet Generator Structure [56]

To develop force and back *emf* expressions, consider the prototype linear translational motor cross section shown in Fig. 5.11. The structure shown is assumed to repeat indefinitely in both directions. In a rotational system producing torque, the two ends would meet halfway around the motor, giving a finite number of magnet poles. Then the equivalent magnetic circuit for the generator is shown in fig. 5.12.

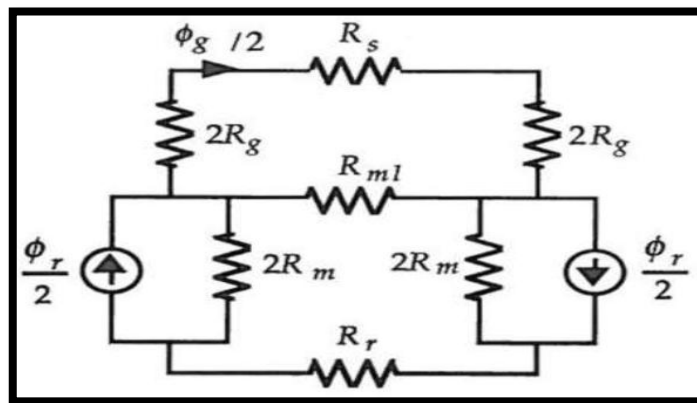


Figure 5.12: Equivalent Magnetic Circuit [56]

After series of circuit simplification we found a simplified circuit as shown in figure 5.13.

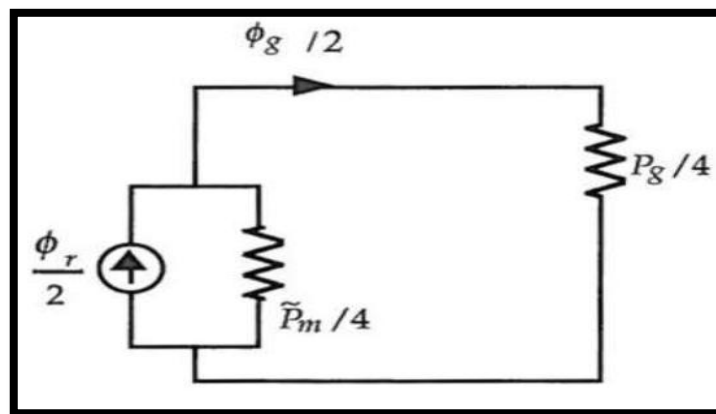


Figure 5.13: Simplified Equivalent Magnetic Circuit [56]

Based on the simplified equivalent circuit the magnet permeance is given by;

$$P_m = \frac{\mu_R \mu_o \alpha_m \tau_p L}{l_m} \quad 5.11$$

And the line permeance for circular arc straight line is;

$$P_{ml} = \frac{\mu_o L}{\pi} \ln \left[1 + \pi \frac{g}{(1 - \alpha_m) \tau_p} \right] \quad 5.12$$

Where the magnet leakage factor k_{ml} is

$$k_{ml} = 1 + \frac{P_{ml}}{P_m} = 1 + \frac{4l_m}{\mu_R \alpha_m \pi} \ln \left[1 + \pi \frac{g}{(1 - \alpha_m) \tau_p} \right] \quad 5.13$$

The air gap permeance describes the net permeance seen by the magnet flux that enters the stator. Because this flux emanates from a cross sectional area of $(\alpha_m \tau_p - 2g)L$ and enters a stator cross sectional area of $\tau_p L$, some approximation of the air gap permeance is required. Using $\tau_p L$ overestimates the air gap permeance, whereas using $\alpha_m \tau_p - 2g)L$ underestimates it. To make things simple, the area is assumed to be the average of these two values, ignoring the $- 2gL$ term.

$$A_g = \frac{\tau_p (1 - \alpha_m) L}{2} \quad 5.14$$

With approximation, the air gap permeance is,

$$P_g = \frac{\mu_R \tau_p (1 - \alpha_m) L}{2g_e} \quad 5.15$$

Where g_e is the effective air gap length it is described as,

$$g_e = g k_c \quad 5.16$$

Finally after some algebraic manipulation the air gap flux is defined as,

$$\phi_g = \frac{1}{1 + \frac{2\mu_R \alpha_m k_{ml} k_c g}{(1 - \alpha_m) l_m}} \quad 5.17$$

Or in terms of permeance coefficient it is given by,

$$\phi_g = \frac{1}{1 + \frac{\mu_R k_{ml} k_c}{P_c}} \phi_r \quad 5.18$$

Where: $P_c = l_m / (g C_\phi)$ and $C_\phi = 2\alpha_m / (1 - \alpha_m)$

The air gap flux density is expressed as,

$$B_g = \frac{C_\phi}{1 + \frac{\mu_R k_{ml} k_c}{P_c}} B_r \quad 5.19$$

It is important to note that this flux density represents the average value crossing the air gap. When the stator is slotted, the actual flux density over the slots will be lower because of the longer flux path there.

5.4 PRELIMINARY ANALYTICAL ANALYSIS

In this section the magnetic, geometrical, and electrical parameters will be determined based on steady state analytical relations. Based on the fundamental concept of axial flux machine and the magnetic circuit analysis the following parameters of the machines are determined. It is important to note at this point the analysis is for the rated power output.

5.4.1 Fixed parameters

Many unknown parameters are involved in the design of brushless generators. As a result, it is necessary to fix some of them and then determine the remaining as part of the design. But the choice is based on the designer constraints and the application required. For this study the fixed parameters are listed at table 5.3.

Table 5.3: Fixed Parameters of the Generator

Parameter	Symbol	Value
Rated output electrical power	P_{ele}	4.5kW
Rated speed(mechanical)	ω_m	10.6rad/sec
Out diameter of the rotor	D_o	500mm
Inner diameter of the rotor	D_i	300mm
Shaft diameter	D_{shaft}	240mm
Number of phases	ϕ	3
Permanent magnet	-	NdFeB
Magnet spacer width	τ_f	0.001m
Magnet length	l_m	0.065m
Air gap	g	0.0015m

5.4.2 Electrical Speed of the Generator

It can be determined from frequency relation,

$$\begin{aligned}\omega_e &= 2\pi f & 5.20 \\ &= 2 \times \pi \times 50\text{Hz} = 314.2\text{rad/sec}\end{aligned}$$

5.4.3 Number of Slots and Magnet Poles

The rotor has an even number of magnets. That is, the number of magnet poles facing the air gap N_m is even, and the number of north South Pole pairs on the rotor is $N_p = N_m/2$. In addition, each stator slot contains the windings of a single phase; i.e., the windings are concentrated. General stator design allows more flexibility. The primary constraint on stator design is that the total number of stator slots be some even integer multiple of the number of phases, i.e.,

Number of stator slots:

$$\begin{aligned}N_s &= N_{sp} \times N_{ph} & 5.21 \\ &= 15 \times 3 = 45\end{aligned}$$

And the other terms can be calculated as follow,

Number of magnet:

$$N_m = \frac{2\omega_e}{\omega_m} \quad 5.22$$

Number of slots per pole per phase:

$$N_{spp} = \frac{N_{sp}}{N_m} \quad 5.23$$

Number of slots per pole:

$$N_{sm} = N_{spp} \times N_{ph} \quad 5.24$$

5.4.4 Coil-Pole Fraction

When N_{spp} is an integer, the distance between the sides of a given coil, i.e., the coil pitch τ_c , is equal to the magnet pole pitch τ_p . However, when N_{spp} has a fractional component, the coil pitch is less than the pole pitch and the winding is said to be chorded or short pitched. In this

case the relationship between the coil pitch and the pole pitch is given by the coil-pole fraction,

$$\alpha_{cp} = \frac{\text{int}(N_{spp})}{N_{spp}} \quad 5.25$$

Table 5.4: Results of the Analysis for Preliminary Parameters of the Generator

Parameter	Symbol	Value
Electrical speed	ω_e	314.2rad/sec
Mechanical speed	ω_m	10.6rad/sec
Number of stator coils	N_s	45
Total number of magnets	N_m	60
Number of slots per pole per phase	N_{spp}	0.25
Number of slots per pole	N_{sm}	0.75
Coil-Pole Fraction	α_{cp}	2
Number of magnetic pole pair	N_p	30

5.4.5 Geometrical Parameter

The angular dimensions of the generator can be determined by the following relations,

$$\theta_p = \frac{2\pi}{N_p} \quad 5.26$$

$$\theta_s = \frac{2\pi}{N_s} \quad 5.27$$

$$\theta_{se} = \frac{2\pi}{N_{sm}} \quad 5.28$$

$$\tau_{pi} = R_i \times \theta_p \quad 5.29$$

$$\tau_{po} = R_o \times \theta_p \quad 5.30$$

$$\tau_{ci} = \alpha_{cp} \times \tau_{pi} \quad 5.31$$

$$\tau_{co} = \alpha_{cp} \times \tau_{po} \quad 5.32$$

$$\tau_{si} = R_i \times \theta_s \quad 5.33$$

Where: θ_p is the angular pole pitch, θ_s is angular slot pitch, θ_{se} is slot pitch, electrical radian, τ_{pi} is inside pole pitch, τ_{po} is outside pole pitch, τ_{ci} is inside coil pitch, τ_{co} is outside coil pitch, and τ_{si} is inside slot pitch.

5.4.6 Distribution Factor

In reality, some reduction in peak back *emf* usually occurs because the peak values of the individual back do not coincide. Clearly, the amount of reduction is highly dependent on the shape of the back *emf* distribution. When the back *emf* is pure sinusoid, the decrease in back *emf* is given by

$$k_d = \frac{\sin\left(\frac{N_{spp} \theta_{se}}{2}\right)}{N_{spp} \sin\left(\frac{\theta_{se}}{2}\right)} \quad 5.34$$

5.4.7 Pitch Factor

The peak flux linked to the coil from the magnet is reduced simply because the net coil area exposed to the air gap flux density is reduced. The degree of reduction is given by the pitch factor k_p , which is the ratio of the peak flux linked when $\tau_c < \tau_p$ to that when $\tau_c = \tau_p$. Because the peak flux linked determines the magnitude of the back *emf* through the *BLv* law, the pitch factor gives the degree of back *emf* reduction due to chording. Therefore, the pitch factor is given by,

$$k_p = \alpha_{cp} \quad 5.35$$

5.4.8 Skew Factor

In contrast to the fractional pitch technique skewing attempts to reduce cogging torque by making dR/dd zero over each magnet face. This is accomplished by slanting or skewing the magnet edges with respect to the slot. The total skew is equal to one slot pitch and can be achieved by skewing either the magnets or the slots. Both have disadvantages. Skewing the magnets increases magnet cost. Skewing the slots increases ohmic loss because the increased slot length requires longer wire. In addition, a slight decrease in usable slot area results. In both cases, skewing reduces and smoothes the back *emf*. As stated above, the benefits of skewing do not come without penalty. The primary penalty of skewing is that it too reduces the total flux linked to the stator windings, the misalignment between each magnet and the corresponding stator winding reduces the peak magnet flux linked to the coil. As before, this

reduction is taken into account by a correction factor, called the skew factor k_s . For the square wave flux density distribution, the skew factor is;

$$k_s = 1 - \theta_{se}/2\pi \quad 5.36$$

5.4.9 Magnet Fraction

The magnet fraction for this topology is given by the following relation,

$$\alpha_m = 1 - \frac{N_m \tau_f}{\pi(R_o - R_i)} \quad 5.37$$

5.4.10 Flux Concentration Factor

It is given by the ratio of the area of the magnet and the air or equivalently it is expressed by magnet fraction as follow;

$$C_\phi = \frac{2\alpha_m}{1 + \alpha_m} \quad 5.38$$

5.4.11 Permeance Coefficient

$$P_c = \frac{l_m}{2gC_\phi} \quad 5.39$$

5.4.12 Magnet Leakage Factor

It is given by the following relation,

$$k_{ml} = 1 + \frac{2l_m N_m}{\pi^2 \mu_R \alpha_m (R_i + R_o)} \ln \left(1 + \pi \frac{g}{\tau_f} \right) \quad 5.40$$

5.4.13 Effective Air Gap for Carter Coefficient

It is expressed by the physical air gap and magnetic permeability, as shown below;

$$g_e = 2g + l_m/\mu_R \quad 5.41$$

5.4.14 Carter Coefficient

There are two more accurate ways of determining air gap permeance in the presence of slotting. The first is based on the observation that the flux crossing the gap over the slot travels a further distance before reaching the highly permeable material across the gap. As a result, the permeance can be written as $P_g = \frac{\mu_o A}{g_e}$. Here $k_c > 1$ is a correction factor that

increases the entire air gap length to account for the extra flux path distance over the slot. One approximation for k_c is known as Carter's coefficient. By applying conformal mapping techniques, Carter was able to determine an analytic magnetic field solution for the case where slots appear on both sides of the air gap. Through symmetry considerations it can be shown that the Carter coefficient for the aligned case, i.e., when the slots are directly opposite each other, is an acceptable approximation to the geometry. There are two expressions for Carter's coefficient but for this application the relation suggested by Nasar (1987) is used, [56]

$$k_c = \left[1 - \frac{1}{\frac{\tau_{sl}}{\omega_s} \left(5 \frac{g_c}{\omega_s} + 1 \right)} \right]^{-1} \quad 5.42$$

5.4.15 Air Gap Area

The air gap area of the generator is expressed by the following relation using the external dimensions (radius) of the generator;

$$A_g = \frac{\pi(1 + \alpha_m)}{2N_m} (R_o^2 - R_i^2) \quad 5.43$$

5.4.16 Air Gap Flux Density

The flux density in the air gap between the rotor and the stator is expressed by the following relation and determined by substitution as follow;

$$\begin{aligned} B_g &= \frac{C_\phi}{1 + \mu_R k_c k_{ml} / P_c} B_r \quad 5.44 \\ &= \frac{0.88}{1 + 1.05 \times 1.0003 \times 4.09 / 24.3} 1.33T = 1.001T \end{aligned}$$

And the air gap flux is the product of the flux density and the air gap area,

$$\begin{aligned} \phi_g &= B_g A_g \quad 5.45 \\ &= 1.001T \times 0.001884m^2 = 0.001885884W \end{aligned}$$

Using the above equations the major geometrical parameters and design factors are determined. The results of the analysis are tabulated at table 5.5.

Table 5.5: Calculated Value of the Geometrical Parameters and Factors of the Generator

Parameter	Symbol	Value
Angular pole pitch	θ_p	0.209rad
Angular slot pitch	θ_s	0.1395rad
Slot pitch, electrical radian	θ_{se}	8.37rad
Inside pole pitch	τ_{pi}	0.03135m
Outside pole pitch	τ_{po}	0.05225m
Inside coil pitch	τ_{ci}	0.0627m
Outside coil pitch	τ_{co}	0.1045m
Inside slot pitch	τ_{si}	0.02093m
Distribution factor	k_d	4
Pitch factor	k_p	2
Skew factor	k_s	0.33
Magnet fraction	α_m	0.8
Flux Concentration Factor	C_ϕ	0.89
Permeance Coefficient	P_c	24.3
Magnet leakage factor	k_{ml}	4.09
Effective Air Gap for Carter Coefficient	g_e	0.065m
Carter Coefficient	k_c	1.0003
Air Gap Area	A_g	0.001884m ²

5.5 EQUIVALENT CIRCUIT

The steady state performance of the AFPM generator is calculated with the use of an equivalent circuit in generator mode. It is sufficient to model only a single phase of an electrical generator [62]. The induced electromotive force (EMF), which is created by the air gap flux linkage, is represented by an ac voltage source, E_{gen} . E_{gen} is connected in parallel with a resistor, R_{eddy} , which models the eddy current losses in the stator. This parallel combination is connected in series with a resistor and an inductor, R_i and L_i , which represents the internal impedance of the AFPM generator. The internal inductance of the generator, L_i , actually consists of the combination of mutual, leakage and end winding leakage inductance, but it is difficult to distinguish between these inductances in a coreless AFPM machine [63].

The resultant current, I_{ac} , is chosen as owing out of the generator model, while the voltage measured across the terminals of the generator is V_{gen} .

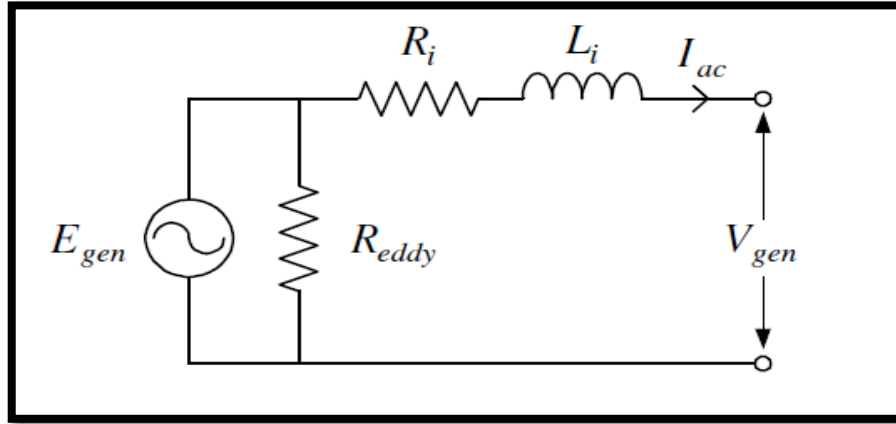


Figure 5.14: Equivalent Circuit of the AFPM Generator

5.5.1 Induced Phase Voltage

The induced phase voltage of the generator is affected by the structure of the winding (i.e. overlapping or non overlapping winding). The RMS value of sinusoidal phase voltage of the non overlapping winding, E_{gen} , can be calculated by [64]

$$E_{gen} = \frac{N_{sp}}{a} \frac{2\sqrt{2}}{N_p} \omega_e B_p N_t R_e l_a k_{pc} k_d \quad 5.46$$

Where: B_p is the peak air gap magnetic flux and given by,

$$B_p = \frac{2\sqrt{3}B_g}{\pi} \quad 5.47$$

k_{pc} is the pitch factor of the non overlapping winding, and can be determined from the following relation.

$$k_{pc} = \frac{\sin\left(\frac{\theta_m(1-k)}{2}\right) \sin\left(\frac{k\theta_m}{2}\right)}{\left(\frac{k\theta_m}{2}\right)} \quad 5.48$$

Where:

$$\theta_m = \frac{\pi N_p}{N_s} \quad 5.48$$

$$k = \frac{\theta_{re}}{\theta_m} \quad 5.49$$

$$\theta_{re} = \left(\frac{R_i + l_g}{R_i} \right) \pi / 3 \quad 5.50$$

$$l_a = R_o - R_i \quad 5.51$$

And, k_d is the distribution factor.

5.5.2 Phase Resistance

The phase resistance models the copper losses in the stator winding of the AFPM machine.

The per phase stator resistance, R_i , can be calculated by [64],

$$R_i = \frac{N_t^2 N_{sp} \rho_t (2l_a + l_e)}{a^2 k_f h_a w} \quad 5.52$$

Where: ρ_t is the resistivity of copper at operating temperature of the machine. The average length of a turn of the winding is calculated by the term in brackets where, l_e is the end winding length of the over- or non overlapping windings, k_f is the filling factor, h_a is the axial height and w is the width of a coil side. ρ_t can be calculated by,

$$\rho_t = \rho_{20} (1 + 0.0039(t_c - 20)) \quad 5.53$$

Where: ρ_{20} is the resistivity of copper at 20°C and t_c is the operating temperature of the machine. The end winding length of the non overlapping winding, l_e , can be calculated by [64],

$$l_e = 2\theta_m (R_o + R_i) \frac{1 - 0.06k}{N_p} \quad 5.54$$

The filling factor, k_f , is defined as the ratio of copper in the area of a coil side. k_f was found from practice to be calculated as 0.42. The coil side width, w , can be calculated by,

$$w = 2R_e \sin \frac{\theta_{re}}{N_p} \quad 5.55$$

5.5.3 Stator Inductance

The inductance of a phase winding consists mainly of mutual and leakage inductances. The AFPM generator utilizes a coreless stator winding topology, which results in a stator winding with a low internal inductance, L_i . The low value of the inductance is very difficult to measure accurately. Therefore, it would be advantageous to calculate the value. A formula for

calculating the inductance of the non overlapping winding was adapted from the air cored multilayer solenoid formula. The inductance of the non overlapping winding, L_i , can be calculated as [66],

$$L_i = \frac{N_{sp}(2l_a + l_e)N_t^2}{h_a} 10^{-7} K_n \quad 5.56$$

During operation the coil is magnetized, which results in the magnetic field no longer being uniform in the winding and therefore a correction factor, referred to as the Nagaoka constant, K_n , is required. The K_n constant can be expressed as [66]

$$K_n = \frac{1}{1 + 0.9 \frac{2l_a + l_e}{2\pi h_a} + 0.32 \frac{2\pi w}{2l_a + l_e} + 0.84 \frac{w}{h_a}} \quad 5.57$$

5.5.4 Eddy Current Loss

The electromagnetic losses in an electrical machine can be divided into iron losses and copper losses, where the iron losses consist of hysteresis and eddy current losses and the copper losses consist of ohmic and eddy current losses [67]. Due to the coreless nature of the AFPM machine there are no iron losses present in the stator core. Also, in a synchronous AFPM machine, the rotor disks rotate at the same speed as the rotating magnetic field in the stator. Therefore, the iron losses in the permanent magnets and the rotor disks can be ignored as there is no change in the flux direction in the rotor back yoke. As a result, the iron loss components for both the rotor and the stator do not need to be modeled and are therefore ignored. The ohmic loss component of the copper losses of the stator windings is modeled by the resistor, R_i .

The eddy current loss component of the copper losses is created by the alternating magnetic fields in the stator winding. The alternating field is created by the permanent magnets sweeping over the conductors in the stator windings. Therefore, if the machine is operated at relatively high frequencies, the induced eddy currents can result in substantial losses within the machine. These losses will result as an increase in the temperature of the stator windings and effectively decrease the efficiency of the machine.

The eddy current loss effect in an AFPM machine for low frequency operation is negligible. But, if the AFPM machine is to be operated at higher rotating speeds or has a higher pole number, thereby effectively increasing the operating frequency, the eddy current loss

component will increase and cannot be ignored. The eddy current losses in the AFPM stator winding, P_{eddy} , can be calculated from [68],

$$P_{eddy} = \frac{\pi l_a d^4 B_p^2 \omega_e^2 N_s N_p}{32\rho} \quad 5.58$$

The eddy current losses in the stator winding of the AFPM machine can be modeled with the use of a resistor, R_{eddy} , which is connected in parallel with the back EMF. The value of the resistor, R_{eddy} , can be calculated by,

$$R_{eddy} = \frac{3E_{gen}^2}{P_{eddy}} \quad 5.59$$

5.5.5 Electromagnetic Torque

The developed torque of the machine, T_d , can be calculated by [64]

$$T_d = k_s k_e k_r C_1 \quad 5.60$$

Where: k_s is the stator factor, k_e is the end winding factor, k_r is the radius factor and C_1 is a machine parameter. The stator factor for non overlapping winding is given by,

$$k_s = k_{wc} \sqrt{\frac{k\pi}{3}} \quad 5.61$$

Where the winding factor of the non overlapping winding, k_{wc} , is calculated by,

$$k_{wc} = k_p k_d \quad 5.62$$

The end winding factor of the non overlapping winding, k_e , is calculated by,

$$k_e = (2 + \delta)^{-\frac{1}{2}} \quad 5.63$$

Where: δ is given by,

$$\delta = \frac{l_e}{l_a} \quad 5.64$$

The radius factor, k_r , is given by,

$$k_r = \sqrt{(1 + \sigma_r)^3 (1 - \sigma_r)} \quad 5.65$$

Where: σ_r is given by equation 5.66,

$$\sigma_r = \frac{R_i}{R_o} \quad 5.66$$

Finally, the machine parameter, C_1 , is given by,

$$C_1 = R_o^2 B_p \sqrt{1.5 P_{cu} k_f h_a / \rho_t} \quad 5.67$$

Where the copper loss is given by,

$$P_{cu} = 3I_{ac}^2 R_i \quad 5.68$$

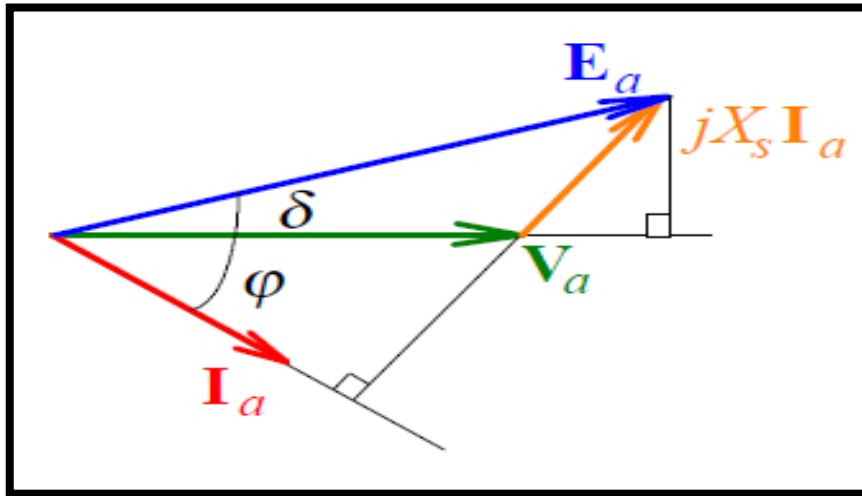


Figure 5.15: Phasor Diagram of the AFPM Generator

From the Phasor diagram of the machine it is possible to develop the following relations,

$$E_{gen} \cos\varphi = V_{gen} - R_i I_{ac} \quad 5.69$$

$$E_{gen} \sin\delta = X_s I_{ac} \cos\varphi \quad 5.70$$

The total generated electrical power at the output terminal can be given as,

$$P_{ele} = 3V_{gen} I_{ac} \cos\varphi \quad 5.71$$

The power factor, $\cos\varphi$, is defined as the ratio of the active power to apparent power, or mathematically,

$$\cos\varphi = \frac{\text{active power}}{\text{apparent power}} = \frac{P_{ele}}{I_{ac}^2 Z} \quad 5.72$$

Where: Z is the impedance of the generator, the combined effect of the resistance and inductance properties of the generator.

$$Z = \sqrt{R_i^2 + (\omega_e L_i)^2} \quad 5.73$$

Using equations 5.69, 5.70, 5.71, and 5.2, the output phase voltage, V_{gen} , the phase current, I_{ac} , the load factor, φ , and the load angle, δ , under rated conditions are determined.

5.5.6 Cut in Speed of the Generator

The rated output voltage of the wind generator, E_{gen} , at the rated speed, n_{rat} , is a function of the cut in speed of the generator, n_{in} , and can be calculated by,

$$E_{gen} = V_{gen} \frac{n_{rat}}{n_{in}} \quad 5.74$$

5.5.7 Efficiency of the Generator

The efficiency of the generator can be determined by calculating the mechanical power and the electrical power supplied and generated, respectively. Mathematically the efficiency of the AFPM generator under the rated conditions is given by the following relation,

$$\eta_{generator} = \frac{P_{ele}}{P_{mecha}} \times 100\% \quad 5.75$$

Then substitution for the electrical and mechanical power will give us,

$$\eta_{generator} = \frac{V_{gen} \cos\phi}{E_{gen} \cos\delta} \times 100\% \quad 5.76$$

Table 5.6: Characteristics of the Design Generator under Rated Conditions

Parameter	Symbol	Value
Generated back EMF	E_{gen}	196.3V
Output phase voltage	V_{gen}	130.V
Output phase current	I_{ac}	9.92Amp
Phase resistance	R_i	0.779Ω
Phase inductance	L_i	0.0563H
Phase impedance	Z	17.76 Ω
Load factor	$\cos\phi$	0.9
Load angle	δ	5.7 degree
Power output	P_{ele}	4.5kW
Cut in speed	n_{in}	3.8m/s
Efficiency	$\eta_{generator}$	0.815
Copper loss	P_{cu}	229.97W
Torque developed	T_d	273.2Nm

In this chapter the design of axial flux permanent magnet generator was completed. the result of the design showed the generator has 3.8m/s cut in speed with 81.5% efficiency so that is capable of generating electricity at lower wind speeds. In the preceding chapter the manufacturing method of components will be discussed.

CHAPTER SIX

MANUFACTURING

6.1 INTRODUCTION

In the preceding chapters the major components and the system are design. Based on the results founded the manufacturing of the components and the assembling techniques will be discussed in this chapter.

The quality of a product and its performance is very dependent on the production method used and the raw materials accessed in addition to the design approaches incorporated. In the first section of this chapter the manufacturing methods for the major electrical and mechanical components will be discussed. The wind blade can be manufactured from wood either by laminating with epoxy or from solid wood only by making the airfoil shape. In the next section prototyping and its test result will be displayed. Finally the performance of the prototype will be compared with the theoretical values. The manufacturing methods are limited to consider the domestic technology advancement so that it is possible to manufacture the components locally.

6.2 BLADE MANUFACTURING

The blades material used for the design was a Douglas fir which is domestically called ‘tid’ laminated with epoxy resin. The basic drawbacks of using wood for engineering material is its moisture content by which its material strength is affected.

The basic principle of laminating wood has been used effectively for many years. The major difference between a standard wood laminate (such as plywood) and the new wood resin composite is that as much as 20 to 25 percent of this new material is resin. The main reason for this change in approach is to provide the wood fiber with maximum protection against moisture. A second reason is to provide sufficient resin to fill the inevitable voids and gaps that can occur with low pressure bonding and thus reduce the number of defects that might act as nuclei for failures [31].

There are two common joints available, scarf and butt joint and both can be used successfully for this application.

As already discussed, most of the problems with wood are moisture related. The basic approach is to seal all wood surfaces with a properly formulated resin system. A typical

laminated using 1/10-in.-thick veneers will have nine glue lines per inch of thickness, and each glue line must be penetrated by water vapor to either increase or decrease the moisture content of the entire laminate. All subsequent joints in the wood/resin composite structure must also be sealed at the same time a proper bond is being made.

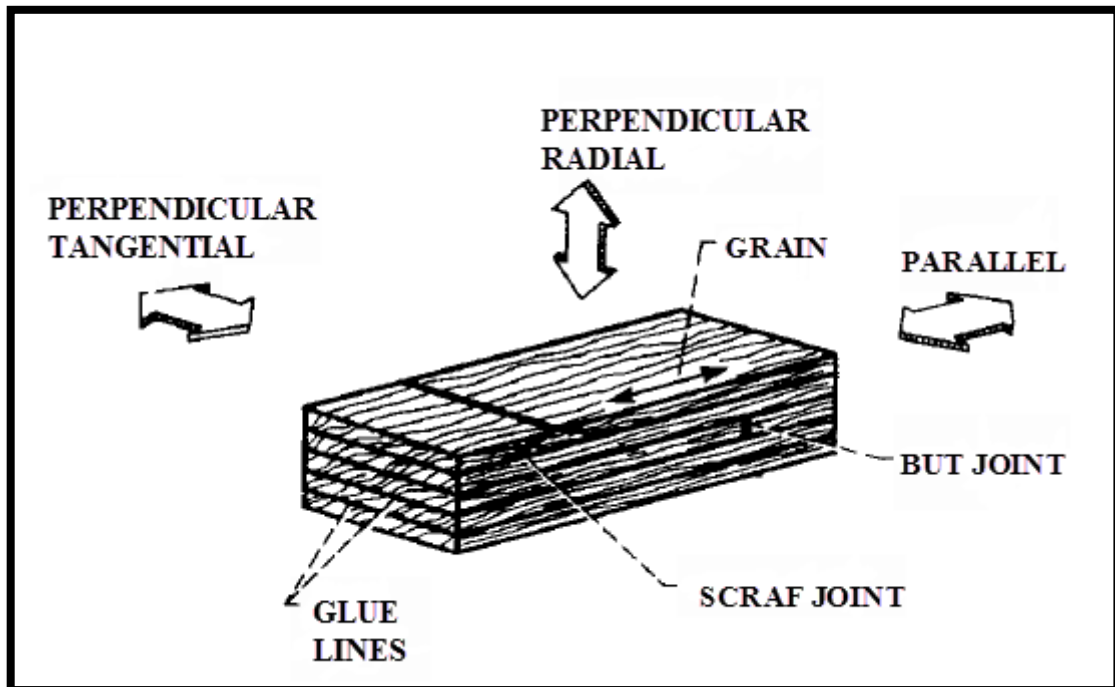


Figure 6.1: Grain Orientation in Laminate and Illustration of Type of Laminate Joints [31]

The complexity of blade manufacturing is directly affected by its airfoil shape and its angle of twist along the span. Airfoils with nearly flat shape at one side are easy to manufacture as compared to symmetrical airfoil. The airfoil selected for this thesis i.e. NACA 4412 is suitable to manufacture by the method suggested by reference [69]. The blade manufacturing process suggested by reference [69] involves forming the curved laminate in a compression mold, removing the excess wood from the edges with band saw, forming the twisted flat bottomed airfoil with an automatic sanding machine, and following by usual manual hard finishing and drilling the completed blade.

One of primary goal of this thesis work is to identify a simple manufacturing technique for the components so that the above manufacturing technique suggested is modified in suitable manner as is can be applicable without using the high cost machines suggested by the inventor.

The manufacturing process for the blade begins by preparing a mold for the lower half of the airfoil (for the flatted bottom side) with the following specification (table 6.1).

After the female mold with the above specification is prepared the thin sheets of Douglas fir veneer will be prepared then after each veneer will be laminated one over the other to form the upper convex airfoil shape on the mold. The wood veneer will form the airfoil shape by laminating with epoxy. The final outlook will look like as shown on figure 6.2.

Table 6.1: Female Mold Width and Twisting Angle Distribution along the Span

Radius	Width	Twist angle relative to the tip(degree)
0.250	0.400	38.52
0.825	0.383	24.33
1.375	0.292	10.75
1.925	0.201	6.831
2.475	0.154	5.780
3.025	0.140	4.730
3.575	0.126	3.679
4.125	0.112	2.629
4.675	0.085	1.578
5.225	0.069	0.528
5.500	0.062	0.003

The twist angle increases as it goes for the tip of the blade to the root.

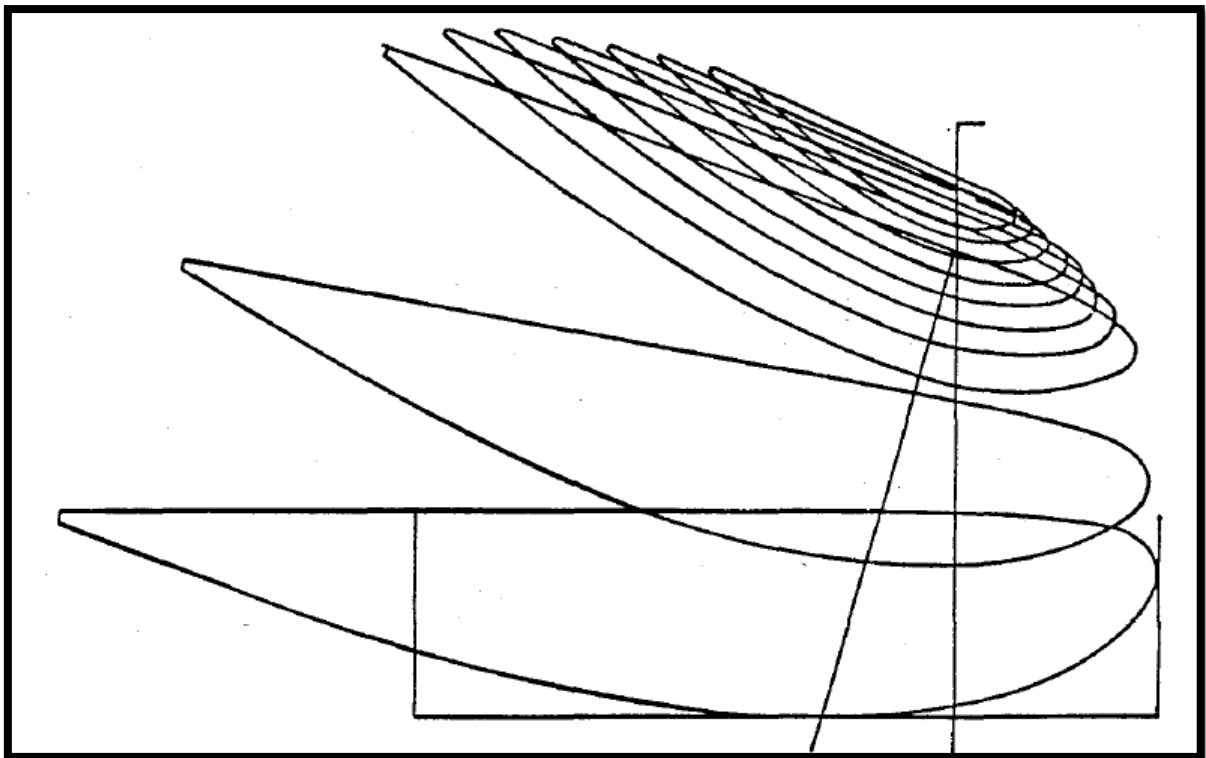


Figure 6.2: Twist of the Blade Airfoil [69]

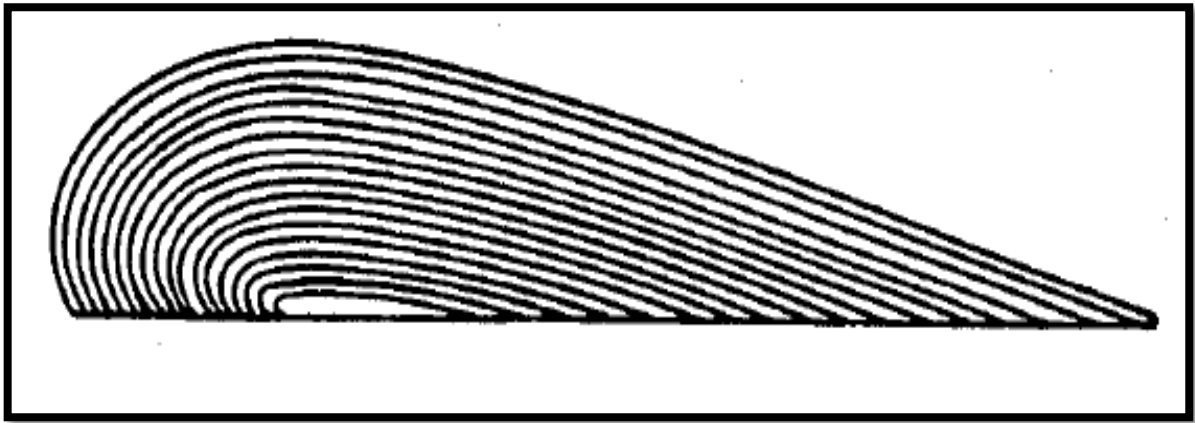


Figure 6.3: The Shape of the Laminated Wood/Epoxy Blade [69]

After the preliminary shape of the blade is construed compression will follow, this may be done using manual screw compression tools and the upper mold pared with similar shape as the outer shape of the blade airfoil. The compression process will harden the wood/epoxy laminate. One full day compression is enough for this application. The final labor intensive work for completing the blade manufacturing process is surface finish and painting to improve its performance. Drilling for bottled joint also will be done as per the part drawing. The detail part drawing for the blade is attached at the annex C.

6.3 HUB MANUFACTURING

Casting is a manufacturing process suggested by many manufactures and literatures. This is because of the structural complexity of the hub assembly and the metal casting process is the simplest, most direct route to a near net shape product, and often the least expensive. This process in its fundamental form requires a mold cavity of the desired shape and molten metal to pour into the mold cavity. The schematic description of casting process is shown below,

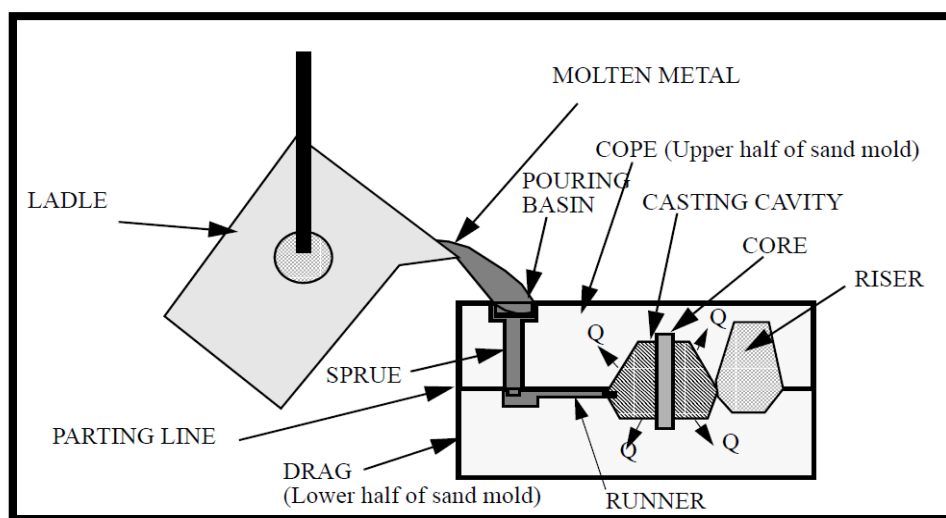


Figure 6.4: Casting Components for Hub Casting [70]

Producing a “good” casting requires a design effort to:

1. Create a gating system (pouring basin, sprue, runner) to bring molten metal into the mold cavity free from entrapped slag, sand or gases.
2. A riser which feeds liquid metal into the casting cavity as the liquid is cooling and solidifying (all liquid metals will shrink as they cool and most liquid metals will shrink as they solidify). The riser may have to provide up to 5 - 7% by volume for the casting as it solidifies.
3. Control heat flow, Q in the above figure, out of the casting so that the last liquid to solidify is in the riser.
4. Control the rate of heat flow so as to control the nature of the solidified product.

Table 6.2: Casting Processes, Mold and Metal Details [70]

Casting Processes	Mold Material	Manner of Entry	State of Metal	State of Mold Cavity
Sand Casting	Sand(Bonded with clay and water or chemicals)	Gravity	100% Liquid	Air
Permanent Mold	Metal	Gravity	100% Liquid	Air
Die Casting	Metal	Pressure	100% Liquid	Air
Investment	Ceramic	Gravity	100% Liquid	Air, Vacuum, Gas
Lost Foam EPC	Sand (Unbounded)	Gravity	100% Liquid	Styrofoam, PMMA
Thixocasting Rheocasting	Metal	Pressure	>50% Liquid Balance Solid	Air
Cosworth	Sand	Vacuum	100% Liquid	Air
V Process	Sand(Unbounded with Vacuum and Enclosing Plastic Film)	Gravity	100% Liquid	Air
Centrifugal	Metal, Graphite	Centrifugal Forces	100% Liquid	Air, Gas Shroud
Ingot - NOT Cast to Shape	Metal or electro-magnetic Field	Gravity	100% Liquid	Air or Gas Shroud
Casting Processes	Mold Material	Manner of Entry	State of Metal	State of Mold Cavity
Sand Casting	Sand(Bonded with clay and water or chemicals)	Gravity	100% Liquid	Air
Permanent Mold	Metal	Gravity	100% Liquid	Air

Modern industrial castings are produced by a wide variety of processes, processes which are broadly defined in terms of: I, the type of mold material (sand, permanent, etc.); II, the manner in which the molten metal is introduced into the cavity (gravity, pressure, vacuum);

III, the state of the metal (percent which is liquid); IV, the state of the mold cavity itself (air, vacuum, solid, gas).

6.3.1 Casting Design Steps

1. Physical design of part to be cast purpose of casting (size, shape), tolerances (manufacturing and engineering), dimensional change in processes, relationship of this part to others to optimize its design (concurrent engineering),
2. Material selection for part to be cast mechanical and physical properties, cast ability, section size sensitivity, fluid flow properties,
3. Pattern production for molds and cores gating and riser design, fluid flow and heat transfer,
4. Casting process selection, casting production limitations due to metal cast, casting size, dimensional requirements cost to produce,
5. After casting processing machining, heat treating, welding,
6. Evaluation of cast product.

The casting design process is an iterative procedure, requiring excellent communication in all steps of the process. Among the casting processes stated sand casting is selected for this application, by taking availability as a major criteria.

6.3.2 Sand Casting Processes

Molding sands account for the production of the major quantity of castings. Sand is used in the ratio of as much as 10 tons of sand per ton of metal to as little as 1/4 ton of sand per ton of metal depending upon the type and size of casting and the molding method employed. The majority of castings are made in green sand molds, molds whose major components are sand (usually silica, SiO₂), clay such as bentonite, and water. The clay - water combination is responsible for the binding action between the sand grains, and can be present in various amounts from 5 to 50 percent by weight. Typical green sand might contain 6 % clay and 3 % water, materials which are replenished as the molding sand is reconstituted and reused again and again. In the ideal world, the sand grains would be reused forever. In actual fact the sand grains themselves suffer some attrition due to mechanical, thermal, and chemical attack in the course of their use and so must be replaced on a consistent basis, usually through the production of cores. The mold should have to be design based on the drawing for the hub dimensions determined during the design process. The drawing is attached at annex C. After

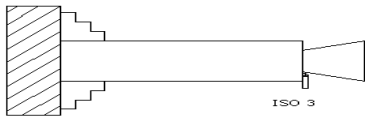
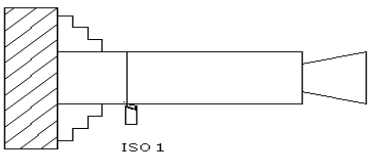
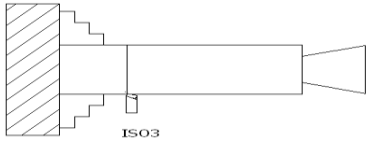
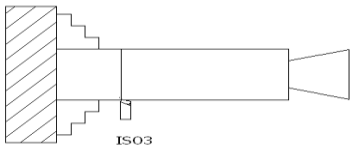
casting process is completed surface finish need to be done for good outcome of the component.

6.4 MAIN SHAFT MANUFACTURING

The main shaft is made of hot rolled steel. The surface finish requirement is the basic constraint for the shaft manufacturing. The manufacturing method for the shaft is machining. The part drawing of the shaft is attached at annex c. the manufacturing process of the shaft is stated below with flow chart.

Step one: preparation of the cylindrical shaft on the lathe machine

Table 6.3: Flow Chart for Shaft Manufacturing

Steps of the operation	Cutting Tools	Possible working value			Illustration with diagram
		Speed (v)m/min	Feed (mm)	n (r.p.m)	
Round shaft having diameter 300mm and length of 800mm. Cutting using power hacksaw.	Depend upon the saw used				
After this the raw material is held in the chuck and facing is done on one side.	Cemented carbide cutting tools tips.ISO ₃ (DIN4978)	75	0.2	450	
After facing, the work piece is held between centers and rough turning is done.	Cemented carbide cutting tools tips. ISO ₁ (DIN4971)	60	0.4	350 450	
After rough Turing, the work piece is held between centers and turning is done.	Cemented carbide cutting tools tips.ISO ₃ (DIN4978)	75	0.2	450	
Finish the long side of the work pieces.	Cemented carbide cutting tool tips.ISO ₃ (DIN4978)	150	0.1	1400	

Step two: Key groove drilling

Key is vital element to connect the hub and shafts to be transmit motion from the hub to the shaft. For this, shaft in a horizontal position and is mounted on a radial drilling (milling) machine since key groove have to be drilled perpendicular to the horizontal axis. Radial drilling, shaper or milling machine is used.

Step three: Heat Treatment

Regarding the steel alloys typically used in high-grade shafts, the desired ultimate (and hence yield and fatigue) strength of the material is produced by a 'heat treatment'. The typical heat-treating process for carbon-steel alloys is first to transform the structure of the rough-machined part into austenite crystalline structure by heating the part in an oven until the temperature throughout the part stabilizes in the neighborhood of 1550°F to 1650°F) in an Induction furnace for about 2 hours (Hardening). Next, the part is removed from the heating oven and rapidly cooled in a medium of oil (Quenching) to extract heat from the part at a rate sufficient to transform a large percentage of the austenitic structure into fine-grained martensite. The desired martensitic post-quench crystalline structure of the steel is the high-strength, high-hardness, form of the iron-carbon solution. The rate of cooling required to achieve maximum transformation varies with the harden-ability of the material, determined by the combination of alloying elements.

After quenching the alloy steel material has reached a very high strength and hardness, but, it lacks sufficient ductility and impact resistance. In order to produce the combination of material properties deemed suitable for a given application, the part is placed in a 'Tempering' oven and soaked for a specific amount of time at temperature of 800 to 900 degree Celsius in order to reduce the hardness to the desired level, hence producing the desired strength, ductility, impact resistance and other desired mechanical properties. For this process induction furnace is used.

Step four: Shot Blasting

Black oxide layer formed during heat treatment process is removed by shot blasting. Shot blasting is a process that is often used to clean the surface of a material. The process usually involves a gun that is used to shoot various types of media, or shot, at the object being blasted. This is a particularly effective method for removing scale, rust, paint, and minor surface flaws from metal objects. In addition it helps to reduce the residual stresses developed during the heat treatment process.

Step five: Greasing

Grease or lubricating oil is applied on all the areas of the shaft which helps to prevent the corrosion on the faces.

Step six: Inspection

Detailed and proper documentation of all inspection results are maintained at various quality assurance stages. The inspection process includes:

- Record for raw material analysis.
- Record of dimensional check at different stages of machining and drilling.
- Measurement of surface roughness using surface roughness meter.
- Using dial Indicators for the measurement of run out.
- Using venire calipers for dimensional checks.

6.5 ROTOR MANUFACTURING

The rotor of the generator is an assembly of the back steel disk and the permanent magnets. The magnets are attached to the steel disk using epoxy. The major determining factor in the rotor manufacturing is the centrifugal force on the joint between the disk and the permanent magnets. The manufacturing process starts with the preparation of the steel disk.

Step one: prepare the still disk having the required dimensions as stated in the design, the detail part drawing is available at annex c. the key way and the inner hole to join with main shaft must be prepared before the magnets are attached.

Step two: during the machine process the rotor disks may have some oiling and unwanted extended objects, for better connection between the disks the magnets clean the disk properly.

Step three: divide the disk using a divider with 12 degree spacing circumferentially and make a mark. These marks are the places to attach the magnets to the disk.

Step four: now it is the final step to finish the rotors, using epoxy resin attach the magnets to the disks at the marked points. It should be noted that the each successive magnets have different magnetic pole, north-south-north arrangement. Then wait till the epoxy resin dried.

6.6 STATOR MANUFACTURING

The stator is mounted at three points around its periphery, using three more 1/2" [12 mm] studs. The coils embedded within it are dimensioned such as to encircle the flux from one

magnet pole at a time. As the magnet blocks pass a coil, the flux through the coil alternates in direction. This induces an alternating voltage in each turn of the coil. The voltage is proportional to the rate of change of flux. Voltage therefore depends on:

- The speed of rotation
- The density of the flux
- The number of turns in the coil.

The number of turns of wire in each coil is used to control the speed of the wind turbine. If the number of turns is large, then the output will reach battery voltage and start to charge the battery at a low rotational speed (rpm). If we use fewer turns of thicker wire in the coils, then it will need to run faster. The number is chosen to suit the rotor blades and also the battery voltage. There are 45 coils in the stator.

Step one: selecting wire

The size and number of turns in each coil has a determining effect on the output of the generator.

Step two: winding the coils

The coils can be wined either manually or using winding machine, with winding dimension 25×41mm and 90turns for each coil.

Step three: connecting the coils

In the previous step 45 coils with 90 numbers of turns are prepared; at this stage they will connect to have combined output. The connection used is series/star connection. The schematic representation is shown below.

Step four: output wiring

The output of the stator must be flexible insulated wire. They need to be more robust than the winding wires because they will be subjected to bending, vibration and abrasion of various kinds.

Step five: stator molding

After these all completed, the connected coils will molded using epoxy resin or other strengthen materials.

6.5 PROTOTYPE MANUFACTURING

The validation of design process that was done till now will be checked using prototype developed in the workshop. To produce accurate result the prototype manufactured from material similar to the materials selected during the design with dimensions scaled as 1:4.6 with the designed dimensions.

The blades are manufactured from local Douglas fir with radius of 1.2m for each blade. Circular saw was used to make the shape of the blade and followed by surface finishing works to improve the outer surface roughness. The dimensions of the prototype are tabulated at table 6.4.

Table 6.4: Dimension of the Blade of the Prototype

Section	Radius	Chord	Maximum Thickness	Maximum Camber	Location of Maximum Camber	of Twist Angle
1	0.06	0.0933	0.0112	0.00373	0.0373	6.420
2	0.18	0.0816	0.0097	0.00326	0.0326	4.055
3	0.3	0.0574	0.0068	0.00229	0.0229	1.792
4	0.42	0.0431	0.00517	0.00172	0.0172	1.138
5	0.54	0.0342	0.00411	0.00137	0.0137	0.963
6	0.66	0.0283	0.00340	0.00113	0.0113	0.788
7	0.78	0.0241	0.00289	0.00096	0.0096	0.613
8	0.9	0.0210	0.00252	0.00084	0.0084	0.438
9	1.02	0.0185	0.00222	0.00074	0.0074	0.263
10	1.14	0.0166	0.00199	0.00066	0.0066	0.0880
tip	1.2	0.0158	0.00190	0.00063	0.0063	0

The blade and hub assembly of the prototype is shown at figure 6.9, and the manufacturing process for the blades is as follow:

Step one: Selecting the Wood

The wood should be well seasoned and free of sap and avoid and knots in the blank prepared. The tree type to be used is has great impact on the strength of the blades it must be carefully selected, cedar, Douglass fir, and larch are good material for this application. For this specific case Douglas fir was used as stated in the design. Then from this material prepare 125×40×1300mm blank for each blades (three blanks)

Step two: create the taper shape along the blade span

As stated in the table 6.4 the blades are narrow at the tip and wider at the root. To make the taper follow the following steps;

- Mark out the stations by measuring from the root of the workpiece.
- Draw a line around the workpiece at each station, using a square.
- Mark the correct width at all station, measuring from the leading edge and join the marks up with a series of pencil line.
- Cut along these lines with a band saw, it is possible to use a circular saw to make the taper.

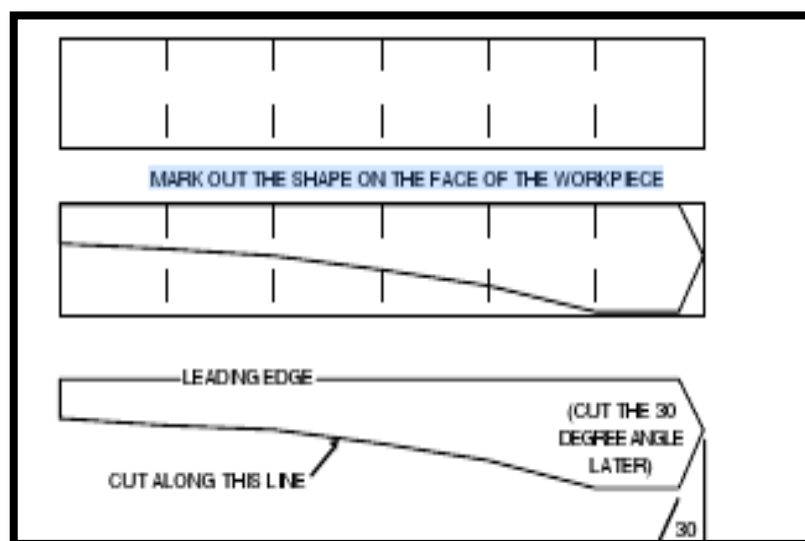


Figure 6.5: Creating the Taper of the Blades [74]

Step three: carving the twisted windward face

The windward face of the blade will be angled, but somewhat flat. Like the underside of the aircraft wing. The angle will be steeper (removing more wood) at the root than it is at the tip. The reason why blades angle should change is because the blade –speed becomes slower as we approach the center. This affects the angle of the apparent air velocity striking the blade at each station.

- Mark the stations on the face you cut out in step one.
- Mark the 'drop' on each of these lines measured from the face of the wood and mark this position of the trailing edge at each station.
- Join these marks to form the line of trailing edge.

- Remove all the wood above the trailing edge line, so that you can place a straight edge between the leading and trailing edges.

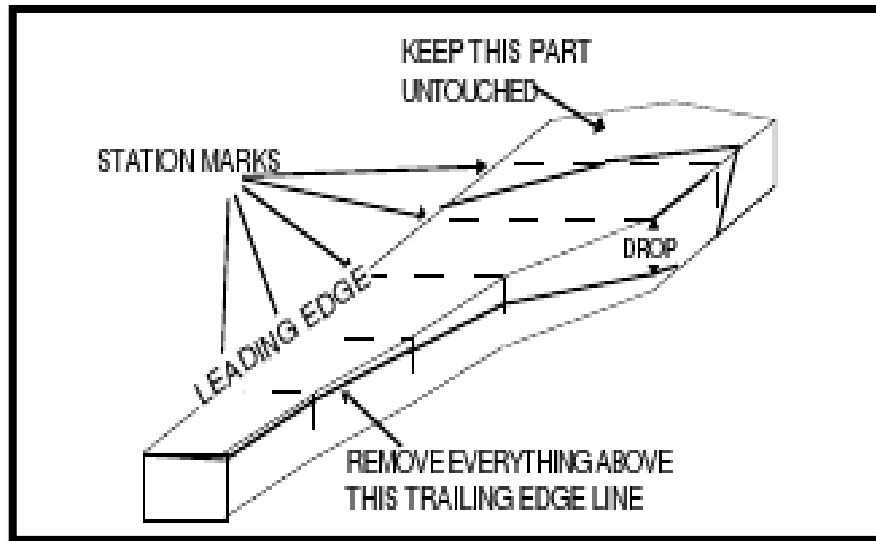


Figure 6.6: Carving the Twisted Windward Face [74]

Step four: carving the thickness

- At each station, measure the appropriate thickness from the windward face, and make a mark. Join the marks to form a line, do this again at the trailing edge.
- Where the thickness runs out at the trailing edge, draw a diagonal line across the back of the workpiece to meet the line at the leading edge.
- These lines will guide you as you carve the section, to achieve the correct thickness. Carve the back of the blade down to these lines.

Both sides of the blade should now be flat and parallel to each other, except at the inner part where this is not possible, because the workpiece is not thick enough to allow full thickness across the whole width. In this area you need not worry about the part nearer to the trailing edge, but try to make the faces parallel where you can. The final blade section will only be full thickness along a line that runs about 30% of the distance from leading to trailing edges.

Step five: Carve the curved shape on the back of the blade

The blade is nearly finished now. The important dimensions, width, angle and thickness are all set. It only remains to give create a suitable airfoil section at each station. If this is not done, the blade will have very high drag. This would prevent it from working well at high tip speed ratio. The first part of this step is to make a feathered trailing edge. Take great care to cut only into the back of the blade. This is the face you just cut out in step three. Do not touch the front face (the carved front face in step two.)

- Draw two lines along the back of the blade, at both 30% and 50% width measured from the leading toward the trailing edge. The 50% line is to guide you in carving the feathered trailing edge.
- Now carve off the part shown hatched, between the trailing edge and the middle of the blade width. This will form the correct angle at the trailing edge. When you have finished, it should be possible to place a straight edge between this line and the trailing edge. The trailing edge should be less than 1 mm thick.
- When this is done, the blade has to be carved into a smoothly curving shape according to the section shown.

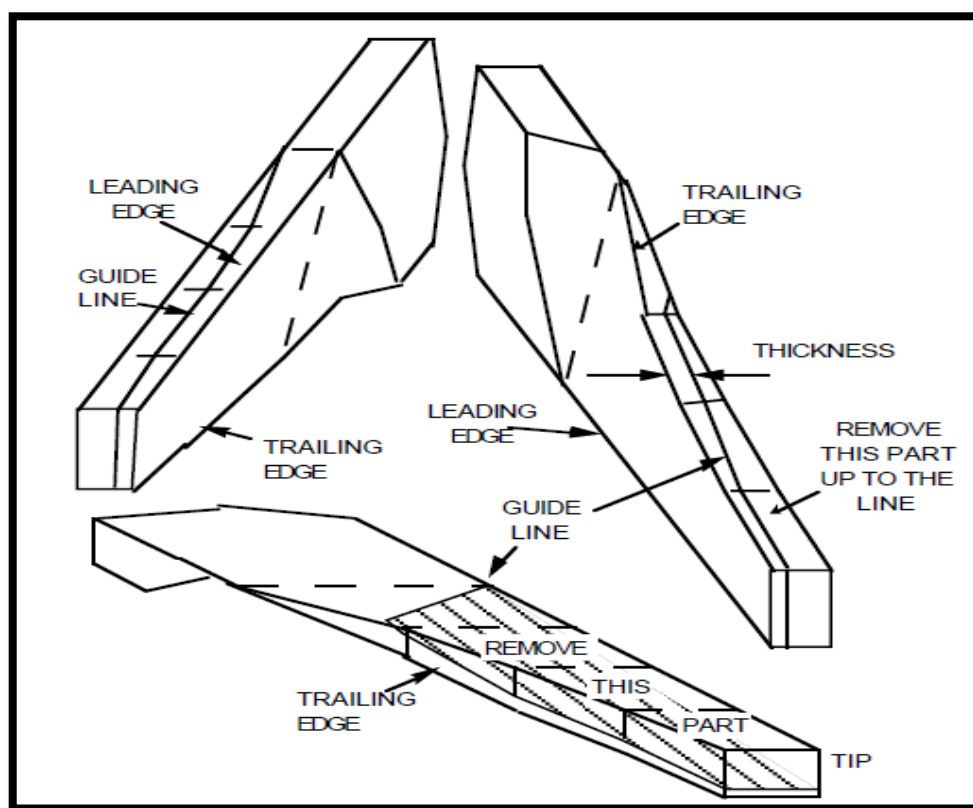


Figure 6.7: Carving the Thickness [74]

It is hard to prescribe exactly how to produce the curve. The best description is simply ‘remove any corners’. As you remove corners, you will produce new corners, which in turn need to be removed. Run your fingers over the wood lightly to feel for corners. Remove less wood each time.

Take care not to remove too much wood. The 30% line represents maximum thickness part and should not be carved down further. Take care not to produce a corner at this thickest point.

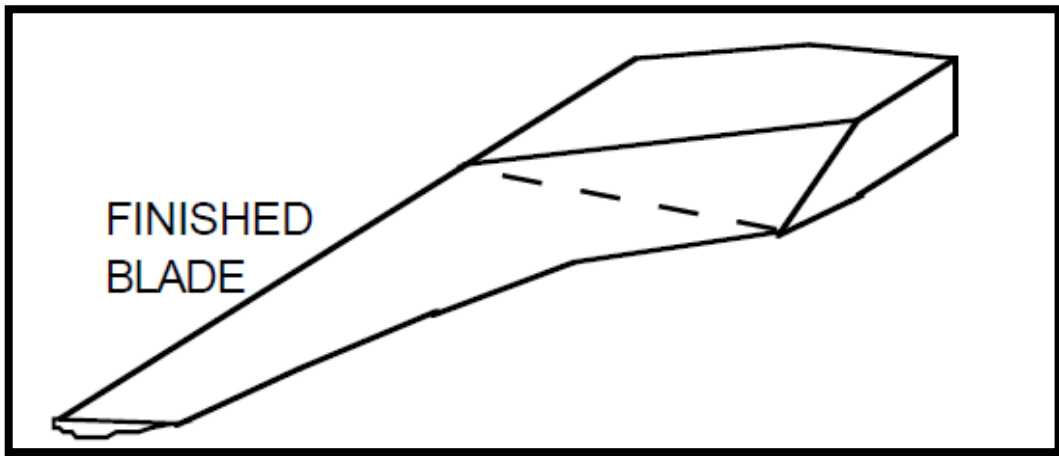


Figure 6.8: Carve the Curved Shape on the Back of the Blade [74]

The final out look of the blade and hub assembly of the 1.2m radius prototype is shown at figure 6.9.

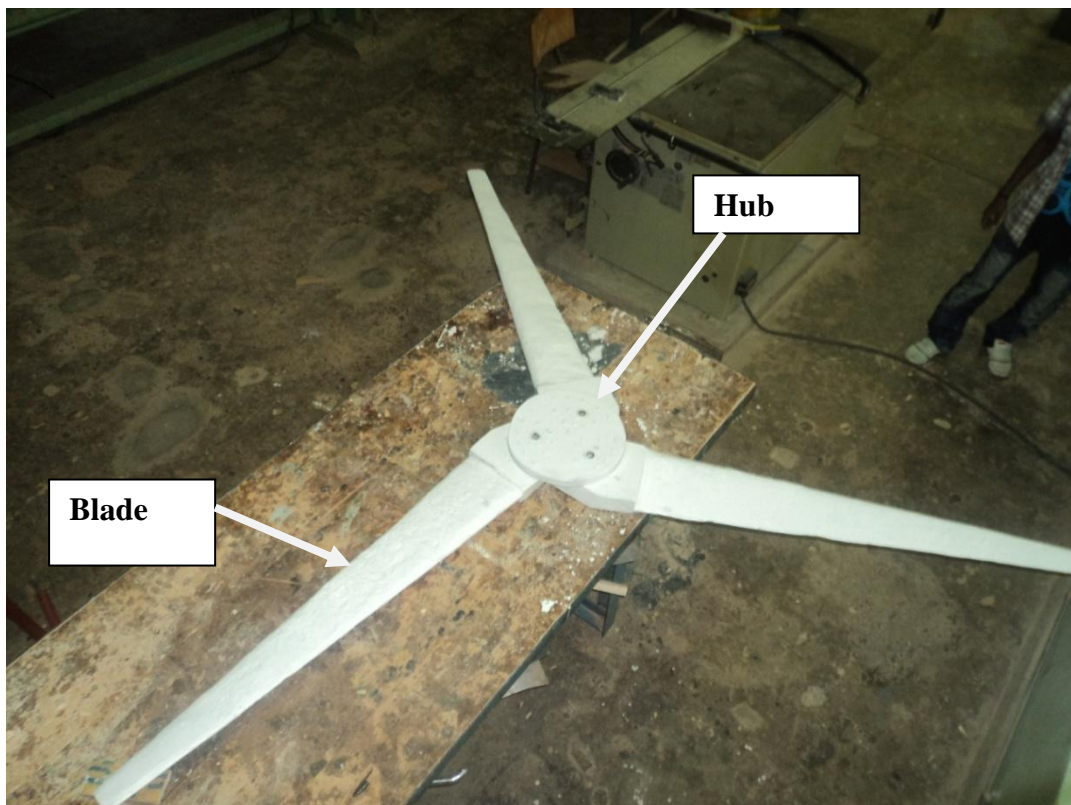


Figure 6.9: Photo of Blade Hub Assembly of the Prototype

The alternator consists of a stator disk sandwiched between two magnet rotors. Strong magnetic flux passed between the two rotors and through the coils in the stator. The movement of the rotors sweeps the flux across the coils, producing alternating voltages in them.

The rotors can be manufactured either by using non magnetic material and by molding the magnets together, the other method using magnetic steel disk and by gluing these magnet on

the surface of the disk. The rotors manufactured in this thesis are used the second option. 12 magnets which are equally spaced are attached to the steel dick using epoxy resin. The dimensions of the rotors are stated in table 6.5.

Table 6.5: Dimension of the Generator of the Prototype

Dimension	Value
Outer diameter	35cm
Inner diameter	30cm
Rotor thickness	5mm
Number of rotor	2
Number of stators coil	9
Number of magnets at each rotor	12
Number of phase	3 phase
Winding layout	Non overlapping
Connection	Star-series connection
Number of turns coil	90 turns
Coil diameter	1.5mm
Back steel disc thickness	6mm

The final rotor assembly manufacture is shown in figure 6.10.

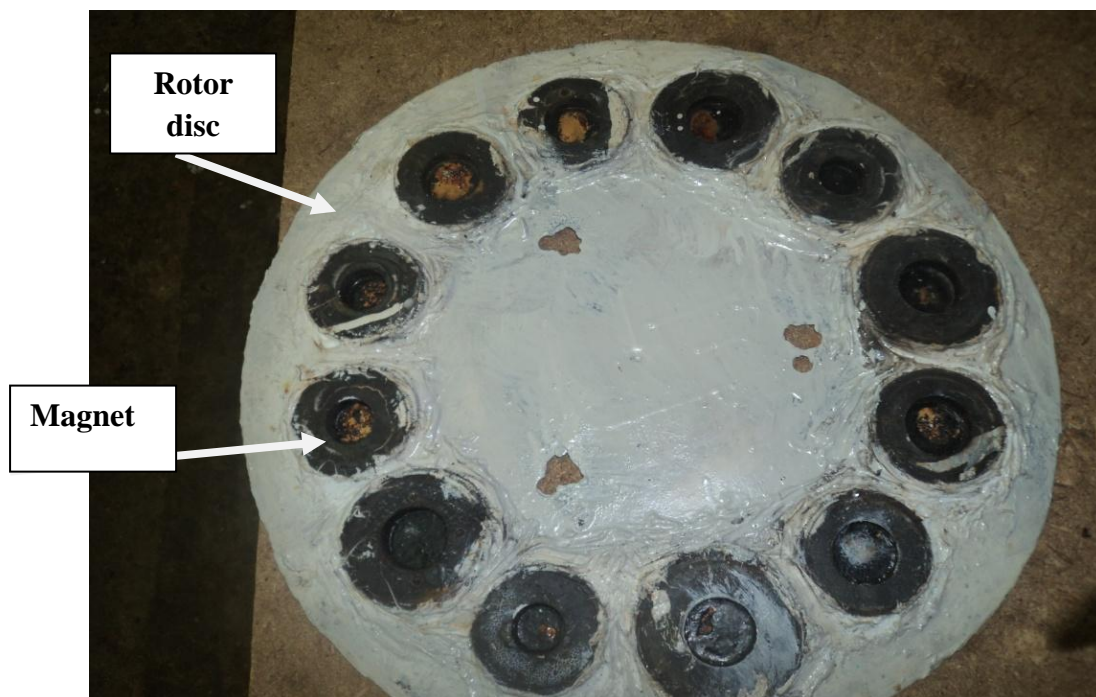


Figure 6.10: Photo of One of the Rotor Assemblies of the Prototype

The stator is mounted at three points around its periphery, using three more 1/2" [12 mm] studs. The coils embedded within it are dimensioned such as to encircle the flux from one magnet pole at a time. As the magnet blocks pass a coil, the flux through the coil alternates in

direction. This induces an alternating voltage in each turn of the coil. The voltage is proportional to the rate of change of flux. Voltage therefore depends on:

- The speed of rotation,
- The density of the flux,
- The number of turns in the coil.

The number of turns of wire in each coil is used to control the speed of the wind turbine. If the number of turns is large, then the output will reach battery voltage and start to charge the battery at a low rotational speed (rpm). If we use fewer turns of thicker wire in the coils, then it will need to run faster. The number is chosen to suit the rotor blades and also the battery voltage. There are ten coils in the stator. The twelve magnet poles pass the coils at different times. This phase lag between coils means that the torque is much smoother than it would be if there were 9 coils. If all the coils were synchronized with each other (single phase) then the machine would vibrate quite intensely when producing power. The manufacturing steps for the prototype stator are as follow;

Step one: selecting wire

The size and number of turns in each coil has a determining effect on the output of the generator. For this specific case, it is based on as stated in table 6.5.

Step two: winding the coils

The coils can be wound either manually or using winding machine, with winding dimension 25×41mm and 90turns for each coil.

Step three: connecting the coils

In the previous step 9 coils with 90 numbers of turns are prepared; at this stage they will connect to have combined output. The connection used is series/star connection.

Step four: output wiring

The output of the stator must be flexible insulated wire. They need to be more robust than the winding wires because they will be subjected to bending, vibration and abrasion of various kinds.

Step five: stator molding

After these all completed, the connected coils will molded using epoxy resin or other strengthen materials. Epoxy resin is not available in the local market there should need for the alternative solution to strengthen the stator. Considering this a 3mm thick mica glass used

in both side and make the stator. The use of this arrangement will create to have a passive cooling mechanism for the coils during its operation. The final work will be finishing stator and painting.

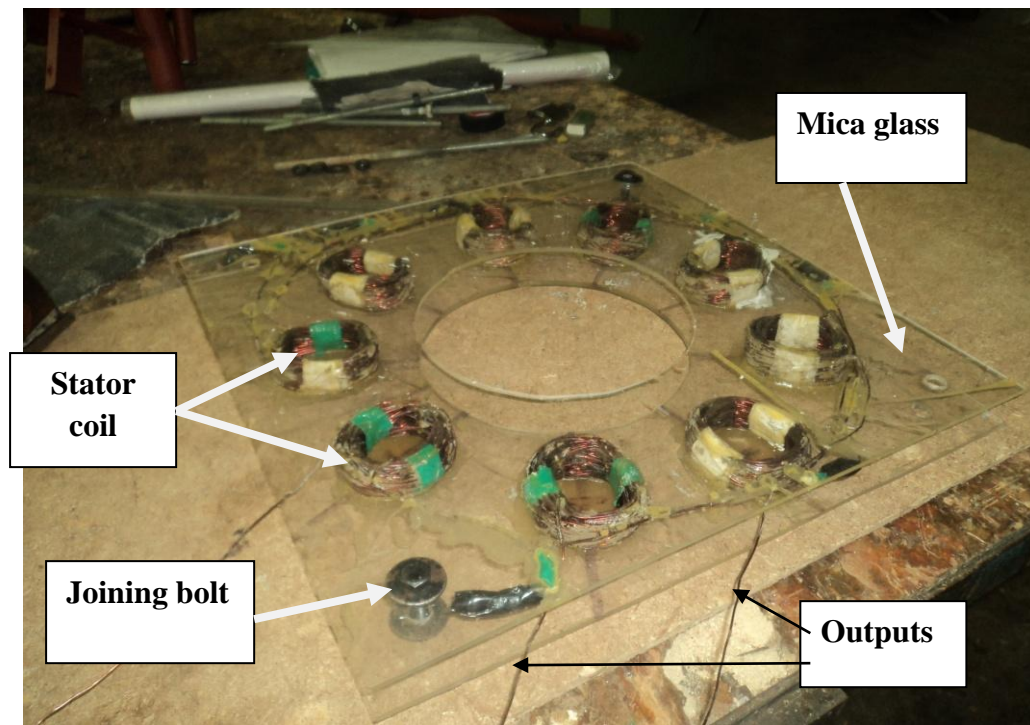


Figure 6.11: Photo of the Stator Assembly of the Prototype

The assembling frames are manufacture from steel pipes and angle irons to reduce the weight of the total system.

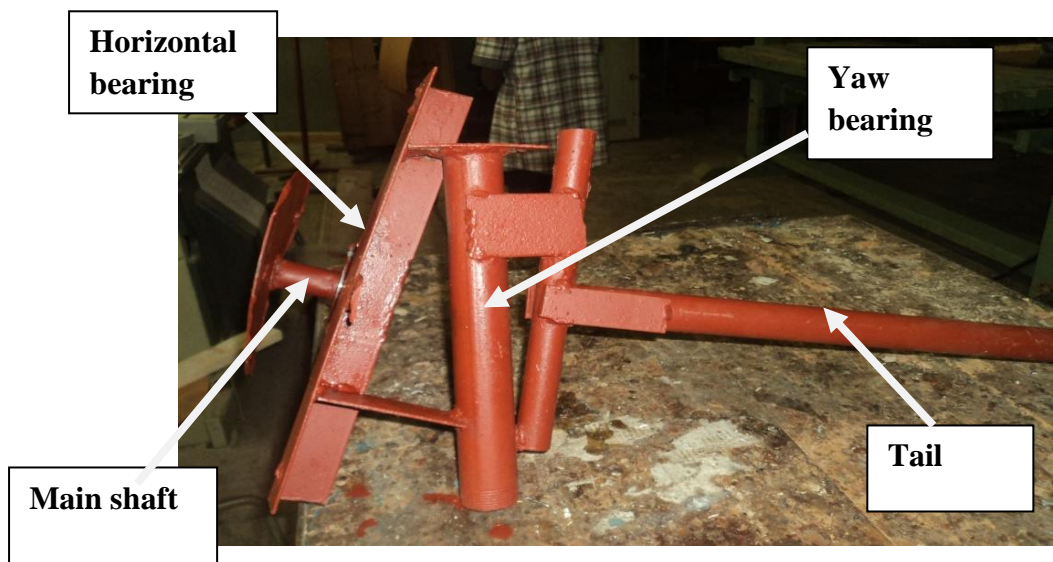


Figure 6. 12: Photo of the Assembling Frame of the Prototype

The assembly of the whole components is shown in figure 6.13.



Figure 6.13: Photo of Assembled Prototype

The prototype was manufactured from very cheap materials having good strength to withstand the loads imposed during operation so that its completion showed us manufacturing this type of system with local constraints is possible for the required application. The manufactured prototype has 22kWh to 164kWh monthly energy production at 3m/s to 7m/s wind speed. The testing procedure for the prototype was required to use a large wind tunnel to evaluate its coefficient of performance and energy generation at different wind speeds but because of lack of this equipment it was not possible to test the prototype manufactured. In the preceding chapter the techno economic analysis will be discussed to evaluate the feasibility of the system design.

CHAPTER SEVEN

OVERALL TECHNO-ECONOMICAL ANALYSIS

So far in the preceding chapters, data collection and analysis, design of system and components, and manufacturing method for the components, generally the technical aspects of the wind energy conversion system were discussed. In this chapter the overall techno economical analysis will be carried out, and will identify the feasibility of the system. The manufacturing cost of components was determined using the empirical relations suggested by reference [75]; the detail components formula for cost determination is attached at annex e.

7.1 CAPITAL INVESTMENT COSTS

It include costs incurred for purchasing equipments and raw materials, manufacturing of components, assembling, transportation and installation of the system, in other words, the total cost needed to bring the project to a commercially operable status.

Table 7.1: Raw Material Costs

S.N	Parameter	Unit	Quantity	Unit price (ETB)	Total price (ETB)
1	Douglass fir wood	Piece	60	190	11,400
2	Epoxy resin	Lit.	57	170	9690
3	Plastic painting	kg	10	70	70
4	Hot rolled steel	kg	300	20/kg	6000
5	Cast iron	kg	1.30	10/kg	370.50
6	Taper roller bearings	Piece	24	450	10,800
7	Hexagonal bolt and nut	piece	216	3	648
8	Yaw system	Piece	6	1500	9000
9	Rotor disks	Piece	12	100	1200
10	Permanent magnets	Piece	360	20	7200
11	Winding wire	kg	20	450	9000
12	Installation wire	m	100	20	2000
13	Frame	m	60	30/m	1800
14	Control	Piece	1	13243	13,243
15	Tower and foundation	Piece	6	12,058	72,350
	Total raw material cost				154,772

The manufacturing cost can be estimated by different approaches, now days many studies are on progress to develop a cost model for the wind turbine components. For this work the relation suggested by reference [75] used. The manufacturing cost for each components and other expenses for the system are determined as attached at annex e. the results are tabulated at table 7.2 and table 7.3.

Table 7.2: Manufacturing Costs of Components

Component	Process	Time required (hour)	Unit price (ETB)	Total Price (ETB)
Blade	Veneer preparation	8	20/hr	160
	Laminating and molding	24	30/hr	720
	Finishing and painting	8	15/hr	120
Main shaft	Turning	4	40/hr	160
	Facing	1	20/hr	20
	Drilling	1	30/hr	30
	Cutting	1	20/hr	20
	Heat treatment	4	20/hr	80
	Finishing and lubrication	1	20/hr	20
Hub	Casting	12	40/hr	480
Rotor	Molding	5	40/hr	200
Stator	Coil Winding	6	40/hr	240
	Molding	5	40/hr	200
Yaw system	Assembling	6	40/hr	240
Total manufacturing cost				2,690

Table 7.3: Miscellaneous Costs

Expense	Cost (ETB)
Transportation cost	10,000
Installation and civil work	15,000
Total	25,000

Based on the above discussion the capital cost of the system is 182,462 ETB.

7.2 ANNUAL COSTS

The annual cost include the operation and maintenance cost and components replacement cost during the system operation period.

7.2.1 Operation and Maintenance Cost (O&M)

Operation and maintenance (O&M) costs constitute a sizeable share of the total annual costs of a wind turbine. It includes expense for insurance, regular maintenance, repair, spare parts, and administration. There are different method to determine the operation and maintenance cost of the wind turbine. For a new turbine, O&M costs may easily make up 20-25 per cent of the total liveliest cost per kWh produced over the lifetime of the turbine. If the turbine is fairly new, the share may only be 10-15 per cent, but this may increase to at least 20-35 percent by the end of the turbine's lifetime. As a result, O&M costs are attracting greater attention, as manufacturers attempt to lower these costs significantly by developing new turbine designs that require fewer regular service visits and less turbine downtime. For this thesis work the operation and maintenance cost estimated by dividing the operation year in 5 groups and considering the following cost pattern,

1. For year 1 the operation and maintenance cost is estimated as 1.5% of the total turbine cost.
2. The O & M cost for each year in the Year 2 – 5 ‘block’ is given as 1.5 % of the turbine cost + 1.5% of the O & M cost for the previous year.
3. Year 6 – 10 = 1.5% of the turbine cost + 3% of the O & M cost for the previous year.
4. Year 11 – 15 = 1.5% of the turbine cost + 4.5% of the O & M cost for the previous year.
5. Year 16 – 20 = 1.5% of the turbine cost + 6% of the O & M cost for the previous year.

Table 7.4: Calculation of the Operation and Maintenance Cost of the System

Year	SYMBOL	OM cost equation	Substitution	Value
1	OM_1	$0.015 \times C$	$= 0.015 \times 182462$	2736.93 ETB
2-5	OM_{2-5}	$0.015 \times C + 0.015 \times OM_1$	$= 2736.93 + 0.015 \times 2736.93$	2777.98 ETB
6-10	OM_{6-10}	$0.015 \times C + 0.03 \times OM_{2-5}$	$= 2736.93 + 0.03 \times 2777.98$	2820.26 ETB
11-15	OM_{11-15}	$0.015 \times C + 0.045 \times OM_{6-10}$	$= 2736.93 + 0.045 \times 2820.26$	2863.84 ETB
16-20	OM_{16-20}	$0.015 \times C + 0.06 \times OM_{11-15}$	$= 2736.93 + 0.06 \times 2863.84$	2908.76 ETB
Total life time operation and maintenance cost				14,115.9 ETB

Finally the total operation and maintenance cost of the system for the total life time will be 14,115.9 ETB, and the annual operation and maintenance cost will be 706 ETB.

7.2.2 Replacement Cost

The major replaceable components in wind energy conversion system are the bearings, the controller, the joints and fastening studs, etc. The replacement cost is expected to be done twice throughout the life time, at the 8th and 14th year of operation. Though much work is under way to Develop more sophisticated models, for this study cost factor \$10.7/kW machine rating is used to calculate the replacement cost of wind turbine [75]. The replacement cost is used to calculate the annualized replacement cost and this cost is not meant to account for inflation. Therefore based on the cost factor suggested by [75] the annual replacement cost of the system will be,

$$\text{Replacement Cost}(\$) = \frac{10.7\$}{kW} \times 27kW = 288.9\$$$

And based on the current currency exchange (17.5ETH=1\$) the annual replacement cost will be 4,920ETB.

Therefore the annual cost of the system will be the sum of the replacement cost and the operating and maintenance costs, i.e.

$$\text{Annual Cost} = O \& M \text{ Cost} + R \text{ Cost} = 706 + 4,920 = 5,617.3\text{ETB}$$

7.3 ANNUAL BENEFITS

The annual benefits of the wind energy conversion system can be divided in to the environmental benefits, social benefits, and the most of all the financial benefit. For this thesis work only the financial benefit was considered, which is the collected money is by selling the energy generated by the system. The annual energy generation by the system is 120MWh/year, and based on the Ethiopian Electric Power Corporation the energy selling price for household use is 0.27ETB/kWh.

$$\text{Annual Benefit} = \text{Energy generated} \times \text{COE} = \frac{120\text{MWh}}{\text{year}} \times \frac{0.27\text{ETB}}{\text{kWh}} = 30,000\text{ETB}$$

Then annual benefit of the system will be 30,000ETB.

7.4 ECONOMICAL EVALUATION OF THE SYSTEM

The economical feasibility of the system can be evaluated by using different techniques either individual or by combining each technique together.

7.4.1 Real Interest Rate

An interest rate that has been adjusted to remove the effects of inflation to reflect the real cost of funds to the borrower, and the real yield to the lender. The real interest rate of an investment is calculated as the amount by which the nominal interest rate is higher than the inflation rate. The real interest rate r is given by fisher equation as [70];

$$r = \frac{1 + i}{1 + E(I)} - 1 \quad 7.1$$

Where: i = Nominal interest rate (the rate at which you could borrow money), it is 8 %

$E(I)$ = Expected inflation rate (11% in Ethiopia), then the real interest rate will be,

$$r = \frac{1 + 0.08}{1 + 0.11} - 1 = -2.7\%$$

A negative real interest rate shows the inflation rate is greater than the interest rate.

7.4.2 Annual Saving

Annual saving is the difference of the total annual expense for the system and the total annual benefit from the system. Mathematically,

$$\text{Annual saving} = \text{Annual benefit} - \text{Annual costs} \quad 7.2$$

$$\text{Annual saving} = 30,000 - 5617.3 = 24,382.7\text{ETB}$$

Then the annual saving will be 24,382.7ETB.

7.4.3 Cost Benefit Ratio (CBR)

Cost–benefit analysis (CBA), sometimes called benefit–cost analysis (BCA), is a systematic process for calculating and comparing benefits and costs of a project for two purposes, to determine if it is a sound investment (justification/feasibility), to see how it compares with alternate projects (ranking/priority assignment). It involves comparing the total expected cost

of each option against the total expected benefits, to see whether the benefits outweigh the costs, and by how much. If the $CBR < 1$ the project will be feasible or gain a profit to the firm, if it is $CBR > 1$ the project will not be feasible and it is at risk, but if $CBR = 1$ the project expense and benefit will be equal so that another criteria required to judge the project feasibility.

$$CBR = \frac{\text{Annual Cost}}{\text{Annual Benefit}} = \frac{5,617.3 \text{ ETB}}{30,000 \text{ ETB}} = 0.2$$

The cost benefit ratio for this system will be, 0.2, and based on the above discussion the system is feasible.

7.4.4 Net Present Value (NPV)

NPV is the amount of money an investment is worth in today's cash, taking into account the amount of the investment, the length of the investment, how long it takes the investment to return a profit and the cost of money (interest and risk). In other way NPV is the current amount of money you would pay for a future investment (always some fraction smaller than one). $NPV > 0$ the investment would add value to the firm, the project may be acceptable. $NPV < 0$ the investment would be subtract value from the firm, the project should be rejected. When $NPV = 0$ the investment would neither gain nor loss value for the firm, the decision based on other criteria. To calculate NPV value it's given by [70]:

$$NPV = -CF_0 + \frac{CF_n(1+i)}{(1+i)} + \dots + \frac{CF_n(1+i)^n}{(1+i)} \quad 7.3$$

Using equation 7.3 the NPV can be calculated on spread sheet package such as Microsoft Excel, and based on the analysis (see table 7.5) the NPV is 203,555.2 ETB.

Or using Dr. Muluwork K. Manuscript project finance equation,

$$NPV = B_d \left[\frac{(1+r)^n - 1}{r(1+r)^n} \right] - C \left[1 + \frac{OM_R}{C} \left(\frac{(1+r)^n - 1}{r(1+r)^n} \right) \right] \quad 7.4$$

Where: B_d : annual benefit, i.e. 30,000 ETB

OM_R : Annual costs, i.e. 5,617.3 ETB

n : project life time, 20 years, and using equation 7.4 the NPV calculated as,

$$NPV = 30,000 \left[\frac{(1 + 0.027)^{20} - 1}{0.027(1 + 0.027)^{20}} \right] - 182,462 \left[1 + \frac{5,617.3}{182,462} \left(\frac{(1 + 0.027)^{20} - 1}{0.027(1 + 0.027)^{20}} \right) \right]$$

$$= 203,555.2 \text{ ETB}$$

The calculated value of the NPV i.e. 203,555.2 ETB is above 1 and the system is feasible based on net present value analysis.

7.4.5 Internal Rate of Return (IRR)

The annual rate of earnings on an investment equates the value of cash returns with the cash invested, taking into consideration the power of compounding interest. The following formula requires a trial-and-error method for solution. The fallacy with the method is its assumption that all cash flows are reinvested at the internal rate of return. The IRR is also the discount rate at which the present value of the net benefit stream in financial terms becomes zero [70].

$$-CF_0 + \frac{CF_n(1 + I)}{(1 + i)} + \dots + \frac{CF_n(1 + I)^n}{(1 + i)} = 0 \quad 7.5$$

The internal rate of return calculated using equation 7.5 on Microsoft Excel (see table 7.5). The IRR rate of return on Microsoft Excel is described on annex f. The result is the internal rate of return using real interest 2.7% is 4% which is above the real interest rate the bank lend, so that based on the internal rate of return analysis the system is feasible.`1

7.4.6 Amortization

In lending, amortization is the distribution of a loan repayment into multiple cash flow installments. The loan principal (A) is given by [70]:

$$A = C \times CRF \quad 7.6$$

Where: *C*: capital investment cost and CFR: is the capital recovery factor recovery factor and given by;

$$CRF = \frac{r(1 + r)^N}{(1 + r)^N - 1} \quad 7.7$$

Where: *N*: loan term, 10 years and *r*: Real interest rate, 2.7%

$$CRF = \frac{0.027 \times (1 + 0.027)^{10}}{(1 + 0.027)^{10} - 1} = 0.115$$

Then the amortization will be,

$$A = 182462 \times 0.115 = 21,063.91 \text{ ETB}$$

Based on the above equations the following table can be formulated. In the table the term loan principal and cash flow can be calculated as [70];

$$\left. \begin{aligned} \text{Principal paid per year} &= \text{loan principal} - \text{Loan interest} \\ \text{Cash flow (net income)} &= \text{Annual Benefit} - \text{loan principal} - OM_R \end{aligned} \right\} 7.8$$

Using equation 7.8 the principal paid per year and cash flow for each can be determined. For year 1 it can be calculated as,

$$\text{Principal paid per year} = 21,063.91 - 4,926.47 = 16,137.44 \text{ ETB}$$

$$\text{Cash flow (net income)} = 30,000 - 21,063.91 - 5,617.3 = 3,318.79 \text{ ETB}$$

And for the second year,

$$\text{Principal paid per year} = 21,063.91 - 4,401.16 = 16,662.76 \text{ ETB}$$

$$\text{Cash flow (net income)} = 30,000 - 21,063.91 - 5,617.3 = 3,318.79 \text{ ETB}$$

It will continue for the other operational years of the system. The results of the analysis based on the relation discussed above are tabulated at the following table 7.5.

7.4.7 Payback Period (PP)

The payback period is the time that it takes for an investment to pay for itself. The basic premise of the payback method is that the more quickly the cost of an investment can be recovered, the more desirable is the investment. The overall measure of cost for the plant accounts for operation and maintenance cost, salvage cost, replacement cost and capital costs of the system component over the twenty years span.

Thus the payback period is given by [70]:

$$PP = \frac{C}{B_d - OM_R} \quad 7.9$$

Where: $B_d - OM_R$: the annual saving = 24,382.7 ETB.

$$PP = \frac{182,462}{24,382.7} = 7.48$$

Substitution will result the payback period to be 8 years from the commencement day of operation of the system.

Table 7.5: Life Time Cash Flow of the System

Years	Capital Cost	O&M R	Loan Interest	Loan Principal	Principal Paid	Annual Benefit	Cash Flow
0	-182462					-182462	-182462
1	-163005.77	5617.3	4926.47	21063.91	16137.44	30000	3318.79
2	-143024.23	5617.3	4401.16	21063.91	16662.76	30000	3318.79
3	-122503.18	5617.3	3861.65	21063.91	17202.26	30000	3318.79
4	-101428.07	5617.3	3307.59	21063.91	17756.33	30000	3318.79
5	-79783.93	5617.3	2738.56	21063.91	18325.36	30000	3318.79
6	-57555.39	5617.3	2154.17	21063.91	18909.75	30000	3318.79
7	-34726.69	5617.3	1554.00	21063.91	19509.92	30000	3318.79
8	-11281.61	5617.3	937.62	21063.91	20126.29	30000	3318.79
9	0	5617.3				30000	3318.79
10		5617.3				30000	24382.70
11		5617.3				30000	24382.70
12		5617.3				30000	24382.70
13		5617.3				30000	24382.70
14		5617.3				30000	24382.70
15		5617.3				30000	24382.70
16		5617.3				30000	24382.70
17		5617.3				30000	24382.70
18		5617.3				30000	24382.70
19		5617.3				30000	24382.70
20		5617.3				30000	24382.70
							NPV
							203,555.2
							IRR
							4%

NB: all the cash list in table 7.4 is in Ethiopian birr (ETB)

7.4.8 Cash Flow

The net cash flow as calculated for each year using equation 7.8, the result for each is tabulated at table 7.5. The life time cash flow of the project is projected to be as shown in figure 7.1

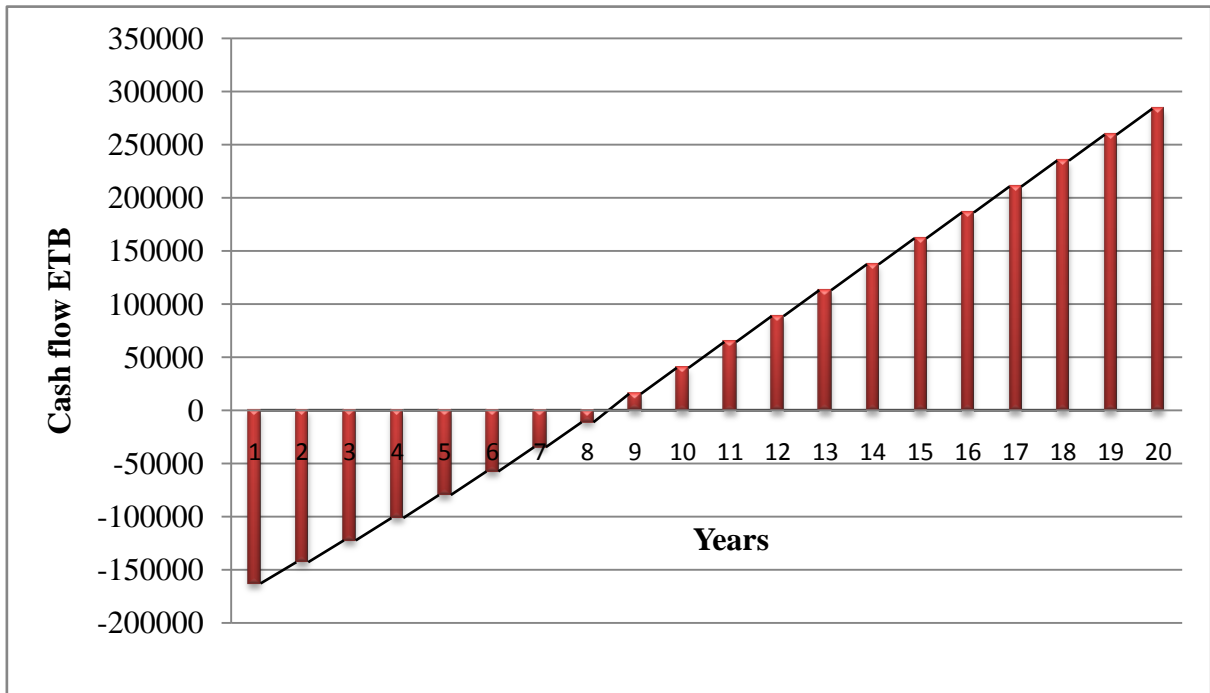


Figure 7.1: Cash Flow of the System

The summary of the economic analysis carried out are tabulated at table 7.5 as shown below.

Table 7.6: Summary of Economic Analysis

Analysis	Value
Initial investment cost	182462 ETB
Annual cost	5,617.3 ETB
Annual saving	24,382.7 ETB
Amortization	21,063.91 ETB
Net present value (NPV)	203,555.2 ETB
Cost benefit ratio	0.2
Internal rate of return (IRR)	4%
Payback period	8

From the above economical evaluation it was founded the cost benefit ratio to be 0.2 which is less than 1, the net present value is 203,555.2 ETB which is above 1, the internal rate of return 4% which is above 2.7% real interest rate the project lend, and the payback period 8 years which is less than 10 years as recommended by many literatures, so that based on this economical analysis the designed standalone direct driven wind energy conversion system is very feasible and promising solution.

CHAPTER EIGHT

CONCLUSION AND RECOMMENDATION

CONCLUSION

In this thesis design and manufacturing of a direct driven, standalone wind energy system with axial flux permanent magnet generator for off-grid electrification application was evaluated. The system was theoretically analyzed and components are designed using analytical relations, the tasks were completed by manufacturing a prototype and techno economic analysis of the system.

Wind turbine aerodynamic design was done using BEM theory by taking in to account, tip loss, drag, wake rotation and finite number of blades will be discussed which will be followed by aerodynamics based on the BEM theory for the specified site conditions and demand requirement and structural design was also completed using IEC 6400-2: *design of small wind turbines* publication as a guide line. The final aerodynamic result showed that the total coefficient of performance of the blade is 0.42 which above the assumed 0.4 value. The structural analysis of the blades also proved that the blades are capable to the intended application. The other components such as the hub, main shaft and the joints are also design to withstand the eight load case they are expected to expose, and the factor of safety showed they can sustain for those loadings.

The electrical components are designed to generate the required 4.5kW electricity at the rated speed of 6m/s. A coreless axial flux permanent magnet generator was theoretically analyzed and different stator winding topologies were evaluated. The generator was designed with coreless stator, non overlapping winding layout, double rotor and permanent magnet excited topology. The final result showed the generator has 81.5 percent efficiency and an output terminal voltage of 130V for each 4.5kW generators.

To validate the performance of the design 1:4.6 scale wind turbine and axial flux generator prototype was developed. The techno economic analysis was carried out to identify the feasibility of the system. Based on the system economical evaluations completed the direct driven standalone wind energy system proved as a feasible system for the required application.

Generally, the present work is devoted to design and manufacture a direct driven and standalone, wind energy conversion system for off gird electrification, and from the completed tasks the following conclusions are drawn;

- There are many useful potential wind sites in Ethiopia for small scale wind energy generation using direct driven permanent generators. In Amhara regional state the major potential sites are Debrebrhan, Gondar, Debremarkos, Aykel, Gorgora, Dangla, Kombolcha, Woreta, and Bahirdar. Based on the criteria stated Aykel city was chosen as working site for this thesis work and the wind resource assessment done showed that the site has 2.67m/s mean wind speed at the 10m height above the ground, to generate the required 27.0kW electricity demand 50 meter above the ground was selected and the wind speed at this height is 6m/s.
- Wind energy system can be used with different alternative configurations, such as, wind turbine with battery storage system, wind turbine connected to grid, standalone wind generator which is directly connected to the load or wind energy hybrid with different energy sources. This thesis select standalone wind generator system with directly coupled axial flux permanent magnet generator.
- It was proved from the design and analysis of the system direct driven wind energy system with axial flux permanent magnet wind generator compatible for small scale wind energy system. The analysis results the generators cut in speed to be 3.8m/s so that the system can start generating electricity at lower wind speed ranges, and it has a capacity of 4.5kW at 6m/s mean wind speed for each.
- The designed mechanical and electrical components are manufactured with 1:4.6 scale in our workshop for 700W rating power. The developed prototype showed the possibility of manufacturing wind turbine and axial flux generator using local manufacturing techniques and equipments. And proved small scale direct driven wind energy system with axial flux permanent magnet generator is a promising solution for the wind speed range Ethiopia have had.
- The economical evaluation showed that the cost benefit ratio to be 0.2 which is less than 1, the net present value is 203,555.2 ETB which is above 1, the internal rate of return 4% which is above 2.7% real interest rate the project lend, and the payback period 8 years which is less than 10 years as recommended by many literatures, so that based on this economical analysis the designed standalone direct driven wind energy conversion system is very feasible and promising solution.

RECOMMENDATION

From this work generally the following points are recommended for the future works,

- The use of renewable energy specifically wind energy has proved benefits for rural areas which are far from the national grid so that the government or private investors can work on it to support the development and life standard of the people.
- The usefulness of a given energy source must be evaluated by throw economic analysis considering the socioeconomically, environmental and other benefits in to account, this thesis did not complete this task and it will be recommended if the detail economic analysis carried out.
- This thesis only considers the wind generator without battery configuration and did not consider other possible alternative configuration with wind generator so that it is more reliable to make feasibility studies to discover different hybrid configurations.
- The manufacturing process was done with many constraints it is recommended to work with team and brainstorming to have better performance and reliable test result.

REFERENCE

- [1] God Frey Boyle, Renewable Energy, *Power for Sustainable Future*, EFN Span Ltd., 1986, UK.
- [2] International Energy Agency, *World Energy Outlook 2000*, 2000, France.
- [3] Aklilu Dalelo (PhD), *Rural electrification in Ethiopia: Opportunities and Bottlenecks*, Addis Ababa University, College of Education, Department of Geography and Environmental Education, Ethiopia.
- [4] L.L. Fresis, *Wind Energy Conversion Systems*, Prentice Hall, 1990, UK.
- [5] Manwell, J. F., McGowan, J. G., Rogers, A. L., *Wind Energy Explained; Theory, Design and Application*, 2nd ed., John Wiley & Sons Ltd, 2002, USA.
- [6] Jill Fehrenbacher. Inhabitat.com, *Ethiopia Announces Largest Wind Farm in Africa*, 2008 October 15th, Jorge Chapa [accessed: February 12, 2011], Available from: <http://inhabitat.com/ethiopia-announces-largest-wind-farm-in-africa/>.
- [7] Mike King, Poul Chapman. Companiesandmarkets.com. *Country profile: Ethiopia*. 2011[accessed: February 12, Available from: <http://www.companiesandmarkets.com/> .
- [8] Ethiopian Electricity Corporation. 2005 [accessed: February 12, 2011], Available from: <http://www.eepco.gov.et>.
- [9] The international Development Research Center. 2009[accessed: February 12, 2011], Available from: www.idrc.ca .
- [10] George Sterzinger, and Matt Svrcek, *Renewable energy policy project (REPP), Technical report on: wind turbine development and location of manufacturers activity*, September, 2004, available from: <http://www.repp.org/articles/static/1/binaries/WindLocator.pdf> .
- [11] *How does solar navigator benefit from wind turbine?* , [accessed: February, 2011], available from: http://www.solarnavigator.net/wind_turbines.htm.
- [12] Kovarik, T., Pipher C., Hurst, J., *Wind Energy*, Prism Press, 1979
- [13] Wikipedia: the free encyclopedia, *Darrieus Wind Turbine*, [accessed: October, 2001], available from: http://en.wikipedia.org/wiki/Darrieus_wind_turbine .
- [14] Le Gourieres, D., *Wind Power Plants, Theory and Design*, Pergamon Press, 1982

- [15] Patpending, *Physical Principles in Wind Turbine Operation & Design Hints for Energy Efficiency in Power Generation*, August 2010 [accessed: October 2011, available from: http://www.bukisa.com/articles/339001_the-physics-engineering-of-the-wind-turbine-with-design-hints-for-efficiency-power-generation .
- [16] Paul Gipe, *Wind Energy Basics: A Guide To Small and Micro Wind Systems*, , August 2008, USA.
- [17] Henk Polinder, Frank F.A. van der Pijl, Gert Jan de Vilder, and Peter J. Tavner, *Comparison of Direct Drive and Geared Generator Concepts for Wind Turbines*, Ieee Transactions on Energy Conversion, Vol.21, No.3, September 2006.
- [18] Lampola, P., *Doctorial thesis on: Directly Driven, Low Speed Permanent Magnet Generators for Wind Power Applications*, Acta Polytechnica Scandinavica, Electrical Engineering Series, No.101, Published by the Finnish Academies of Technology, ISBN 951-666-539-X. ISSN 0001-6845. UDC 621.313.8/.12:621.311.245.
- [20] P. Sivachandrar, P. Venkatesh, *Paper on: Design and analysis of dual rotor radial flux permanent magnet generator for direct coupled standalone wind energy system*, department of electrical and electronics engineering, Thiagaraja collage of engineering, India.
- [21] Paul Noel, Paper on: *how parallel path gets over unity*, March 7, 2006, [accessed: October 2011], Available from: http://www.pureenergysystems.com/academy/papers/How_Parallel_Path_Gets_Over_Unity/.
- [22] Andrew Jan, *A Direct Drive to Sustainable Wind Energy*, March 2010, [accessed: October 2011], Available from: <http://www.windsystemsmag.com/> .
- [23] Grant Ingram, *Wind Turbine Blade Analysis Using the Blade Element Momentum Method*, version 1.0, December 13, 2005.
- [24] S.E. Skaar, O. Krovel, R. Nilssen and H. Erstad, *Slotless, Toroidal Wound, Axially Magnetized Permanent Magnet Generator For Small Wind Turbine Systems*, Department of Electrical Power Engineering Norwegian University of Science and Technology, Norway.
- [25] Frances Drake and Yacob Mulugetta, *Assessment of Solar and Wind Energy Resources in Ethiopia, I, Solar Energy*, School of Geography, University of Leeds, and Leeds LS2 9JT, May 1996, U.K.
- [26] *The Operational Life time of Wind Turbines in Denmark Government Data*, 19 December, 2008 [accessed: February 2011], Available from: <http://www.dailykos.com>.

- [27] The British wind energy association, *Wind Turbine Technology*, 2004 [accessed: February 2011], Available from: <http://www.bwea.com/energy/rely.html>.
- [28] HOMER Energy, *Homer user guide*, Homer energy, LLC, 8885 Arapahoe Ave. Boulder Co.80302, July 24 2009, USA.
- [29] Spora D.A., *Wind Turbine Technology*, Asme press, 1998.
- [30] J.L. Tanglor, D. M. Somers, *Airfoil Families for HAWTs*, and National Renewable Energy Laboratory of US Department of energy: prepared under task number: we429180, January 1995.
- [31] David A. Spera, Jack B. Esgar, Meade Gougeon and Michael D. Zuteck, *Structural properties of laminated Douglas fir/epoxy composite material*, Work performed for U.S. Department of Energy Conservation and Renewable Energy Wind/Ocean Technology Division, Washington DC.
- [32] International Electrotechnical Commission, *Wind Turbines- Part 2: Design Requirement for Small Wind Turbines (IEC -614002)*, 2nd edition, 2006, Switzerland.
- [33] Richard Budynas, J. Keith Nisbett, *Mechanical Engineering Design*, 8th edition, The McGraw Hill Companies, NY , 2008, USA.
- [34] Tony Burton, David Sharpe, Nick Jenkins, Ervin Bossanyi, *Wind Energy Handbook*, John Wiley & Sons, Ltd, 2001, England.
- [35] Pramod Jain, *Wind Energy Engineering*, McGraw-Hill Companies, Inc., 2011., USA.
- [36] Maarten J. Kamper, RongJie Wang , Jacek F. Gieras, *Axial Flux Permanent Magnet Brushless Machines*, Kluwer Academic Publishers, 2005, USA.
- [37]Wang R., and Kamper M.J. (2002), *Evaluation of Eddy current losses in axial flux Permanent Magnet (AFPM) machine with an ironless stator*, IEEE 37thI as Meeting, Pittsburgh, PA, USA.
- [38] A. Parvairinen and P. Kontkorene, *Axial Flux Permanent Magnet Generator for Wind Power Application*, flux magazine, p. 4-5, 2005.
- [39] B. J. Chalmers and E. Spooner, *Axial Flux Permanent Magnet Generator for Gearless Wind Energy System*, IEEE Transactions on energy conversion, Vol.14, p. 251-257, 1999.

- [40] Seyed Mohsen Hosseini, Mojtaba Agha Mirsalim, and MehranMirzaei, *Paper on: Design, Prototyping, and Analysis of a Low Cost Axial Flux Coreless Permanent Magnet Generator*, IEEE Transactions on Magnetics, Vol. 44, No. 1, January 2008.
- [41] D. Platt, *Permanent Magnet Synchronous Motor with Axial Flux Geometry*, IEEE Transactions on Magnetics, Vol. 25, p. 3076-3079, 1989.
- [42] F. Magnussen and C. Sadarangani, *Winding Factors and Joule Losses of Permanent Magnet Machines with Concentrated Windings*, presented at IEEE International electrical machines and drives conference IEMDC 03, Madison, Wisconsin, 2003, USA,.
- [43] Gieras, J. F. & Wing, M., *Permanent Magnet Motor Technology: Design and Applications*, 2nd ed., Marcel Dekker, 2002, New York.
- [44] Gieras, J. F., Wang, R. & Kamper, M. J., *Axial Flux Permanent Magnet Brushless Machines*, Dordrecht, The Netherlands: Kluwer, 2004, Netherland.
- [45] Lombard, N. F. & Kamper, M. J., *Analysis and Performance of an Ironless Stator Axial Flux PM Machine*. IEEE Transaction Energy Conversion, Vol. 14, No. 4, p. 1051–1056, 1999
- [46] Chalmers, B. J. & Spooner, E. *An Axial Flux Permanent Magnet Generator For a Gearless Wind Energy System*, IEEE Transactions on Energy Conversion, Vol. 14, No. 2, pp. 251 – 257, 1999.
- [47] Wallace R. R., Lipo T. A., Moran L. A., and Tapia J. A., *Design and Construction of a Permanent Magnet Axial Flux Synchronous Generator*, Electric Machines and Drives Conference Record, IEEE International 18-21 May 1997 Page(s): MA1/4.1 -MA1/4.3, 1997.
- [48] Mirzaei M., Mirsalim M., and Abdollahi E., *Analytical Modeling of Axial Air-Gap Solid Rotor Induction Machines Using a Quasi Three Dimensional Method*. IEEE Transactions on Magnetics, Vol. 43, No. 7, 2007.
- [49] Wang, R. J., Kamper, M. J., Westhuizen, K. V. D. & Gieras, J. F. (2005). *Optimal Design of a Coreless Permanent Magnet Generator*, IEEE Transaction on Magnetics, Vol. 41, No. 1, p. 55-64.
- [50] Fitzgerald, A. E. & Kingsley, C., *Electrical Machinery*, 2nded. McGraw-Hill, 1961, New York.
- [51] Atherton W. A., *From Compass to Computer; a History of Electrical and Electronics Engineering*, The Macmillan Press Ltd, p. 337, 1984, London.

- [52] Strnat K. J., *Modern Permanent Magnets for Applications in Electro-Technology*, Proceedings of the IEEE, Vol. 78, No. 6, pp. 923-946, 1990.
- [53] Deshpande, U. S., *Recent Advances in Materials for Use in Permanent Magnet Machines Review*, In Proceedings of IEEE Electric Machines and Drives Conference, IEMDC'03, Madison, 1-4 June 2003, Vol. 1, pp. 509-515, 2003, USA.
- [54] Dailymag Magnetic Technology (Ningbo) Limited, *Magnetic Properties of Sintered NdFeB magnet*, Accessed: June 2011, Available from: <http://www.magnet-ndfeb.com/magnetic-properties-of-ndfeb-magnets.htm>.
- [55] Densis L. Feucht, *Wire Packing Factor Magnetic Design*, accessed: May 2011, available from: http://www.analogzone.com/col_1204.pdf.
- [56] Duane C. Hanselman, *Brushless Permanent Magnet Motor Design*, 1st ed., McGraw-Hill, inc., 1994, USA.
- [57] Profumo F., Tenconi A., Zhang Z., and Cavagnino A, *Novel Axial Flux Interior PM Synchronous Motor Realized with Powdered Soft Magnetic Materials*, IEEE-IAS Annual Meeting, Vol. 1, pp. 152–159, 1998.
- [58] Christine A. Hult, *Researching and Writing an Interdisciplinary Approach*, Wadsworth publishing company, 1986, California.
- [59] JuhaPyrhönen, TapaniJokinen and Val´eriaHrabovcov´am, *Design of Rotating Electrical Machines*, John Wiley & Sons, Ltd. ISBN: 978-0-470-69516-6, 2008, New Delhi, India.
- [60] Nicolette ArnaldaCencelli, Master's thesis on: *Aerodynamic Optimization of a Small Scale Wind Turbine Blade for Low Wind Speed Conditions*, Stellenbosch University, December 2006, South Africa.
- [61] R. Wang, *Design Aspects and Optimization of an Axial Field Permanent Magnet Machines with an Ironless Stator*, Ph.D. dissertation, University of Stellenbosch, 2003, South Africa.
- [62] S. Drouilhet, E. Muljiadi, R. Holz, and V. Gevorgian, *Optimizing Small Wind Performance in Battery Charging Applications*, Windpowers, 95, 1995.
- [63] R. J. Wang, M. Kamper, K. Van der Westhuizen, and J. Gieras, *Optimal Design of a Coreless Stator Axial Flux Permanent Magnet Generator*, Magnetics, IEEE Transactions on, Vol. 41, No. 1, pp. 55-64, 2005.

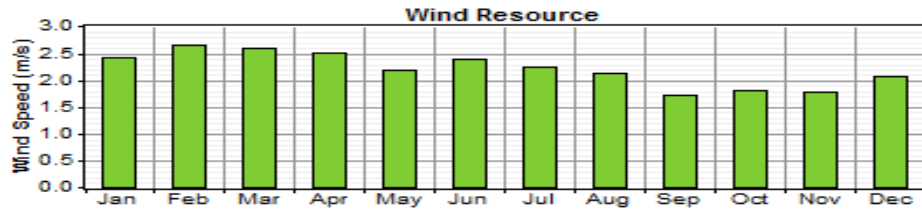
- [64] M. Kamper, R. Wangs, and F. Rossouw, *Analysis and Performance of Axial Flux Permanent Magnet Machine With Air Cored Non Overlapping Concentrated Windings*, IAS, 2008.
- [65] F.W. Grover, *Inductance Calculations Working Formula and Tables*, D. Vamd Nostrand Company Inc, 1946.
- [66] V.G. Welsby, *The Theory and Design of Inductance Coils*, MacDonald and Co, 1950.
- [67] K. Nilsson, E. Segergren, and M. Leijon, *Simulation of Direct Drive Generators Designed For Under Water Vertical Axis Turbine*, in fifth European wave energy conference, 2003.
- [68] R.J. Wang, M. Kamper, *Optimal Calculation of Eddy Current Loss in Axial Field Permanent Magnet Machine with Coreless Stator*, energy conversion, IEEE Transaction, Vol. 19, No. 3, pp. 532-538, 2004.
- [69] Clint Coleman, *Wooden Wind Turbine Blade Manufacturing Process*, United State Patent, Patent No. 4, 597,715, July 1 1986, USA.
- [70] Chans Park, *Fundamental of Engineering Economics*, by Pearson Education, Inc. Upper Saddle River, 2004, New Jersey.
- [71] AltE University, *Power Ratings (typical) for Common Appliances*, Accessed May 2011, available from: <http://www.altestore.com/howto/Power-Ratings-typical-for-Common-Appliances/a21/>.
- [72] Accessed: May 2011, Available from: http://www.sungrowpower.com/en/product_display.php?id=233.
- [73] Missouri Wind and Solar, *Charge Controller Speciation*, Accessed: May 2011, Available from: www.missouriwindandsolar.com.
- [74] Hugh Piggot, *A Wind Turbine Recipe Book: The Axial Flux Windmill Plans*, August 2009, German.
- [75] L. Fingersh, M. Hand, and A. Laxson. *Wind Turbine Design Cost and Scaling Model*. 1617 Cole Boulevard, Golden 80401-3393 : National Renewable Energy Laboratory available at www.nrel.gov, 2009, Colorado.

ANNEX A

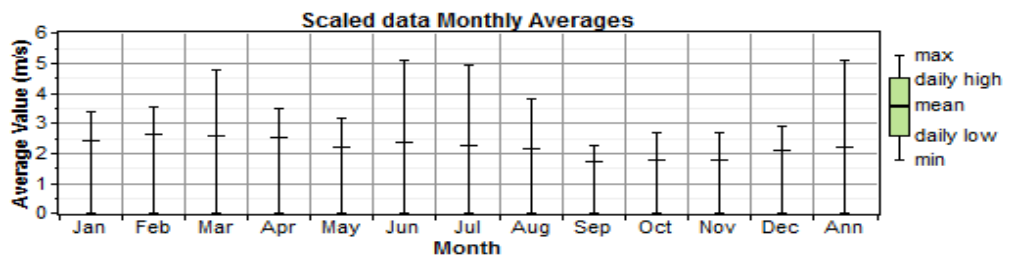
WIND RESOURCE ASSESSMENT RESULT

Wind Resource Assessment Result for Aykel: 1989

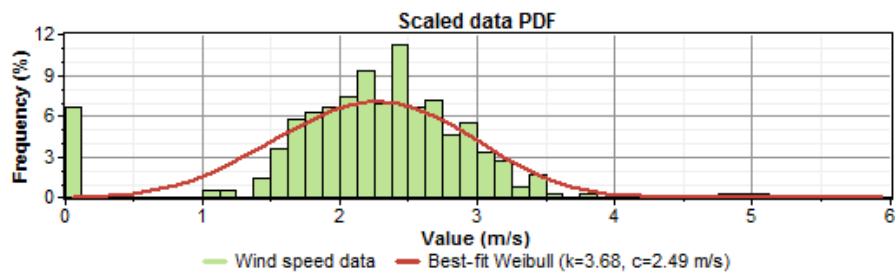
1. Wind Resource of the Year for Each Month



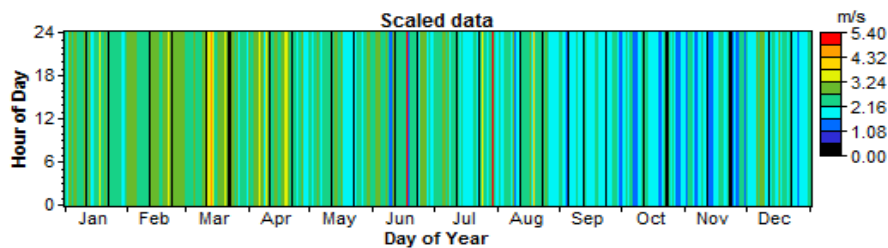
2. Monthly Average Wind Distribution of the Year



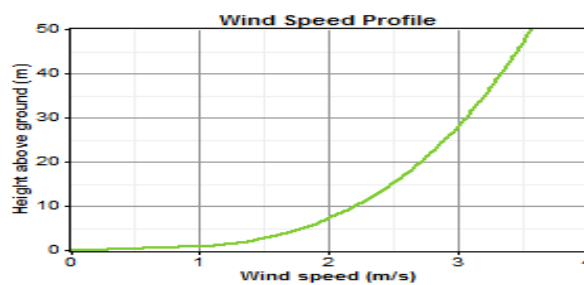
3. Probability Density Function of the Wind of Aykel at the Year



4. Diurnal Pattern Strength of the Wind of the Year

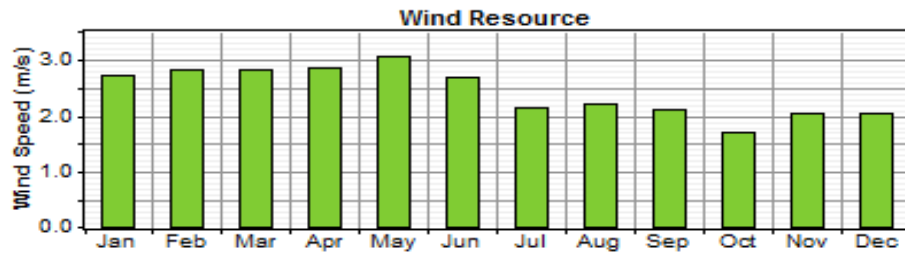


5. Wind Speed Variation with Height of Aykel at the Year

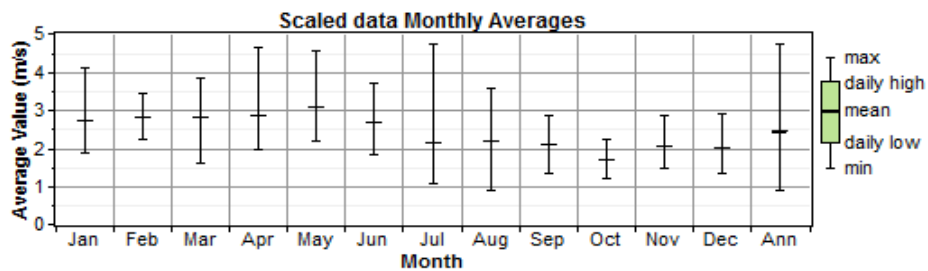


Wind Resource Assessment Result for Aykel: 2005

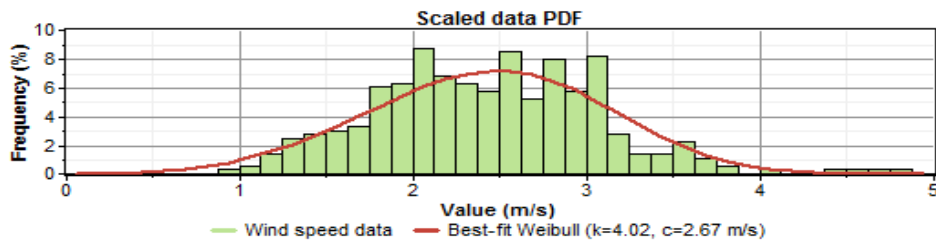
1. Wind Resource of the Year for Each Month



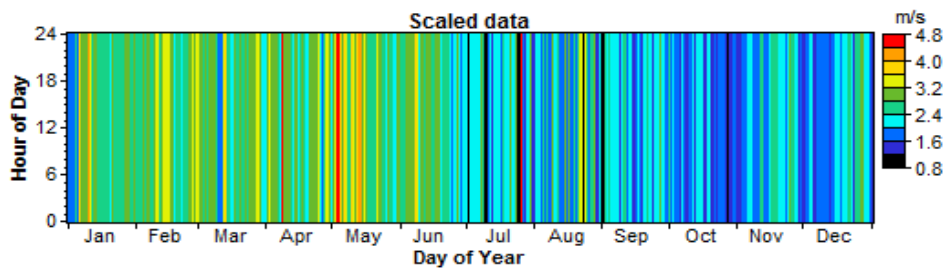
2. Monthly Average Wind Distribution of the Year



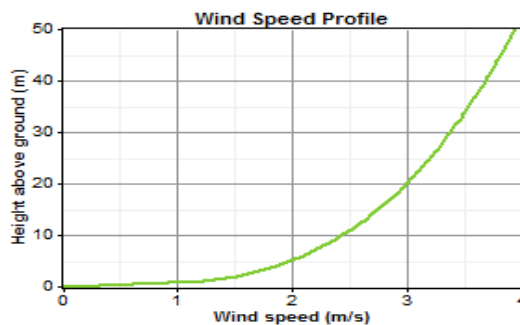
3. Probability Density Function of the Wind of Aykel at the Year



4. Diurnal Pattern Strength of the Wind of the Year

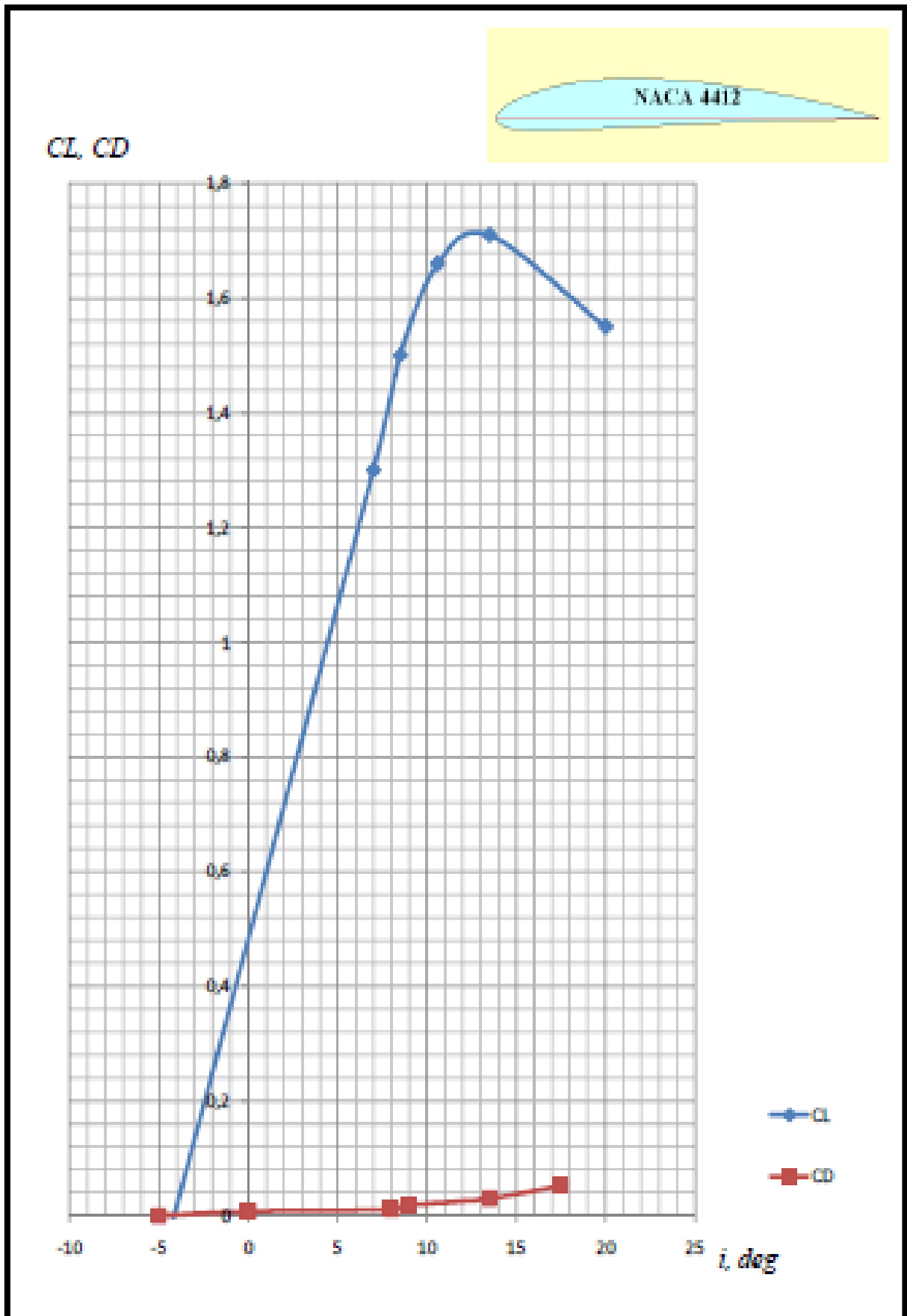


5. Wind Speed Variation with Height of Aykel at the Year



ANNEX B

Airfoil Profile for NACA 4412 [60]



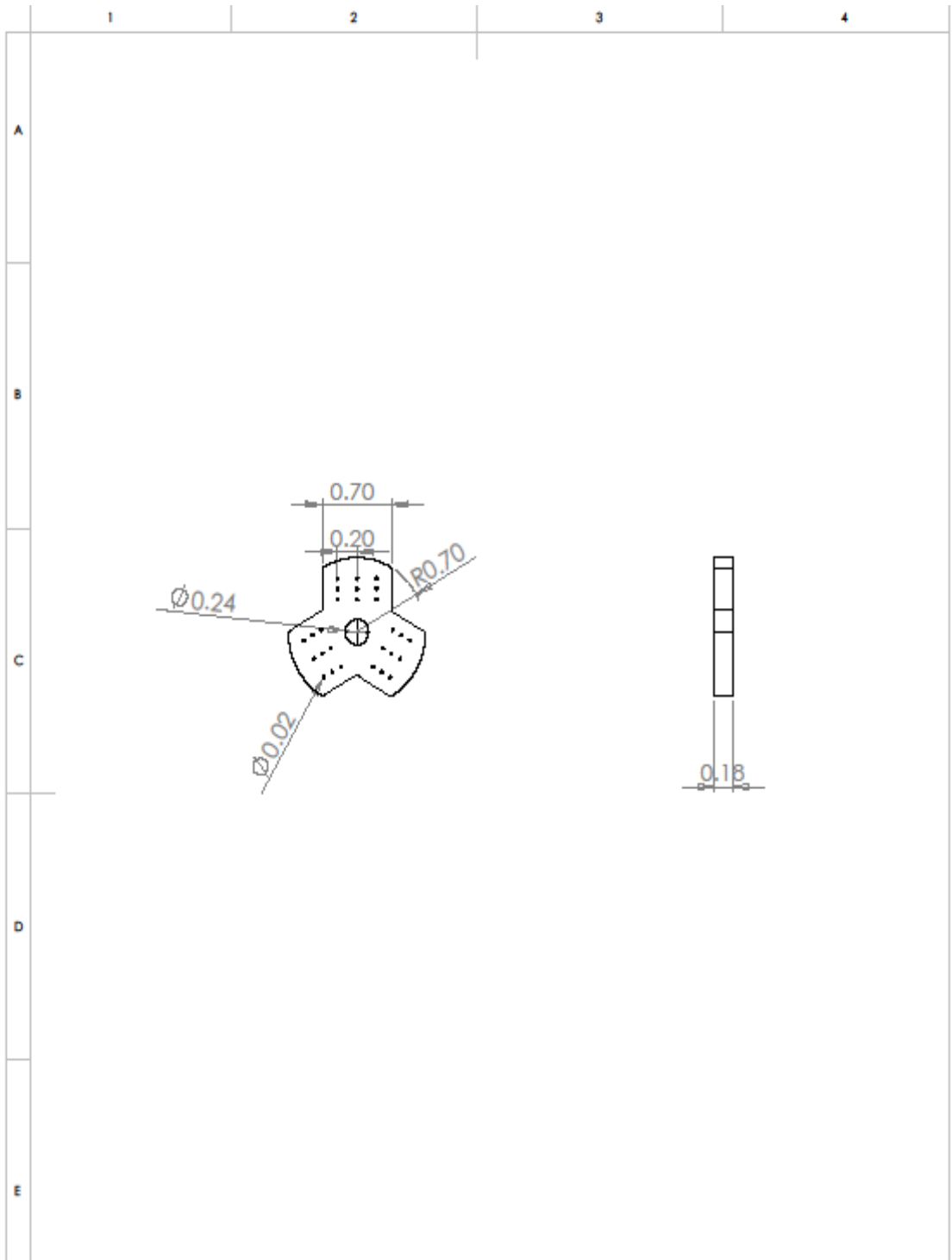
ANNEX C
PART DRAWINGS



All dimensions in meter

	NAME	SIGNATURE	DATE		
DRAWN	MESFIN B				
CHKD					
APPVD					
F MFG					
QA	3				

TITLE: BLADE	
MATERIAL: DOUGLASS FIR	DWG NO. 1
SCALE:1:100	A4

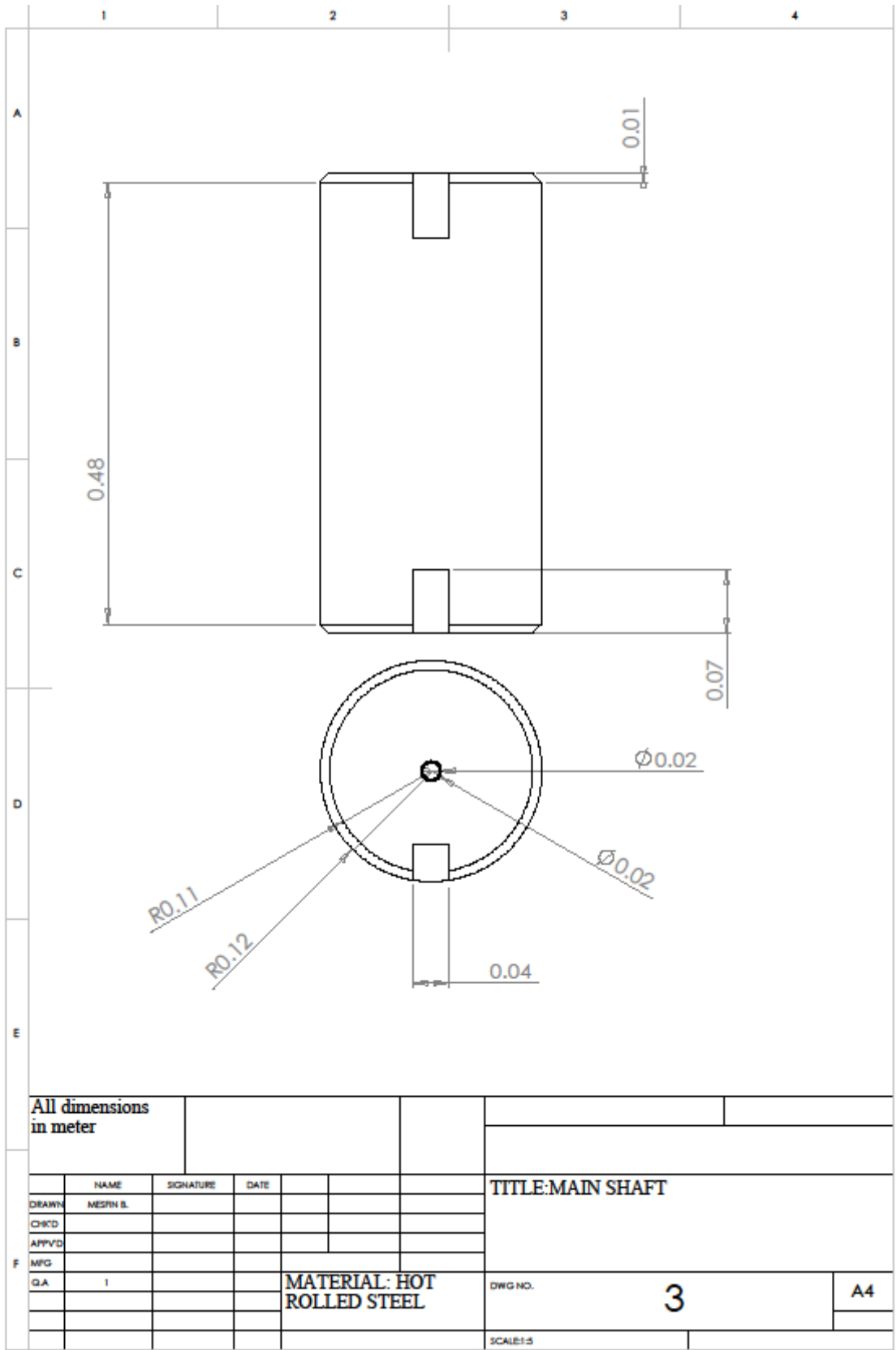


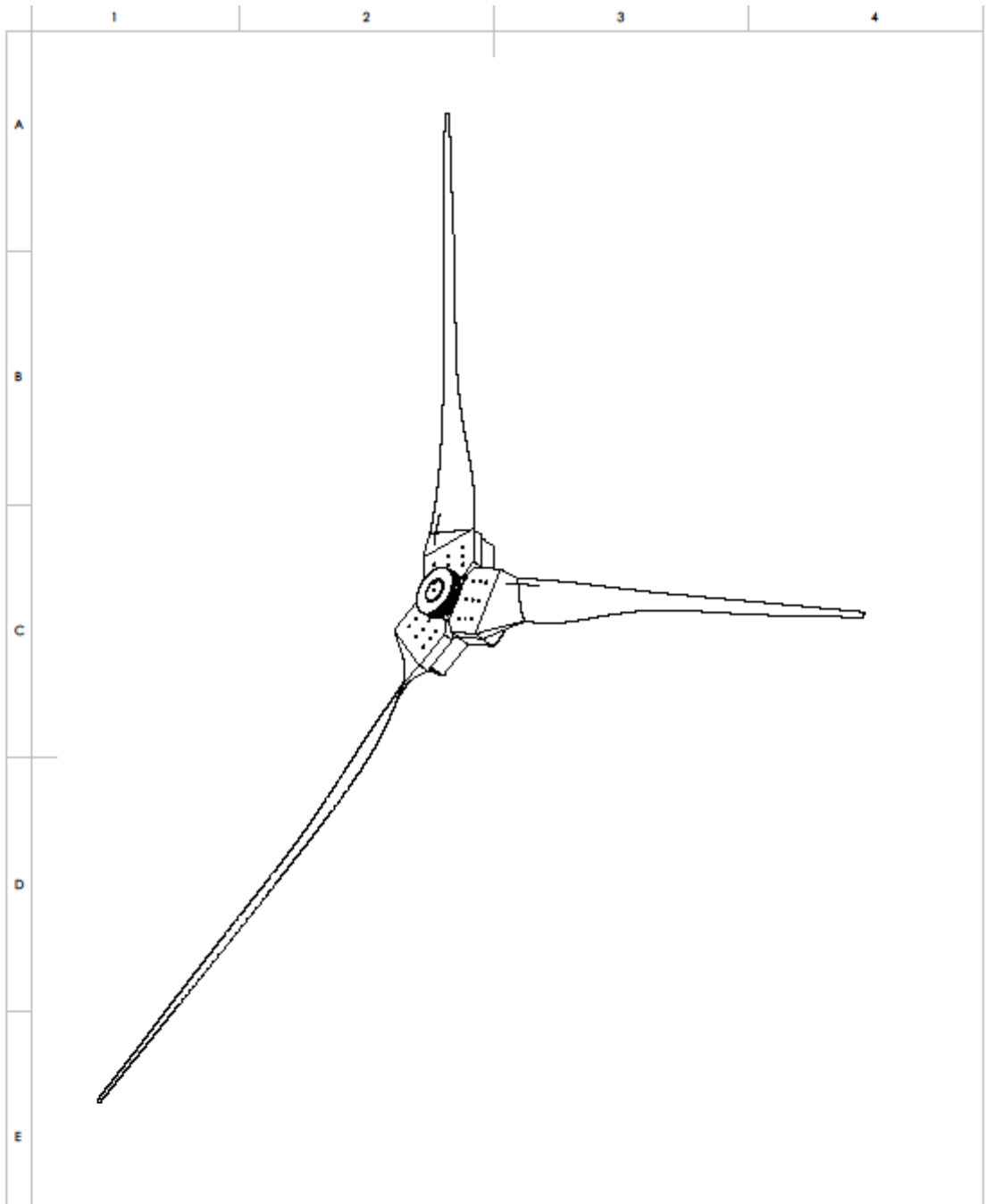
All dimensions in meter

	NAME	SIGNATURE	DATE			
DRAWN	MESIN B					
CHECKED						
APPROVED						
MFG						
QA						

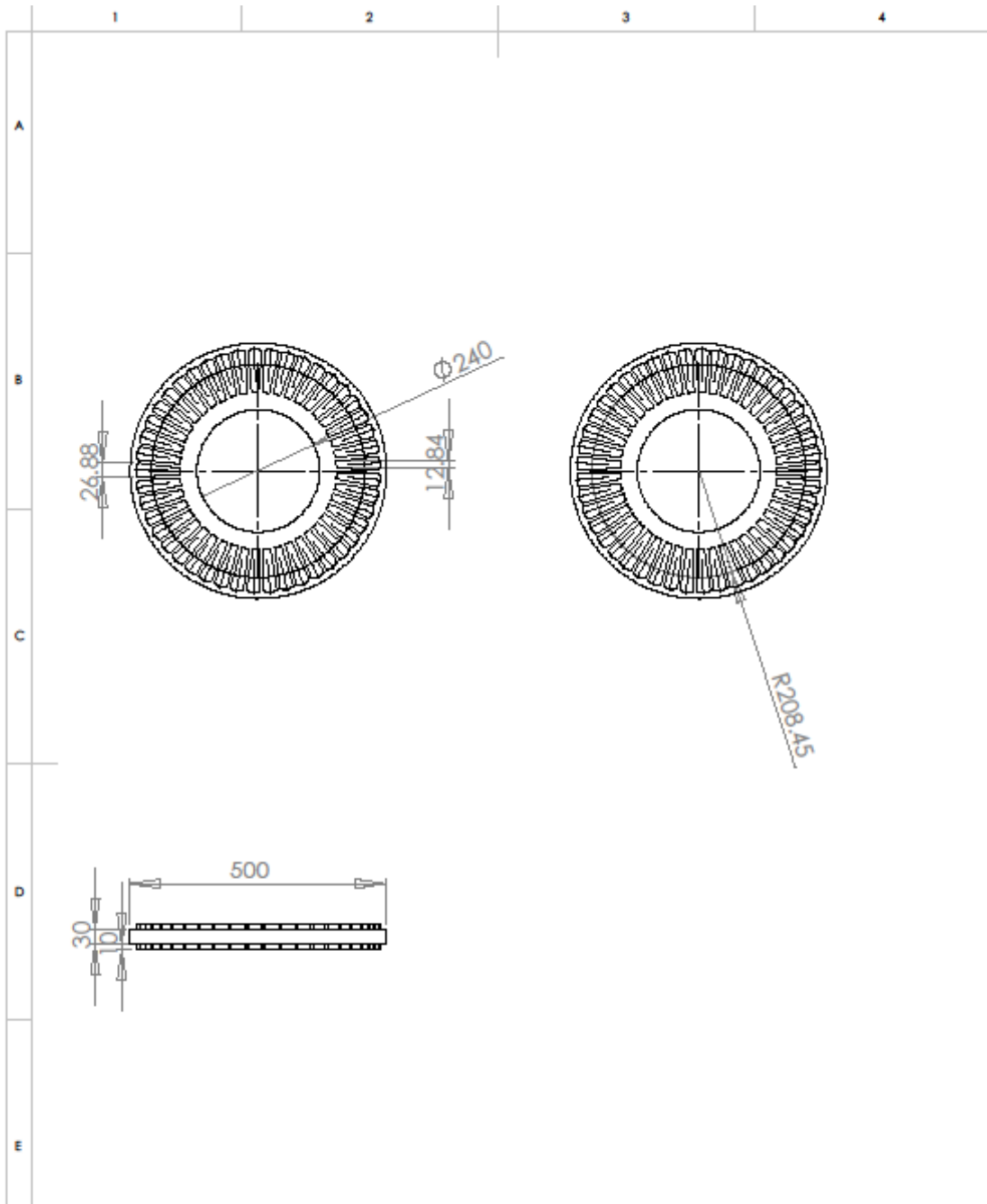
TITLE: HUB		DWG NO.	2	A4

MATERIAL: CAST IRON

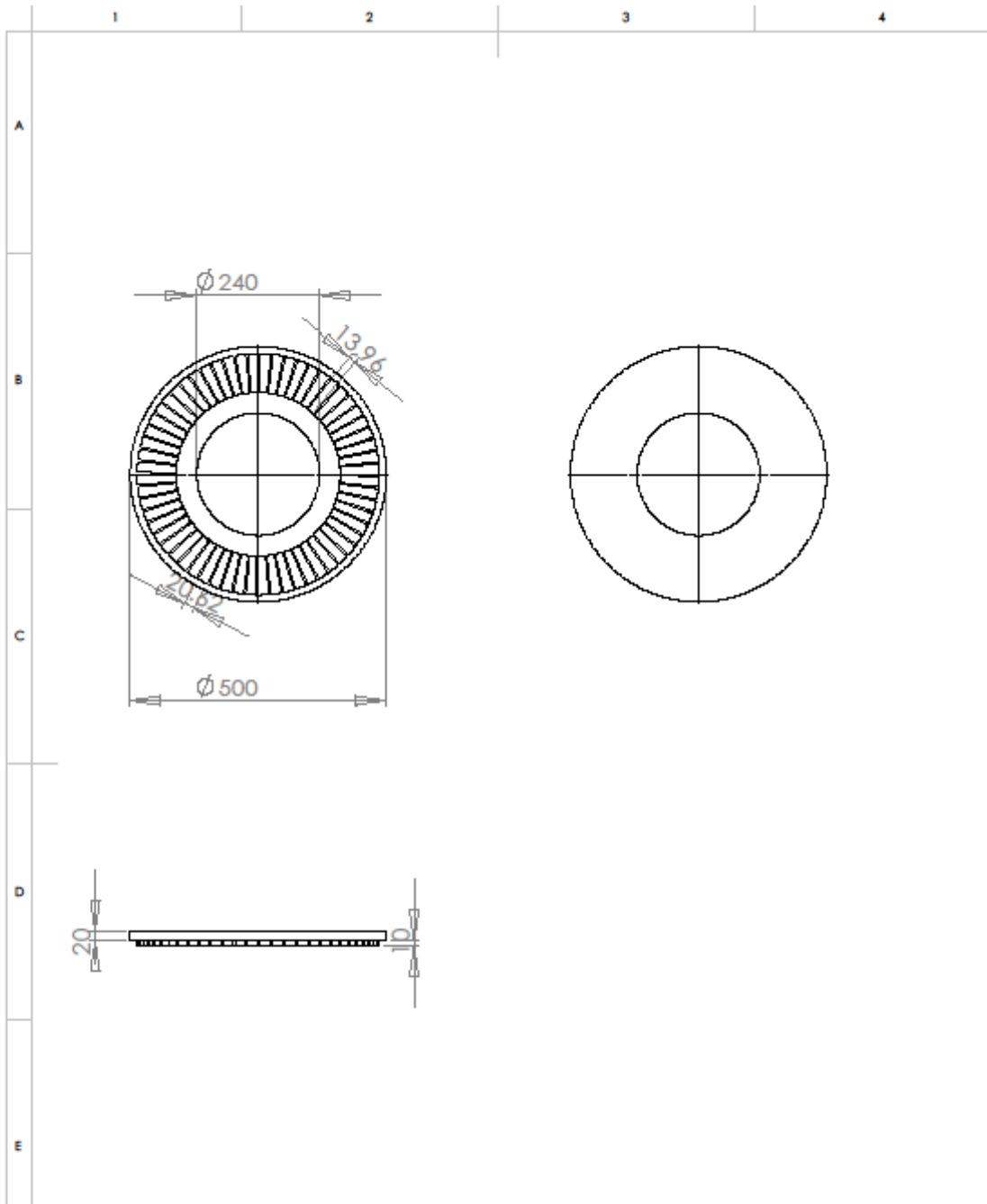




All dimensions in meter				DO NOT SCALE DRAWING		REVISION	
						TITLE: ASSEMBLY OF THE SYSTEM	
DRAWN	NAME	SIGNATURE	DATE				
CHKD							
APPVD							
MFG							
QA				MATERIAL: assembly		DWG NO. 4	
						A4	
				WEIGHT:	SCALE:1:500		



All dimensions are in millimete.		FINISH:			
				TITLE: stato of the axial flux generator	
DRAWN	NAME	SIGNATURE	DATE		
	Meefin B				
CHKD	Mr. Assefin A				
APPVD	Dr. Solomon T				
MFG	Meefin B				
QA	I			MATERIAL: copper wire and epoxy mold	DWG NO. 5
					A4
				SCALE:1:10	



All dimensions in millimeter							
	NAME	SIGNATURE	DATE		TITLE: rotor of the axial flux generator		
DRAWN	MESPN B						
CHECKED							
APPROVED							
MFG							
Q.A				MATERIAL: steel disk and permanent magnets	DWG NO.	6	A4
					SCALE: 1:30		

ANNEX D
ITERATION RESULT

FIRST ITERATION					
Section	C_l	AOA	Relative wind angel	a	a'
1	1.362671326	7.626	41.93741597	0.302727587	0.538270502
2	1.344266751	7.4426675	21.91410458	0.335993115	0.089083373
3	1.326043444	7.26	13.80164499	0.353553467	0.034093536
4	1.332216824	7.3	9.935655758	0.362525907	0.017741089
5	1.389765825	7.8	8.156775002	0.343131463	0.010836879
6	1.378368314	7.8	6.673382158	0.345908359	0.007284793
7	1.280307385	6.8	4.633732295	0.441708502	0.005219229
8	1.180194231	5.8019423	2.867605965	0.608759225	0.003915405
9	1.38330492	7.8330492	4.308542623	0.34532143	0.002999916
10	1.22012347	6.2012347	2.209270575	0.56538109	0.00193783
SECOND ITERATION					
1	1.379169929	7.79	42.10141597	0.303383178	0.550554304
2	1.379527361	7.7952736	22.26671068	0.334448485	0.091884137
3	1.389744161	7.89	14.43164499	0.343720535	0.035892503
4	1.410527948	8.05	10.68565576	0.342167606	0.018849196
5	1.42192051	8.08	8.436775002	0.333090625	0.011098376
6	1.416540078	8.08	6.953382158	0.333553781	0.007492446
7	1.437468298	8.14	5.973732295	0.348147361	0.005876466
8	1.251013764	6.5101376	3.575801295	0.514675598	0.00415423
9	1.431276046	8	4.475493423	0.335885021	0.003104968
10	1.278286449	6.78286449	2.790900365	0.46059374	0.002031295
THIRD ITERATION					
1	1.371972802	7.719	42.03041597	0.303094065	0.54517
2	1.357578248	7.5757825	22.04721958	0.335414279	0.09014
3	1.336359532	7.36	13.90164499	0.351992396	0.03438
4	1.325751646	7.3	9.935655758	0.36140241	0.017653
5	1.376020218	7.6	7.956775002	0.352174722	0.010723
6	1.361800214	7.62	6.493382158	0.35563547	0.007194
7	1.247901665	6.5	4.333732295	0.468575582	0.005084357
8	1.325304959	7.2530496	4.318713245	0.435012831	0.00441
9	1.38330492	7.8330492	4.308542623	0.34532143	0.002999916
10	1.367064783	7.67064783	3.678683705	0.344460135	0.002174583
FOURTH ITERATION					
1	1.375095847	7.75	42.06141597	0.303217909	0.54750287
2	1.371386789	7.7138679	22.18530498	0.334808282	0.091234672
3	1.381919339	7.82	14.36164499	0.344665454	0.035671626
4	1.410527948	8.05	10.68565576	0.342167606	0.018849196
5	1.450916717	8.2	8.556775002	0.331279376	0.011330842
6	1.446924602	8.2	7.073382158	0.330651492	0.007656373
7	1.442943289	8.21	6.043732295	0.343725922	0.005899743
8	1.30393556	7.0393556	4.105019255	0.456089119	0.004333423

Cont...					
9	1.431276046	8	4.475493423	0.335885021	0.003104968
10	1.304263704	7.04263704	3.050672915	0.42167346	0.00207314
FIFTH ITERATION					
1	1.373733618	7.737	42.04841597	0.303158001	0.546491179
2	1.362755569	7.6275557	22.09899278	0.335187718	0.090547944
3	1.342770532	7.43	13.97164499	0.35076993	0.034564649
4	1.325751646	7.3	9.935655758	0.36140241	0.017653473
5	1.354455511	7.54	7.896775002	0.352035973	0.010551817
6	1.335556536	7.33	6.203382158	0.372325958	0.007050363
7	1.230597959	6.3	4.133732295	0.488691008	0.005012202
8	1.320484395	7.204844	4.270507605	0.439645538	0.004389593
9	1.38330492	7.8330492	4.308542623	0.34532143	0.002999916
10	1.373469397	7.73469397	3.742729845	0.337746801	0.002184951
SIXTH ITERATION					
1	1.374305131	7.743	42.05441597	0.303176878	0.546922673
2	1.368172893	7.6817289	22.15316598	0.334949818	0.090978738
3	1.37629608	7.76	14.30164499	0.345657185	0.035511487
4	1.410527948	8.05	10.68565576	0.342167606	0.018849196
5	1.458999241	8.15	8.506775002	0.335127529	0.011393175
6	1.487959532	8.35	7.223382158	0.327535284	0.007877823
7	1.439062696	8.2	6.033732295	0.343866958	0.005883674
8	1.308401894	7.0840189	4.149682595	0.451567492	0.004348576
9	1.431276046	8	4.475493423	0.335885021	0.003104968
10	1.290478704	6.90478704	2.912822915	0.441762509	0.002050926
SEVENTH ITERATION					
1	1.374041401	7.74	42.05141597	0.30317083	0.546720441
2	1.364781421	7.6478142	22.11925128	0.335098852	0.090708954
3	1.348170414	7.48	14.02164499	0.350040188	0.034716278
4	1.325751646	7.257	9.892655758	0.363417063	0.017651119
5	1.363578777	7.6	7.956775002	0.35010531	0.01062521
6	1.300404707	7.0001	5.873482158	0.391877784	0.006859321
7	1.233114841	6.3	4.133732295	0.489201549	0.005022505
8	1.317719546	7.2	4.265663655	0.439688883	0.004380334
9	1.383304921	7.8330492	4.308542623	0.34532143	0.002999916
10	1.372625457	7.72625457	3.734290445	0.338620445	0.002183585

ANNEX E

MANUFACTURING COST OF COMPONENTS

The manufacturing cost of the wind turbine components can be estimate by using empirical relation developed by earlier studies. For this work the methods suggested by reference [75] was used. Unless otherwise noted, all dimensions are in meters and all masses are in kilograms. The outputs of all formulas will be in 2002 dollars, unless otherwise noted. An escalation can then be applied using the PPIs or GDP.

Blade	$\begin{aligned} \text{Advanced Material Cost} &= 0.04019R^3 - 21,051 \\ \text{Labor Costs} &= 2.7445R \\ \text{Baseline Material Cost} &= 0.4019R^3 - 955.24 \\ \text{Total Blade Cost} &= \frac{(\text{Material} + \text{Labor})}{(1 - 0.28)} \end{aligned}$
Hub	$\begin{aligned} \text{Hub mass} &= 0.954 \times \left(\text{blade} \frac{\text{mass}}{\text{single blade}} \right) + 5680.3 \\ \text{Hub cost} &= \text{hub mass} \times 4.25 \end{aligned}$
Pitch System	$\begin{aligned} \text{Total Pitch Bearing Mass} &= 0.1295 \times \text{total blade mass (three blades)} + 491.31 \\ \text{Total pitch system mass} &= (\text{Total Pitch Bearing Mass} \times 1.328) + 555 \text{ kg} \\ \text{Total pitch system cost (three blades)} &= 2.28 \times (0.2106 \text{Rotor diameter})^{2.6578} \end{aligned}$
Main Bearing	$\begin{aligned} \text{Bearing mass} &= \left(\text{rotor diameter} \times \frac{8}{600} - 0.033 \right) \times 0.0092 \times \text{rotor diameter}^{2.5} \\ \text{Total bearing system cost} &= 2 \times \text{bearing mass} \times 17.6 \end{aligned}$
Mechanical Brake, High-Speed Coupling,	$\begin{aligned} \frac{\text{Brake}}{\text{coupling}} \text{cost} &= 1.9894 \times \text{machine rating} - 0.1141 \\ \frac{\text{Brake}}{\text{coupling}} \text{mass} &= \left(\text{brake coupling} \frac{\text{cost}}{10} \right) \end{aligned}$
Generator	$\begin{aligned} \text{Mass} &= 661.25 \times \text{low speed shaft torque} \times 0.606 \\ \text{Total Cost} &= \text{machine rating} \times 219.33 \end{aligned}$
Yaw Drive And Bearing	$\begin{aligned} \text{Total yaw system mass} &= 1.6 \times (0.0009 \times \text{rotor diameter} \times 3.314) \\ \text{Total Cost} &= 2 \times (0.0339 \times \text{rotor diameter} \times 2.964) \end{aligned}$
Mainframe	$\begin{aligned} \text{Mainframe mass} &= 1.228 \times \text{rotor diameter} \times 1.953 \\ \text{Mainframe cost} &= 627.28 \times \text{rotor diameter} \times 0.85 \end{aligned}$
Electrical Connections	$\text{Electrical connection cost} = \text{machine rating} \times 40$
Cooling System	$\begin{aligned} \text{Hydraulic, cooling system mass} &= 0.08 \times \text{machine rating} \\ \text{Hydraulic, cooling system cost} &= \text{machine rating} \times 12 \end{aligned}$
Nacelle	$\text{Nacelle cost} = 11.537 \times \text{machine rating} + 3849.7$
Tower	$\begin{aligned} \text{Advanced: mass} &= 0.2694 \times \text{swept area} \times \text{hub height} + 1779 \\ \text{Baseline: mass} &= 0.3973 \times \text{swept area} \times \text{hub height} - 1414 \\ \text{Total Cost} &= \text{mass} \times 1.50 \end{aligned}$
Foundation	$\text{Foundation cost} = 303.24 \times (\text{hub height} \times \text{rotor swept area})^{0.4037}$
Transportation	$\begin{aligned} \text{Transportation cost factor } \$/kW & \\ &= 1.581^{-5} \times \text{machine rating}^2 - 0.0375 \times \text{machine rating} \\ &+ 54.7 \end{aligned}$
Road And Civil Works	$\begin{aligned} \text{Roads, civil work cost factor } \$/kW & \\ &= 2.17^{-6} \times \text{machine rating}^2 - 0.0145 \times \text{machine rating} + 69.54 \end{aligned}$
Installation	$\text{Assembly and installation} = 1.965 \times (\text{hub height} \times \text{rotor diameter})^{1.1736}$

ANNEX F

INTERNAL RATE OF RETURN USING MICROSOFT EXCEL

Return the internal rate of return for a series of cash flows represented by the numbers in values. These cash flows do not have to be even, as they would be for an annuity. However, the cash flows must occur at regular intervals, such as monthly or annually. The internal rate of return is the interest rate received for an investment consisting of payments (negative values) and income (positive values) that occur at regular periods. To calculate Internal Rate of Return using the IRR formula in Excel, you need a series of periodic cash flows like that shown in the figure E.1 below.

	A	B
1	t	Values
2	0	(20,000)
3	1	7,000
4	2	5,000
5	3	8,000
6	4	9,000
7		
8	IRR:	15.64%

Figure E.1: Sample Microsoft Excel Table

Syntax: IRR (values,guess)

Values: is an array or a reference to cells that contain numbers for which you want to calculate the internal rate of return.

- Values must contain at least one positive value and one negative value to calculate the internal rate of return.
- IRR uses the order of values to interpret the order of cash flows. Be sure to enter your payment and income values in the sequence you want.
- If an array or reference argument contains text, logical values, or empty cells, those values are ignored.

Guess: is a number that you guess is close to the result of IRR.

- Microsoft Excel uses an iterative technique for calculating IRR. Starting with guess, IRR cycles through the calculation until the result is accurate within 0.00001 percent. If IRR can't find a result that works after 20 tries, the #NUM! error value is returned.
- In most cases you do not need to provide guess for the IRR calculation. If guess is omitted, it is assumed to be 0.1 (10 percent).
- If IRR gives the #NUM! error value, or if the result is not close to what you expected, try again with a different value for guess.